Universidade de Aveiro Departamento de Química
2014

Leandro Miguel de Oliveira Lourenço

Ftalocianinas: Interação com estruturas de carbono e como agentes em PDT

Phthalocyanines: Interaction with carbon structures and as PDT agents

Universidade de Aveiro Departamento de Química
2014

Leandro Miguel de Oliveira Lourenço

Ftalocianinas: Interação com estruturas de carbono e como agentes em PDT

Phthalocyanines: Interaction with carbon structures and as PDT agents

Tese apresentada à Universidade de Aveiro para cumprimento dos requisitos necessários à obtenção do grau de Doutor em Química, realizada sob a orientação científica do Doutor João Paulo Costa Tomé, Investigador Principal do Departamento de Química da Universidade de Aveiro e Professor Auxiliar da Universidade de Gent, e co-orientação do Doutor José Abrunheiro da Silva Cavaleiro, Professor Catedrático do Departamento de Química da Universidade de Aveiro.

Este trabalho de doutoramento foi financiado pela FCT (Fundação para a Ciência e Tecnologia) através da bolsa com a referência de doutoramento SFRH/BD/64526/2009.

Dedico esta tese à minha Mãe, às minhas Irmãs e ao meu Pai que sempre me apoiaram, acarinharam e incentivaram na execução desta tese.

A coisa mais bela que podemos experimentar é o mistério. Essa é a fonte de toda a arte e ciências verdadeiras.

Albert Einstein

o júri

presidente

Doctor Fernando Manuel dos Santos Ramos
Cathedratic Professor - Department of Communication and Art – University of Aveiro

Doctor Tomás Torres Cebada (Vowel, principal examiner)
Cathedratic Professor - Department Organic Chemistry – Autonoma University of Madrid

Doctor Dirk Michael Guldi (Vowel, principal examiner)
Cathedratic Professor - Institute for Physical Chemistry- Friedrich-Alexander-Universität Erlangen-Nürnberg

Doctor Uwe Pischel (Vowel)
Associate Professor – Department of Chemistry Engineering, Physical-Chemistry and Organic Chemistry – University of Huelva

Doctor Pedro Miguel Pimenta Góis (Vowel)
Principal Researcher – Faculty of Pharmacy – University of Lisbon

Doctor Maria da Graça de Pinho Morgado da Silva Neves (Vowel)
Associated Professor with Habilitation – Department of Chemistry – University of Aveiro

Doctor Maria do Amparo Ferreira Faustino (Vowel)
Auxiliar Professor - Department of Chemistry – University of Aveiro

Doctor João Paulo Costa Tomé (Supervisor)
Principal Researcher – Department of Chemistry – University of Aveiro

agradecimentos

Agradeço à Fundação para a Ciência e a Tecnologia a bolsa de doutoramento (Referência: SFRH/BD/64526/2009) concedida ao longo de 4 anos para a realização dos objectivos propostos.

Ao grupo de investigação de Química Orgânica, Produtos Naturais e Agroalimentares (QOPNA) da Universidade de Aveiro, que me facultou as condições logísticas e materiais necessárias para o desenvolvimento do meu projeto de investigação científica.

Um agradecimento especial ao Doutor João Tomé pela orientação, amizade e ensinamentos que sempre me ajudaram ao longo da minha formação e elaboração dos trabalhos científicos. O meu muito obrigado pelo apoio e dedicação ao longo destes últimos anos que me fizeram ver a Química com "outros olhos".

À Doutora Graça Neves, agradeço a sua amizade, ajuda e discussões científicas muito pertinentes, sempre numa abordagem muito construtiva, ao longo do doutoramento.

Ao Professor Cavaleiro pela oportunidade de ter ingressado no grupo de investigação QOPNA para a elaboração dos diversos trabalhos.

Ao Professor Tomás Torres "muchas gracias" pela amizade, boa disposição, conhecimentos científicos e oportunidade de trabalho na síntese de ftalocianinas nos seus laboratórios de Química Orgânica na Universidade Autónoma de Madrid.

Ao Professor Dirk Guldi "Danke" pela oportunidade concedida de integrar um grupo excepcional de fotofísica na Universidade de Erlangen, que permitiram adquirir conhecimentos na funcionalização supramolecular de nanoestruturas de carbono. Um grande obrigado aos seus alunos e amigos Georgios Katsukis, Anita Hausmann, Marc Rudolf, Christina Schubert, Juergen Bartelmess, Konstantin Dirian e Leonie Wibmer pela elaboração dos trabalhos e também pelo convívio durante a minha estadia em Erlangen. Obrigado aos meus amigos Oana Tamasoiu, Irene Sanchez-Molina, Noelia Rubio Carrero, Ruben Casillas e Alejandro López que foram sempre companheiros muito importantes em Erlangen pela forma como me acolheram na cidade alemã. A vocês um grande "Prost".

À Doutora Rosário Domingues pela amizade, apoio e ensinamentos relevantes durante a elaboração dos estudos por espectrometria de massa.

Ao Doutor Fernando Domingues e à Doutora Mónica Válega pela excepcional dedicação dos estudos por cromatografia líquida.

À Doutora Amparo Faustino, Rosa Fernandes, Adelaide Almeida e Ângela Cunha pelas suas contribuições nos multidisciplinares estudos biológicos que se encontram descritos nesta dissertação, com um especial agradecimento pela amizade e dedicação à Patrícia Pereira, Clara Gomes e Andreína Sousa.

Ao Doutor Artur Silva agradeço a sua amizade, companheirismo, disponibilidade e ensinamentos científicos ao longo das distintas avaliações do Programa Doutoral em Química. Também um especial apreço pela sua capacidade de liderança e organização nas suas múltiplas funções que tem desenvolvido neste mesmo programa doutoral na Universidade de Aveiro.

agradecimentos

Ao Doutor Uwe Spichel deixo aqui o meu agradecimento pelo estágio científico na Universidade de Huelva, pelos ensinamentos na Química Supramolecular e pelas discussões objectivas nos trabalhos de ambição científica elevada. Agradeço também à Vânia Pais pela amizade, acolhimento e conhecimentos transmitidos durante a minha estadia em Huelva.

Um muito obrigado aos companheiros de laboratório Ana Gomes, Nuno Moura, Andreia Farinha e Mário Calvete pela amizade, ensinamentos, paciência e disponibilidade, principalmente durante a minha formação inicial na Química Orgânica.

Um agradecimento aos técnicos do Departamento de Química da Universidade de Aveiro pela capacidade e competência no desempenho das suas funções que me ajudaram sempre na obtenção dos melhores resultados científicos.

Ao pessoal da orgânica deixo aqui um grande obrigado por todos estes anos que me receberam muito bem e mesmo com alguns contratempos sempre conseguimos funcionar como um bom grupo de trabalho em prol da ciência.

Um abraço e um muito obrigado aos amigos da farra, boa disposição e das viagens: Sónia Pires, Diana Resende, Clara Gomes, Dora Costa, Joana Brás Pereira, Carla Pereira, Raquel Silva, Bernardo Iglésias, Lucía Fernández, Djeni Rocha, Joana Torrão e Rita Craveiro.

Aos campeões Sérgio Vilela, Flávio Figueira, João Rodrigues e Ricardo Carvalho deixo aqui um forte abraço e um sinal de enorme gratidão pela amizade e o apoio durante estes anos de luta numa "maratona" que não foi fácil de chegar ao fim. Muito obrigado pelos Vossos conselhos que foram sempre importantes e levados em boa consideração.

Um agradecimento especial aos meus amigos Roberto Paradinha, Sara Seiça, Nélio Silva, Diana Lopes, Diogo Carvalhais, Salomé Marques, Luís Bastião, Renato Cardoso e Ana Ventura pela amizade, apoio nos momentos mais difíceis e que me deram sempre uma outra perspectiva para levar tudo a "bom porto".

À Joana Lagarinhos agradeço todo o amor, carinho e compreensão principalmente durante esta "caminhada" final para terminar o doutoramento. Um forte abraço e o meu muito obrigado por tudo.

palavras-chave

Ftalocianinas, fulerenos (C_{60}), nanotubos de carbono (CNT), nanofolhas de grafeno, química supramolecular, matrizes supramoleculares, assembleias dador-aceitador, transferência de energia, terapia fotodinâmica (PDT), fotossensibilizador, células de cancro de bexiga humana UM-UC-3, fotoinativação de micorganismos (PDI).

resumo

Esta dissertação descreve a síntese e caracterização de diferentes derivados de ftalocianina (Pc), assim como de algumas porfirinas (Pors), para interação supramolecular com diferentes nanoestruturas de carbono para potencial aplicação em nanodispositivos eletrónicos. Igualmente, é também reportado a preparação e avaliação biológica de interessantes conjugados de Pc para a terapia fotodinâmica (PDT) de cancro e para a fotoinativação de microrganismos (PDI).

Neste trabalho científico são discutidas as propriedades gerais das Pcs e metodologias sintéticas usadas na sua preparação, bem como algumas das suas importantes aplicações.

Os precursores ftalonitrilo foram preparados a partir de ftalonitrilos comerciais por substituições nucleofílicas de grupos -NO_2, -Cl ou -F, presentes no núcleo ftalonitrilo, por unidades tiol ou piridilo. As correspondentes Pcs foram preparadas por ciclotetramerização dos ftalonitrilos, previamente sintetizados, na presença de um sal metálico a temperaturas elevadas. Uma segunda estratégia envolveu a pós-funcionalização na periferia do macrociclo da ftalocianina hexadecafluor de zinco(II) com unidades de mercaptopiridina ou ciclodextrina.

Os diferentes compostos foram caracterizados estruturalmente por diversas técnicas espectroscópicas, nomeadamente espectroscopia de ressonância magnética nuclear de ^{1}H, ^{13}C e ^{19}F (atendendo à composição elementar de cada estrutura), espectroscopia de absorção e de emissão, e espectrometria de massa. Para estudos fotofísicos específicos foram também usadas a caracterização electroquímica, espectroscopia de femtossegundo e raman, microscopia de transmissão eletrónica e de força atómica. Foi realizado a derivatização não covalente de nanoestruturas de carbono, principalmente nanotubos de carbono de parede simples (SWNT) e nanofolhas de grafeno, com os conjugados de ftalocianina preparados, para dessa forma estudar as propriedades fotofísicas dessas nanoassembleias supramoleculares. Também, a partir de Pors-piridilo e ftalocianinas de ruténio (RuPcs) foram realizadas matrizes de Por-RuPcs *via* química de coordenação. Os resultados obtidos mostraram interessantes interações eletrónicas doador-aceitador e podem ser considerados candidatos atrativos para diversos dispositivos nanotecnológicos.

Por outro lado, os conjugados anfifílicos de ftalocianina-ciclodextrina (Pc-CD) foram testados em ensaios biológicos para avaliar a sua capacidade de inibir células cancerígenas UM-UC-3 da bexiga humana. Os resultados obtidos demonstraram que estes conjugados fotoativos são altamente fototóxicos contra este tipo de células, mostrando-se bastante promissores como agentes em PDT.

keywords

Phthalocyanines, fullerenes (C_{60}), carbon nanotubes (CNTs), graphene nanosheets, supramolecular chemistry, supramolecular arrays, donor-acceptor assemblies, energy transfer, photodynamic therapy (PDT), photosensitizer, UM-UC-3 human bladder cancer cells, microorganisms photodynamic inactivation (PDI).

abstract

This dissertation describes the synthesis and characterization of different phthalocyanine (Pc) derivatives, as well as some porphyrins (Pors), for supramolecular interaction with different carbon nanostructures, to evaluate their potential application in electronic nanodevices. Likewise, it is also reported the preparation and biological evaluation of interesting phthalocyanine conjugates for cancer photodynamic therapy (PDT) and microorganisms photodynamic inactivation (PDI).

The phthalonitrile precursors were prepared from commercial phthalonitriles by nucleophilic substitution of -NO_2, -Cl, or -F groups, present in the phthalonitrile core, by thiol or pyridyl units. After the synthesis of these phthalonitriles, the corresponding Pcs were prepared by ciclotetramerization using a metallic salt as template at high temperatures. A second strategy involved the post-functionalization of hexadecafluorophthalocyaninato zinc(II) through the adequate substituents of mercaptopyridine or cyclodextrin units on the macrocycle periphery.

The different compounds were structurally characterized by diverse spectroscopic techniques, namely ^{1}H, ^{13}C and ^{19}F nuclear magnetic resonance spectroscopies (attending the elemental composition of each structure); absorption and emission spectroscopy, and mass spectrometry. For the specific photophysical studies were also used electrochemical characterization, femtosecond and raman spectroscopy, transmission electron and atomic force microscopy. It was highlighted the noncovalent derivatisation of carbon nanostructures, mainly single wall carbon nanotubes (SWNT) and graphene nanosheets with the prepared Pc conjugates to study the photophysical properties of these supramolecular nanoassemblies. Also, from pyridyl-Pors and ruthenium phthalocyanines (RuPcs) were performed Por-RuPcs arrays *via* coordination chemistry. The results obtained of the novel supramolecular assemblies showed interesting electron donor-acceptor interactions and might be considered attractive candidates for nanotechnological devices.

On the other hand, the amphiphilic phthalocyanine-cyclodextrin (Pc-CD) conjugates were tested in biological trials to assess their ability to inhibit UM-UC-3 human bladder cancer cells. The results obtained demonstrated that these photoactive conjugates are highly phototoxic against human bladder cancer cells and could be applied as promising PDT drugs.

Index

Abbreviations

δ	Chemical shift
ε	Molecular absorption coefficient
λ	Wavelength
τ	Life time
φ	Quantum yield
0D	Zero-dimensional
1D	One-dimensional
2D	Two-dimensional
AFM	Atomic Force Microscopy
C_{60}	Fullerene
CD	Cyclodextrin
CFU	Colony-forming unit
CNT	Carbon nanotube
COSY 2D	Two dimensional homonuclear correlation spectroscopy
d	Doublet
DBN	1,5-diazabicyclo[4.3.0]non-5-ene
DBU	1,8-diazabicyclo[5.4.0]undec-7-ene
DCF	2´,7´-dichlorodihydrofluorescein
DCFDA	2´,7´-dichlorodihydrofluorescein diacetate
dd	Doublet of doublets
DEA	Diethylamine
DIPEA	*N*,*N'*-diisopropylethylamine
DMAE	*N*,*N'*-dimethylaminoethanol
DMF	*N,N'*-dimethylformamide
DMSO	Dimethyl sulfoxide
DPBF	Diphenylisobenzofuran
E. coli	*Escherichia coli*
ESI	Electrospray ionization
Gal	Galactose
GalPro	Protected D-galactose
H_2DCFDA	6-carboxy-2',7'-dichlorodihydrofluorescein diacetate

HOMO	Highest occupied molecular orbital
HPLC	High-performance liquid chromatography
HR	High resolution
HSA	Human serum albumin
IC	Incubation concentration
ISC	Intersystem crossing
IUPAC	International Union of Pure and Applied Chemistry
J	Coupling constant
L.C.	Light control
L.D.	Dark control
LED	Light emitting diode
LUMO	Lowest unoccupied molecular orbital
m	Multiplet
m/z	Mass/charge relation
MALDI-TOF-MS	Matrix-assisted laser desorption/ionization-Time of flight-Mass spectrometry
MPc	Metallophthalocyanine
MS	Mass spectrometry
MTT	3-(4,5-dimethylthiazol-2-yl)-2,5-diphenyltetrazolium bromide
MWNT	Multi Walled Carbon Nanotube
nIR	Near-infrared
NLO	Nonlinear optic
NMR	Nuclear magnetic resonance
PBS	Phosphate buffered saline
Pc	Phthalocyanine
Pc-CD	Phthalocyanine-cyclodextrin
PDI	Photodynamic inactivation
PDT	Photodynamic Therapy
PEG	Polyethylene glycol
Por	Porphyrin
Por-Pc	Porphyrin-Phthalocyanine
ROS	Reactive oxygen species
rt	Room temperature

s	Singlet
S_0	Ground singlet state
S_1	Excited state of higher energy
SDBS	Sodium dodecylbenzenesulphate
SWNT	Single Walled Carbon Nanotube
T	Triplet
TCSPC	Time correlated single photon counting
TEM	Transmission electronic microscopy
TFA	Trifluoroacetic acid
TLC	Thin-layer chromatography
TMS	Tetramethylsilane
TSA	Tripic Soy Agar
TSB	Tripic Soy Broth
UV-Vis	Ultraviolet-visible

Chapter 1

General Introduction

1.1 Phthalocyanines: General considerations

The term phthalocyanine was suggested by Linstead, in 1933, to describe a class of blue-green pigments. This term comes from the combination of the prefix *phthalo*, highlighting the origin from phthalic anhydride and derivatives, and *cyanine* due to their dominating blue colour.[1] Phthalocyanines are a class of compounds of synthetic origin, structurally close to the analogous porphyrins (Pors), but with a core constituted by four isoindole units linked through aza bridges (**H_2Pc**, Figure 1.1).[1]

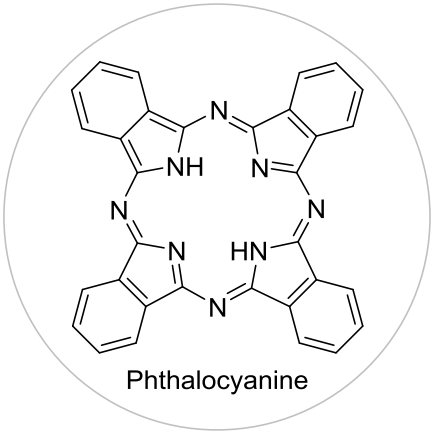

Figure 1.1 Structure of free-base phthalocyanine **H_2Pc**.

Pcs are one of the most widely used and studied classes of chromophores, as revealed by the plethora of applications were they are included.[1-3]

The vast number of publications since their discovery[4] and a high interest in the physical-chemical properties characterization attracted many researchers from 20th century.[5-13] In 1907, Braun and Tscherniak detected the formation of a small amount of a blue compound when heated the *o*-cyanobenzamide.[14] In 1927, Diesbach and von der Weid of the University de Fribourg described a high stable blue material during the chemical reaction of 1,2-dibromobenzene with copper cyanide in pyridine under reflux.[15-17] However, these researchers proposed an incorrect molecular formula of $C_{26}H_{18}N_6Cu$.[15] Six years later, in 1933, Linstead continued this investigation and identified the compounds as being the free and the Cu(II) complex of phthalocyanine. In the same period, *Scottish Dyes Ltd*. detected a highly stable and insoluble blue impurity when their employees were trying to produce phthalimide from phthalic anhydride and ammonia; this compound showed a high potential to be used as a pigment. In 1929, the economic interest of this pigment leads

to create a patent, even without knowing the exact structure.[18] In this sense, the company decided to send some quantity of this sample to Linstead. Finally, between 1933 and 1934, this researcher proved that the blue compound was the Fe(II) complex of phthalocyanine and the structure was confirmed by Robertson using the X-ray crystallography.[19-23] Following the Linstead study, the first one to use the name of *phthalocyanine*, two distinct synthetic routes were described to prepare phthalocyanines: one of them involved the use of *o*-cyanobenzamide as starting material, and the other the use of phthalonitrile precursors.[24-27] With these developments, in 1935, the Cu(II) phthalocyanine was synthesized at industrial scale and used as a blue pigment until nowadays. The Linstead investigations were encouraging for the paint industry, but in case of the scientific areas the insolubility of these pigments limited their use.

Only in the 60s, when Lukyanets tried to continue the Pcs investigation and reported the synthesis of highly soluble Pc derivatives, the phthalocyanine chemistry won importance among many synthetic organic researchers. In the period of 1965-2001, over 5000 works on Pcs and their derivatives, including research papers and patents, concerning the synthesis, characterization and applications were published.[28] Interestingly, in 1983, Frank H. Moser and Arthur L. Thomas published two volumes on Pcs[29,30] dedicating a especial chapter focused on the physical properties of these dyes with information related to the effects of temperature, pressure, electromagnetic radiation and particle impact on Pcs. These books also cover the properties of the Pcs in solutions and on surfaces, experimental techniques and analytical methods used for their characterization, and also theoretical calculations.[1]

In 2000, it was also published a concise review of the physical properties of Pcs written by Lobbert[31] in the Ullmann's Encyclopedia of Industrial Chemistry, which offers the information about: density, appearance, sublimation points, solubility and thermal stability of Pcs; particle size; colour properties; crystal structure and polymorphism; surface and interfacial properties; physical investigations [absorption, fluorescence, phosphorescence, nuclear magnetic resonance (NMR), infrared (IR) and Raman spectra; determination of electric, photoelectric and magnetic properties; Mossbauer analysis, ESCA, inelastic tunnelling spectroscopy, field ion and field electron microscopy].[31] In the last 13 years, from 2002 until 2014, occurred a boom in the phthalocyanine research and were published over 12000 works (923 papers per year) in scientific journals which considerably reveal the enormous interest of the phthalocyanines until nowadays.

However, the evolution of the chemistry of phthalocyanines has not only been focused at finding synthetic strategies that provide increasingly "sophisticated" phthalocyanine structures. The called analogues of phthalocyanines, namely subphthalocyanine, naphtophthalocyanine, tetrapirazinoporphyrazine and hemiporphyrazine (Figure 1.2) also represent a number of structural variations of the basic macrocycle ring.[32,33]

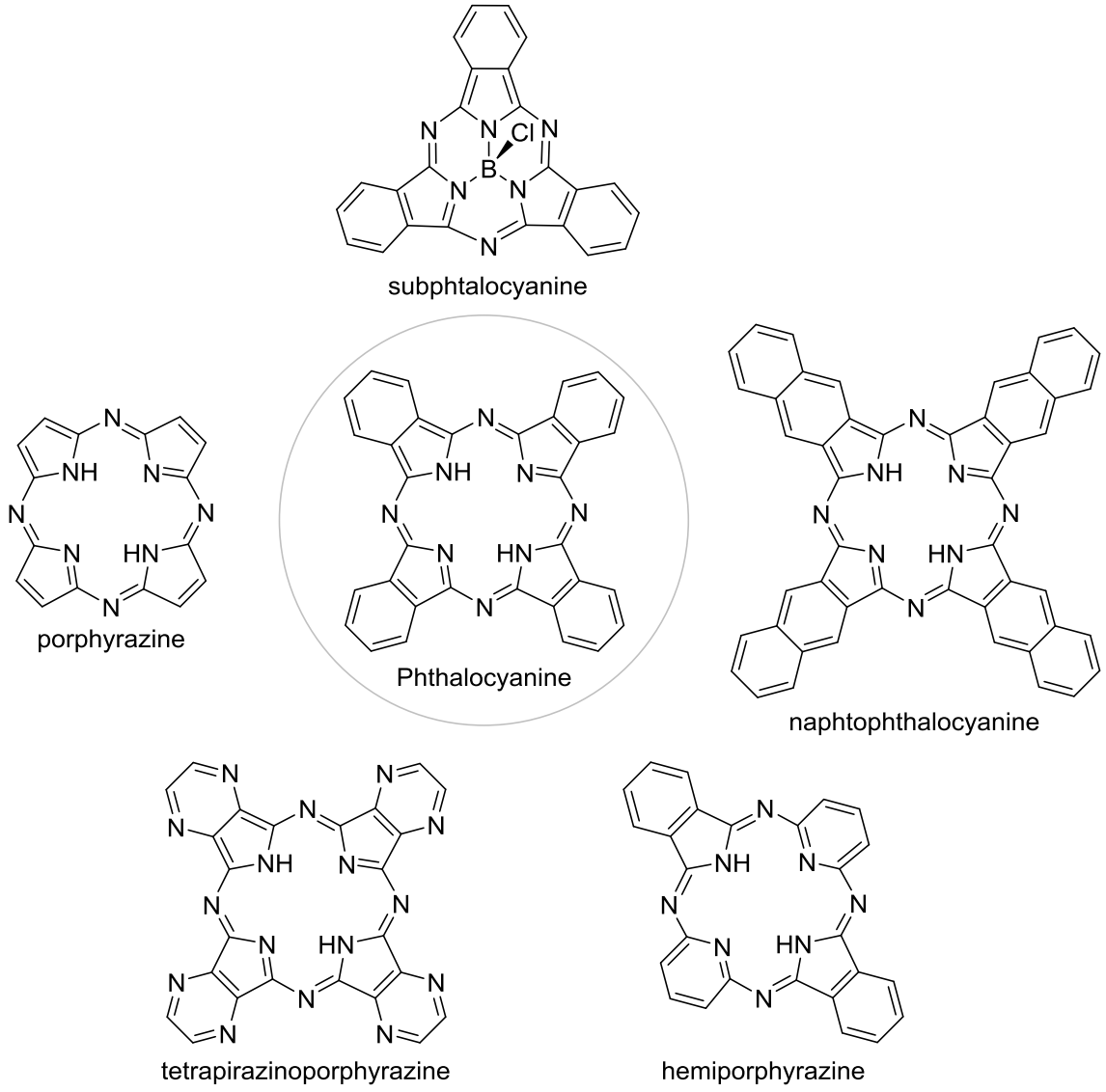

Figure 1.2 Examples of phthalocyanine analogue structures.

1.2 Aromaticity and optical properties

Phthalocyanines are structurally related with porphyrins but contrarily to the last ones do not occur in nature. These aromatic compounds were one of the first macrocycles

synthesised in the organic chemistry laboratories. The main attention devoted to these structures is correlated with the striking resemblance with the heme group and chlorophylls were the phthalocyanines have being used as models for these biomolecules. The aromatic structure of the metal-free unsubstituted phthalocyanine molecule is constituted by 18 π-electron pairs and according with the *International Union of Pure and Applied Chemistry* (IUPAC), all atoms are numbered except the fused carbons between the pyrrole ring and the benzene ring (Figure 1.3).[34] This type of macrocycle formed by four isoindole groups can also be called tetrabenzotetraazoporphyrin or tetrabenzoporphyrazine. The macrocycle evidences sixteen possible sites for substitution in the four benzo-subunits: eight peripheral β-positions (2,3,9,10,16,17,23,24) and eight non-peripheral α-positions (1,4,8,11,15,18,22,25). These positions can be substituted by several organic units. Substitutions in the α,β-positions improve the solubility of the phthalocyanines in the most organic and aqueous solvents depending on the groups.[35]

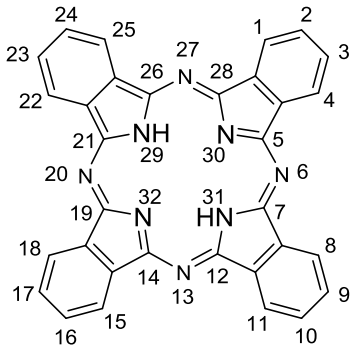

Figure 1.3 IUPAC numeration of the free-base phthalocyanine.

One of the most extraordinary features of the Pc macrocycle core is their versatility to incorporate some chemical elements. One of the first systematic studies on the variations of nonlinear optic (NLO) properties of modulated Pcs was presented in 1991 and concerned the characterization of Pcs having different central metal atoms "M" (Figure 1.4).[36] The hydrogen atoms of the central cavity of the Pc may be replaced by more than seventy elements of the periodic table giving rise to metallophthalocyanine (MPc), which can be regarded as very weak dibasic acid.[37] Hence, one of the most synthesized MPc in large scale was phthalocyaninato Cu(II).

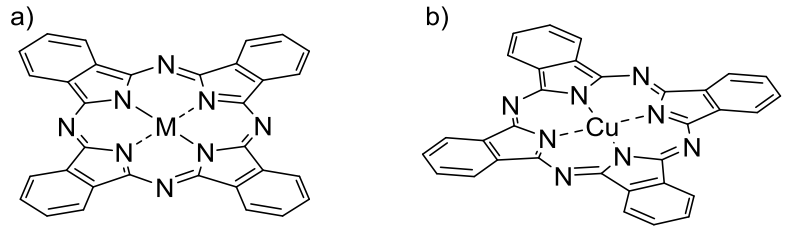

Figure 1.4 a) Disposition of MPc, which symbol "M" can represent monovalent or divalent entities. b) Structure of phthalocyaninato Cu(II).

The unsubstituted phthalocyanines exhibit high thermal and chemical resistance, which is an important role for the most technological applications. Their major drawback lies with the fact of the highly insoluble compounds, are only dissolved in solvents with high boiling point such as quinoline, chlorobenzene or 1-chloronaphthalene, or strong mineral acids due to their natural tendency to stack (π-π stacking). Also, the versatility of these aromatic structures, not only allows the incorporation of specific substituents, in the isoindole rings, but also certain central metals can be co-axially functionalized. Usually, co-axially functionalized derivatives are highly soluble, since the π-π-stacking is drastically decreased.[38-40]

Phthalocyanines and their analogues have been used as components of artificial photosynthetic devices, due to their unequivocal photophysical features.[41-47] In this respect, phthalocyanines hold some advantages comparing to other photoactive porphyrinoids. Attending to the extended network of conjugated electrons, which are delocalized over four isoindole units bridged by eight azamethines, these compounds have subsequently high molar absorption coefficients in the red region of the electromagnetic spectrum and fast energy and/or electron transfer abilities to electron acceptor counterparts. The explanation for this phenomenon is the structural differences of the two tetrapyrrolic macrocycles: the higher electronegativity of the nitrogen atoms in the aza bridges than of carbon atoms, which attract a self-around the π-electron density and the benzene rings fused allow the extend the π-electronic system.[48,49]

The typical electronic spectrum of a metal phthalocyanine complex shows a broad band around 300-400 nm called Soret-band (S- or B-band) and an intense Q-band situated in the range of 600-750 nm (Figure 1.5).[50-52] This narrow and intense Q-band is responsible for the blue-green colour of these dyes. In case of free-base phthalocyanines, the macrocycle have less symmetry and consequently show a split of the Q-band (Figure

1.5).[49] The strongest Q-band absorption of **H_2Pc** and **ZnPc**, can be attributed to the absorption of light and consequently excitation of electrons from the highest occupied molecular orbital (HOMO), namely the π-transitions, to a transition of the lowest unoccupied molecular orbital (LUMO), namely the π*-transitions (Figure 1.6).[48,49]

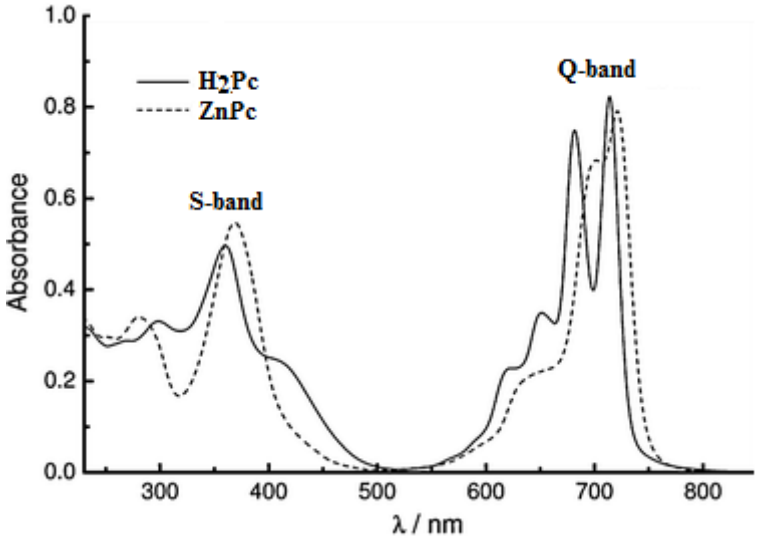

Figure 1.5 Ultraviolet–visible (UV-Vis) spectra of free-base **H_2Pc** (D_{2h}) and metal complex **ZnPc** (D_{4h}).[53]

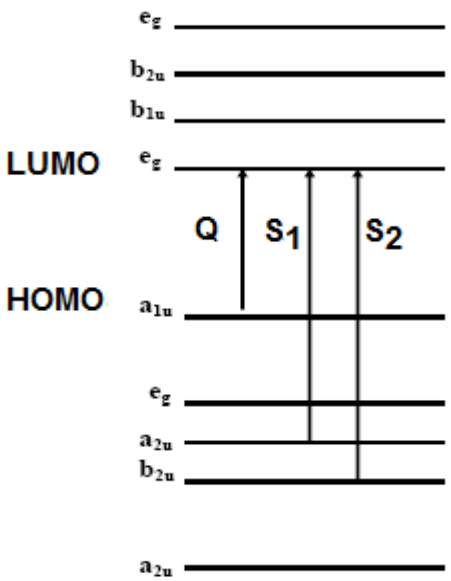

Figure 1.6 Electronic transitions of the Q- and S-bands of the phthalocyanine.

It is also noteworthy, that the position, appearance and intensity of the Q-bands depend on the Pc peripheral substituents, metal insertion, solvent and if the macrocycle is

aggregate or not. The nature and the oxidation state of the metal ion and the expansion of the macrocycle aromatic system can also affect its electronic features.[49]

1.3 Synthesis of phthalocyanines

A great variety of precursors can be used in the synthesis of phthalocyanines, such as: *o*-cyanobenzamide, phthalic acid, phthalic anhydride, phthalimide, diiminoisoindoline and phthalonitrile (Figure 1.7). One of the most common precursors are the phthalonitriles, that depending on the reaction conditions can initially be transformed into a diiminoisoindoline derivative *via* reaction with ammonia, followed of condensation, usually in alcoholic solutions at high temperatures. It is noteworthy, that the use of a catalytic organic base, for example, 1,8-diazabicyclo[5.4.0]undec-7-ene (DBU) or 1,5-diazabicyclo[4.3.0]non-5-ene (DBN) in pentanol[54,55] or 2-dimethylaminoethanol (DMAE) as solvent, is possible to get many desired Pcs in high yields.[56]

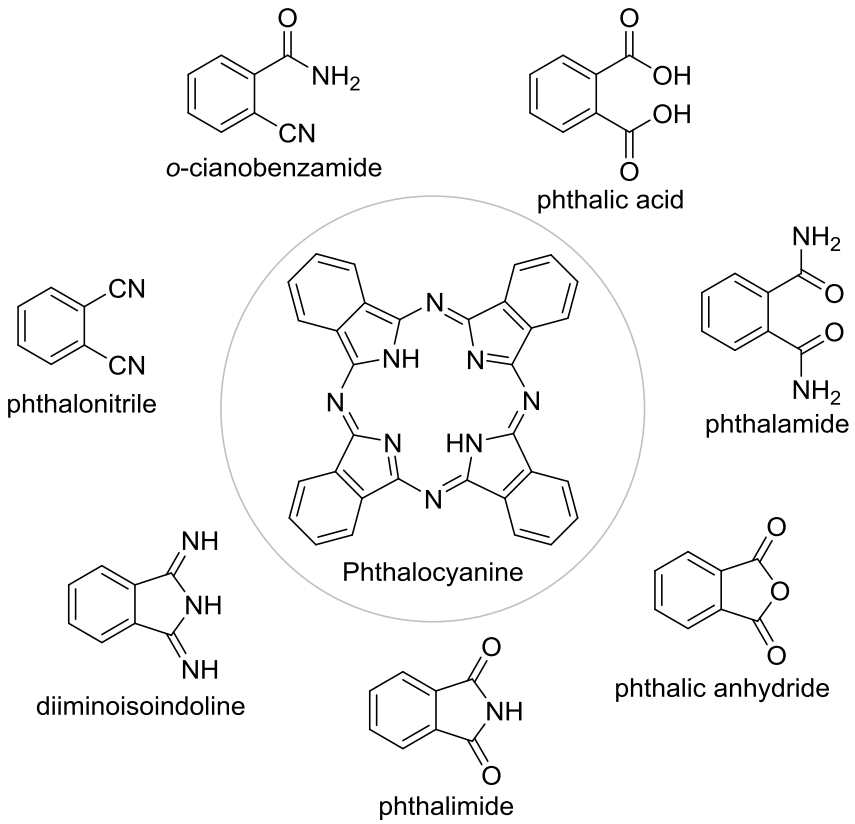

Figure 1.7 Synthetic routes for the synthesis of free-base **H_2Pc**.

However, reactions with other precursors, like phthalimide, phthalic acid and phthalic anhydride require urea as nitrogen donor. In order to prepare free-base Pcs, it is common the use of lithium or magnesium, as template, followed by demetallation of the obtained Pc complexes in dilute acidic conditions.

The access to MPcs can involve two different approaches: in one of them the metal is inserted directly in the macrocycle during the tetramerization process using a phthalonitrile and an adequate metal salt;[57] and other strategy is by metallation of **H_2Pc** previously prepared (Scheme 1.1).[58]

The synthesis of free-base and metal complex phthalocyanines containing the same type of substituents in all four isoindole rings (A_4) can be performed by cyclotetramerization of the same suitable substituted precursor (Scheme 1.2).[59] Depending on the precursor, nature of the substituents and metal to be inserted into the macrocycle, have been used a wide range of reaction conditions: reaction time, temperature, solvent, type of atmosphere, base and catalyst selected.[60]

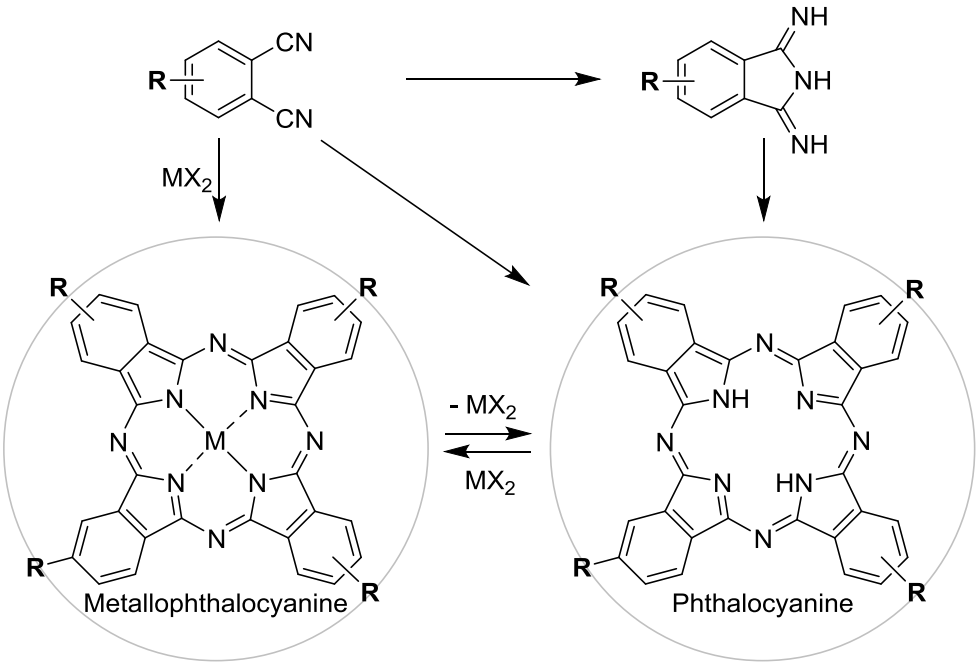

Scheme 1.1

To prepare metal complexes of phthalocyanines it is necessary to heat a mixture of a phthalonitrile derivative and a metallic salt choosing a solvent with a high boiling point, such as DMAE, *N,N'*-dimethylformamide (DMF) or 1-chloronaphthalene.[28] On the other

hand, there are procedures that can be carried out at lower temperatures, by using for example a basic catalyst such as DBU in pentan-1-ol,[54] or even at room temperature by using lithium in DMAE.[61] This methodology allows the synthesis of MPcs with different metallic salts in specific heating conditions (Schemes 1.1 and 1.2).

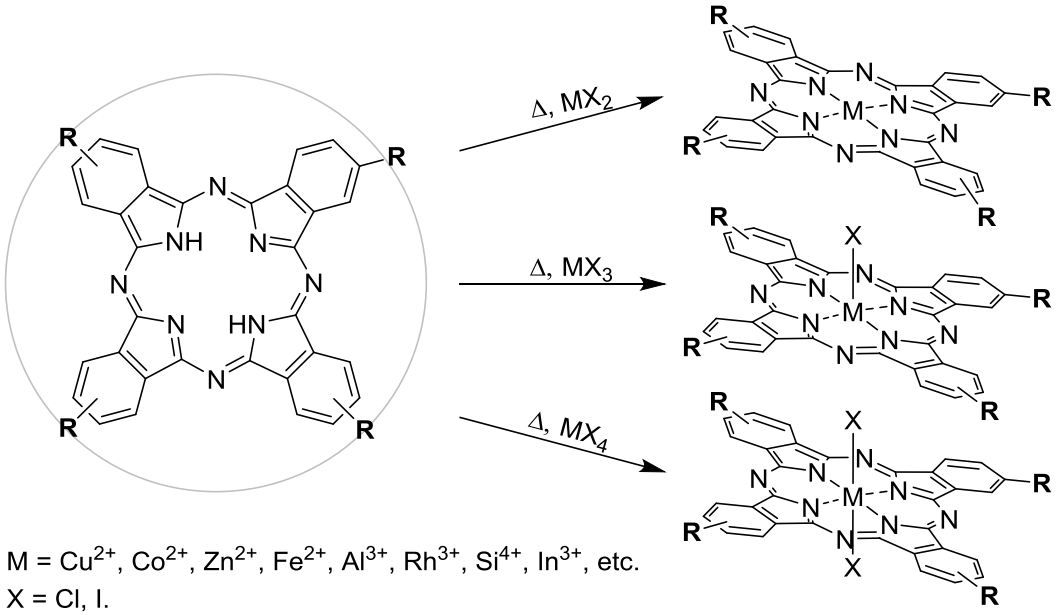

Scheme 1.2

Taking advantage of established knowledge about synthesis or chemical modifications of Pcs[35] and also about the linkage of some species,[62,63] different synthetic approaches were considered to obtain several conjugates.[35] In most of those approaches, the different suitable groups are incorporated previously in the precursors during the first synthetic procedure to allow and simplify the achievement of the desired phthalocyanines. In this sense, when chosen a symmetrically disubstituted precursor, the final product is a symmetric phthalocyanine derivative with all α- or β-positions completely substituted (Figure 1.8).[35] On the other hand, the use of monosubstituted precursor in the position 3 or 4 (IUPAC numeration, Figure 1.3) is generated a mixture of four isomers (Figure 1.9) which are particularly difficult to separate by chromatography techniques. Nevertheless, mono-, di, tri- and tetra-substituted phthalocyanines have interesting applications[35] and in these cases several chromatography techniques have been developed to purify all the structural isomers.[64,65]

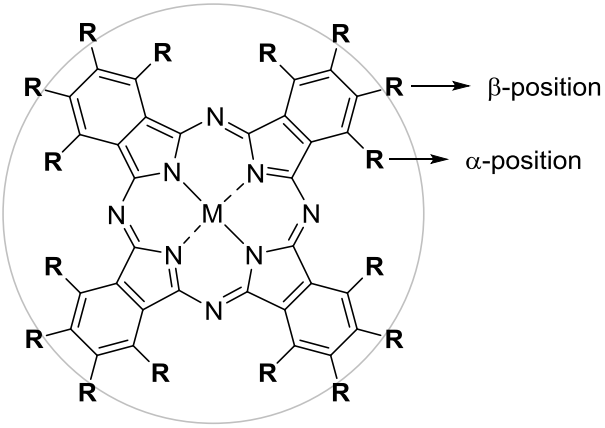

Figure 1.8 Structural of symmetric phthalocyanines.

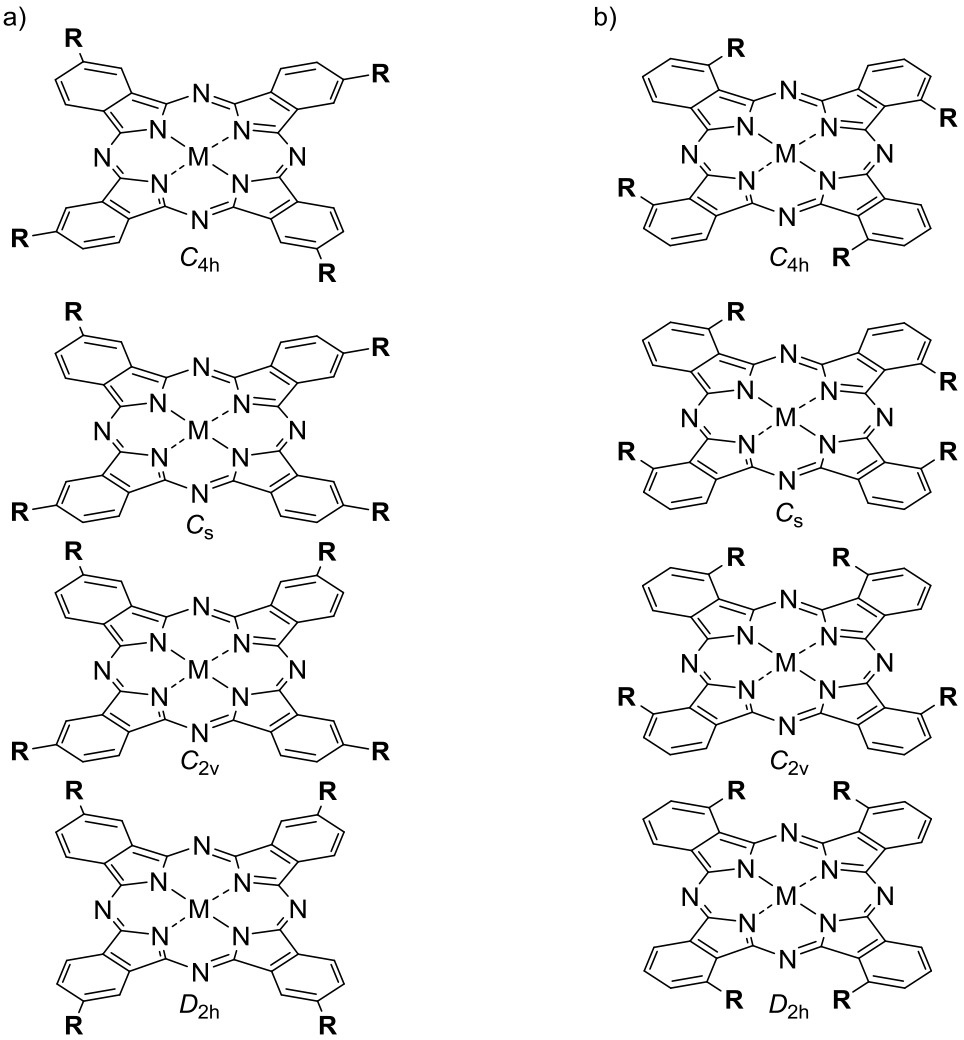

Figure 1.9 Four structural a) β-isomers and b) α-isomers of phthalocyanines performed from a monosubstituted precursors.

The details of the phthalocyanine mechanism and the exact and unambiguous course remain still unclear. A purposed mechanism of the synthesis of MPcs is exemplified in Figure 1.10 where it is possible to observe stepwise the formation of potentials intermediaries.[28]

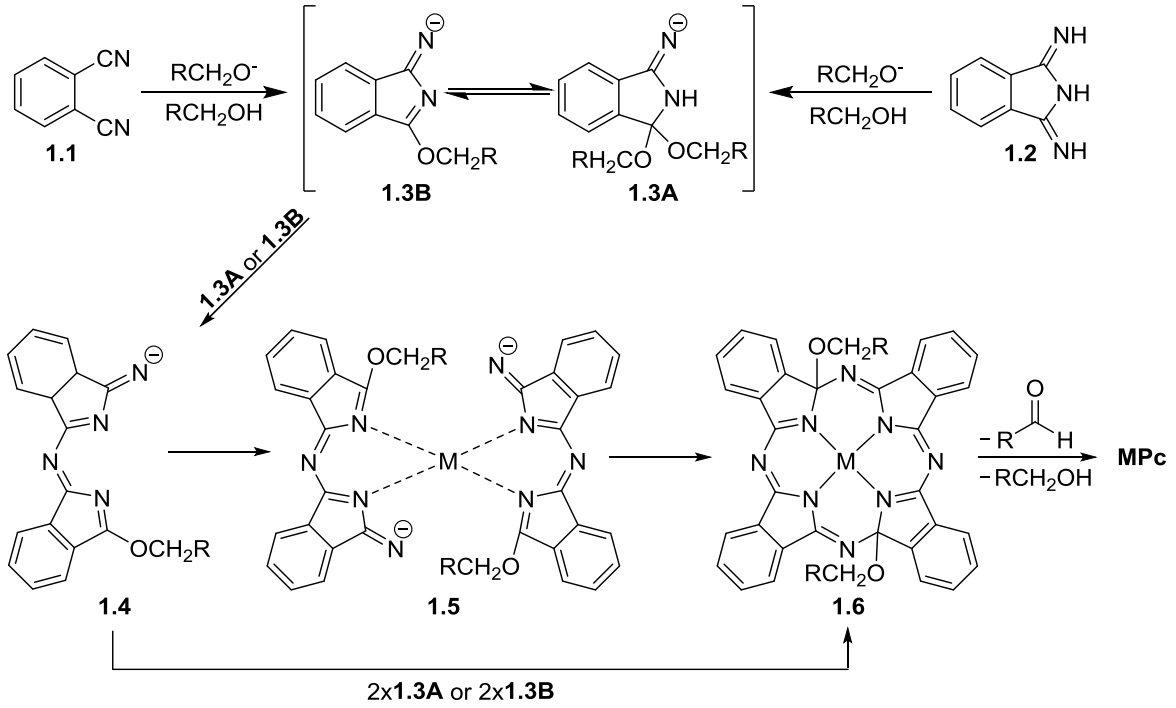

Figure 1.10 Possible mechanism of the MPc formation with the corresponding intermediaries.

The tetramerization of phthalonitriles in the presence of alkali metals, such as Li or Na, using an alcohol as solvent with a high boiling point, resulted initially in the specie RCH_2O^- and in the separation of the anionic forms **1.3A** and **1.3B**. It is noteworthy that the obtained structure **1.3A** can be formed and preferential favoured in the presence of alcohols with a short chain, such as methanol or ethanol, while other alcohols with a larger chain favoured the formation of **1.3B**. It is possible that both forms are in the reaction as intermediates leading the formation of the phthalocyanine in pentan-1-ol at high temperature.[28] Curiously, the intermediate of type **1.4** is formed in good yield when the reaction is carried out between the 4-nitrophtalonitrile and lithium methoxide around 120 °C.[55] In case of the intermediate **1.5**, composed by coordination of two moieties **1.4** with a metal ion of Ni(II), was isolated after reaction in pentan-1-ol at reflux. Subsequently, heating the obtained complex **1.5** in the same solvent assisted the formation of metallated

phthalocyanine with Ni(II) that leads concomitantly pentanol and pentanal liberation.[66] The cyclization of the ring and the corresponding intermediary eventually depends of the intermediary **1.6** where the ring closure is driven by the thermodynamic stabilization and the aromaticity involved. The formation of **1.6** can also occurs *via* sequential addition of two phthalonitrile molecules or diiminoisoindoline to the intermediate **1.4**.[28]

The synthetic procedures from diiminoisoindoline with addition of an organic base, such as DBU, DBN or NH_3, provide a tetramerization mechanism similar to the previously one described, however the alkoxide RCH_2O^- is formed by the action of the organic base.[28]

The synthesis of phthalocyanines involves nucleophilic aromatic substitution reactions and obviously electrophilic aromatic substitutions. However, when preceded to the halogenation, sulphonation or nitration of the phthalocyanine macrocycle results inevitably a mixture of compounds with different substitution degrees.[34] These compounds are particularly difficult to dissolve and subsequently their functionalization wins a high interest. In this sense, the use of substituted precursors[67] enables the achievement of substituted phthalocyanines with appropriate groups.[28,32]

1.4 Phthalocyanine applications

Phthalocyanines[34] have also been intensively studied due to their unequivocal applications in several scientific areas, namely as: i) biomimetic models of photosynthetic primary processes;[34] ii) catalysts[68,69] or photocatalysts[68,70] and iii) photosensitizers (PSs) or markers in photomedicine.[71] More recently they have also been combined with nanomaterials to exploit the nanohybrid material features in nanosciences and different nanotechnological applications.

1.4.1 Phthalocyanines as electroactive molecules for supramolecular interaction with carbon nanostructures

The preparation of supramolecular carbon nanostructures (graphene, single-walled carbon nanotubes and fullerenes) with organic compounds present a certain degree of order (where it is possible to observe nanoscopic to macroscopic multiple scales), highly

desirable with the fast-growing of nanoscience and nanotechnology fields.[72-74] In this perspective, the use of self-assemblies is an attractive strategy for the functionalization of organized structures to perform multifunctional systems by efficient noncovalent interactions. Among the organic compounds, the π-conjugated phthalocyanine molecules are interesting candidates for the construction of such supramolecular arrays due to their self-assemble capabilities.[75]

The interesting organization capability of Pc derivatives and their exceptional physicochemical features have prompted their utilization as photoactive components in different technological fields, such as nanosensors, molecular photovoltaics, liquid crystals and nanotransistors, where the supramolecular organization is considered fundamental for an efficient application.[58]

Among the most important photoactive phthalocyanine features, it is noteworthy their redox reactions and their strong extinction coefficients of absorption in the red/near-infrared (NIR) region of the solar spectrum and also high fluorescence quantum yields, which render them attractive candidates for light-harvesting antenna structures. Thus, these unequivocal photophysical properties have promoted their utilization as multifunctional nanomaterials in donor-acceptor arrays.[74] In this sense, Pcs have been employed for the preparation of covalent and noncovalent donor-acceptor systems based on Pcs with graphene, carbon nanotubes (CNTs) or fullerenes (C_{60}). In this approach, the relevant synthetic strategies for the preparation of supramolecular heterochromophoric systems, based on phthalocyanine derivatives, leads to a large variety of carbon nanostructures assemblies. In these systems, the degree of electronic interaction between the components is highly dependent on their electronic characteristics, interaction type, and molecular topology of the ensemble.

Photoinduced electron process

The process of photoinduced electron transfer (PET) is a key role in supramolecular chemistry and/or biology areas.[76] It is noteworthy that in chemistry during the last century have been developed supramolecular-based artificial solar energy harvesting systems with ability to absorb light from the sun for convert it to useful and storable forms. In this sense, one procedure to store solar energy is in chemical energy form, evidenced efficiently for example during photosynthesis of the plants.[77]

For an efficient artificial solar energy converting systems, some requirements are needed: i) the light irradiation must be absorbed by antenna molecules as sensitizers, leading to excited states; ii) the light absorption must allow the transference of an electron to the acceptor unit; iii) the electron transference must be steered; and iv) the lifetimes of the excited states must be high for electron transfer. Indeed, the intermolecular PET is just an easy process where an electron is transferred from an electron-donor specie (D) to an electron-acceptor specie (A), producing the radical cation of the donor ($D^{\bullet+}$) and the radical anion of the acceptor ($A^{\bullet-}$), when one of these species is photoexcited upon irradiation.[78,79] If these charged species are used as electrons and holes to line up electrical energy or provide chemical reactions before back electron transference driving to the initial states of the reactants arises (Figure 1.11), which the light energy is converted into electrical or chemical energy. A critical factor in PET is evidenced in the successful matching of D and A with suitable electrochemical and photophysical characteristics for the existence of an exothermic ET.[77,78] It is important to know that the excited state energies of the chromophores and the redox potentials of D and A species are unequivocally an essential condition to study PET processes. The main interest on the phthalocyanines photochemistry is the challenge to mimic the photosynthetic processes, where phthalocyanine derivatives have been extensively used as sensitizers and as electron donor system.[80,81]

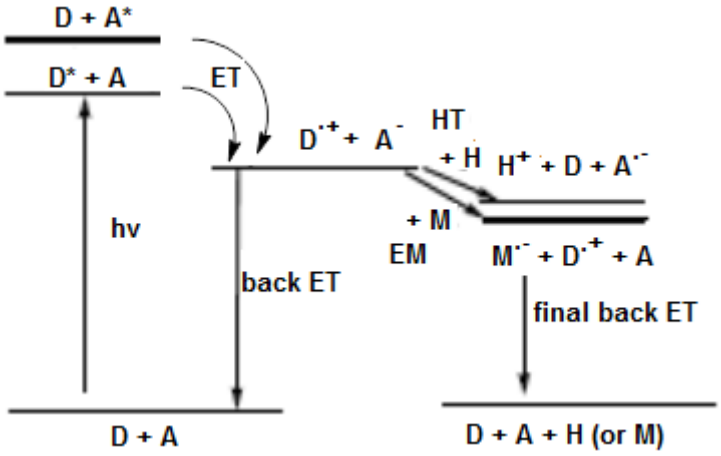

Figure 1.11 Energy diagram of the PET processes in donor-acceptor systems: HT refers to hole transfer step in the presence of hole acceptor (H) and EM refers to an electron mediation step in the presence of an electron mediator (M).

Interesting is that each intramolecular decay step of an excited molecule is characterized by their own rate constant and each excited state is evidenced by their lifetime. In solution, when the intramolecular deactivation processes are not fast, mainly when the lifetime of the excited state is appropriately long, an excited molecule *A may have a chance to find a molecule of another solute, B. In this case, specific interactions can lead to the deactivation of the excited state by second order kinetic processes. The two most important types of interactions in an encounter are those leading to electron or energy transfer observed below:

$^*A + B \rightarrow A^+ + B^-$ oxidative electron transfer (eq. 2.1)

$^*A + B \rightarrow A^- + B^+$ reductive electron transfer (eq. 2.2)

$^*A + B \rightarrow A + {}^\bullet B$ energy transfer (eq. 2.3)

It will be emphasized the electronic interactions between carbon nanostructures and phthalocyanine derivatives, as well in multichromophoric supramolecular arrays.

A short view of graphene, carbon nanotubes and fullerenes chemistry

In the last years, the nanoscience field has had over the years a considerable growth in all areas of research and technologies. A prove of this importance can be obtained from Figure 1.12, which show fantastic economic scenarios for nanotechnology. Although the forecasts differ significantly from each other they both predict a substantial increase of nanotechnological products starting in the early 2010s.[82,83]

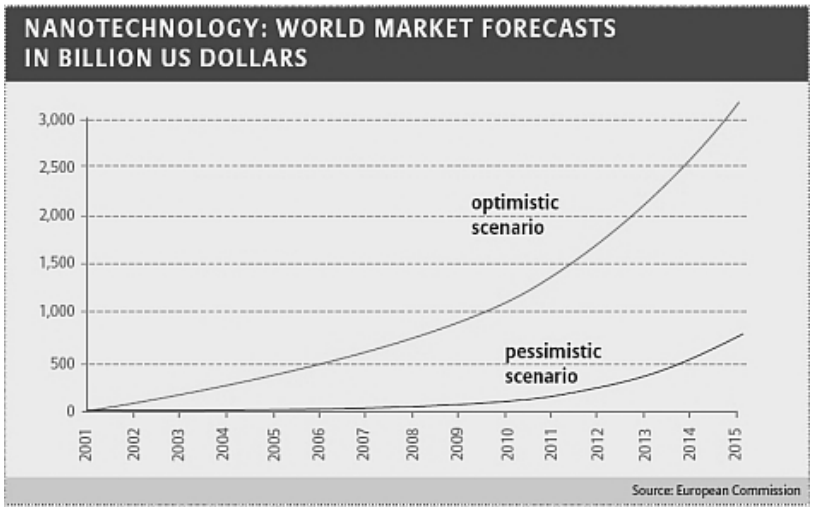

Figure 1.12 World market forecasts for nanotechnology in billion US Dollar.[84]

The nanotechnology is the conception and exploitation of materials, devices, and systems through the control of matter on the nanometer-length scale, *i.e.*, at the level of atoms, molecules, and supramolecular structures. This term is applied to describe the creation and employment of functional structures with at least one typical dimension measured in nanometers (a nanometer is one billionth of the meter – 10^{-9} m).[85]

Carbon nanostructures can be associated with many structures/molecules, such as Pors and Pcs by covalent or supramolecular interactions. These porphyrinoids are multiconjugated chromophores able to absorb UV-Vis light and can be excellent electronic donor-acceptors. With these systems it can be possible to combine the unique optical properties of both components; dyes (Por and Pc) and carbon nanostructures, and prepare hybrids with interesting properties.[74,86] The unidirectional and exponential growth of materials to create nanostructures has attracted a colossal interest in the middle of 20th century, with the discovery and proposed term of graphene as a combination of *graphite* and the suffix *-ene* by Hanns-Peter Boehm.[87] He described the carbon nanosheets in 1962,[88,89] but the structure was just isolated in 2004 by Novoselov.[90,91] Since the pioneering work by Novoselov *et al*. graphene is one of the first two-dimensional (2D) atomic material, which is readily available. This nanostructure revealed interesting electrical, mechanical, and thermal features, namely high carrier mobility, ambipolar electrical field effect, tunable band gap, room temperature quantum hall effect, high elasticity, superior thermal conductivity, etc.[92] Taking the aforementioned into concert, graphene bears great promises to replace existing materials in emerging applications.[93] In Figure 1.13 are represented four kinds of π-conjugated systems of different dimensions, namely polyacetylene (Figure 1.13a); a 1D system which can be rolled up to form a series of annulenes (Figure 1.13b), each being a quasi-0D system; graphene a 2D system, which can be rolled up to perform a series of SWNTs (Figure 1.13c), each being a quasi-1D system.

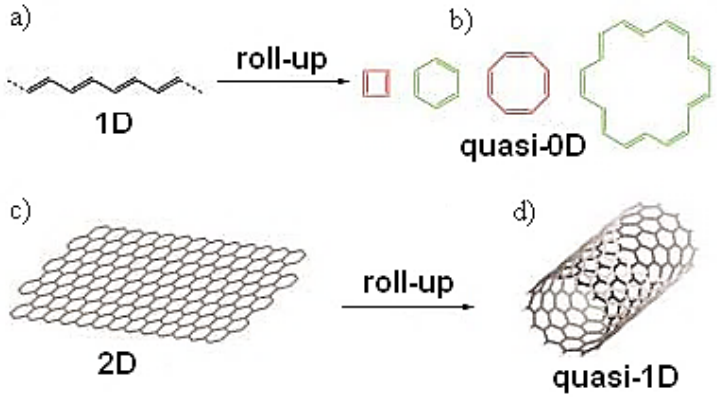

Figure 1.13 Four π-conjugated systems of different dimensionalities: a) polyacetylene; b) annulenes (cyclobutadiene, benzene, cyclooctatetraene, annulene, etc.); c) graphene; d) SWNT. Classical aromatic and antiaromatic structures are painted green and red, respectively.[109]

After the discovery of the firsts nanomaterials, fullerenes surged in 1985[94] followed of the CNTs that were immediately discovered in 1991,[95] and since then the research in this exciting field has been in continuous evolution.[96,97] CNT consist on graphene nanosheets, which have been rolled up into a tubular and cylindrical shape generating single-walled carbon nanotube (SWNT) and multi-walled carbon nanotube (MWNT), all represented in Figures 1.14 and 1.15.

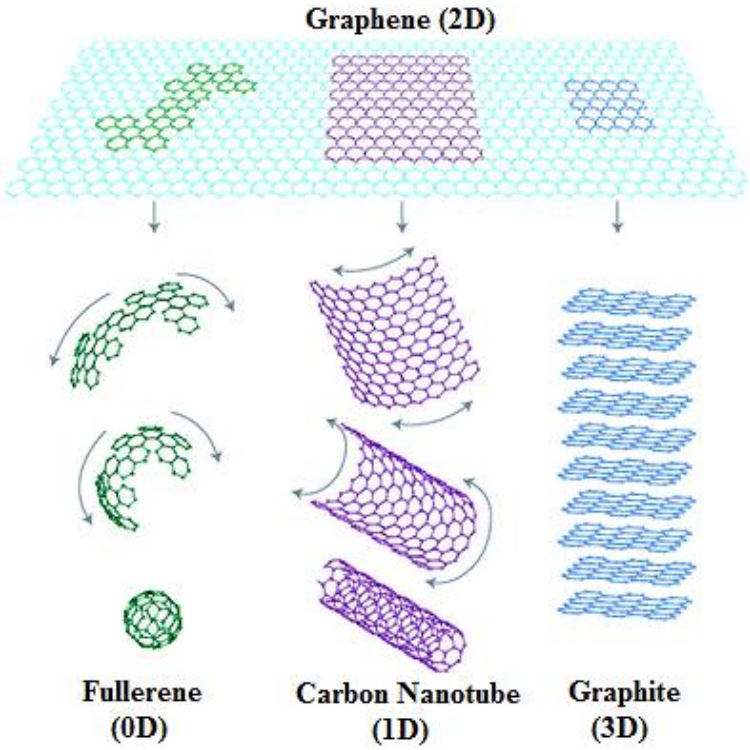

Figure 1.14 Graphene as the rudimentary unit of fullerene (0D), carbon nanotubes (1D) and graphite (3D).[92]

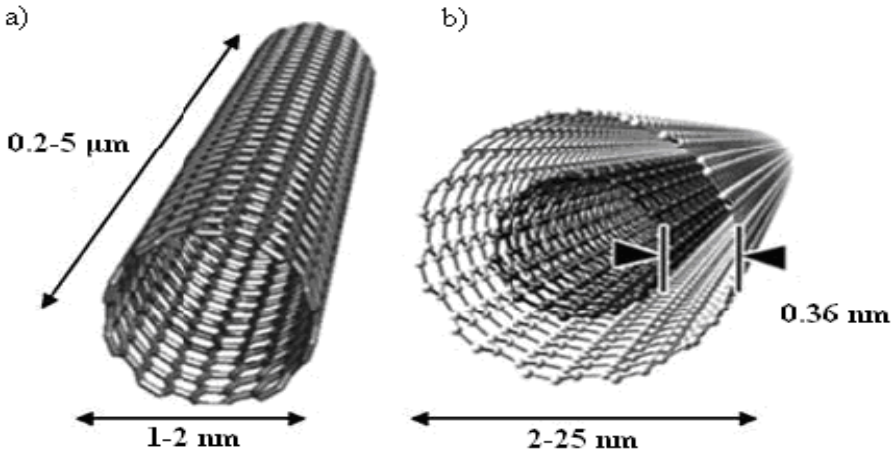

Figure 1.15 – Conceptual diagram of a) SWNT and b) MWNT showing typical dimensions of length, width and separation distance between graphene rolled layers in MWNTs.

It is noteworthy that the length of CNT is in the size of micrometres with diameters up to 100 nm. CNT form bundles, which are entangled together in the solid state giving rise to a highly complex network. Thus, CNTs can be metallic or semiconducting depending on the arrangement of the hexagon rings along the tubular surface. A major critical issue toward their widespread application in nanotechnology is the control of their electronic properties, in their pristine form, which depends on their diameter and chirality.[98,99]

The concepts of aromaticity, highest occupied molecular orbital (HOMO), and lowest unoccupied molecular orbital (LUMO) are of fundamental significance in understanding the chemical stability and reactivity of CNTs conductivity, namely of their metallic or semiconducting properties. Both metallic and semiconducting carbon nanotubes have positive resonance energies, although "metallic" nanotubes are slightly less aromatic than the semiconducting ones.[100-102] This aromaticity confers to both types of nanotubes a relative similar thermodynamic stability. On the other hand, the kinetic stability of polycyclic aromatic complexes is usually more associated to their HOMO-LUMO energy gap than to their resonance energy.[103,104] Indeed, the effect of the geometric structure of CNTs on their electronic arrangement and chemical reactivity can be intuitively appreciated by an illustrative analogy between the imaginary process of rolling up a polyacetylene to form annulenes and the roll-up of graphene to form SWNTs.[105,106] Thus, semiconducting nanotubes are equivalent to [4*n*+2]annulenes, which are usually considered aromatic by the Hückel rule, whereas metallic nanotubes are corresponding to

[4*n*]annulenes, which are often considered nonaromatic by the Hückel rule, even though only small ones, such as cyclobutadiene, have negative resonance energies.[107-109]

Nevertheless, the lack solubility and the complicated handling in any solvents have imposed enormous limitations to the use of carbon nanostructures, mainly graphene and carbon nanotubes. In fact, when graphene and carbon nanotubes are prepared they are insoluble in all organic solvents and aqueous solutions. They can be dispersed in several solvents by ultrasonication, but a precipitation occurs immediately when it is interrupted the sonication process. On the other hand, it has been demonstrated that these structures can interact with diverse classes of compounds.[110-116] The structure of supramolecular complexes allows a better processing of carbon nanostructures toward the fabrication of unique and specific nanodevices. More, they can suffer chemical reactions that can provide solubility, making easier their integration into inorganic, organic, and biological systems.[74,116,117]

The key approaches to change the physicochemical properties of these carbon allotropes can involve the following two approaches: i) covalent derivatization with functional groups directly on their skeleton; or ii) noncovalent interactions, through adsorption or wrapping with functional molecules. However, in case of CNTs is possible to occur an endohedral filling of their internal empty cavity.

1.4.2 Covalent and noncovalent functionalization of carbon nanostructures

The covalent functionalization is based on covalent linkage of functional entities onto the carbon nanostructures scaffold. This functionalization can occur on their sidewalls of the graphene,[118] CNTs[119] and fullerenes,[120] but also in the termini of the graphene nanosheets or nanotubes. Direct covalent sidewall functionalization is related with a change of hybridization from sp^2 to sp^3 and a simultaneous loss of electronic conjugation. It is noted that defect functionalization takes disadvantage of chemical modifications of defect sites because it can open ends and holes in the sidewalls, terminated, for example, by carboxylic groups, and irregularities in the hexagon graphene framework. Also oxygenated sites, formed through oxidative purification, can be considered as defects (Figure 1.16).[118-124] On the other hand, the noncovalent functionalization of the carbon

allotropes is principally based on supramolecular assemblies using various adsorption forces, such as Van der Waals and π-stacking interactions.[118,123,126-129]

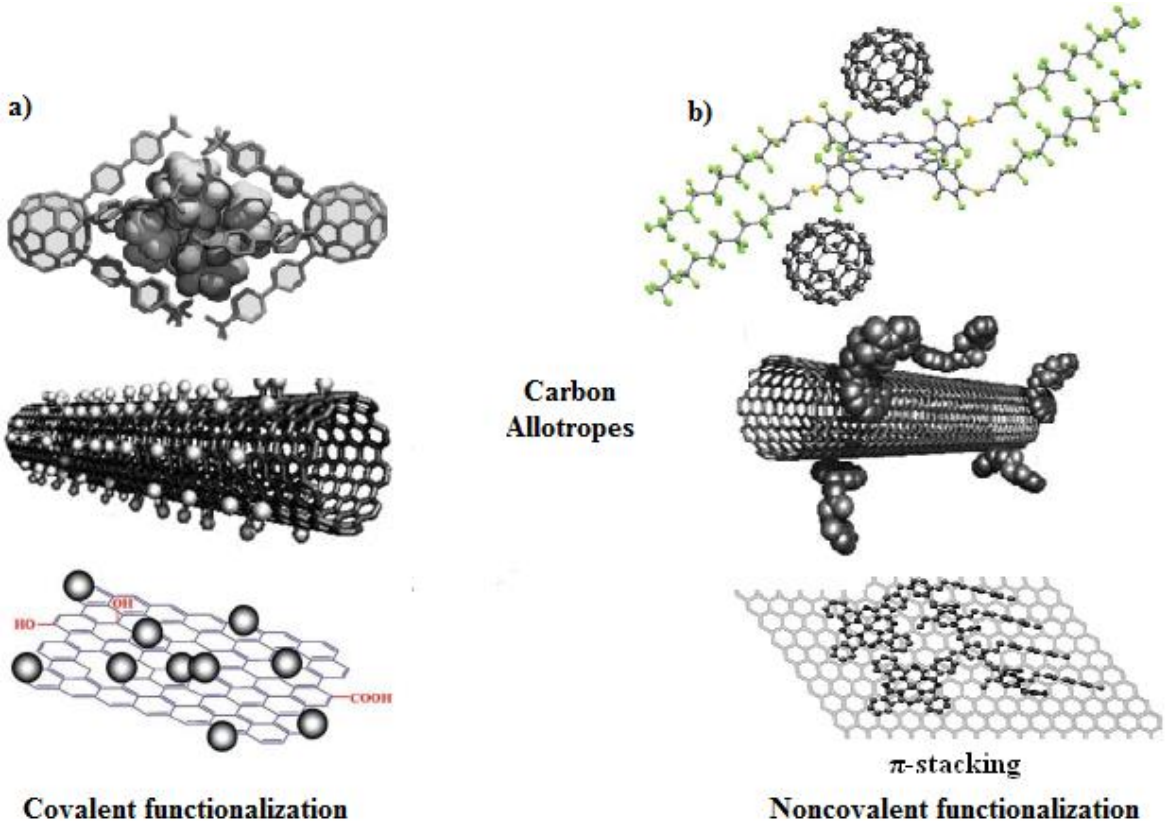

Figure 1.16 Functionalization of carbon allotropes: a) Covalent functionalization of fullerenes,[130] CNTs[131] and graphene[118]; and b) Noncovalent functionalization of fullerenes,[132] CNTs[131] and graphene.[133]

Covalent and noncovalent functionalization of carbon nanostructures conjugates

In the case of covalent functionalization sidewalls are directly functionalized by oxidation or reduction, and subsequently derivatised with a variety of different molecules, and by several addition reactions.[134,135,137] The outside skeletal functionalization is possible using various methodologies, namely: fluorination, ozonolysis, hydrogenation, halogenation, cycloadditions, radical additions, electrophilic additions, osmylation, and nucleophilic additions.[136-138]

The structures of graphene and carbon nanotubes can react with different reagents, which proportionate the addition of some groups/molecules to the structure side-wall.[118,139] Studies of the chemical reactivity of these derivatives had attributed a main role to induced local strain, which arises from disruption of the sp^2-hybridized (trivalent) carbon atoms and

π-orbitals misalignment between adjacent carbon atoms.[100,118,139,140] This methodology represents a chemical view of the electronic structure of carbon nanostructures, which fits into the molecular orbitals description of organic reaction mechanisms.[140] This surface modification of the scaffold is important because allows the incorporation of external molecules allowing a significantly hydrosolubility when attached to biopolymers, for example.[118,119,139-141]

Moreover, it is necessary to take into account the type of interaction with the carbon allotropes, because the global properties of these compounds are modified according the covalent or noncovalent attachment.[118,130-132] Indeed, the photophysical properties are different with the incorporation of some molecules such as phthalocyanines.[142] Thus, the advance of novel porphyrinoid-based systems capable to absorb a higher scale of the solar emissions evidences an unquestionable importance, mainly the functions ranging from light harvesting through most of the visible part of the solar spectrum to electron transport.[142] The redox properties of phthalocyanine derivatives can be analysed by electrochemistry or spectroelectrochemistry because the electro donor-acceptor features are an interesting point for interaction with carbon allotropes. The remarkable characteristics of phthalocyanines, as well as porphyrins, can form building blocks with carbon allotropes as light-harvesting systems. These planar chromophores share important electronic features, mainly the redox conditions and simultaneously photoinduced energy and/or electron transfer, which these features can be modified with incorporation of different peripheral substituents and metal centres.[92,142]

An alternative way to render carbon nanostructures soluble in a wide range of solvents is based on their noncovalent hydrophobic and π-π stacking interactions with interesting phthalocyanine derivatives attending their electronic features. The main goal of these carbon allotropes is their functionalization *via* noncovalent interactions, where the aromatic structure and their electronic characteristics are preserved.[133,143,144]

In this sense, the exfoliation and supramolecular derivatization of graphite was achieved, for example, using a zinc phthalocyanine oligomer that is also an electron donor (Figure 1.17) as described by Guldi and co-workers.[133] The Pc derivatives interact tightly and reversibly with graphene, performing stable dispersions with high concentrations of mono- to few-layer graphene.

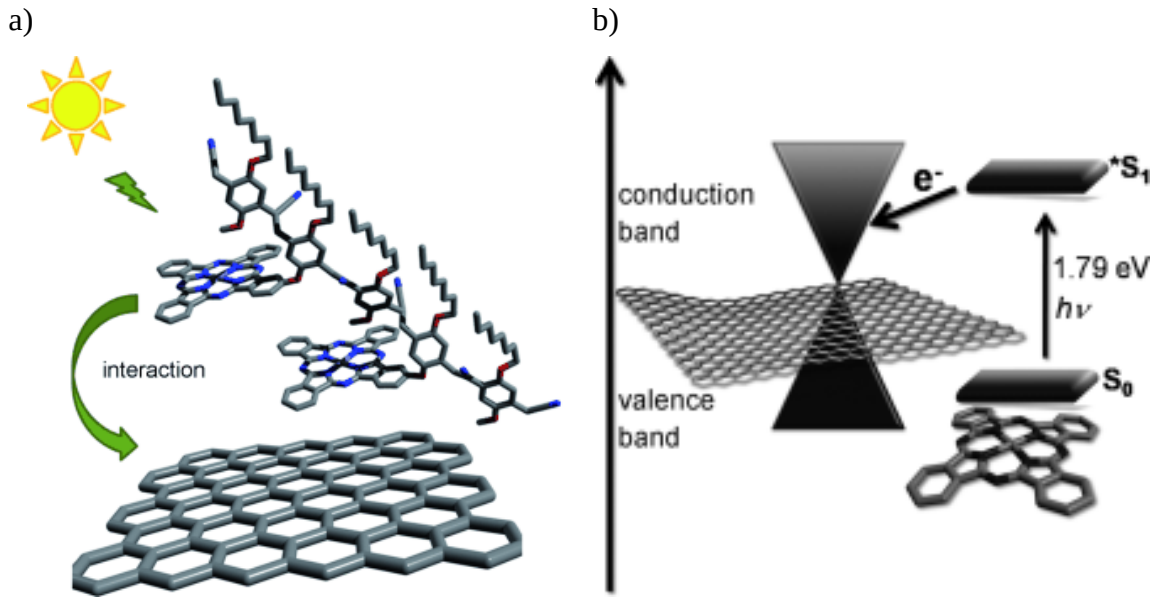

Figure 1.17 a) Supramolecular exfoliated NG/Pc assembly; b) Electron-transfer pathway in the exfoliated NG/Pc hybrid.[133]

In fact, it was observed interesting exfoliated NG/Pc hybrids with strong electronic coupling between the single components (Figure 1.17a) that allows characteristic absorptions and a close quantitative fluorescence quenching. Moreover, the transient absorption measurements determined interactions with electron transfer from the Pc derivative to the graphene nanosheets (Figure 1.17b), both in the ground and excited state. This methodology was used to prepare individual graphene nanolayers by wrapping on their surface several organic Pc molecules and these hybrid materials are constructed as active layer and transparent electrode materials for solar-cell systems.

For example, another supramolecular approach based on π-π stacking interactions between pyrene derivatives and SWNTs has also an advantage of being non-destructive sp^2 structures with respect to the nanotubes, and consequently is useful for applications where the conducting properties of the CNTs are nowadays exploited (Figure 1.18).[145]

The noncovalent modification of the CNT surface has emerged as a potent and viable strategy safeguarding unequivocally the unique electronic, physicochemical and mechanical properties of CNTs.[146] In this context, pyrene derivatives have played a leading role to immobilize Por **1.7**,[147-150] chlorins **1.8**[151] or fullerenes **1.9**[152] onto CNTs (Figure 1.18).

Interactions between different dyes with planar structures have been showing interesting adsorption properties and play a significant role also in supramolecular

chemistry.[153] It has been well documented that different conjugated aromatic units have preferences to associate on the SWNT surface by host-guest interactions promoting aromatic association.[154-157] These macrocyclic dyes can be planar or non-planar with a flexible or rigid framework[158] enhances a specific face-to-face orientation around the SWNT scaffold.[159] Depending of these molecules type it's possible to obtain electronic transitions between the aromatic macrocycle and SWNT, establishing potential electronic donor-acceptor properties.[152] The association of SWNT with electron-donors or acceptors produces active materials, which are able to generate electrical energy when irradiated.[160] Indeed, the development of trustworthy and reproducible procedures to incorporate CNT into functional assemblies, like donor/acceptor hybrids to convert sunlight into electrical or chemical energy, has emerged as an interesting research area. In this way, phthalocyanines and SWNT are promising building blocks in donor-acceptor devices for solar energy conversion, which is nowadays an important research topic to produce innovative materials, composites, and electronic devices of greatly reduced size.

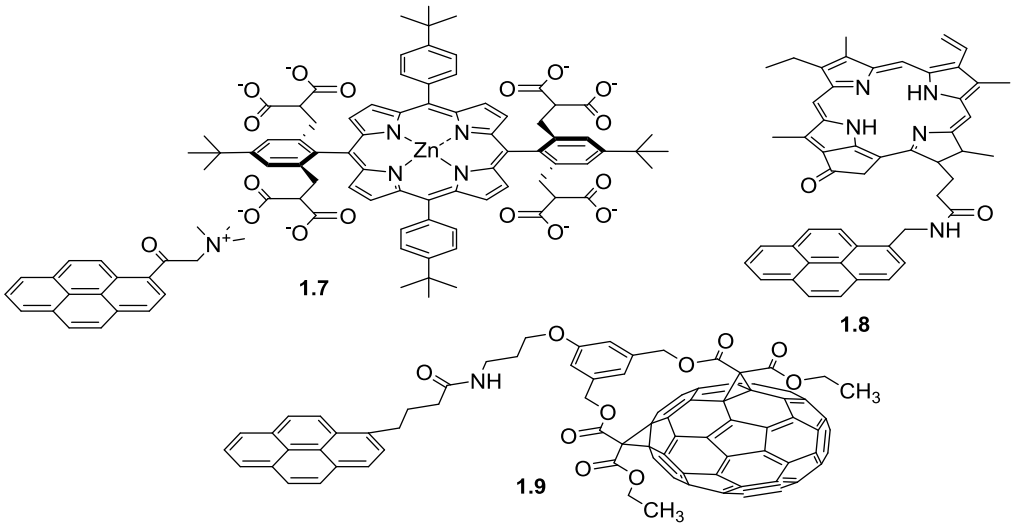

Figure 1.18 Pyrene derivatives as electroactive units for immobilization onto the CNT surface.

Guldi and co-workers developed an strategy to immobilize functional Pcs onto the SWNT surface without covalent functionalization, using substituted poly(*p*-phenylene vinylene)-oligomers (or PPV-oligomers) with a different electronic character.[161] The complementary use of a series of microscopy and spectroscopy techniques is fundamental, particularly to gather a comprehensive representation of the supramolecular interactions. After photoexcitation of an SWNT/Pc **1.10** hybrid, it was evidenced a metastable radical

ion pair state, namely oxidized Pc and reduced SWNT (Figure 1.19). In this sense, rather significant is the ratio of charge separation to charge recombination, specifically near of 3 orders of magnitude, which is promising to construct photovoltaic cells established, for example, on different carbon nanostructures.[161]

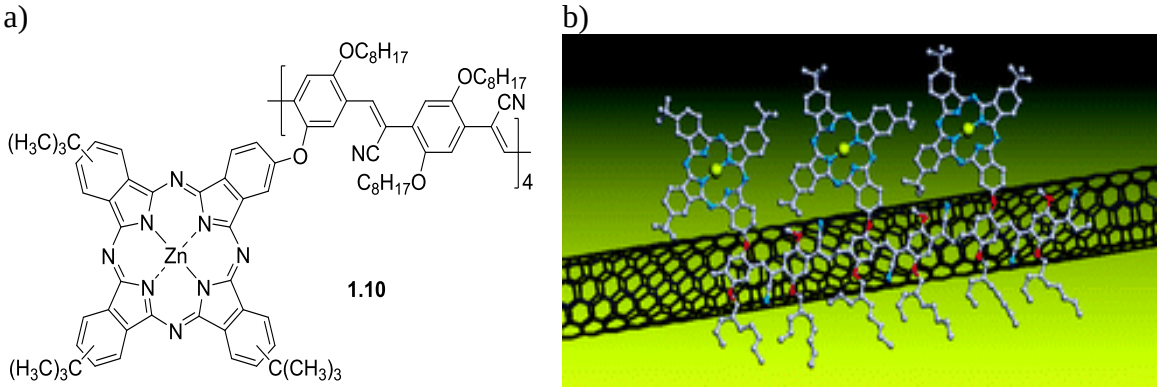

Figure 1.19 a) Pc-oligomer **1.10** derivative; b) Tuning and optimizing the intrinsic interactions between phthalocyanine-based oligomers **1.10** and SWNTs toward *n*-type/π-type systems.

Likewise, Nyokong have been developed interesting pyridyl Pcs **1.11** due to their assembly properties with SWNTs.[162,163] The authors functionalized covalently SWNTs with amine groups using a previously developed diazonium approach, to improve the dispersion in organic solvents. The amine functionalized SWNTs showed a significant increase in the intensity of the D-band upon amine functionalization, a feature indicative of disruption of the sp^2 carbon hexagonal lattice to sp^3 bonded carbons. The authors showed a sidewall functionalization as a result of the covalent attachment of the ethylamine groups, the increased D-band intensity is more accurately expressed with respect to the G-band in the form of a D:G ratio (sp^3:sp^2 carbon ratio).[162] After that, was shown a SWNT/Pc **1.11** supramolecular complex obtained *via* supramolecular π–π stacking interactions between the Pc planar units and the unpristine carbon nanotube surface (Figure 1.20).

The presence of a covalent bond in the linked form limits the extent of decomposition attainable, for the same functional groups. Indeed, rapid deactivation of fluorescence was found upon introduction of SWNTs as revealed by the fluorescence spectra and showed also low fluorescence quantum yields.[162] Additionally, it was expected that the pyridine groups could coordinate with the central metal of the macrocycle core of the neighbouring molecules, and in that way forming a random 3D network able to

encapsulate the SWNTs. This strategy could bring closer the Pc macrocycles around the SWNTs providing a compact assembly also *via* coordination chemistry.

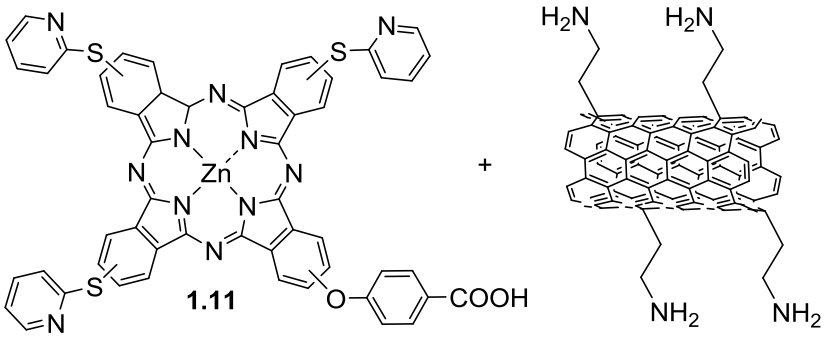

Figure 1.20 Pc **1.11**/SWNT supramolecular complex.

The importance of the presence of pyridyl units in dye derivatives it is a methodology to prepare compact supramolecular array as reported by Cook and co-workers.[164,165] Pyridyl groups placed at the bay region of a porphyrin coordinate with ruthenium phthalocyanine (**RuPc**) units to perform structural hybrids to promote electronic coupling systems. The starting topic of synthetic photosynthesis is an arrangement of light-induced energy- and electron-transfer reactions. In this way, centres mimicking the light-harvesting and reaction processes should comprise light-absorbing chromophores, acting as antenna molecules and excited-state electron donors, and additional electron acceptors.[166]

Torres and co-workers proved as a versatile approach for designing a novel electron donor/acceptor hybrid perylenediimide-$[RuPc]_4$ **1.12** *via* metal coordination, in which four pyridines placed at the bay region of a perylenediimide coordinate with four **RuPc** units (Figure 1.21). The structural system was projected to provide electronic coupling between the electron donors-acceptors, confirmed by physicochemical properties. Indeed, the absorption and electrochemical assays revealed a remarkable redistribution of electron density from the electron-donating **RuPc** to the electron-accepting perylenediimide. It is noteworthy, that the **RuPc** are oxidized and the perylenediimide reduced rendered more difficult in the supramolecular array than in the individual building blocks. Therefore, in the excited state, strong electronic communication is the inception for a rapid charge-transfer process in photoexcitation process.

a) b)

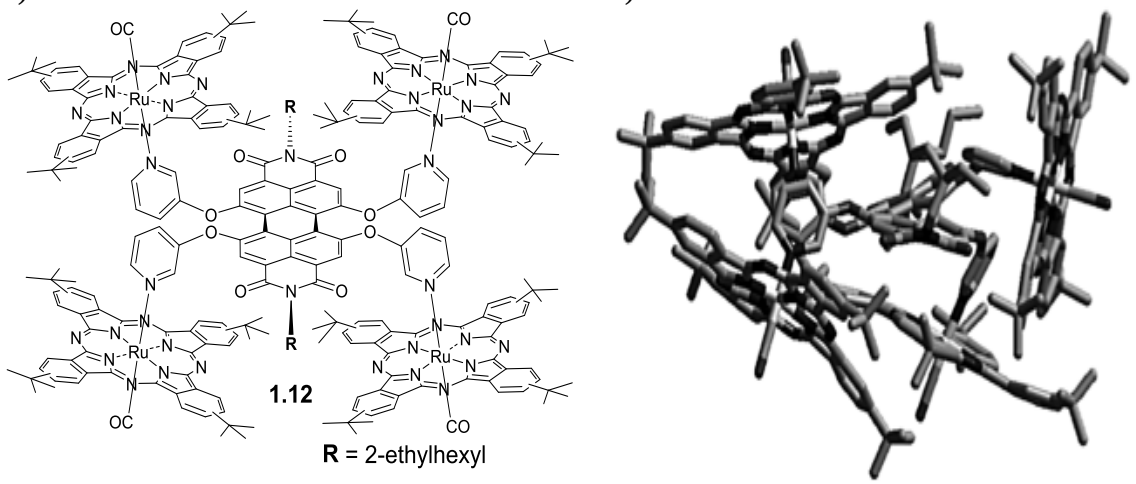

Figure 1.21 a) Structure of perylenediimide-$[RuPc]_4$ **1.12**; b) Energy-minimized of structure **1.12**.

1.4.3 Phthalocyanine derivatives as photodynamic therapy agents

In addition to the electronic applications previously described, phthalocyanines have also a prominent role in medicine, particularly in photodynamic therapy (PDT)[167,168] photodynamic inactivation (PDI)[169] and as markers.[170] Since Pcs are photoactive molecules that can absorb and emit light in a large range of the UV-Vis spectrum, these characteristics make them also useful probes for photodiagnostic applications and/or in the study of basic cellular processes.[171] For all this, in biomedical/environmental applications are necessary to guarantee a good solubility in biological media. This can be reached by combining different amphiphilic units, such as cationic pyridinium groups[172,173] or cyclodextrin (CD) units[174,175] to the macrocycle. In presence of molecular oxygen $^3O_2$ and upon photoexcitation with a specific light, this class of compounds can promote the production of reactive oxygen species (ROS), mainly singlet oxygen ($^1O_2$), which can induce cellular dead.[28] The combination of these characteristics makes them potential photosensitizer agents in PDT, PDI and/or fluorescent tags.

In general, the topical or systemic administration of a PS is initiated by its preferential accumulation in cells of rapidly division like neoplastic tissues. Then, the target tissue is irradiated with a suitable light that enables the excitation of the PS from its singlet ground state (S_0) to excited state of higher energy (S_1) – Figure 1.22. This excited state can then decay through a phenomenon of intersystem crossing (ISC) to a lower

energy state with a longer life time, the triplet excited state (T_1).[176,177] The PS, in this excited state, can instantaneously respond in two different ways:

- Type I mechanism which involve reactions of electron transfer from the photosensitizer in the triplet excited state to a substrate yielding radical ions. When the substrate is the molecular oxygen occurs formation of $O_2^{\cdot -}$ species, which easily converts in radical species, followed of easily conversion in reactive radical specie of $OH^{\cdot}$. These cytotoxic species can subsequently react with other organic substrates yielding a chain of oxidative processes.[178]

- Type II mechanism which involves energy transfer from the triplet state of the PS to the triplet ground state of the molecular oxygen ($^3O_2$) converting into singlet oxygen ($^1O_2$). This reactive cytotoxic specie is able to oxidize biomolecules such as proteins, lipids and nucleic acids.[179]

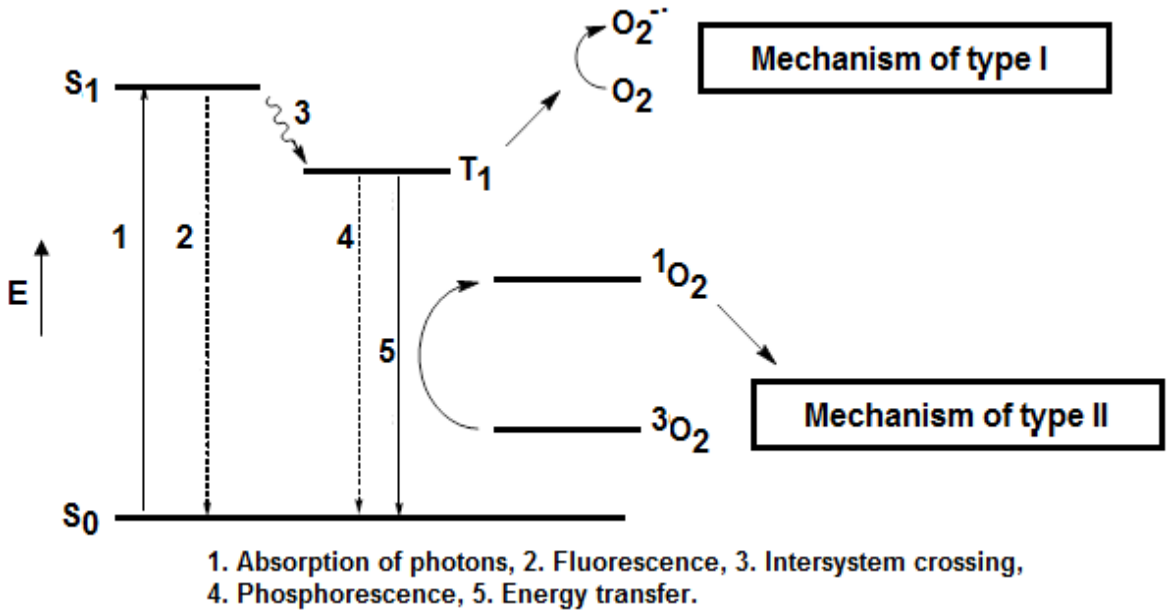

Figure 1.22 Jablonski modified diagram representing the excitation and relaxation of a PS, and type I and type II photoreactions. S_0 = ground singlet state; S_1 = first excited singlet state; T_1 = first excited triplet state.

Probably the two processes act in simultaneous. However, the mechanism of type II is predominantly and the singlet oxygen is considered the most important cytotoxic specie in the photodynamic process; however mechanism of type I can be more significant in environments with low oxygen level. In addition, the ROS in both mechanisms provide oxidative reactions that induce cell death and consequently tumour destruction.

The increase of pathogenic of resistance microorganisms in infection diseases[180-184] and/or in contaminated environments[185,186] have been exploited by many researchers to develop new methodologies to guarantee their well-successful inactivation.[187] The same can be said about the successful development of new methodologies for cancer treatment. In both applications, several molecules have been used as PSs,[188-192] for several infection, cancer and environmental problems.

The emergent antibiotic resistance of pathogenic bacteria has encouraged numerous research groups to investigate the principle of PDI as an alternative antimicrobial therapy, where the metallated Pcs, upon photoexcitation with light, are able to photoinactivate different pathogenic microorganisms and could be an excellent approach to inactivate bacteria.[169,193]

Despite of the existence of medical procedures against cancer cells (surgery, chemotherapy and radiotherapy), PDT has the advantage of being a selective treatment for early diagnosis and locally identified carcinomas, without harming the surrounding healthy tissues. The PS and light can be selectively focused to the damage localization[176] and the high reduced life time of the main cytotoxic oxygen species in biological media, especially the singlet oxygen, limit the treatment exclusively to the area to be treated.[194] The photodamage processes, initialized by PDT, lead to necrosis and/or to apoptosis and autophagy. The leading mechanism of the cell inactivation depends on the specific protocol used, such as the drug and light doses.[179]

However, PDT efficiency is dependent of several other aspects, such as: the PS structure, its subcellular localization at the time of irradiation, irradiation magnitude and wavelength, sensitivity of tumour cells, tumour oxygenation level, among others.[178,195-198] Indeed, the efficiency of this medical procedure depends on the high light absorption features of the PS, mainly at the red region of the visible spectrum, its great selectivity to the target cells, minimal dark toxicity, and high singlet oxygen quantum yields formation, amphiphilicity features and others.[176,178,199,200] PDT is considered an excellent strategy for the treatment of a large variety of tumours, age-related macular degeneration, and promising for the treatment of cardiovascular and infectious diseases.[176,182,201-203] On the other hand, antimicrobial PDT has been suggested for dental applications, burn wounds and acne, mainly due to the easy access of the light source to these areas.[180,182,184]

Amongst the various types of PSs used in PDT, Pors are the most extensively studied and the ones firstly approved for clinical applications. However, it is recognized

that even the most widely used formulation (Photofrin®) is far from being an ideal PS. It comprises a mixture of hematoporphyrin oligomeric derivatives, with considerable skin accumulation and reduced light absorbance capabilities in the red region of the electromagnetic spectrum, where light penetrates deepest into tissues.[202] Due to this disadvantage, it has emerged a second generation of PDT agents based on chlorins[204] and Pcs.[205] These new PSs have an extraordinary absorbance in the visible red region of the electromagnetic spectrum, enabling both phototherapy and imaging to go deeper into tissues. However, all these types of macrocycle cores do not have appropriate biocompatibility requirements, mainly solubility in physiological fluids. For that, different delivery formulations, such as incorporation into liposomes,[206] biopolymers,[207] cyclodextrins[208] and more recently into dendrimers[209] have been explored. In fact, the different photodynamic activities can be associated to their different extent of cellular uptake and aggregation effect. Indeed, the progress of more effective PDT agents has been accomplished by appending second generation PSs with "bio"molecular recognition motifs, such as: carbohydrates,[63] polysaccharides,[181] amino acids,[210] proteins,[211] monoclonal antibodies,[212] pyridinium[213,214] and ammonium units,[215] sulphonate groups,[216] polyethylene glycol (PEG) units,[217] etc. The PSs prepared by the later strategy are known as third generation of PSs because these moieties/groups target specific cancer cells.[218]

The attractive properties of phthalocyanines, namely the strong absorption band (e.g. Photosens: $\varepsilon = 110000\ M^{-1}\ cm^{-1}$) in the region of 620-800 nm, which is considered the ideal photodynamic therapeutic window. In case of Photosens®, that is a PS in the second stage of clinical trials by the selection of the water-soluble aluminium sulphonated phthalocyanine **1.13**, (Figure 1.23) by several Moscow medical institutions (Oncological Scientific Centrum, Oncological Institute, Moscow Medical Academy and Institute of Laser Surgery). In fact, this PS used as a mixture of regioisomers, is now in the second stage of clinical trials for the treatment of malignant and non-malignant tumours, ulcers, and festering wounds with very promising results.[219-223] A review from Lukyanets has been published concerning the success of clinical studies using Pcs as PSs.[224]

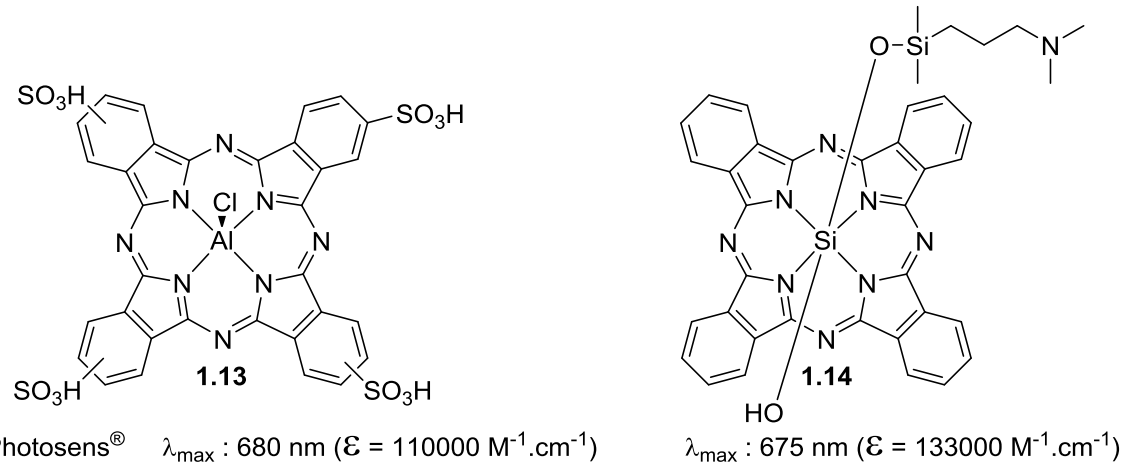

Photosens® λ_{max} : 680 nm (ε = 110000 $M^{-1}.cm^{-1}$) λ_{max} : 675 nm (ε = 133000 $M^{-1}.cm^{-1}$)

Figure 1.23 Structures of photosensitizers based on phthalocyanines.

Another promising photosensitizer is the phthalocyaninato silicon(IV) **1.14** (Figure 1.23) which as a single compound has shown effective feasibility in the treatment of skin diseases.[225]

In order to get an ideal PS, using these photoactive structures, several groups have developed synthetic strategies in order to incorporate pyridinium[226] and cyclodextrin[208] units into the Pc core. The new compounds can be excellent alternatives to overcome the tremendous limitations of the first and second generation PSs have been prepared and studied in order to give their higher solubility in aqueous media and cell/tissue recognition.[167,173,227,228] In fact, phthalocyanine derivatives can open the possibility to build smart photoactive molecules by the combination of their unique photophysical and photochemical properties.[210,229,230]

Phthalocyanines as photosensitizer drugs against microorganisms

It is well-known that for an efficient photoinactivation of Gram-negative bacteria is essential the use of a cationic PS,[231-233] where the positive charged can interact electrostatically with the negative charged of the outer wall (lipoproteins, lipopolysaccharides) allowing their binding and relative entrance.[234] The positive charged groups provides a strait electrostatic interaction with negatively charged sites at the outer membrane surface of the Gram-negative bacteria, increasing the efficiency of the photodynamic activity. Furthermore, inactivation of Gram-positive bacteria is guaranteed by neutral, anionic or cationic PSs that quickly cross the cell membrane.[234,235] Nevertheless, the typical damages involved in the antimicrobial PDI are not well clarified.

For example, Brown and co-workers reported uptake studies using cationic groups on the Pc core to perform interesting water-soluble pyridinium zinc phthalocyanine **1.15**[236] (Figure 1.24) as a powerful photosensitizer able to inactivate *Escherichia coli* (or *E. coli*).[237] This PS was applied in the incubation of *E. coli* cells in the dark, which produced modifications in the outer membrane permeability barrier, rendering the bacteria sensitive to hydrophobic compounds.[238] Interesting, is the addition of Mg^{2+} to the medium prior to the cells incubation with the PS preventing these modifications in the outer membrane. Moreover, the use of Mg^{2+} in the medium also prevents the photoinactivation of *E. coli*. The binding of divalent cations, such as Mg^{2+}, prevents electrostatic repulsion of the outer leaflet membrane of lipopolysaccharides being responsible for protecting the structure of the membrane surface.[239]

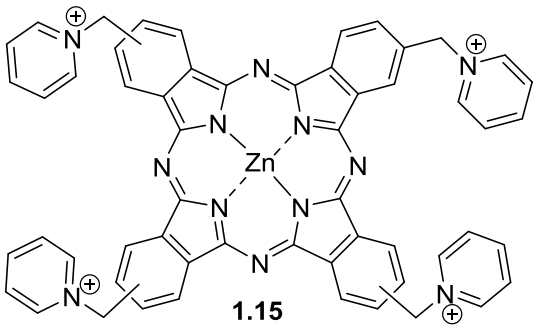

Figure 1.24 Structure of water-soluble pyridinium zinc(II) phthalocyanine.

However, the authors have reported that the obtained results are consistent where the metallated pyridinium phthalocyanines access across the outer membrane of *E. coli* by self-promoted uptake pathway in Gram-negative bacteria.[237]

Kaliya and co-workers showed the photophysical and photosensitizing properties of two octacationic oxotitanium phthalocyanines with pyridiniomethyl **1.16** or cholinyl **1.17** units (Figure 1.25) that were studied in aqueous and alcohol solutions.[240]

The phototoxicity of the Pc derivatives has been studied against coliform bacteria from a contaminated Moscow River water, by generating singlet oxygen $^1O_2$ and hydroxyl radicals upon light exposure. It is proposed that both OH and $^1O_2$ might be responsible for the observed bactericidal effects to achieve the water disinfection. However, the authors mentioned that in these conditions it is more difficult to achieve disinfection than on pure bacterial cultures. The photodisinfection study was performed in microorganisms, which

are standardized in drinking water supply reservoirs, specifically total germs, *E. coli*, spores of sulphite-reducing *Clostridium* and coliphages.[240]

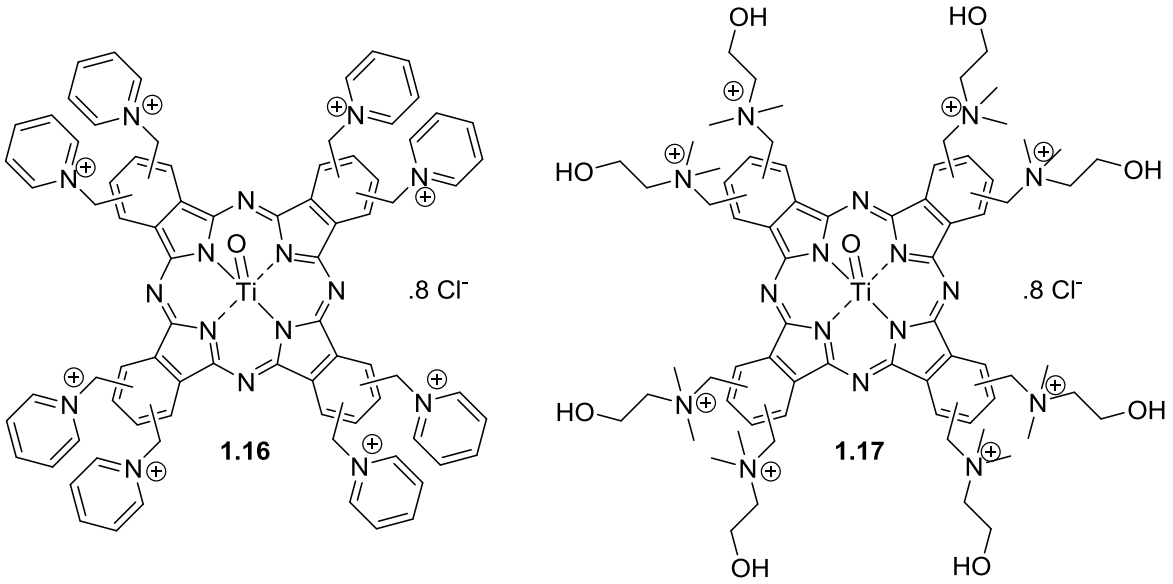

Figure 1.25 Structures of octa-pyridiniomethyl phthalocyanine oxotitanium **1.16** and **1.17**.

Phthalocyanines for cancer PDT

A different strategy to obtain soluble Pcs in biological media is to insert different carbohydrates (CHs) in the Pc core. The combination of these two characteristics makes them possible PS drugs in PDT. Carbohydrates are largely disseminated in all living organisms, appearing as monomers, oligomers or polymers and as components of many other natural molecules and playing vital roles in metabolic processes.[241,242] Also, these molecules can appear conjugated to other biological components, such as: proteins, lipids and nucleic acids. It is well-known that carbohydrates are involved in many cellular processes (e.g., cell-substrate and cell-cell recognition, drug transport, etc.).[243-245] In this sense, CH derivatives have been incorporated on the structures of several drugs, to give them the adequate physicochemical properties for biomedical proposes. This methodology has attracted the search for therapeutic applications in the medical field, being an exciting strategy to solve many of the biocompatibility and selectivity problems of several active molecules.[243]

Cavaleiro and co-workers[174] reported the synthesis of glyco-Pcs with four protected D-galactose (GalPro) units linked to the same isoindole by the hydroxyl group located in carbon C-6 (Scheme 1.3). The Pc **1.19** was obtained by statistical cross-condensation of

glycophthalonitrile **1.18** with an excess of 1,2-dicyanobenzene phthalonitrile, in the presence of zinc chloride The reaction was performed in DMAE at 100 ºC, affording the desired Pc **1.19** in 30% yield, accompanied by the symmetric zinc Pc formed by self-condensation of phthalonitrile. The Pc **1.20** was obtained in 85% yield, after removal of the CH protecting groups with aqueous trifluoroacetic acid (TFA) and purification by reverse-phase column chromatography (Scheme 1.3). The UV-Vis spectrum of **1.20**, in dimethyl sulfoxide (DMSO), indicates the presence of monomeric species. A different situation occurs in water where a significant reduction in the Q-band suggests intermolecular aggregation due to macrocycles cofacial arrangements.

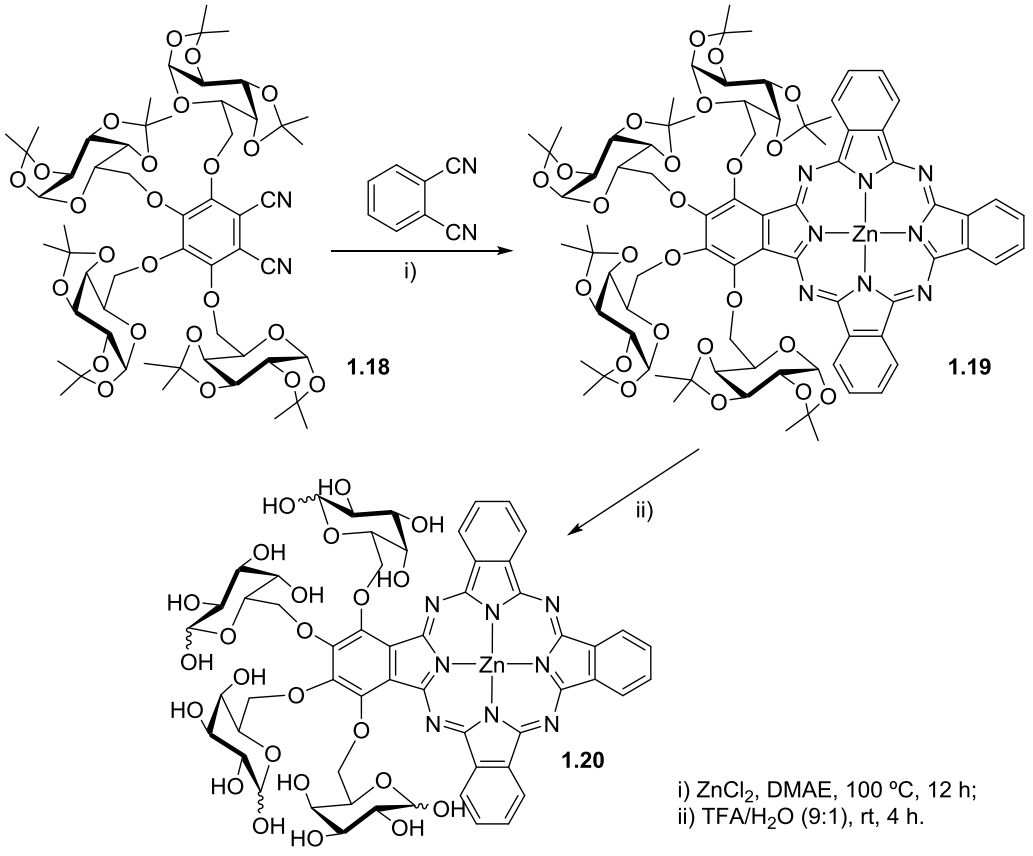

Scheme 1.3

The asymmetric structure of the Pc **1.20** provides an amphiphilic character useful for drug administration (hydrophilicity) and membrane crossing (lipophilicity).[246] In addition, considering the specific affinity of carbohydrates for cancer cells and their strong influence on the bioavailability of the corresponding conjugates, good perspectives can be anticipated for this new generation of photosensitizers based on Pc-carbohydrate derivatives.[247-250]

The synthesis of glyco-Pcs where the CH units are linked by a short or a long spacer, it was idealized in order to avoid any steric disturbance of the macrocycle in the recognition source, and simultaneously to allow multiple carbohydrate recognition.[251] In this context, Cavaleiro and co-workers[227] reported the synthesis of Pcs with eight galactose (Gal) units separated from macrocycle by methylenic (CH_2) bridges (Scheme 1.4). The synthetic route involved the tetramerization of phthalonitrile **1.21** in DMAE at 140 ºC under argon atmosphere for 16 h in the presence of $ZnCl_2$ giving the glyco-Pc **1.22** as a dark blue solid in 62% yield. The deprotection of the CH units under acidic conditions afforded Pc **1.23** in 87% yield (Scheme 1.4).

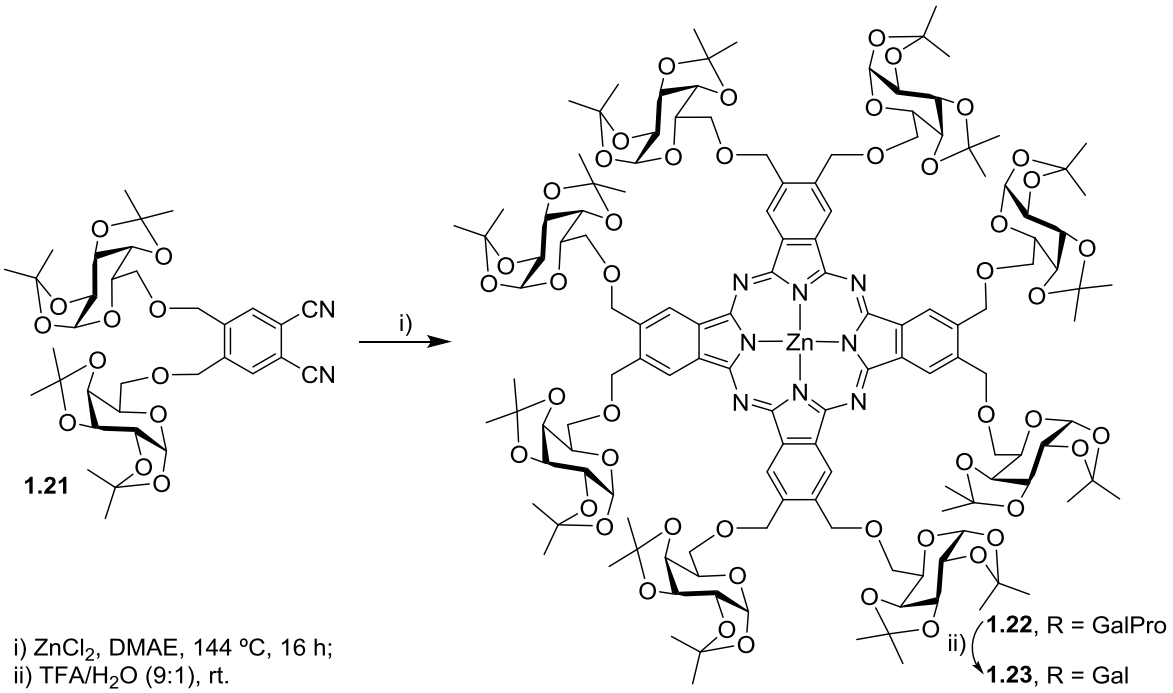

Scheme 1.4

The optical properties of the octa-glycophthalocyanine suggest good perspectives for the potential application of such compounds as photosensitizers in PDT depending of the specific affinity for tumour tissues.

Tomé and co-workers[167] selected also the post glycoconjugation approach to obtain the phthalocyanines decorated with sixteen galactose units (Scheme 1.5), where the preliminary photophysical and photochemical features of the glycodendrimer conjugates, namely their high singlet oxygen production and interaction with human serum albumin (HAS) suggest that they might be used as promising PDT agents. In the this publication, the authors reported an efficient and elegant access to the glycodendritic unit **1.27** that involved in a first step the reaction of 2,4,6-trichlorotriazine **1.24** with the adequate

protected galactose **1.25** in the presence of *N,N'*-diisopropylethylamine (DIPEA) in dry toluene. Then, the reaction of intermediate **1.26** obtained in 92%, with propane-1,3-dithiol, afforded the glycodendritic unit **1.27** in 89% yield. The synthetic approach involving the reaction of the commercial available perfluorinated phthalocyanine **ZnPcF$_{16}$** with the dendritic unit **1.27**, afforded the protected glycodendrimer **1.28** in 81% yield (Scheme 1.5). The hydrolysis of the isopropylidene protective groups with TFA/H_2O (9:1) produced the unprotected glycodendrimer conjugate **1.29** in 78% yield, as a mixture of α/β stereoisomers.

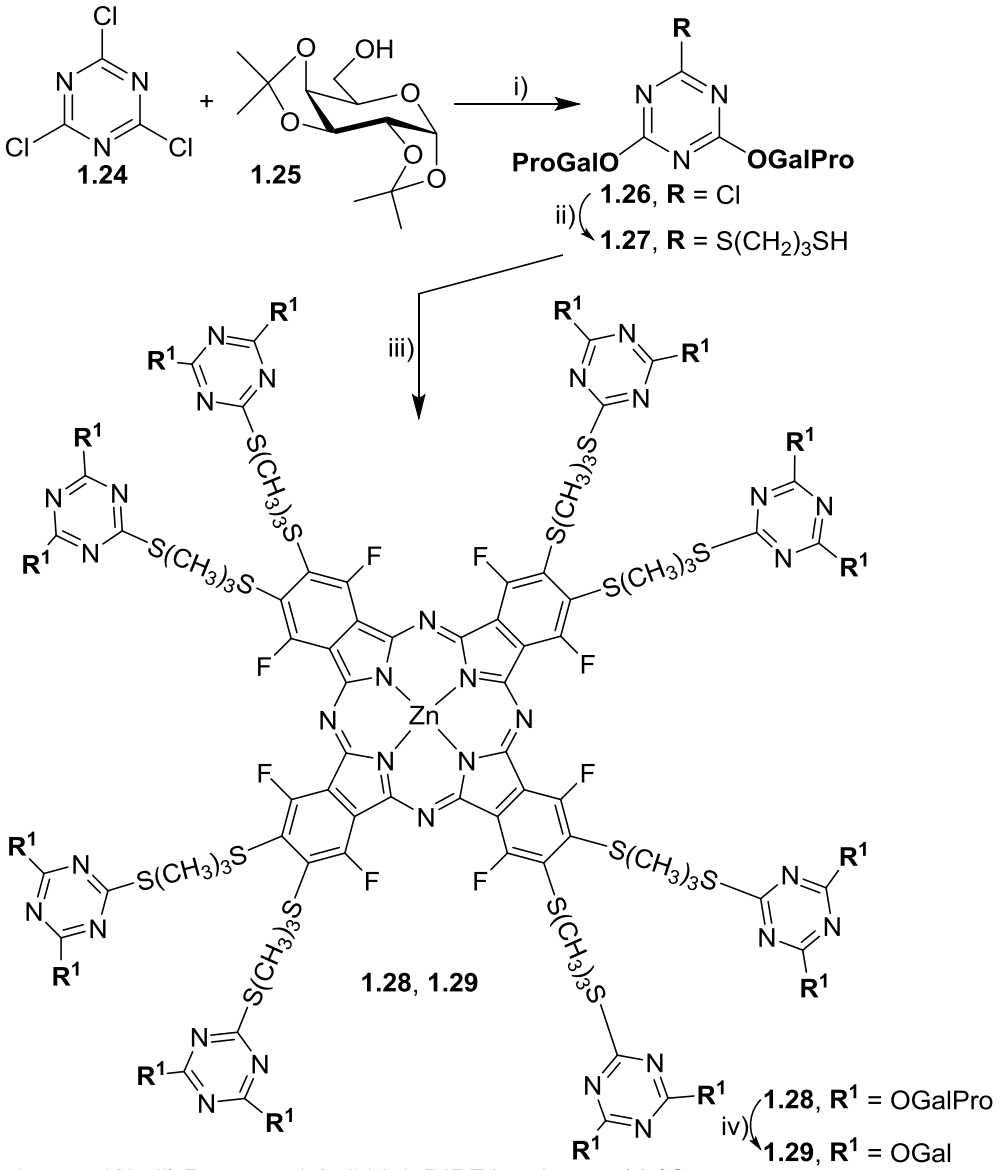

i) DIPEA, toluene, 48h; ii) Propane-1,3-dithiol, DIPEA, toluene, 80 ºC, 48h; iii) **ZnPcF$_{16}$**, DIPEA, DMF, 50 ºC, 24h; iv) TFA/H_2O (9:1)

Scheme 1.5

Cavaleiro and co-workers synthesized the first water-soluble phthalocyanine-β-cyclodextrin conjugate *via* a statistical cross condensation of a 4-(β-cyclodextrin)phthalonitrile with known phthalonitriles.[174] The purpose work was to obtain stable water solutions of Pcs using a covalent linkage to the β-cyclodextrin (Figure 1.26). The use of the CD moiety was related with the high amphiphilicity character to the performed water soluble hybrids. The exterior hydrophilic properties of the CD combined with its hydrophobic cavity in the centre allow the solubilisation of these Pcs in water. Moreover, the CDs have the capacity of inclusion of small molecules in their cavity.[252]

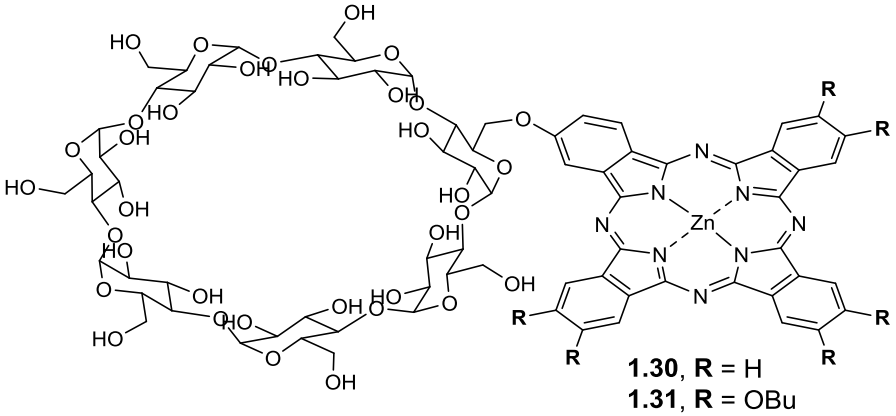

Figure 1.26 Water-soluble phthalocyanine-β-cyclodextrin conjugates **1.30** and **1.31**.

In the same context, Ng and co-workers developed a series of symmetrical and unsymmetrical silicon(IV) phthalocyanines based on permethylated β-cyclodextrin units or on this unit combined with a sugar or a diamino moiety as the axial substituents.[253,254] In Scheme 1.6 are shown the structures of unsymmetrical phthalocyanines **1.35** and **1.36** as examples of this series of Pcs, which were obtained in yields ranging from 10 to 14% .

The photodynamic activities for **1.35** and **1.36** were investigated against HT29 human colorectal carcinoma and HepG2 human hepatocarcinoma cells, showing IC_{50} between 21-36 nM; it was also highlighted that **1.35** has a greater photocytotoxicity and efficiency to generate ROS than **1.36**.

The extension of the previous studies to the tetra-ethyleneglycol-linked 1,2:5,6-di-*O*-isopropylidene-α-D-glucofuranose unit **1.34** allowed to prepare the glucoconjugated silicon(IV) phthalocyanines **1.38** and **1.39** (Scheme 1.7).[229]

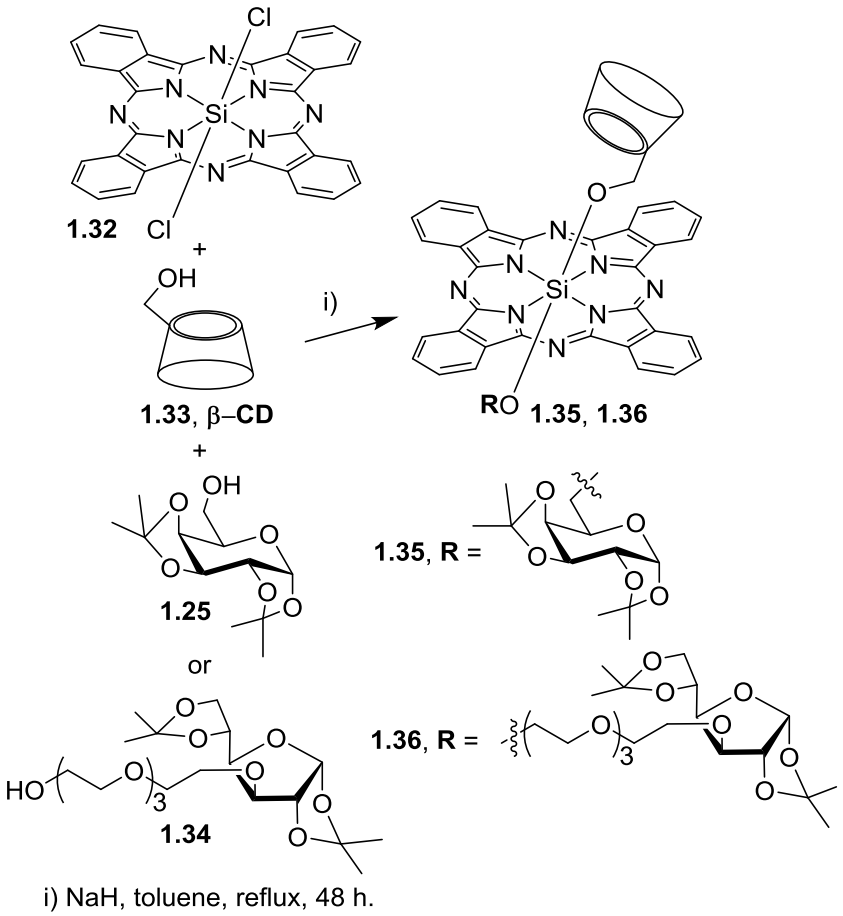

Scheme 1.6

The diglucosylated phthalocyanine **1.38** was obtained in 13% yield after refluxing in toluene **1.34** with the readily available silicon(IV) phthalocyanine dichloride **1.32** in the presence of sodium hydride (NaH) for 48 h, followed by chromatographic purification. The authors highlighted that the purification must be performed by column chromatography using neutral alumina followed by gel permeation chromatography, due to the susceptibility of the compound towards silica gel acidic nature to its decomposition.[229]

The silicon 2,3-dichlorophthalocyanine dichloride **1.37**, used as precursor of **1.39**, (Scheme 1.7) was prepared *via* a "3+1" mixed cyclisation involving 1,3-diiminoisoindoline, dichloro-1,3-diiminoisoindoline and $SiCl_4$ and was performed in reflux quinoline. The authors mentioned that the crude **1.37** owing to its poor solubility was treated directly with the protected glucose derivative **1.34** and NaH. The A_3B-type silicon(IV) phthalocyanines **1.39** was isolated in 3.1% after a similar chromatographic process described for **1.38**.[229]

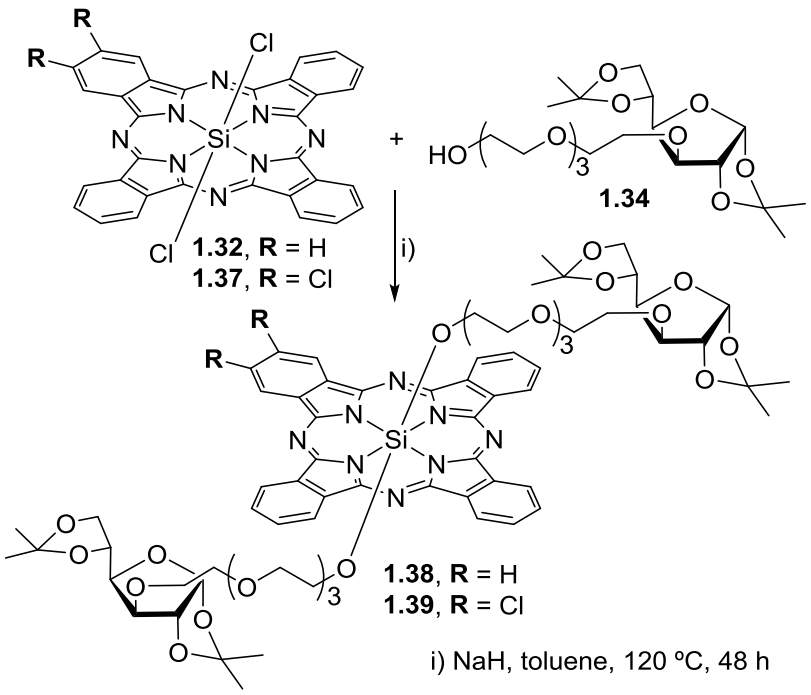

Scheme 1.7

Both compounds **1.38** and **1.39** show high solubility in common organic solvents and exhibit substantial solubility in water. The *in vitro* photodynamic activities of both compounds showed highly photocytotoxicity against HepG2 human hepatocarcinoma and HT29 human colon adenocarcinoma cells, principally the nonchlorinated Pc **1.38** due to its smaller tendency to aggregate in biological media when compared with **1.39**. The studies indicated also that Pc **1.38** presents a highly selective subcellular localization property targeting the lysosomes of HT29 cells.

For all aforementioned, in the next five chapters it will be emphasized the preparation of novel phthalocyanine derivatives with suitable groups on their periphery for different applications: electronic supramolecular interactions (Chapters 2-4), microorganisms PDI (Chapter 5) and cancer PDT (Chapter 6).

Objectives

The global goal of this project comprise the synthesis and characterization of innovative compounds/materials based on neutral and cationic phthalocyanines (Pcs) and to study their potential in electron donor-acceptor and biomedical applications.

To achieve that goal, new phthalocyanine derivatives were prepared with adequate motifs and suitable units on their periphery in order to study their interactions with carbon nanostructure and their use as photosensitizers (PSs) in photodynamic therapy (PDT) of cancer cells and in the photodynamic inactivation of microorganisms (PDI).

So, the present PhD work is divided in the 5 specific aims summarized below:

Specific Aim 1 – Develop suitable substituted precursors to prepare the corresponding thiopyridyl Pc derivatives and it will be studied their supramolecular interactions with graphene nanosheets (GN) – Figure 1.27.

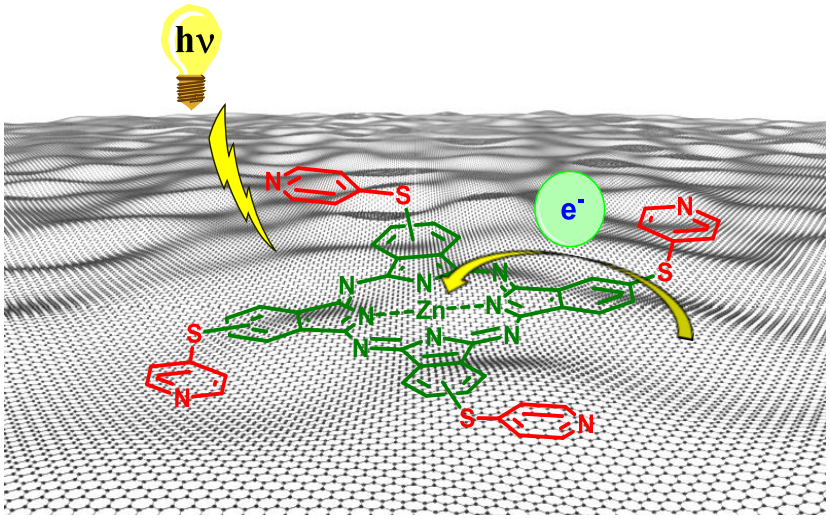

Figure 1.27 Example of one of the targets thiopyridyl-Pc/graphene nanohybrids

Specific Aim 2 – Synthesis and characterization of new cationic Pcs, based on thiopyridinium motifs, to interact with single wall carbon nanotubes (SWNTs) in water media. It will be analysed the photophysical properties of the possible supramolecular systems (Figure 1.28).

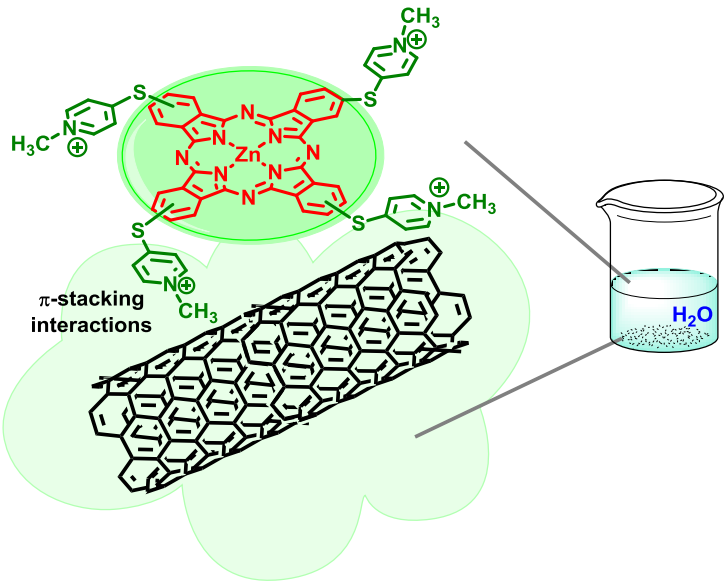

Figure 1.28 Example of one of the targets thiopyridinium-Pc/SWNT nanohybrid.

Specific Aim 3 – Develop new supramolecular arrays from coordination of ruthenium phthalocyanine (RuPc) and thiopyridylporphyrins to perform multichromophoric assemblies (RuPc-PorSPy, Figure 1.29). The photophysical characterization of the supramolecular arrays it will be analysed.

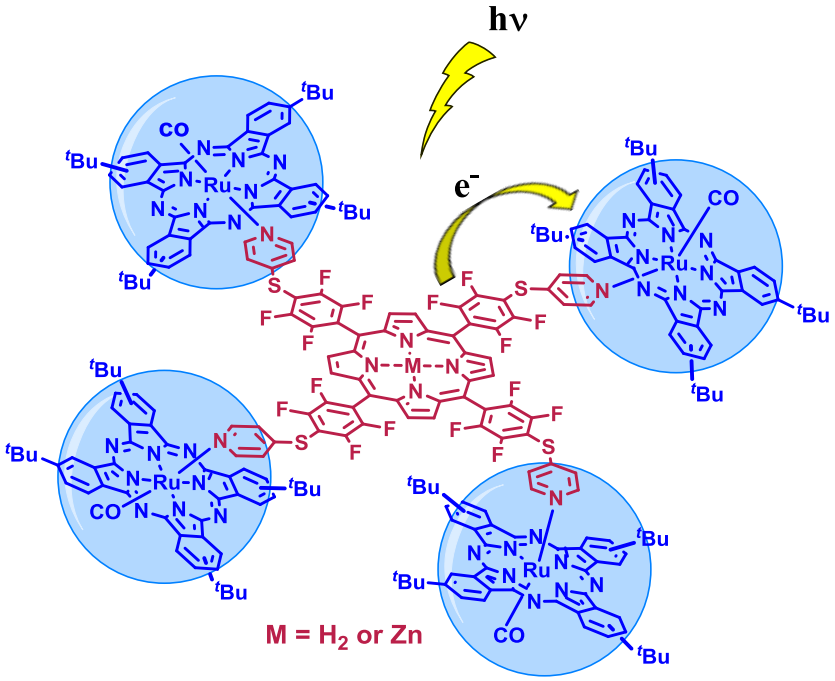

Figure 1.29 Example of synthesised supramolecular RuPc-PorSPy pentads.

Specific Aim 4 – Synthesis and characterization of new amphiphilic phthalocyanines, based on methoxypyridinium derivatives to be evaluated as potential "photoantibiotics"/photoactive molecules against antibiotic resistant microorganisms. The

new Pc-pyridinone molecules initially prepared will be subsequently methylated to yield the corresponding target cationic Pcs (Figure 1.30). The biological screen on Gram-negative bacteria (*Escherichia coli*) performed in collaboration with the microbiology group of the University of Aveiro, it will be investigated to evaluate the potential of these compounds in the photoinactivation of Gram-negative bacteria.

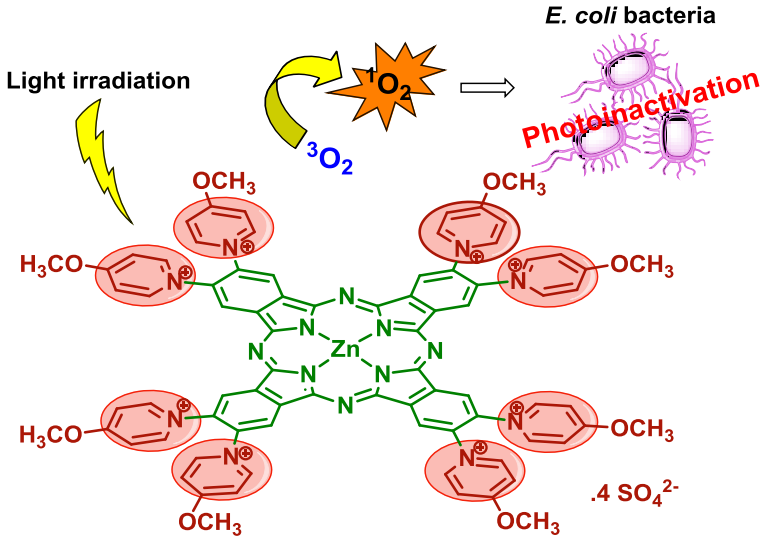

Figure 1.30 Example of a cationic Pc used as PS agent.

Specific Aim 5 – Synthesis and characterization of novel photosensitizing agents, based on phthalocyanine-cyclodextrin (Pc-CD) conjugates. In this project, the particular concern is to design and synthesize new asymmetric Pc-CD formulations covalently conjugated, which may show water solubility and marked selectivity towards UM-UC-3 human bladder cancer cells (Figure 1.31). The physicochemical and photobiological properties will be assessed and the *in vitro* studies on bladder cancer cells examined to select the most effective PSs.

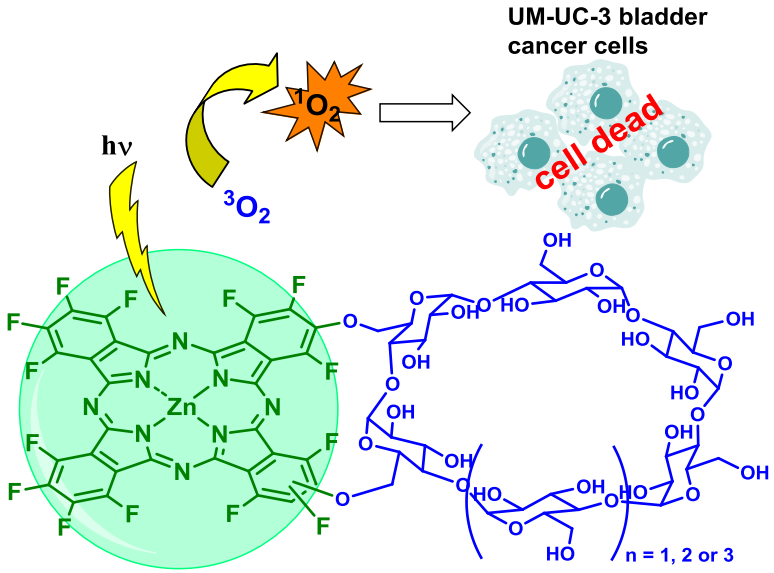

Figure 1.31 Example of target Pc-CD conjugates.

1.5 References

1. Moser, F. H., Thomas, A. L., in Phthalocyanine Compounds, American Chemical Society, Reinhold Publishing, New York, NY, USA, 1963.
2. Mansuy, D., Battioni, P., in Bioinorganic Catalysis, Reedijk, J., Ed., Marcel Dekker, New York, NY, USA, p. 395, 1993.
3. Lever, A. B. P., *Adv. Inorg. Chem. Radiochem*., **1965**, 7, 27–114.
4. Bedioui, F., *Coord. Chem. Rev*., **1995**, 144, 39–68.
5. Breck, D. W., Zeolite Molecular Sieves - Structure, Chemistry and Use, Robert, E., Publishing Co., 1–18, 1984.
6. Shilov, A. S., *J. Molec. Catal*., **1988**, 47, 351–362.
7. Collman, J. P., Zhang, X., Lee, V. J., Uffelman, U. U., Brauman, J. L., *Science*, **1993**, 261, 1404–1411.
8. Mansuy, D., *Coord. Chem. Rev*., **1993**, 125, 129–142.
9. Karlin, K. D., *Science*, **1993**, 261, 701–708.
10. Flanigan, E. M., in Introduction to Zeolite Science and Practice. *Zeolites and molecular sieves: An historical perspective*, Bekkum, H. V., Flanigan, E. M., Jacobs, P. A., Jansen, J. C., Eds., Elsevier, Amsterdam, Netherlands, *Studies in Surface Science and Catalysis*., vol. 137, Chapter 2, pp. 11–36, 2001.
11. Dyer, A., in An Introduction to Zeolite Molecular Sieves, Wiley, New York, NY, USA, 1–164, **1988**.
12. Bekkum, H. V., Flanigan, E. M., Jansen, J. C., in Introduction to Zeolite Science and Practice, Elsevier, Amsterdam, Netherlands, pp. 1-753, **1991**.
13. McCusker, L. B., Baerlocher, C., in Introduction to Zeolite Science and Practice. *Zeolite structures*, Bekkum, H. V., Flanigan, E. M., Jacobs, P. A., Jansen, J. C., Eds., Elsevier, Amsterdam, Netherlands, *Studies in Surface Science and Catalysis.*, vol. 137, Chapter 3, pp. 37–67, 2001.
14. Braun, A., Tscherniak, F. J., *J. Ber.*, **1907**, 40, 2709–2714.
15. Diesbach, H., von der Weid, E., **1927**, 10, 886–888.
16. McKeown, N. B., in An introduction to the phthalocyanines. Phthalocyanine Materials: Synthesis, Structure and Function, McKeown, N. B., Ed., Cambridge University Press, Cambridge, UK, Chapters 1 and 2, pp. 1–31, 1998.

17. Thomas, A. L., in Phthalocyanine Research and Applications, CRC Pres: Baton Rouge, FL, USA, p. 2, **1990**.
18. Dandridge, A. G., Drescher, H. A. E., Thomas, J., *Dyes. British patent 322*, 169, **1929**.
19. Robertson, J. M., *J. Chem. Soc.*, **1935**, 615–621.
20. Robertson, J. M., *J. Chem. Soc.*, **1936**, 1195–1209.
21. Robertson, J. M., *J. Chem. Soc.*, **1936**, 1736–1738.
22. Robertson, J. M., Woodward, I., *J. Chem. Soc*., **1937**, 219–230.
23. Robertson, J. M., *J. Chem. Soc*., **1940**, 36–48.
24. Linstead, R. P., *J. Chem. Soc*., **1934**, 1016–1017.
25. Byrne, G. T., Linstead, R. P., Lowe, A. R., *J. Chem. Soc*., **1934**, 1017–1022.
26. Dent, C. E. Linstead, R. P., *J. Chem. Soc*., **1934**, 1027–1032.
27. Dent, C. E., Linstead, R. P., *J. Chem. Soc*., **1934**, 1033–1039.
28. McKeown, N. B., in The Porphyrin Handbook, *The synthesis of symmetrical phthalocyanines*, Kadish, K. M., Smith, K. M., Guilard, R., Eds., Academic Press, New York, NY, USA, vol. 15, cap. 98, pp. 61–124, 2003.
29. Davis, M. E., Lobo, R. F., *Chem. Mater*., **1992**, 4, 756–768.
30. Mortier, W. J., Compilation of Extra Framework Sites in Zeolites, Butterworth & Co., Guildford, England, 1–67, 1982.
31. Löbbert, G., in Ullmann's Encyclopedia of Industrial Chemistry, *Phthalocyanines*, Wiley-VCH, Ed., 2000.
32. Rodríguez-Morgade, M. S., de la Torre, G., Torres, T., in The Porphyrin Handbook, *Design and Synthesis of Low-Symmetry Phthalocyanines and Related Systems*, Kadish, K. M., Smith, K. M., Guilard, R., Eds., Academic Press, New York, NY, USA, vol. 15, cap. 99, 2003.
33. Kobayashi, N., in The Porphyrin Handbook, *Synthesis and Spectroscopic Properties of Phthalocyanine Analogs*, Kadish, K. M., Smith, K. M., Guilard, R., Eds., Academic Press, New York, NY, USA, vol. 15, cap. 100, 2003.
34. Leznoff, C. C., in Phthalocyanines – Properties and Applications; Leznoff, C. C., Lever, A. B. P., Eds., VCH Publishers, New York, NY, USA, vol. 1, cap. 1., 1989.
35. Lourenço, L. M. O., Neves, M. G. P. M. S., Cavaleiro, J. A. S., Tomé, J. P. C., *Tetrahedron review*, **2014**, 70, 2681–2698.

36. Shirk, J. S., Lindle, J. R., Bartoli, F. J., Kafafi, Z. H., Snow, A. W., in Materials for Nonlinear Optics-Chemical Perspectives, Marder, S. R., Sohn, J. E., Stucky, G. D., Eds., Series 455, Chapter 42, p. 626, ACS Symposium 1991.
37. Dini, D., Hanack, M., in The Porphyrin Handbook, *Physical Properties of Phthalocyanine-based Materials*, Kadish, K. M., Smith, K. M., Guilard, R., Eds, vol. 17, cap. 107, Academic Press, New York, NY, USA, 2003.
38. Brewis, M., Clarkson, G. J., Goddard, V., Helliwell, M., Holder, A. M., McKeown, N. B., *Angew. Chem. Int. Ed*., **1998**, 37, 1092–1094.
39. Hanack, M., Heckmann, H., *Eur. J. Inorg. Chem.*, **1998**, 367–373.
40. Yang, G. Y., Hanack, M., Lee, Y. W., Chen, Y., Lee, M. K. Y., Dini, D., *Chem. Eur. J*., **2003**, 9, 2758–2762.
41. Guldi, D. M., *Chem. Soc. Rev*., **2002**, 31, 22–36.
42. Imahori, H., Mori, Y., Matano, Y., *J. Photochem. Photobiol*. *C*, **2003**, 4, 51–83.
43. El-Khouly, M. E., Ito, O., Smith, P. M., D'Souza, F., *J. Photochem. Photobiol*. *C*, **2004**, 5, 79–104.
44. de la Torre, G., Claessens, C. G., Torres, T., *Chem. Commun*., **2007**, 20, 2000–2015.
45. Fukuzumi, S., *Phys. Chem. Chem. Phys*., **2008**, 10, 2283–2297.
46. Wasielewski, M. R., *Acc. Chem. Res*., **2009**, 42, 1910–1921.
47. Special issue in *Renewable Energy*, Nocera, D., Guldi, D. M., *Chem. Soc. Rev*., **2009**, 38, 1–293.
48. Milgrom, L. R., in The colours of Life: an Introduction to the Chemistry of Porphyrins and Related Compounds, Oxford University Press: Oxford, USA, 1–256, 1997.
49. Rio, Y., Rodríguez-Morgade, M. S., Torres, T., *Org. Biomol. Chem*., **2008**, 6, 1877–1894.
50. Gouterman, M., in The Porphyrins, Part A. Physical Chemistry, Dolphin, D., Ed., Academic Press, New York, NY, USA, vol. 3, 1–654, 1978.
51. McHugh, A. J., Gouterman, M., Weiss, C., *Theoret. Chim. Acta*, **1987**, 24, 246.
52. Schaffer, A. M., Gouterman, M., Davidson, E. R., *Theoret. Chim. Acta*, **1973**, 30, 9–30.
53. Dehe, D., Lothschütz, C., Thiel, W. R., *New J. Chem*., **2010**, 34, 526–532.
54. Tomoda, H., Saito, S., Ogawa, S., Shiraishi, S., *Chem. Lett*., **1980**, 1277–1280.

55. Oliver, S. W., Smith, T. D., *J. Chem. Soc. Perkin Trans*., **1987**, 2, 1579–1584.
56. Brach, P. J., Grammatica, S. J., Ossanna, O. A., Weinberger, L., *J. Heterocyclic. Chem*., **1970**, 7, 1403–1405.
57. Piechocki, C., Thèse Docteur Spécialisé, Strasbourg, **1982**.
58. de la Torre, G., Bottari, G., Hahn, U., Torres, T., in Functional Phthalocyanine Molecular Materials, *Structure and Bonding*, Jiang, J., Ed., Springer, vol. 135, pp. 1–44, 2010.
59. Martínez-Díaz, M. V., Quintiliani, M., Torres, T., *Synlett*, **2008**, 1, 1–20.
60. Tomoda, H., Hibiya, E., Nakamura, T., Ito, H., Saito, S., *Chem. Lett*., **1976**, 9, 1003–1006.
61. Leznoff, C. C., Hu, M., Nolan, K. J. M., *Chem. Commum*., **1996**, 1245–1246.
62. Cavaleiro, J. A. S., Tomé, J. P. C., Faustino, M. A. F., in Heterocycles from Carbohydrate Precursors, Topics in Heterocyclic Chemistry, *Synthesis of Glycoporphyrins*, Ashry, E. S. H. E., Ed., Springer, vol. 7, 179–248, 2007.
63. Cavaleiro, J. A. S., Faustino, M. A. F., Tomé, J. P. C., in Carbohydrate Chemistry, *Porphyrinyl-type sugar derivatives: synthesis and biological applications*, The Royal Society of Chemistry, vol. 35, pp. 199–231, 2009.
64. Hanack, M., Schmid, G., Sommerauer, M., *Angew. Chem. Int. Ed*., **1993**, 32, 1422–1424.
65. Rodríguez-Morgade, M. S., Hanack, M., *Chem. Eur. J*., **1997**, 3, 1042–1051.
66. Hurley, T. J., Robinson, M. A., Trotz, S. I., *Inorg. Chem*., **1967**, 6, 389–392.
67. Sharman, W. M., van Lier, J. E., in The Porphyrin Handbook, *Synthesis of Phthalocyanine Precursors*, Kadish, K. M., Smith, K. M., Guilard, R., Eds, Academic Press, New York, NY, USA, vol. 15, cap. 97, 2003.
68. Kaliya, O. L., Lukyanets, E. A., Vorozhtsov, G. N., *J. Porphyrins Phthalocyanines*, **1999**, 3, 592–610.
69. Bench, B. A., Brennessel, W. W., Lee, H.-J., Gorun, S. M., *Angew. Chem. Int. Ed.*, **2002**, 41, 750–754.
70. Tsaryova, O., Semioshkin, A., Wöhrle, D., Bregadze, V. I., *J. Porphyrins Phthalocyanines*, **2005**, 9, 268-274.

71. Lam, M., Lee, Y., Deng, M., Hsia, A. H., Morrissey, K. A., Yan, C., Azzizudin, K., Oleinick, N. L., McCormick, T. S., Cooper, K. D., Baron, E. D., *Adv. Hematol.*, **2010**, 2010, 1–8.
72. Special Issue in *Supramolecular Chemistry and Self-Assembly*, *Science*, **2002**, 295, 2395–2421.
73. Special Issue in *Supramolecular Approaches to Organic Electronics and Nanotechnology*, *Adv. Mater*., **2006**, 18, 1227–1329.
74. Bottari, G., Suanzes, J. A., Trukhina, O., Torres, T., *J. Phys. Chem. Lett*., **2011**, 2, 905–913.
75. Hoeben, F. J. M., Jonkheijm, P., Meijer, E. W., Schenning, A. P. H. J., *Chem. Rev*., **2005**, 105, 1491–1546.
76. V. Krishnan, in Electron Transfer in Chemistry and Biology – The Primary Events in Photosynthesis, Springer (Ad.), vol. 2, pp.77–86, **1997**.
77. El-Khouly, M. E., Ito, O., Smith, P. M., D'Souza, F., *J. Photochem. Photobiol., C*, **2004**, 5, 79–104.
78. Wasielewski, M. R., in Photoinduced Electron Transfer, Connolly, J. S., Bolton, J. R., Fox, M. A., Chanon, M., Eds., Elsevier, Amsterdam, 1988.
79. Ceroni, P., Balzani, V., in Electron Transfer in Chemistry, Balzani, V., Ed., vol. I-V, Wiley, 2001.
80. Gust, D., Moore, T. A., in The Porphyrin Handbook, Kadish, K. M., Smith, K., Guilard, R., Eds., Academic Press, vol. 8, 2000, pp. 153–190.
81. Yoshihara, K., Kumazaki, S., *J. Photochem. Photobiol. C: Rev. 1*, 22, 2000.
82. Hullmann, A., *The economic development of nanotechnology – An indicators based analysis*, European Commission, DG Research, Unit *Nano S&T - Convergent Science and Technologies*, Version: 28, November **2006**.
83. Youtie, J., Shapira, P., Porter. A. L., *J. Nanopart. Res.*, **2008**, 10, 981–986.
84. Schünemann, A., *Nanotechnology: No small matter*, *Risk future*, 8–11, 2009.
85. Singh, I., Rehni, A. K., Kumar, P., Kumar, M., Aboul-Enein, H. Y., in Fullerenes, Nanotubes and Carbon Nanostructures, *Carbon Nanotubes: Synthesis, Properties and Pharmaceutical Applications*, Taylor & Francis, vol. 17, pp. 361–377, 2009.

86. Bartelmess, J., Soares, A. R. M., Martínez-Díaz, M. V., Neves, M. G. P. M. S., Tomé, A. C., Cavaleiro, J. A. S., Torres, T., Guldi, D. M., *Chem. Commun.*, **2011**, 47, 3490–3492.
87. Boehm, H. P., Setton, R., Stumpp, E., *Pure Appl. Chem*., **1994**, 66, 1893–1901.
88. Boehm, H. P., Clauss, A., Fischer, G. O., Hofmann, U., *Z. Naturf.*, **1962**, 17, 150–153.
89. Schniepp, H. C., Li, J.-L., McAllister, M. J., Sai, H., Herrera-Alonso, M., Adamson, D. H., Prud'homme, R. K., Car, R., Saville, D. A., Aksay, I. A., *The Journal of Physical Chemistry B*, **2006**, 110, 8535–8539.
90 Novoselov, K. S., Geim, A. K., Morozov, S. V., Jiang, D., Zhang, Y., Dubonos, S. V., Grigorieva, I. V., Firsov, A. A., *Science*, **2004**, 306, 666–669.
91. Geim, A. K., Novoselov, K. S., *Nat. Mater*., **2007**, 6, 183–191.
92. Huang, L., Wu, B., Yu, G., Liu, Y., *J. Mater. Chem*., **2011**, 21, 919–929.
93. Edwards, R. S., Coleman, K. S., *Nanoscale*, **2013**, 5, 38–51.
94. Kroto, H. W., Heath, J. R., O'Brien, S. C., Curl, R. F.; Smalley, R. E., *Nature*, **1985**, 318, 162–163.
95. Iijima, S., *Nature*, **1991**, 354, 56–58.
96. Kratschmer, K., Lamb, L. D., Fostiropoulos, K., Huffman, R. D., *Nature*, **1990**, 347, 354–358.
97. Iijima, S., Ichihashi, T. *Nature*. **1993**, 363, 603–605.
98. Wildoer, J. W. G., Venema, L. C., Rinzler, A. G., Smalley, R. E., Dekker, C., *Nature*, **1998**, 391, 59–61.
99. Hatton, R. A., Miller, A. J., Silva, S. R. P., *J. Mater. Chem*., **2008**, 18, 1183–1192.
100. Niyogi, S., Hamon, M. A., Hu, H., Zhao, B., Bhowmik, P., Sen, R., Itkis, M. E., Haddon, R. C., *Acc. Chem. Res*., **2002**, 35, 1105–1113.
101. Joselevich, E., *Angew. Chem. Int. Ed*., **2004**, 43, 2992–2994.
102. Dragoman, D., Dragoman, M., *Physica E*., **2006**, 33, 178–181.
103. Aihara, J., *J. Phys. Chem. A*., **1999**, 103, 7487–7495.
104. Gao, X., Zhou, Z., Zhao, Y., Nagase, S., Zhang, S. B., Chen, Z., *J. Phys. Chem. C*., **2008**, 112, 12677–12682.
105. Odom, T. W., Huang, J. L., Kim, P., Lieber, C. M., *J. Phys. Chem. B*., **2000**, 104, 2794–2809.

106. Monthioux, M., Serp, P., Flahaut, E., Razafinimanana, M., Laurent, C., Peigney, A., Bacsa, W., Broto, J.-M., in Springer Handbook of Nanotechnology, *Introduction to Carbon Nanotubes* Part A, Bhushan, B., Ed., pp. 39–98, 2004.
107. Wannere, C. S., Moran, D., Allinger, N. L., Hess, Jr. B.A., Schaad, L. J., Schleyer, P. v. R., *Org. Lett*., **2003**, 5, 2983–2986.
108. Basiuk, V. A., *J. Phys. Chem. B*., **2004**, 108, 19990–19994.
109. Joselevich, E., *Chem. Phys. Chem*., **2004**, 5, 619–624.
110. O'Neill, A., Khan, U., Nirmalraj, P. N., Boland, J., Coleman, J. N., *J. Phys. Chem. C*, **2011**, 115, 5422–5428.
111. Dai, L., Mau, A. W. H., *Adv. Mater.*, **2001**, 13, 899–913.
112. Hirsch, A., *Angew. Chem., Int. Ed*., **2002**, 41, 1853–1859.
113. Dyke, C. A., Tour, J. M., *Chem. Eur. J.*, **2004**, 10, 812–817.
114. Sinnott, S. B., *J. Nanosci. Nanotechnol*., **2002**, 2, 113–123.
115. Lu, X., Chen, Z., *Chem. Rev*., **2005**, 105, 3643–3696.
116. Kharisov, B. I., Kharissova, O. V., Gutierrez, H. L., Méndez, U. O., *Ind. Eng. Chem. Res.*, **2009**, 48, 572–590.
117. Yang, W., Thordarson, P., Gooding, J. J., Ringer, S. P., Braet, F., *Nanotechnology*, **2007**, 18, 1–12.
118. Georgakilas, V., Otyepka, M., Bourlinos, A. B., Chandra, V., Kim, N., Kemp, K. C., Hobza, P., Zboril, R., Kim., K. S., *Chem. Rev*., **2012**, 112, 6156–6214.
119. Hirsch, A., Vostrowsky, O., in Functional Molecular Nanostructures, *Topics in Current Chemistry*, Schlüter, A. D., Ed., Springer, vol. 245, pp. 193–237, 2005.
120. Zhu, S.-E., Li, F., Wang, G.-W., *Chem. Soc. Rev*., **2013**, 42, 7535–7570.
121. Chen, J., Hammon, M. A., Hu, H., Chen, Y. S., Rao, A. M., *Science*, **1998**, 282, 95–98.
122. Bahr, J. L., Tour, J. M., *J. Mater. Chem*., **2002**, 12,1952–1958.
123. Burghard, M., *Surf. Sci. Rep.*, **2005**, 58, 1–109.
124. Singh, P., Campidelli, S., Giordani, S., Bonifazi, D., Bianco, A., Prato, M. *Chem. Soc. Rev*. **2009**, 38, 2214–2230.
125. Coleman, K. S., *Annu. Rep. Prog. Chem., Sect. A*, **2008**, 104, 379–393.
126. Sgobba, V., Guldi, D. M., *Chem. Soc. Rev*., **2009**, 38, 165–184.
127. Mann, J. A., Dichtel, W. R., *J. Phys. Chem. Lett*., **2013**, 4, 2649–2657.

128. Yoshimoto, S., Itaya, K., *J. Porphyrins Phthalocyanines*, **2007**, 11, 313–333.
129. Li, M., Ishihara, S., Ji, Q., Akad, M., Hill, J. P., Ariga, K., *Sci. Technol. Adv. Mater*., **2012**, 13, 1–14.
130. Kennedy, R. D., Halim, M., Khan, S. I., Schwartz, B. J., Tolbert, S. H., Rubin, Y., *Chem. Eur. J*., **2012**, 18, 7418–7433.
131. Jeon, I.-Y., Chang, D. W., Kumar, N. A., Baek, J. B., in Carbon Nanotubes – Polymer Nanocomposites, *Functionalization of Carbon Nanotubes*, Yellampalli, S., Ed., InTech, Chapter 5, 2011.
132. Radivojevic, I., Varotto, A., Farley, C., Drain, C. M., *Energy Environ. Sci*., **2010**, 3, 1897–1909.
133. Malig, J., Jux, N., Kiessling, D., Cid, J.-J., Vázquez, P., Torres, T., Guldi, D. M., *Angew. Chem. Int. Ed*., **2011**, 50, 3561–3565.
134. Zhao, B., Hu., H., Haddon, R. C., *Adv. Funct. Mater*., **2004**, 14, 71–76.
135. Campidelli, S., Sooambar, C., Diz, E. L., Ehli, C., Guldi, D. M., Prato, M., *J. Am. Chem. Soc*., **2006**, 128, 12544–12552.
136. Tasis, D., Tagmatarchis, N., Bianco, A., Prato, M., *Chem. Rev*., **2006**, 106, 1105–1136.
137. Krueger, A., Carbon Materials and Nanotechnology, WILEY-VCH Verlag GmbH & Co. KGaA, Weinheim, 2010.
138. Ragoussi, M. E., Malig, J., Katsukis, G., Butz, B., Spiecker, E., de la Torre, G., Torres, T., Guldi, D. M., *Angew. Chem. Int. Ed*., **2012**, 51, 6421–6425.
139. Strano, M. S., Dyke, C. A., Ursey, M. L., Barone, P. W., Allen, M. J., Shan, H., Kittrell, C., Hauge, R. H., Tour, J. M., Smalley, R. E., *Science*, **2003**, 301, 1519–1522.
140. Chen, Z., Thiel, W., Hirsch, A., *Chem. Phys. Chem*., **2003**, 1, 93–97.
141. Banerjee, S., Hemraj-Benny, T., Wong, S. S., *Adv. Mater*., **2005**, 17, 17–29.
142. de la Torre, G., Bottari, G., Sekita, M., Hausmann, A., Guldi, D. M., Torres, T., *Chem. Soc. Rev*., **2013**, 42, 8049–8105.
143. Britz, D. A., Khlobystov, A. N., *Chem. Soc. Rev*., **2006**, 35, 637–659.
144. Liu, J. Q., Xiao, T., Liao, K., Wu, P. *Nanotechnology*, **2007**, 18, 165701–165706.
145. Chen, R. J., Zhang, Y., Wang, D., Dai, H., *J. Am. Chem. Soc*., **2001**, 123, 3838–3839.

146. Ehli, C., Guldi, D. M., Herranz, M. A., Martín, N., Campidelli, S., Prato, M., *J. Mater. Chem*. **2008**, 18, 1498–1503.
147. Guldi, D. M., Rahman, G. M. A., Jux, N., Tagmatarchis, N., Prato, M., *Angew. Chem. Int. Ed*., **2004**, 43, 5526–5530.
148. Guldi, D. M., Rahman, G. M. A., Jux, N., Balbinot, D., Tagmatarchisc, D., Prato, M., *Chem. Commun*., **2005**, 2038–2040.
149. Chitta, R., Sandanayaka, A. S. D., Schumacher, A. L., D'Souza, L., Araki, Y., Ito, O., D'Souza, F., *J. Phys. Chem. C*., **2007**, 111, 6947–6955.
150. Ehli, C., Rahman, G. M. A., Jux, N., Balbinot, D., Guldi, D. M., Paolucci, F., Marcaccio, M., Paolucci, D., Melle-Franco, M., Zerbetto, F., Campidelli, S., Prato, M., *J. Am. Chem. Soc*., **2006**, 128, 11222–11231.
151. Kavakka, J. S., Heikkinen, S., Kilpeläinen, I., Mattila, M., Lipsanen, H., Helaja, J., *Chem. Commun*., **2007**, 519–521.
152. Guldi, D. M., Menna, E., Maggini, M., Marcaccio, M., Paolucci, D., Paolucci, F., Campidelli, S., Prato, M., Rahman, G. M. A., Chergna, S., *Chem. Eur. J*., **2006**, 12, 3975–3983.
153. Inokuma, Y., Osuka, A., *Dalton Trans.*, **2008**, 2517–2526.
154. Boul, P. J., Cho, D. G., Rahman, G. M. A., Marquez, M., Ou, Z., Kadish, K. M., Guldi, D. M., Sessler, J. L., *J. Am. Chem. Soc*., **2007**, 129, 5683–5687.
155. Komatsu, N., in Heterocyclic Supramolecules I, Topics in Heterocyclic Chemistry, *Heterocyclic Supramolecular Chemistry of Fullerenes and Carbon Nanotubes*, Matsumoto, K., Ed., Springer, vol. 17, pp. 161–198, 2008.
156. Geng, J., Ko, Y. K., Youn, S. C., Kim, Y.-H., Kim, S. A., Jung, D.-H., Jung, H.-T., *J. Phys. Chem. C.*, **2008**, 112, 12264–12271.
157. Guo, Z., Mao, J., Ouyang, Q., Zhu, Y., He, L., Lv, X., Liang, L., Ren, D., Chen, Y., Zheng, J., *J. Dispersion Sci. Technol.*, **2010**, 31, 57–61.
158. Gros, C. P., Brisach, F., Meristoudi, A., Espinosa, E., Guilard, R., Harvey, P. D., *Inorganic Chemistry*, **2009**, 48 2571–2582.
159. Chichak, K. S., Star, A., Altoé, M. V. P., Stoddart, J. F., *Small*, **2005**, 1, 452–461.
160. Spänig, F., López-Duarte, I., Fischer, M. K. R., Martínez-Díaz, M. V., Bäuerle, P., Torres, T., Guldi, D. M., *J. Mater. Chem*., **2011**, 21, 1395–1403.

161. Bartelmess, J., Ehli, C., Cid, J.-J., García-Iglesias, M., Vázquez, P., Torres, T., Guldi, D. M., *Chem. Sci.*, **2011**, 2, 652–660.
162. Chidawanyika, W., Nyokong, T., *Carbon*, **2010**, 48, 2831–2838.
163. Moeno, S., Nyokong, T., *J. Photochem. Photobiol., A*, **2009**, 201, 228–236.
164. Berber, G., Cammidge, A. N., Chambrier, I., Cook, M. J., Hough, P. W., *Tetrahedron Lett.*, **2003**, 44, 5527–5529.
165. Cammidge, A. N., Berber, G., Chambrier, I., Hough, P. W., Cook, M. J., *Tetrahedron*, **2005**, 61, 4067–4074.
166. Rodríguez-Morgade, M. S., Torres, T., Atienza-Castellanos, C., Guldi, D. M., *J. Am. Chem. Soc*., **2006**, 128, 15145–15154.
167. Silva, S., Pereira, P. M. R., Silva, P., Paz, F. A. A., Faustino, M. A. F., Cavaleiro, J. A. S., Tomé, J. P. C., *Chem. Commun.*, **2012**, 48, 3608–3610.
168. Pereira, P. M. R., Carvalho, J. J., Silva, S., Cavaleiro, J. A. S., Schneider, R. J., Fernandes, R., Tomé, J. P. C., *Org. Biomol. Chem.*, **2014**, 12, 1804–1811.
169. Mantareva, V., Kussovski, V., Angelov, I., Borisova, E., Avramov, L., Schnurpfeild, G., Wöhrle, D., *Bioorg. Med. Chem.*, **2007**, 15, 4829–4835.
170. Boyle, R. W., Leznoff, C. C., van Lier, J. E., *Br J. Cancer.*, **1993**, 67, 1177–1181.
171. Lv, F., Cao, B., Cui, Y., Liu, T., *Molecules*, **2012**, 17, 6348–6361.
172. Gomes, M. C., Woranovicz-Barreira, S. M., Faustino, M. A. F., Fernandes, R., Neves, M. G. P. M. S., Tomé, A. C., Gomes, N. C. M., Almeida, A., Cavaleiro, J. A. S., Cunha, Â., Tomé, J. P. C., *Photochem. Photobiol. Sci*., **2011**, 10, 1735–1743.
173. Pereira, J. B., Carvalho, E. F. A., Faustino, M. A. F., Neves, M. G. P. M. S., Cavaleiro, J. A. S., Gomes, N. C. M., Cunha, A., Almeida, A., Tomé, J. P. C., *Photochem. Photobiol*., **2012**, 88, 537–547.
174. Ribeiro, A. O., Tomé, J. P. C., Neves, M. G. P. M. S., Tomé, A. C., Cavaleiro, J. A. S., Serra, O. A., Torres, T., *Tetrahedron Lett.*, **2006**, 47, 6129–6132.
175. Silva, J. N., Silva, A. M. G., Tomé, J. P. C., Ribeiro, A. O., Domingues, M. R. M., Cavaleiro, J. A. S., Silva, A. M. S., Neves, M. G. P. M. S., Tomé, A. C., Serra, O. A., Bosca, F., Filipe, P., Santuse, R., Morliere, P., *Photochem. Photobiol. Sci.*, **2008**, 7, 834–843.

176. Bonnett, R., in Chemical Aspects of Photodynamic Therapy, *Singlet Oxygen*, Gordon and Breach Science Publishers: Amesterdam, Netherlands, vol. 1, Chapter 3, 39–56, 2000.
177. Nyman, E. S., Hynninen, P. H., *J. Photochem. Photobiol. B*, **2004**, 73, 1–28.
178. Ethirajan, M., Chen, Y., Joshi, P., Pandey, R. K., *Chem. Soc. Rev*., **2011**, 40, 340–362.
179. Mroz, P., Yaroslavsky, A., Kharkwal, G. B., Hamblin, M. R., *Cancers*, **2011**, 3, 2516–2539.
180. Almeida, A., Cunha, Â., Faustino, M. A. F., Tomé, A. C., Neves, M. G. P. M. S., in Photodynamic Inactivation of Microbial Pathogens, Medical and Environmental Applications, *Porphyrins as Antimicrobial Photosensitizing Agents*, Hamblin, M. R., Jori, G., Eds., RSC Publishing: Cambridge, England, Chapter 5, pp. 83–160, 2011.
181. Gad, F., Zahra, T., Hasan, T., Hamblin, M. R., *Antimicrob. Agents Chemother*., **2004**, 48, 2173–2178.
182. Tomé, J. P. C., Neves, M. G. P. M. S., Tomé, A. C., Cavaleiro, J. A. S., Soncin, M., Magaraggia, M., Ferro, S., Jori, G., *J. Med. Chem*., **2004**, 47, 6649–6652.
183. Nagata, J. Y., Hioka, N., Kimura, E., Batistela, V. R., Terada, R. S. S., Graciano, A. X., Baesso, M. L., Hayacibara, M. F., *Photodiagn. Photodyn. Ther.*, **2012**, 9, 122–131.
184. CIBA Foundation Symposium, Photosensitizing Compounds: Their Chemistry, Biology and Clinical Use; Bock, G., Harnett, S., Eds., John Wiley: Chichester, UK, vol. 727, pp. 1–32 and 60–130, 2008.
185. Dumoulin, F., Durmuş, M., Ahsen, V., Nyokong, T., *Coord. Chem. Rev*., **2010**, 254, 2792–2847.
186. Kussovski, V., Mantareva, V., Angelov, I., Orozova, P., Wöhrle, D., Schnurpfeil, G., Borisova, E., Avramov, L., *FEMS Microbiol. Lett*., **2009**, 294, 133–140.
187. Jemal, A., Siegel, R., Ward, E., Murray, T., Xu, J. Q., Thun, M. J., *CA: Cancer J. Clin*., **2007**, 57, 43–66.
188. Sallas, F., Darcy, R., *Eur. J. Org. Chem.*, **2008**, 957–969.
189. Cheng, Y., Samia, A. C., Meyers, J. D., Panagopoulos, I., Fei, B., Burda, C., *J. Am. Chem. Soc.*, **2008**, 130, 10643–10647.

190. Ma, J., Chen, J.-Y., Idowu, M., Nyokong, T., *J. Phys. Chem. B*, **2008**, 112, 4465–4847.
191. Liu, W., Jensen, T. J., Fronczek, F. R., Hammer, R. P., Smith, K. M., Vicente, M. G. H., *J. Med. Chem.*, **2005**, 48, 1033–1041.
192. Verdree, V. T., Pakhomov, S., Su, G., Allen, M. W., Countryman, A. C., Hammer, R. P., Soper, S. A., *J. Fluoresc.*, **2007**, 17, 547–563.
193. Fu, X.-J., Fang, Y., Yao, M., *BioMed Research International*, **2013**, 2013, 1–9.
194. Niedre, M., Patterson, M. S., Wilson, B. C., *Photochem. Photobiol*., **2002**, 75, 382–391.
195. Lovell, J. F., Liu, T. W. B., Chen, J., Zheng, G., *Chem. Rev.*, **2010**, 110, 2839–2857.
196. Park, S. Y., Baik, H. J., Oh, Y. T., Oh, K. T., Youn, Y. S., Lee, E. S., *Angew. Chem. Int. Ed.*, **2011**, 50, 1644–1647.
197. Manthe, R. L., Foy, S. P., Krishnamurthy, N., Sharma, B., Labhasetwar, V., *Mol. Pharmaceutics*, **2010**, 7, 1880–1898.
198. Kaestner, L., Cesson, M., Kassab, K., Christensen, T., Edminson, P. D., Cook, M. J., Chambrier, I., Jori, G., *Photochem. Photobiol. Sci.*, **2003**, 2, 660–667.
199. Oliveira, K. T., Assis, F. F., Ribeiro, A. O., Neri, C. R., Fernandes, A. U., Baptista, M. S., Lopes, N. P., Serra, O. A., Iamamoto, Y., *J. Org. Chem.*, **2009**, 74, 7962–7965.
200. Králová, J., Bříza, T., Moserová, Dolenský, B., Vašek, P., Poučková, P., Kejík, Z., Kaplánek, R., Martásek, P., Dvořák, M., Král, V., *J. Med. Chem.*, **2008**, 51, 5964–5973.
201. Silva, J. N., Galmiche, A., Tomé, J. P. C., Boullier, A., Neves, M. G. P. M. S., Silva, E. M. P, Capiod, J. C., Cavaleiro, J. A. S., Santus, R., Maziere, J. C., Filipe, P., Morliere, P., *Biochem. Pharmacol.*, **2010**, 80, 1373–1385.
202. Celli, J. P., Spring, B. Q., Rizvi, I., Evans, C. L., Samkoe, K. S., Verma, S., Pogue, B. W., Hasan, T., *Chem. Rev.*, **2010**, 110, 2795–2838.
203. Carvalho, C. M. B., Tomé, J. P. C., Faustino, M. A. F., Neves, M. G. P. M. S., Tomé, A. C., Cavaleiro, J. A. S., Costa, L., Alves, E., Oliveira, A., Cunha, Â., Almeida, A., *J. Porphyrins Phthalocyanines*, **2009**, 13, 574–577.
204. Singh, S., Aggarwal, A., Thompson, S., Tomé, J. P. C., Zhu, X., Samaroo, D., Vinodu, M., Gao, R., Drain, C. M., *Bioconjugate Chem.*, **2010**, 21, 2136–2146.

205. Vittar, N. B. R., Awruch, J., Azizuddinc, K., Rivarola, V., *The International Journal of Biochemistry & Cell Biology*, **2010**, 42, 1123–1131.
206. Chen, B., Pogue, B. W., Hasan, T., *Expert. Opin. Drug Deliv.*, **2005**, 2, 477–487.
207. Brady, C., Bell, S. E. J., Parsons, C., Gorman, S. P., Jones, D. S., McCoy, C. P., *J. Phys. Chem. B*, **2007**, 111, 527–534.
208. Mazzaglia, A., Micali, N., Scolaro, L. M., Sciortino, M. T., Sortino, S., Villari, V., *J. Porphyrins Phthalocyanines*, **2010**, 14, 661–677.
209. Nishiyama, N., Jang, W. D., Kataoka, K., *New J. Chem.*, **2007**, 31, 1074–1082.
210. Taquet, J.-P., Frochot, C., Manneville, V., Barberi-Heyob, M., *Curr. Med. Chem.*, **2007**, 14, 1673–1687.
211. Caughey, W. S., Raymond, L. D., Horiuchi, M., Caughey, B., *Proc. Natl. Acad. Sci. USA*, **1998**, 95, 12117–12122.
212. Vrouenraets, M. B., Visser, G. W. M., Snow, G. B., van Dongen, G. A. M. S., *Anticancer Res.*, **2003**, 23, 505–522.
213. Ragàs, X., He, X., Agut, M., Roxo-Rosa, M., Gonsalves, A. R., Serra, A. C., Nonell, S., *Molecules*, **2013**, 18, 2712–2725.
214. Lourenço, L. M. O., Fernandes, J. A., Neves, M. G. P. M. S., Cavaleiro, J. A. S., Tomé, J. P. C., Paz, F. A. A, *Acta Cryst*., **2011**, E67, o3157–o3158.
215. Han, Y., Bu, J., Zhang, Y., Tong, W., Gao, C., *Macromol. Biosci.*, **2012**, 12, 1436–1442.
216. Selbo, P. K., Weyergang, A., Eng, M. S., Bostad, M., Mælandsmo, G. M., Høgset, A., Berg, K., *J. Controlled Release*, **2012**, 159, 197–203.
217. Master, A. M., Rodriguez, M. E., Kenney, M. E., Oleinick, N. L., Gupta, A. S., *J. Pharm. Sci.*, **2010**, 99, 2386–2398.
218. Figueira, F., Cavaleiro, J. A. S., Tomé, J. P. C., *J. Porphyrins Phthalocyanines*, **2011**, 15, 518–533.
219. Stranadko, E. F., Skobelkin, O. K. Vorozhtsov, G. N., Mironov, A. F., Markichev, N. A., Riabov, M. V., *Proc. SPIE*, **1996**, 2924, 298–304.
220. Vakoulovskaia, E. G., Chental, V. V., Abdoulin, N. A., Kuvshinov, Y. P., Tabolinovskaia, T. D., Edinak, N. J., Poddubny, B. K., Kondratjeva, T. T., Meerovich, G. A., Stratonnikov, A. A., Linkov, K. G., Agafonov, V. V., *Proc. SPIE*, **1997**, 3191, 232–236.

221. Sokolov, V. V., Chissov, V. I., Yakubovskaya, R. I., Filonenko, E. V., Sukhin, D. G., Nemtsova, E. R., Belous, T. A., Zharkova, N. N., *Proc. SPIE*, **1996**, 3191, 322–329.
222. Sokolov, V. V., Stranadko, E. F., Zharkova, N. N., Yakubovskaya, R. I., Filonenko, E. V., Astrakhankina, T. A., *Voprosy. Onkol.*, **1995**, 41, 134–138.
223. Budzinskaia, M. V., Likhvantseva, V. G., Shevchik, S. A., Loshchenov, V. B., Kuz'min, S. G., Vorozhtsov, G. N., *Vestn. Oftalmol.*, **2005**, 121, 13–16.
224. Lukyanets, E. A., *J. Porphyrins Phthalocyanines*, **1999**, 3, 424–432.
225. Ke, M. S., Xue, L., Feyes, D. K., Azizuddin, K., Baron, E. D., McCormick, T. S., Mukhtar, H., Panneerselvam, A., Schluchter, M.-D., Cooper, K. D., Oleinick, N. L., Stevens, S. R., *Photochem. Photobiol.*, **2008**, 84, 407–414.
226. Wainwright, M., Amaral, L., *Antibiotics*, **2013**, 2, 182–190.
227. Soares, A. R. M., Tomé, J. P. C., Neves, M. G. P. M. S., Tomé, A. C., Cavaleiro, J. A. S., Torres, T., *Carbohydr. Res.*, **2009**, 344, 507–510.
228. Soares, A. R. M., Neves, M. G. P. M. S., Santos, S. M., Tomé, J. P. C., Tomé, A. C., Cavaleiro, J. A. S., Torres, T., Domingues, M. R. M., *Rapid Commun. Mass Spectrom.*, **2013**, 27, 1019–1026.
229. Lo, P.-C., Chan, C. M. H., Liu, J.-Y., Fong, W.-P., Ng, D. K. P., *J. Med. Chem.*, **2007**, 50, 2100–2107.
230. Lyubimtsev, A., Iqbal, Z., Crucius, G., Syrbu, S., Ziegler, T., Hanack, M., *J. Porphyrins Phthalocyanines*, **2012**, 16, 434–463.
231. Spesia, M. B., Rovera, M., Durantini, E. N., *Eur. J. Med. Chem.*, **2010**, 45, 2198–2205.
232. Junqueira, J. C., Jorge, A. O. C., Barbosa, J. O., Rossoni, R. D., Vilela, S. F. G., Costa, F. A. C. B. P., Primo, L., Gonçalves, J. M., Tedesco, A. C., Suleiman, J. M. A. H., *Lasers Med. Sci.*, **2012**, 27, 1205–1212.
233. Spesia, M. B., Durantini, E. N., *J. Photochem. Photobiol., B*, **2013**, 125, 179–187.
234. Malik, Z., Ladan, H., Nitzan, Y., *J. Photochem. Photobiol. B*, **1992**, 14, 262–266.
235. Kuznetsova, N. A., Makarov, D. A., Kaliya, O. L., Vorozhtsov, G. N., *J. Hazard. Mater.*, **2007**, 146, 487–491.
236. Griffiths, J., Schofield, J., Wainwright, M., Brown, S. B., *Dyes Pigm.*, **1997**, 33, 65–78.

237. Minnock, A., Vernon, D. I., Schofield, J., Griffiths, J., Parish, J. H., Brown, S. B., *Antimicrob. Agents Chemother*., **2000**, 44, 522–527.
238. Vaara, M., *Microbiol. Rev*., **1992**, 56, 395–411.
239. Nikaido, H., Vaara. M., *Microbiol. Rev*., **1985**, 49,1–32.
240. Kuznetsova, N., Makarov, D., Yuzhakova, O., Strizhakov, A., Roumbal, Y., Ulanova, L., Krasnovsky, A., Kaliya, O., *Photochem. Photobiol. Sci*., **2009**, 8, 1724–1733.
241. Ernst, B., Hart, G. W., Sinaý, P., in Carbohydrates in Chemistry and Biology, *Part I: Chemistry of Saccharides: Chemical Synthesis of Glycosides and Glycomimetics*, Ernst, B., Hart, G. W., Sinay, P., Part I, Wiley-VCH, vols. 1 and 2, 2008.
242. Ferrier, R. J., in Carbohydrate Chemistry, *Monosaccharides, Disaccharides and Specific Oligosaccharides* (A Review of the Literature Publishing During 1998), Royal Society of Chemistry, vol. 32, 2001.
243. Nicolaou, K. C., Mitchell, H. J., *Angew. Chem. Int. Ed*., **2001**, 40, 1577–1624.
244. Seeberger, P. H., Werz, D. B., *Nature*, **2007**, 446, 1046–1051.
245. Galonic, D. P., Gin, D. Y., *Nature*, **2007**, 446, 1000–1008.
246. Mroz, P., Sharma, S. K., Zhiyentayev, T., Huang, Y.-Y., Hamblin, M. R., in Drug Delivery in Oncology: From Basic Research to Cancer Therapy, *Photosensitizer Targeting and Delivery*, Kratz, F., Senter, P., Steinhagen, H., John Wiley & Sons, vol. 2, pp. 1569–1604, 2011.
247. del Rey, B., Keller, U., Torres, T., Rojo, G., Agulló-López, F., Nonell, S., Marti, C., Brasselet, S., Ledoux, I., Zyss, J., *J. Am. Chem. Soc*., **1998**, 120, 12808–12817.
248. Claessens, C. G., González-Rodríguez, D., Torres, T., *Chem. Rev*., **2002**, 102, 835–853.
249. de la Escosura, A., Martínez-Díaz, M. V., Thordarson, P., Rowan, A. E., Nolte, R. J. M., Torres, T., *J. Am. Chem. Soc*., **2003**, 125, 12300–12305.
250. Guldi, D. M., Gouloumis, A., Vázquez, P., Torres, T., Georgakilas, V., Prato, M., *J. Am. Chem. Soc*., **2005**, 127, 5811–5813.
251. Zorlu, Y., Dumoulin, F., Bouchu, D., Ahsen, V., Lafont, D., *Tetrahedron Lett.*, **2010**, 51, 6615–6618.
252. Kurkov, S. V., Loftsson, T., *Int. J. Pharm.*, **2013**, 453, 167–180.
253. Leng, X., Choi, C.-F., Lo, P.-C., Ng, D. K. P., *Org. Lett*., **2007**, 9, 231–234.

254. Lau, J. T. F., Lo, P.-C., Tsang, Y.-M., Fong, W.-P., Ng, D. K. P., *Chem. Commun.*, **2011**, 47, 9657–9659.

Chapter 2

Decorating Graphene Nanosheets with Electron Accepting Pyridyl Phthalocyanines

2.1 Overview

Since the pioneering work of Novoselov *et al*. graphene is one of the first two-dimensional (2D) atomic crystals, which is readily available.[1,2] An overwhelming number of its properties including mechanical stiffness,[3,4] strength and elasticity – a Young's modulus of 1 TPa and intrinsic strength of 130 GPa[5,6], electrical and thermal conductivity, above 3,000 W mK^{-1},[7] among others, are simply outstanding, especially when compared to conventional materials. Taking the aforementioned features together, graphene bears great promises to replace existing materials in emerging applications.[8]

To meet the full potential of graphene in general, and the requirements for specific applications in particular, dozens of methods for preparing graphene featuring various dimensions, shapes and quality, are either in use or under development.[9] A leading example is the micromechanical exfoliation of graphite, which yields high-quality single-layer graphene with room-temperature electron and hole mobility up to 15000 cm^2/Vs,[10] but comes short of scalability.

Alternatively, bottom-up fabrication strategies of graphene by means of, for example, epitaxial growth[11] and/or chemical vapour deposition[12] opened the doors for technological applications. This approach can be used to prepare transparent conductive layers[13] for photonics[14] and nanoelectronic systems.[15] Only a few substrates such as copper and others are, however, suitable for the growth of graphene films and a fairly problematic transfer step is required to facilitate combination with other materials.[16]

In stark contrast, liquid-phase exfoliation of graphite is a widespread method that bears great potential for mass-production of graphene.[17] Liquid-phase exfoliation is currently been conducted in the area of coatings,[18] composites,[19] conductive inks,[20] transparent conductive layers,[21] and energy generation/storage.[22] As such, it is based on bringing graphite with the aid of sonication into contact with a solvent, which, in turn, assists in disintegrating graphite into individual platelets. Exfoliation efficiencies and yields are, however, rather moderate in pure solvents, due to high activation barrier and high thermodynamic stability of graphite.[17,23]

Somewhat related is the approach of transforming graphite into graphite oxide by means of harsh oxidation, dispersing the resulting flakes by sonication, and

re-reducing it back to graphene.[24] Although this method guarantees processability on one hand, and covalent functionalization on the other, it comes along with a significant alteration of the physicochemical properties of pristine graphene.[25-27] To avoid such setbacks and to secure the efficient exfoliation of graphite the necessity of employing molecular building blocks in the form of amphiphilic intercalators has evolved.[28,29]

One key aspect in graphene research is to tune its electronic properties by chemical doping with molecular building blocks, while preserving its unique band structure.[30] Importantly, covalent methodologies affect the electronic structure of graphene and in that way potentially reduce the charge carrier mobility. On the contrary, noncovalent strategies not only tune the electronic properties of graphene but also minimize the damage to the sp^2-conjugated lattice.[31] Here, relevant advances are particularly in the area of self-ordering/self-assembling,[32,33] π-stacking,[34,35] as well as charge transfer[36,37] interactions. Such approach is particularly useful to link photo- and/or redoxactive chromophores to graphene, and, thereby, adding light harvesting and electron transfer features. To this date, a fairly large number of molecular building blocks, such as porphyrins,[27] porphycenes,[30] phthalocyanines (Pcs),[31] perylenes,[38,39] among others, have successfully been immobilized onto the basal plane of graphene.

In the current study, we focus on Pc/graphene nanohybrids[40] as promising electron donor-acceptor building blocks in, for example, solar energy conversions schemes. This constitutes a contemporary research topic, especially in terms of producing innovative materials of greatly reduced sizes.[41] In this context, we report herein the immobilization of pyridyl-appended Pcs **2.6**-**2.8** (Figure 2.1) onto graphene. The unique absorption features of Pcs throughout the solar spectrum render them well suited for our proposal.[42,43] Furthermore, in contrast to the standard tetra-*tert*-butyl phthalocyanines (ZnPcs), the newly synthesized pyridyl Pcs show electron accepting properties.

Usually, phthalocyanines are poorly soluble and tend to aggregate in many solvents. Nevertheless, a careful selection of peripheral substituents may minimized/overcome these disadvantages. The synthesis of all the target compounds follows previous procedures already reported by us.[44]

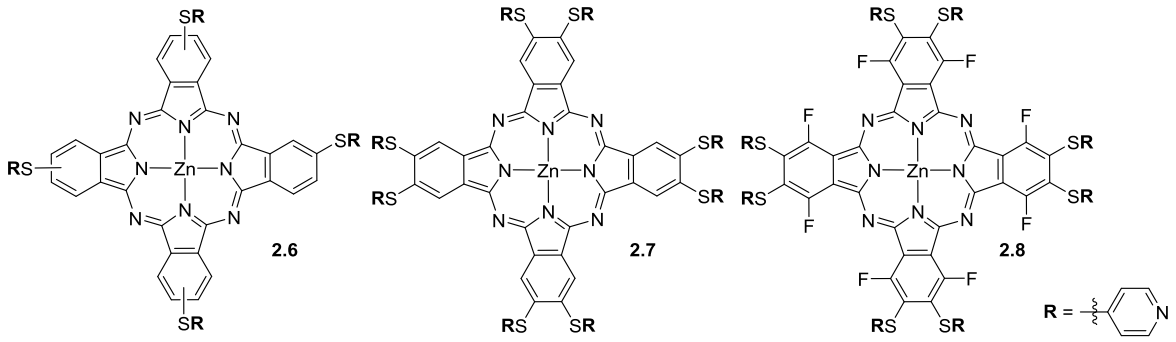

Figure 2.1 Structures of thiopyridylphthalocyanines **2.6**-**2.8**.

2.2 Syntheses of thiopyridylphthalocyanines

The thiopyridylphthalocyanines **2.6**-**2.8** were chosen for the proposed study not only due to the unique optical features of this type of macrocycles covering a large range of the UV-Vis spectrum, but also due to the presence of the mercaptopyridyl groups, which can favour noncovalent interactions with the metal present in the macrocycle core of neighbour molecules.[45] These interactions can approach the Pc macrocycles around the graphene nanosheets providing a compact assembly, not only due to the approximation of these molecules but also by the π-π stacking interactions between the macrocycle and graphene structure.

2.2.1 Syntheses of mono- and di-thiopyridylphthalonitrile precursors

The access to the innovative pyridyl-phthalocyanines **2.6** and **2.7** required the previous synthesis of the adequate the thiopyridylphthalonitriles **2.3** and **2.5** (Scheme 2.1). The mono-thiopyridylphthalonitrile **2.3** was obtained by nucleophilic substitution of the nitro group in 4-nitrophthalonitrile **2.1** by the sulphanyl group of the mercaptopyridine **2.2**. The reaction was carried out in dimethylformamide (DMF) under basic conditions for 5 h at 60 ºC. The evolution of the reaction was followed by thin-layer chromatography (TLC) and the desired product **2.3** (70 % yield) was directly obtained from the reaction medium by addition of water.

A similar procedure was used in the synthesis of the di-thiopyridylphthalonitrile **2.5** but the coupling involved 4,5-dichlorophthalonitrile (**2.4**) and 4-mercaptopyridine (Scheme 2.1). In this case, the reaction was carried out at room temperature and after stirring for 2 h,

it was confirmed by TLC the presence of the di-thiopyridylphthalonitrile **2.5**. The crude product was precipitated from the reaction medium with water, filtered and washed several times with water. Finally, product **2.5** was isolated in 50% of yield, after crystallization from a mixture of MeOH/CH_2Cl_2.

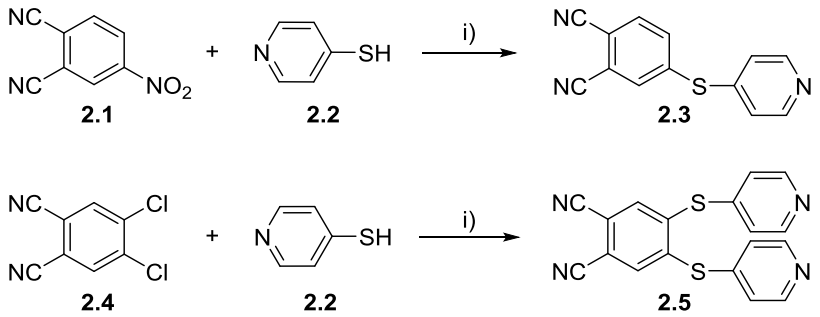

Scheme 2.1

The thiopyridylphthalonitrile **2.3** was previously characterized by ^{1}H, ^{13}C NMR, and mass spectroscopy (MS) using electrospray (ESI) in positive mode. The 7 aromatic protons distributed between both aromatic rings appear at δ 7.35, 7.91, 8.15, 8.28 and 8.53 ppm (Figure 2.2). The pyridyl protons *ortho*-H^d and *meta*-H^e appear as two doublet of doublets at δ 7.35 and 8.53 ppm, respectively, due to the different shielding influenced mainly by the nitrogen atom.

Figure 2.3 shows the ^{1}H NMR spectrum of the symmetrical phthalonitrile **2.5**, where the resonance signals of the pyridyl protons *ortho*-H^b and *meta*-H^c appear as two doublet of doublets respectively at δ 7.25 and 8.67 ppm. The resonances of the phthalonitrile ring H^a are situated as a singlet at δ 7.57 ppm. The structures of the 4-thiopyridylphthalonitrile (**2.3**) and 4,5-dithiopyridylphthalonitrile (**2.5**) were also confirmed by ESI-MS presenting, respectively, the molecular ion peaks $[M+H]^+$ at *m/z* 237 and 347.

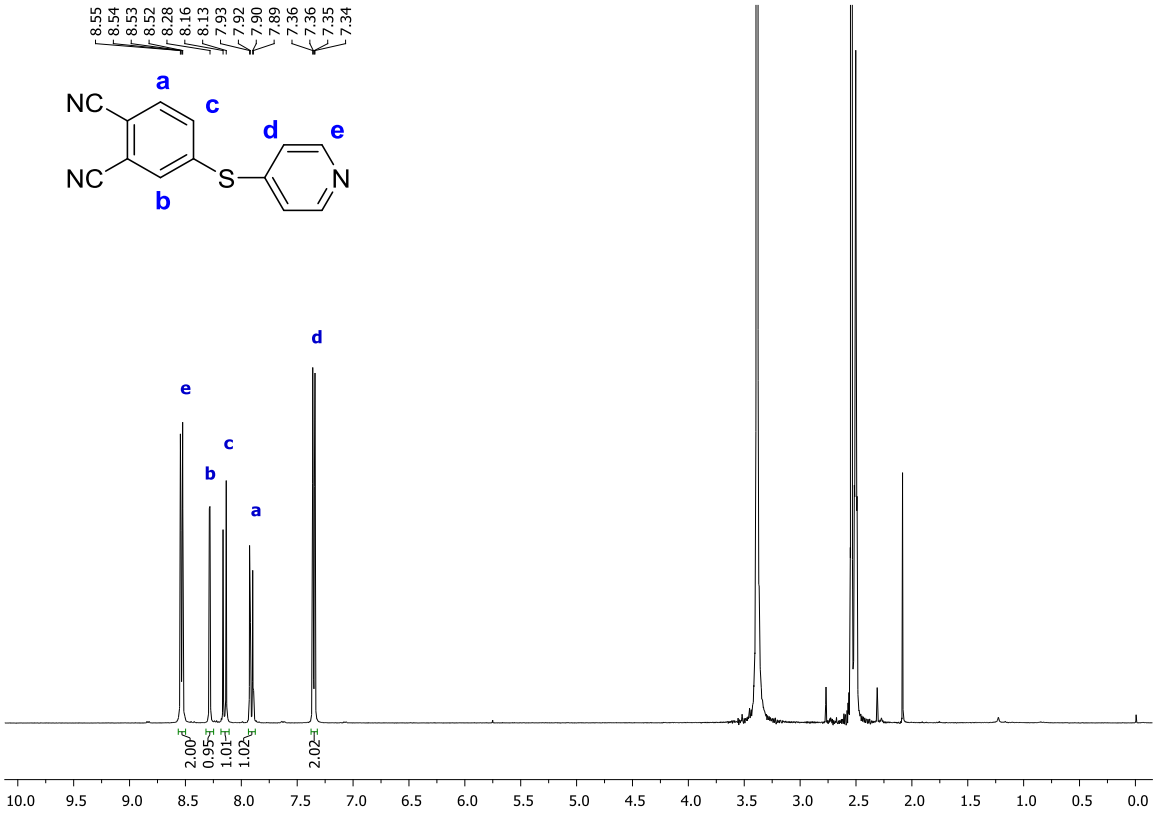

Figure 2.2 ^{1}H NMR spectrum of compound **2.3** in DMSO-d_6.

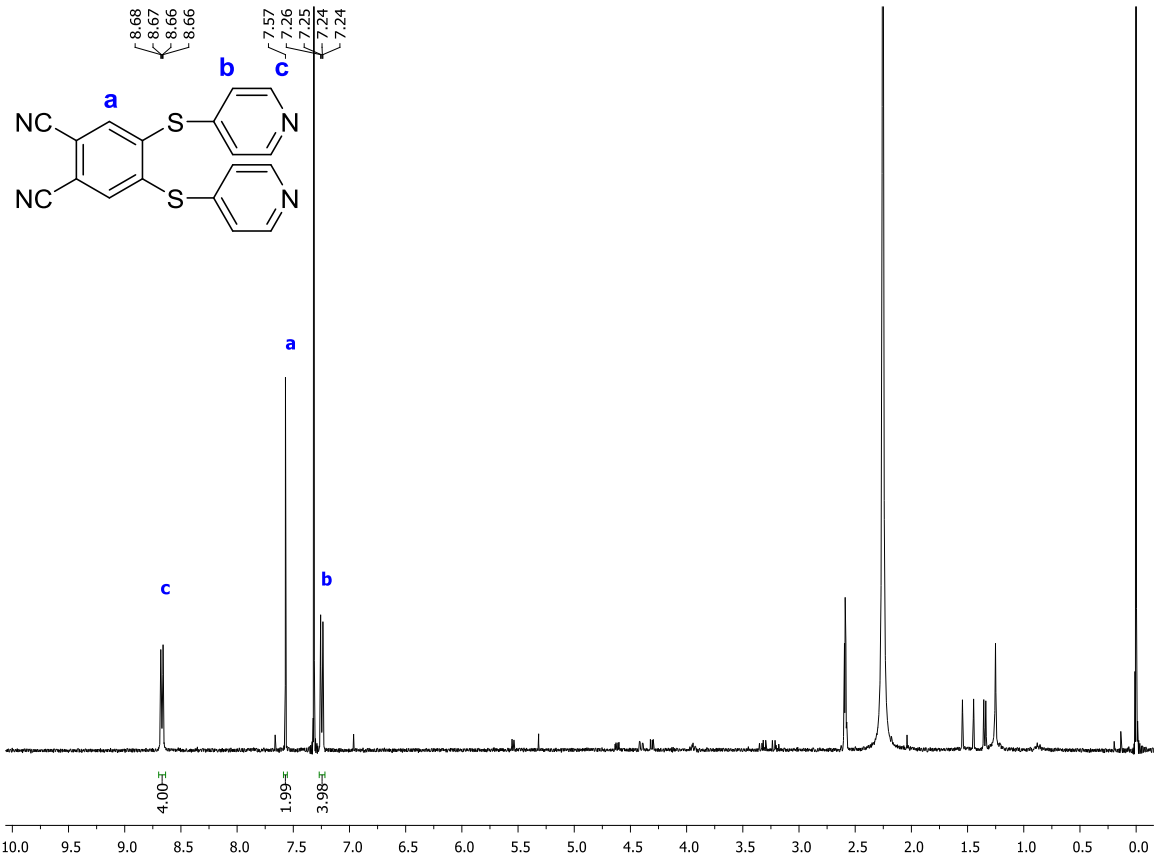

Figure 2.3 ^{1}H NMR spectrum of compound **2.5** in $CDCl_3$.

2.2.2 Syntheses and characterization of the thiopyridylphthalocyanines

The Pc **2.6** was synthesized *via* cyclotetramerization of 4-thiopyridylphthalonitrile **2.3** in dimethylaminoethanol (DMAE) at 140 ºC, in the presence of anhydrous zinc(II) chloride ($ZnCl_2$) (Scheme 2.2). The reaction mixture was maintained under reflux overnight and then it was added methanol. The resulting precipitated was washed several times with methanol and water in order to remove the excess of metallic $ZnCl_2$ salt. After drying under vacuum, product **2.6** was obtained in 82% yield.

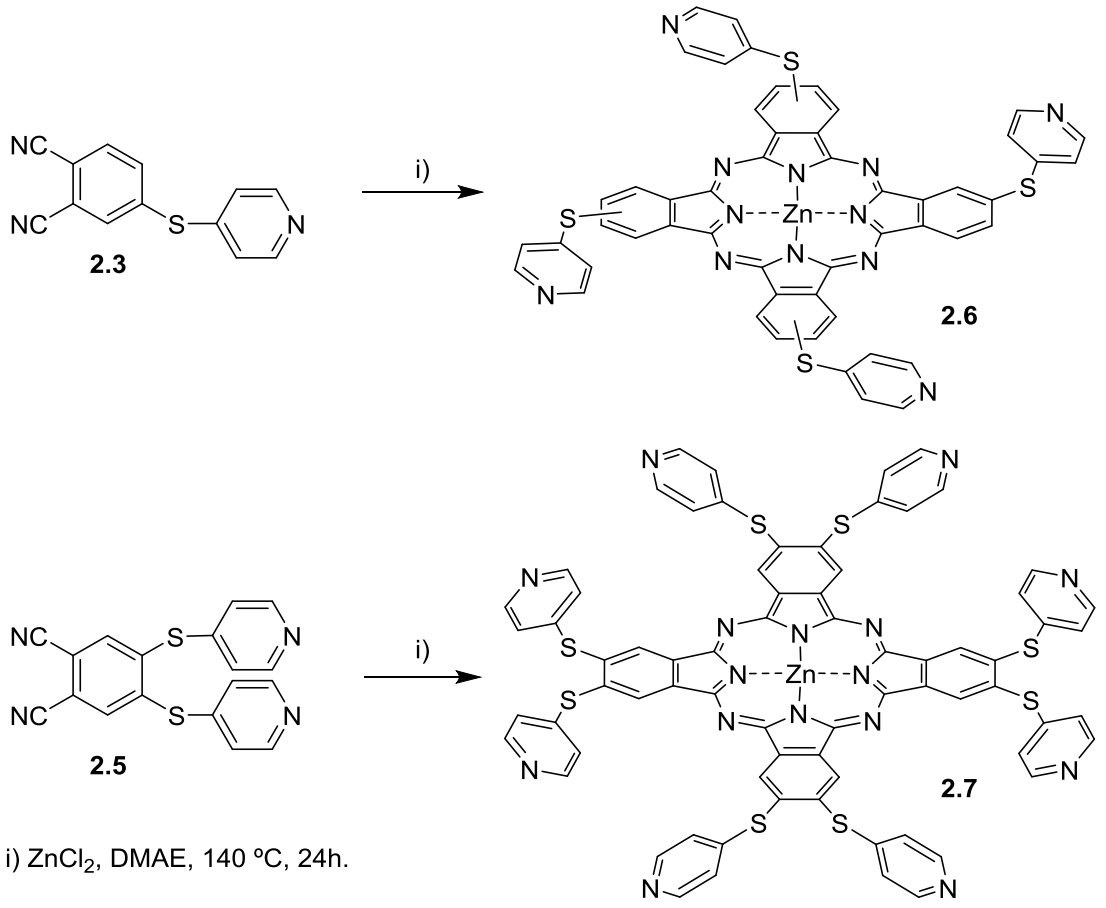

Scheme 2.2

The octa-substituted Pc **2.7** was obtained by self-tetramerization of 4,5-dithiopyridylphthalonitrile (**2.5**) using a synthetic procedure similar to the one outlined above for **2.6** (Scheme 2.2); this Pc was isolated in 85% yield after purification.

The central zinc metal was chosen to favour noncovalent interactions with the pyridyl assemblies, but also to tune the features of the final materials. The photophysical properties of metallated Pcs are influenced by the metal nature. Closed shell diamagnetic

ions, like Zn^{2+}, Ga^{3+} and Si^{4+}, give to Pc complexes excellent properties such as high triplet yields and long lifetimes.[46] In particular, ZnPcs have been extensively studied because of d^{10} configuration of the central Zn^{2+}, which contributes for simple optical spectra. ZnPcs have an intense absorption at the red-visible region and high singlet and triplet yields, making them valuable photosensitizers for PDT and for supramolecular applications.[47,48]

The ^{1}H NMR spectrum of **2.6** illustrate all proton resonances as multiplets for the α- and β-aromatic proton atoms of the Pc macrocycle between δ 8.88–9.45 and 8.26–8.48 ppm, respectively, corresponding to the 8 α-protons α-$H^{a,b}$ and 4 β-protons β-H^{c}. Furthermore, the proton resonances of the mercaptopyridyl moiety are more shielded than the macrocycle aromatic α-protons and consequently the *ortho*-H^{d} and *meta*-H^{e} protons appear at δ 7.74–8.00 and 8.52–8.79 ppm, respectively (Figure 2.4).

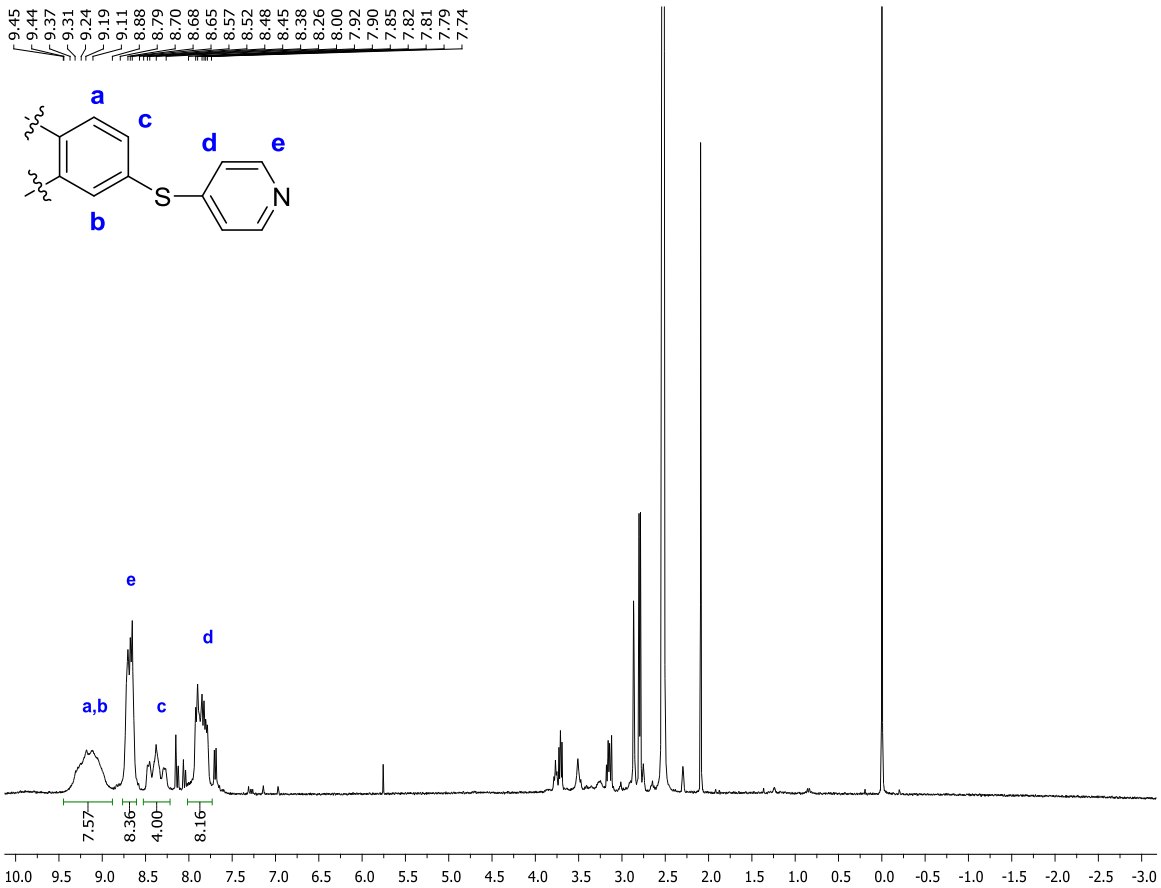

Figure 2.4 ^{1}H NMR spectrum of compound **2.6** in DMSO-d_6 + TFA.

The ^{1}H NMR spectrum of tetra-substituted Pc derivative **2.6** shows a complex pattern due to the presence of the different positional isomers resulting from possible

combinations of the mercaptopyridyl moiety on the β-positions of the four isoindole units of the macrocycle.

In ^{1}H NMR spectrum of Pc **2.7** bearing mercaptopyridyl groups in both β-positions, the resonances due to the 16 *ortho*-H^{b} and 16 *meta*-H^{c} proton of the pyridyl moiety were observed at δ 8.02 and 8.70 ppm, respectively. Moreover, it was also observed a singlet corresponding to the 8 α-H^{a} of the Pc ring at δ 10.15 ppm (Figure 2.5); these protons suffer a deshielding comparatively with the analogous ones of the Pc **2.6** (8.88 – 9.45 ppm). The MALDI-TOF-MS spectra confirmed the structures of **2.6** and **2.7** showing the presence of the protonated molecular ion peaks $[M+H]^{+}$at *m/z* 1013 and 1448, respectively.

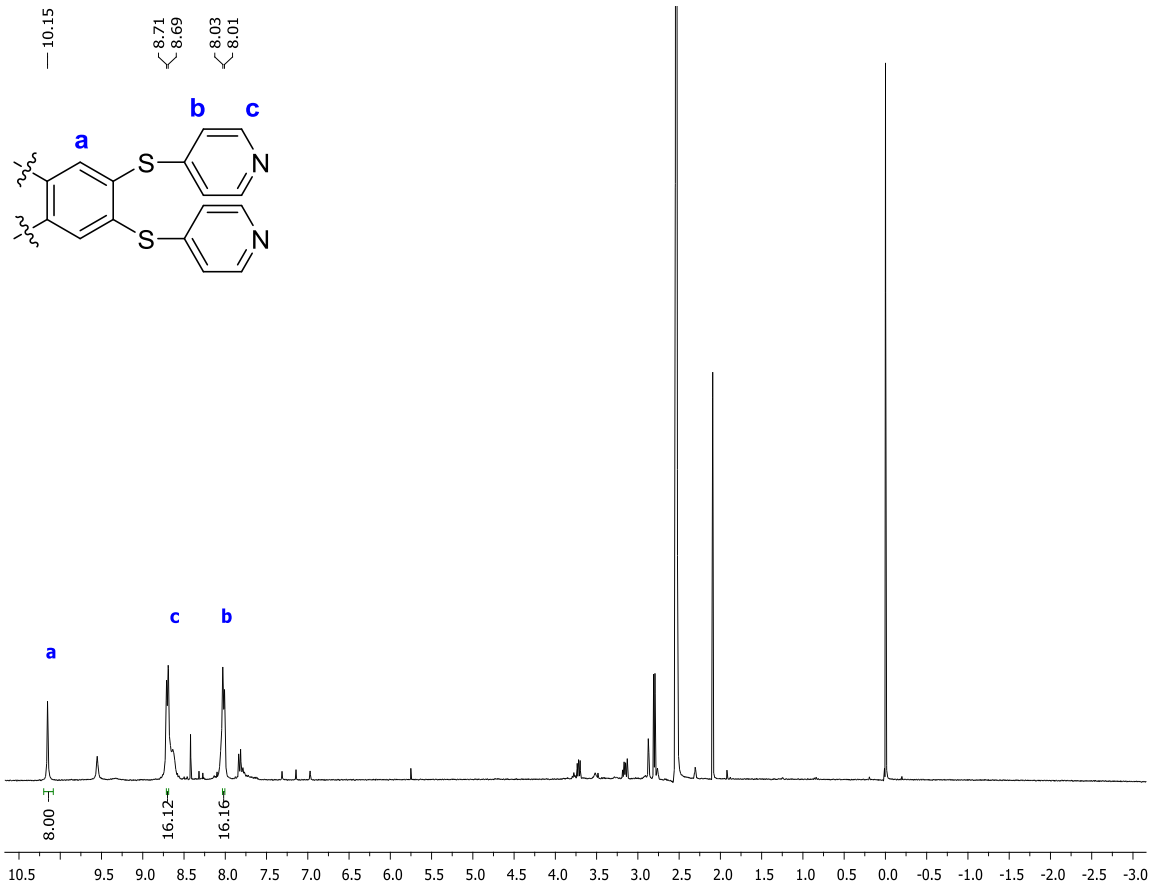

Figure 2.5 ^{1}H NMR spectrum of compound **2.7** in DMSO-d_6 + TFA.

The octa-substituted Pc **2.8** also considered in the preparation of graphene nanohybrids was synthesized from the commercial available hexadecafluorophthalocyaninato zinc(II) (**ZnPcF$_{16}$**) and mercaptopyridine (Scheme 2.3). In Pc **2.8** both α-positions of the Pc macrocycle bear fluorine atoms instead of hydrogen atoms as in **2.7.** It will be important to compare how the main spectroscopic features of

these two octa-substituted Pcs are affected by the presence or absence of the electronegative fluorine atoms.

The nucleophilic substitutions of all 8 β-fluorine atoms by mercaptopyridine (10 equivalents) took place overnight at room temperature in basic conditions. The reaction was ended by precipitation in water and the resulting green solid, after being filtered and washed several times with water and acetone, was identified as Pc **2.8** (89% yield).

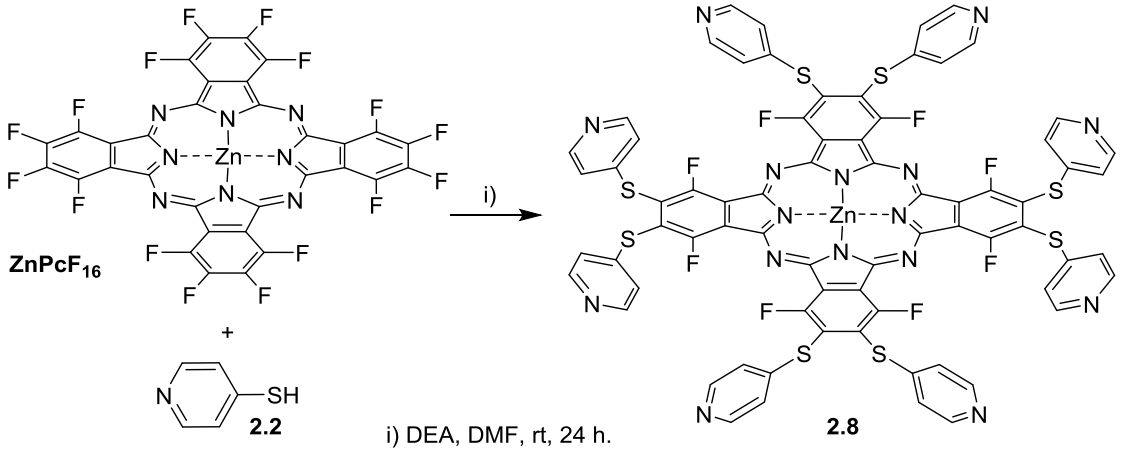

Scheme 2.3

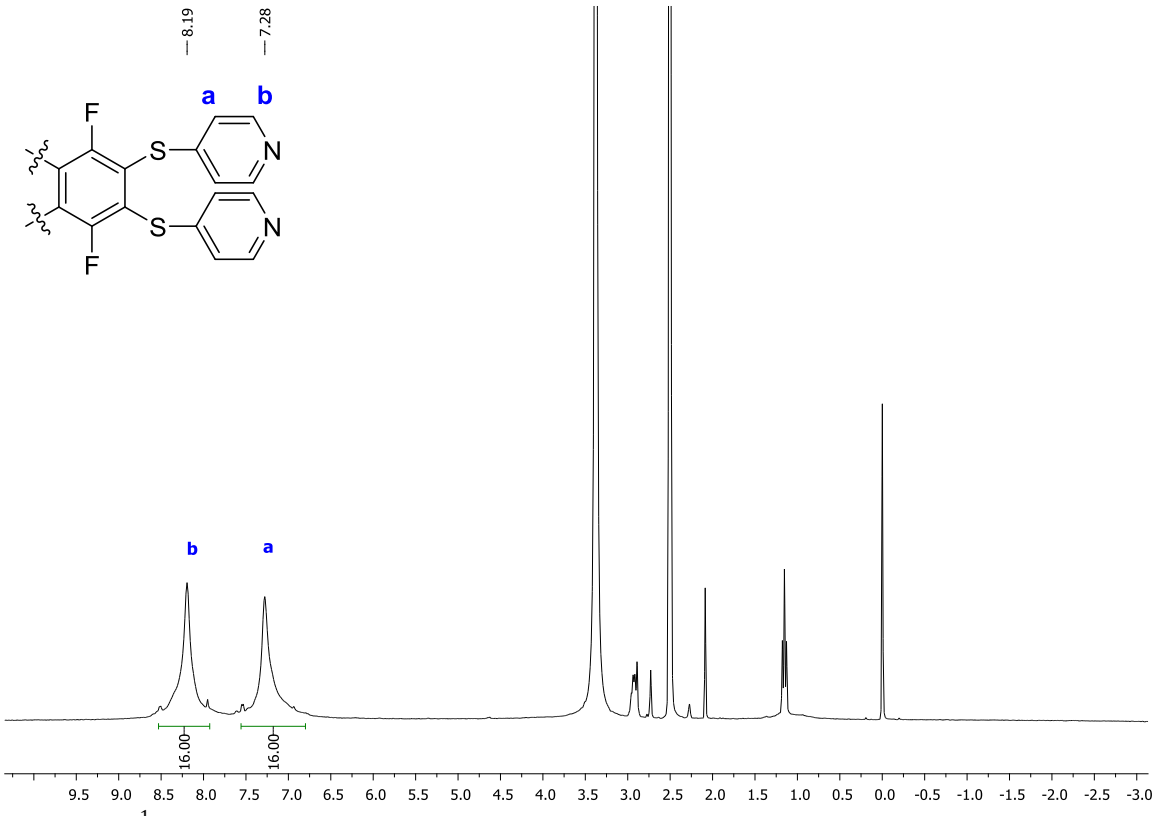

Figure 2.6 ^{1}H NMR spectrum of compound **2.8** in DMSO-d_6 + TFA.

The ^{1}H NMR spectrum of **2.8** shows the resonances of the *ortho*-H^{a} and *meta*-H^{b} protons of the peripheral pyridyl groups as two broad singlets, respectively at δ 7.28 and 8.19 ppm (Figure 2.6). Interesting, it is the influence of the fluorine atoms of the Pc **2.8** where is observed a shift of the pyridyl proton resonances comparatively with the analogous resonances of **2.7**. In case of **2.8**, occurs a high field shift for both pyridyl protons *ortho*-H^{a} and *meta*-H^{b} when compared with the equivalent Pc **2.7** (δ 8.02 and 8.70 ppm) due to the shield effect of the electronegative fluorine atoms on the Pc **2.8**. The ^{19}F NMR spectrum of **2.8** shows clearly the presence of the fluorine atom resonances as a duplet at δ -126.91 ppm (Figure 2.7). Likewise, the MALDI-TOF-MS spectrum confirmed the structure of **2.8** showing the presence of the protonated molecular ion peak $[M+H]^{+}$ at *m/z* 1595.

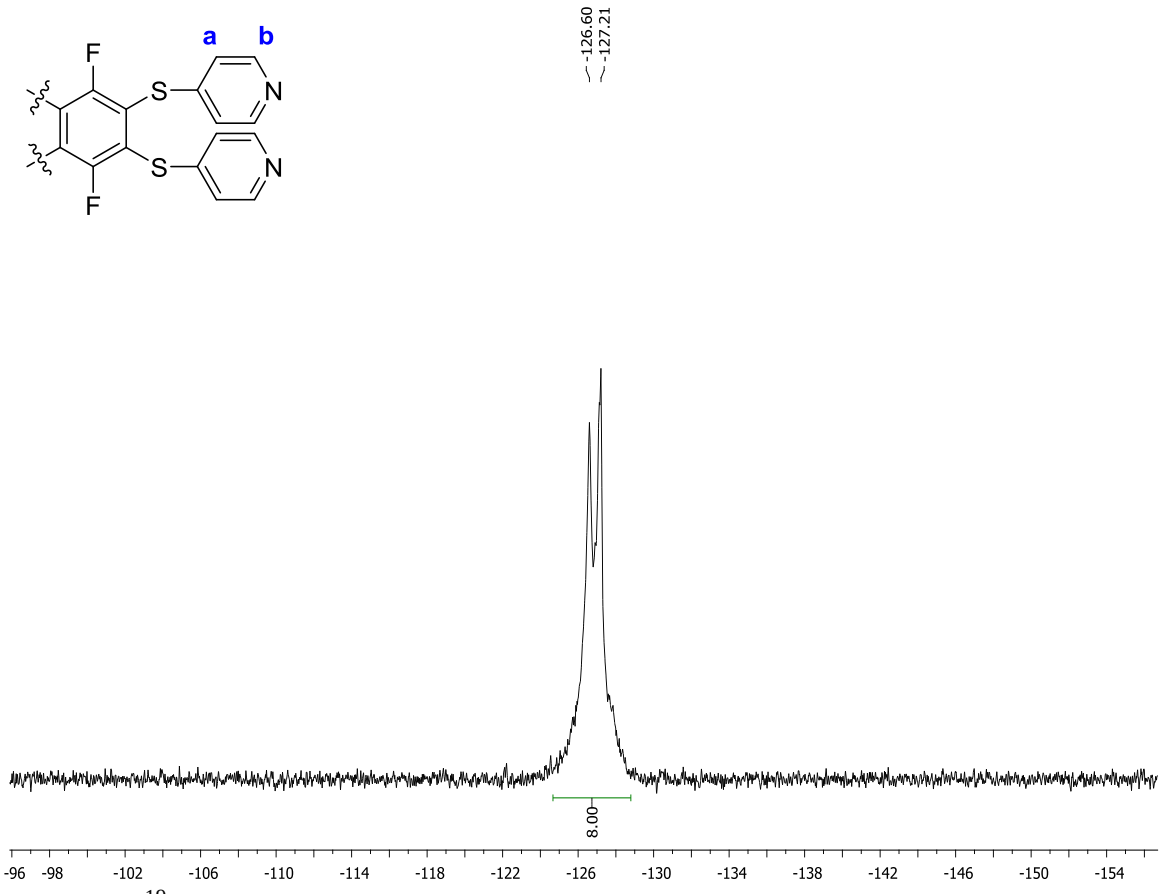

Figure 2.7 ^{19}F NMR spectrum of compound **2.8** in DMSO-d_6 + TFA.

2.3 Photophysical studies*

2.3.1 Optical characterization of thiopyridylphthalocyanines

The initial measurements regarding the ground and excited state features of **2.6**-**2.8** were performed in DMF. The occurrence of aggregation was detected at concentrations, higher than 10^{-5} M from the broadening and asymmetry observed in the Q-band region (data not shown). This fact can be rationalized by the presence of pyridyl groups as an inception to form intermolecular complexes by coordination with the metal present in the inner core of the macrocycle. Evidence for monomeric **2.6**-**2.8** with Q-band maxima at 684, 703, and 722 nm, respectively, were gathered at concentrations below 10^{-5} M (Figure 2.8). Interestingly, as the number of substituents at the β-position increases the Soret- and the Q-bands shift bathochromically. Figure 2.8 shows also the fluorescence spectra of **2.6**-**2.8** monomers upon excitation at 630 nm in DMF. These spectra reveal maxima at 689, 710 and 730 nm, respectively, and the quantum yields found for **2.6** (0.23), **2.7** (0.18) and **2.8** (0.12) – Table 2.1), are slightly lower than the quantum yield of **ZnPc** used as reference (0.3).[49]

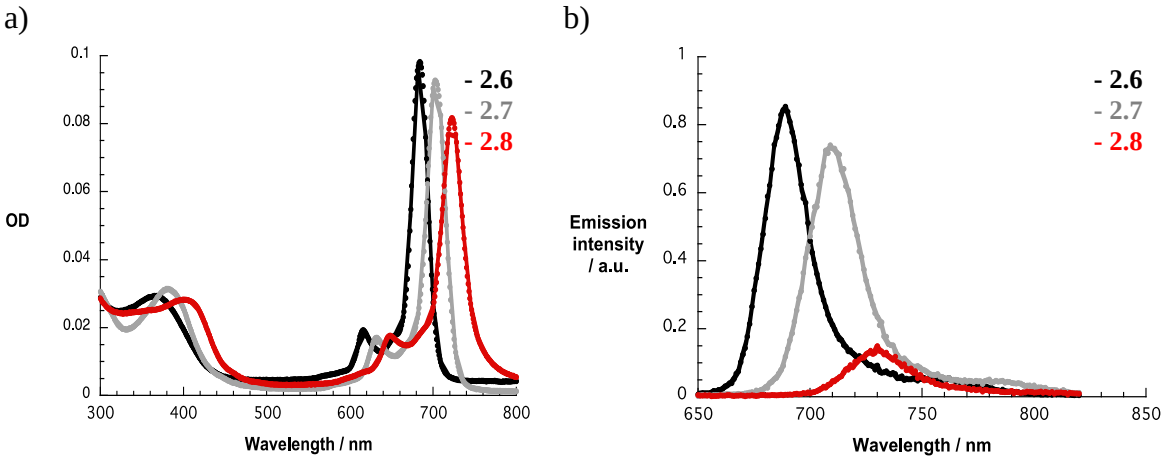

Figure 2.8 a) Absorption and b) fluorescence spectra of **2.6**-**2.8** in DMF, upon excitation at 630 nm, at concentration of 10^{-6} M.

*These compounds were tested by **Leonie Wibmer**, **Alexandra Roth** and **Georgios Katsukis Hausmann** who kindly provided their results for a comprehensive analysis of the photophysical values of these supramolecular assemblies.

As a complement, time-correlated single photon counting (TCSPC) measurements were performed following 403 nm excitation (Figure 2.9). The resulting fluorescence time profiles for the thiopyridylphthalocyanines are best fit monoexponentially. The resulting lifetimes are respectively 2.5 ns for **2.6**, 2.1 ns for **2.7** and 1.9 ns for **2.8**.

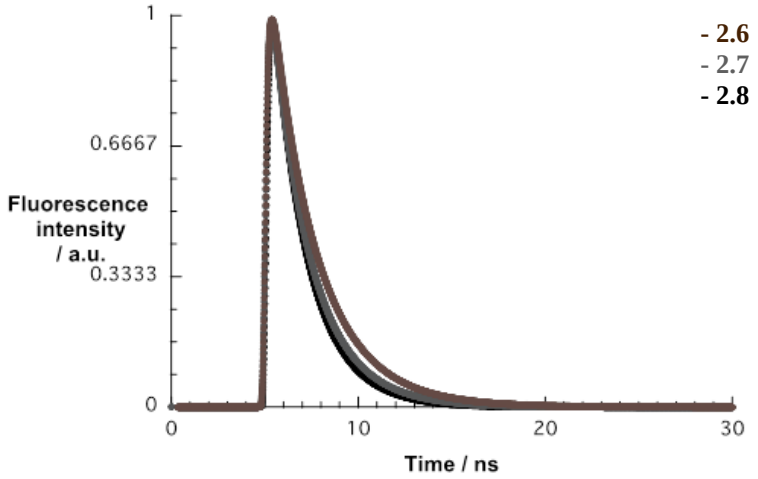

Figure 2.9 Emission time profiles of **2.6**-**2.8** in DMF, upon excitation at 403 nm.

Table 2.1 The molar extinction coefficient (ε), Q-band maxima (λ_{max}), fluorescence quantum yields (ϕ_F), and time correlated single photon counting (τ) in DMF.

Compounds	ε ($M^{-1}cm^{-1}$)	λ_{max} / nm	ϕ_F	τ_1 (ns)
2.6	2.50×10^4	684	0.23	2.5
2.7	0.85×10^4	703	0.18	2.1
2.8	2.03×10^4	722	0.12	1.9

2.3.2 Femtosecond transient absorption spectroscopy of thiopyridylphthalocyanines

The transient absorption spectra of **2.6**-**2.8** and **ZnPc** were recorded following 387 nm femtosecond excitation. The differential absorption characteristics of their singlet excited state obtained right after the excitation is discernable in Figure 2.10 for **Pc 2.7**. The minima which evolve at 632 and 705 nm and also the maxima at 500, 840 and 1200 nm are ascribed to the ground state bleaching in the range of the Q-band transitions. The singlet excited state is, however, metastable and during its decay a notable red-shift moves the maximum from 500 nm to 524 nm. This underlying trend reflects the superimposition of two different transients driven by intersystem crossing. One hand is due to the decay from the singlet excited state and the other to the concurrently developing triplet excited state

with maxima at 524, 564 and 605 nm. The analyses of the absorption time profiles at 500 nm, etc. shed light onto the kinetics. In particular, a short lifetime of 10 ± 0.8 ps, a long lifetime of 2.7 ± 0.3 ns, and an intermediate lifetime with minor amplitude of 250 ± 60 ps can be correlated with internal conversion, intersystem crossing, and the presence of aggregates, respectively.

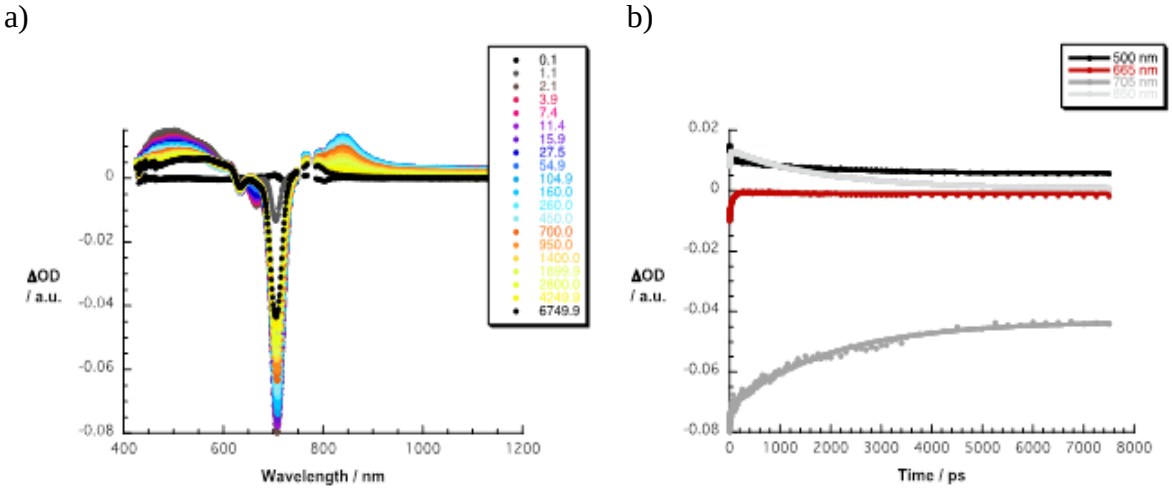

Figure 2.10 a) Differential absorption spectra (visible and near infrared) obtained upon femtosecond pump probe experiments (387 nm) of **2.7** in DMF with time delays between 0.1 and 6750.1 ps at room temperature – for time delays see figure legend. b) Time absorption profiles of the spectra shown at 500, 665, 705 and 850 nm.

The lifetime of the triplet excited state exceeds the time resolution of our experimental setup. The behaviour of **2.6**, **2.8** and also **ZnPc** is quantitatively similar to the one described for **2.7** (Figure 2.11), only showing slightly different lifetimes.

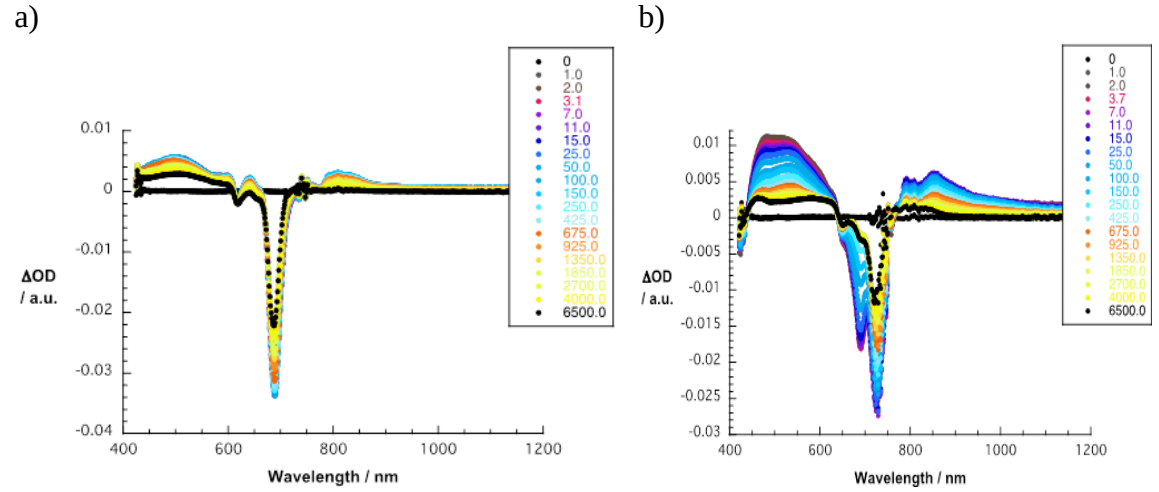

Figure 2.11 Differential absorption spectra (visible and near infrared) obtained upon femtosecond pump probe experiments (387 nm) of a) **2.6** and b) **2.8** in DMF with addition of pyridine to ensure monomeric Pcs with time delays between 0 and 6500.0 ps at room temperature – for time delays see figure legend.

2.3.3 Electrochemistry characterization of thiopyridylphthalocyanines

The electrochemical properties of **2.6-2.8** were studied by electrochemistry techniques using distilled DMF as solvent. In terms of reductions, the reduction potentials are -1.22 V for the first two Pc followed by a second reduction at -1.56 V for **2.6**, -1.04 V for **2.7**, and -0.86 V and -1.25 V for **2.8**. In terms of oxidation, only for **2.6** an oxidation potential was noted at +0.51 V. For **2.7** and **2.8** within our experimental range, namely up to 1.3 V, no oxidation potential was found. An extrapolation from absorption data gives an oxidation potential of +0.7 V and +0.9 V for **2.7** and **2.8**, respectively. In this respect, the choice of different solvents including DMSO, THF (or in these solvents but with addition of 4-(dimethylamino)-pyridine for guaranteeing monomeric Pcs), DCM and an acetonitrile/toluene (3/1 v/v) mixture did not change the results. In contrast, **ZnPc** revealed a reduction at -1.43 V and oxidation at +0.24 V in DMF.

As a complement, spectroelectrochemical assays were performed in DMF. In the case of **2.7**, applying a voltage of -0.4 V *vs* Ag-wire leads to changes in the absorption spectra, which are ascribed to the formation of the one electron reduced phthalocyanine. In particular, next to the bleaching of the Soret- and Q-bands, new maxima in the visible region at 467, 594 and 740 nm as well as in the near infrared region at 876, 913, 952 and 1000 nm arise in the differential absorption spectra (Figure 2.12a). For **2.6** and **2.8**, similar results are noted at, however, slightly different potentials (Figures 2.12b and 2.13).

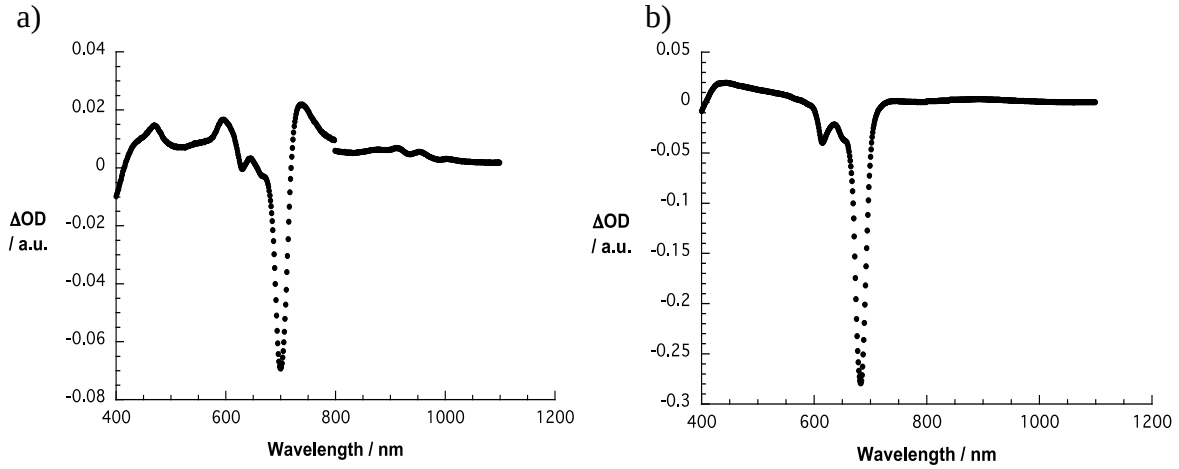

Figure 2.12 Differential absorption spectrum (visible and near infrared) in DMF obtained upon spectroelectrochemical one electron reduction with a voltage of a) -0.4 V *vs* Ag-wire for **2.7** and b) -0.6 V *vs* Ag-wire for **2.6**.

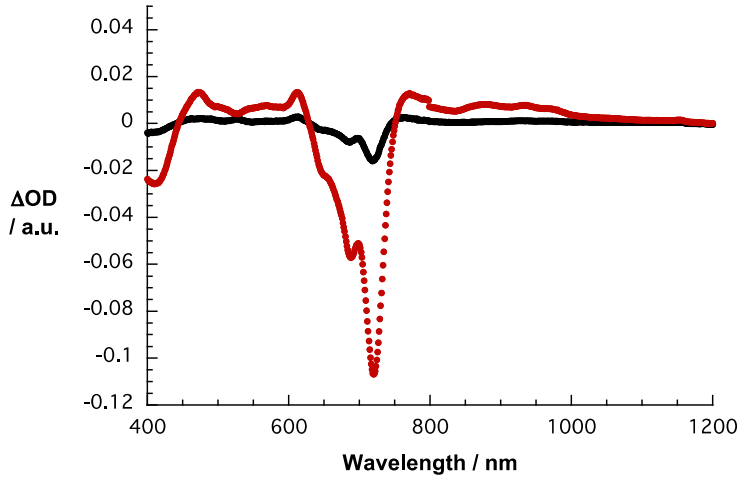

Figure 2.13 Differential absorption spectra (visible and near infrared) obtained upon spectroelectrochemical one electron (black spectrum) and two electron (red spectrum) reductions of **2.8** in DMF with voltages of -0.2 and -0.6 V *vs* Ag-wire, respectively.

For example, the signature of one electron reduced phthalocyanine **2.6** evolves at an applied potential of -0.6 V *vs* Ag-wire. For **2.8**, an applied potential of only -0.2 V *vs* Ag-wire is sufficient to form the one electron reduced phthalocyanine, while at -0.6 V its two electrons reduced form is generated. In other words, the electron accepting properties scale with increasing number of substituents at the β-position of the phthalocyanine. Interestingly, no appreciable changes in the absorption spectra were seen upon applying positive voltages in any of the used solvents. For **ZnPc**, in contrast, a spectroelectrochemical oxidation was possible in dichloromethane at an applied potential of 0.5 V. Here, features at 411, 525, 835 and 916 nm are due to the characteristic and well known signature of the one electron oxidized phthalocyanine.

2.3.4 Supramolecular preparation of nanographene/Pc nanohybrids G2.6-G2.8

After the establishment of the key features of **Pc 2.6-2.8**, the respective nanographene/Pc nanohybrids **G2.6-G2.8** were prepared; for comparison the nanohybrid **GZnPc** (using the standard **ZnPc**) following a previously reported procedure.[50] In particular, 1-2 mg of natural graphite was added to a 10^{-5} M DMF solution of thiopyridylphthalocyanines, which were ultrasonicated for 45 min and subsequently centrifuged at 20 G for 20 min. The supernatants were then extracted and again subjected to ultrasonication with newly added natural graphite.

2.3.5 Optical characterization of nanographene/Pc nanohybrids G2.6-G2.8

During the preparation of the nanographene/Pc nanohybrids **G2.6**-**G2.8**, the absorption spectra were recorded after each enrichment cycle and were compared to those of the corresponding Pc **2.6**-**2.8** references. Overall, an increase in absorbance is discernable with each enrichment cycle when using **G2.6**-**G2.8** as well as **GZnPc** with equal contributions from absorption and scattering processes of exfoliated graphite (Figure 2.15 for graphene assembly with Pc **2.7**). Notably, the exact amount of exfoliated graphite cannot be calculated due to superimposing absorption features of exfoliated graphite and **G2.6**-**G2.8**. No additional changes are detected in the absorption spectra of **GZnPc**. In contrast, new absorption features evolve for **G2.6**-**G2.8** namely a red shift with respect to the original Q-band which intensifies after each enrichment cycle. The maxima of the new Q-bands appear at 718, 737 and 760 nm for **G2.6**, **G2.7** and **G2.8**, respectively (Figure 2.14).

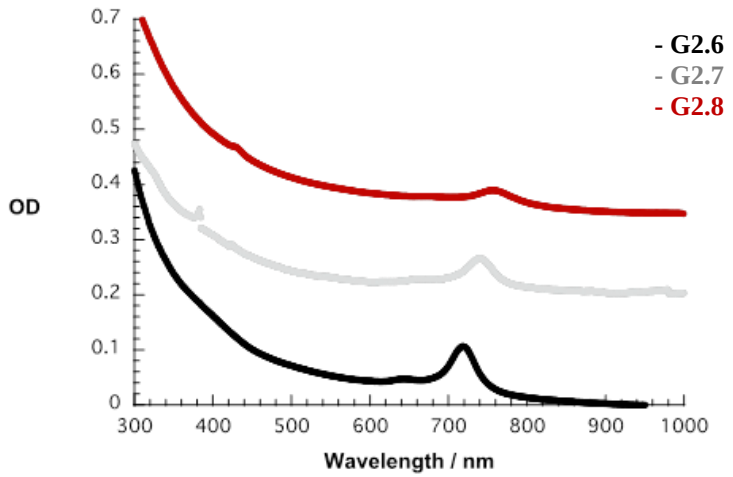

Figure 2.14 Absorption spectra of **G2.6**-**G2.8** in DMF.

Notably, in the end the original Q-bands have completely disappeared. Instead, merely the new 35 nm red-shifted Q-bands are visible. In the case of **G2.7**, only four enrichment cycles are necessary (Figure 2.15) to obtain the fully shifted Q-band for **G2.6** and **G2.8**, at least 5-6 enrichment cycles are needed.

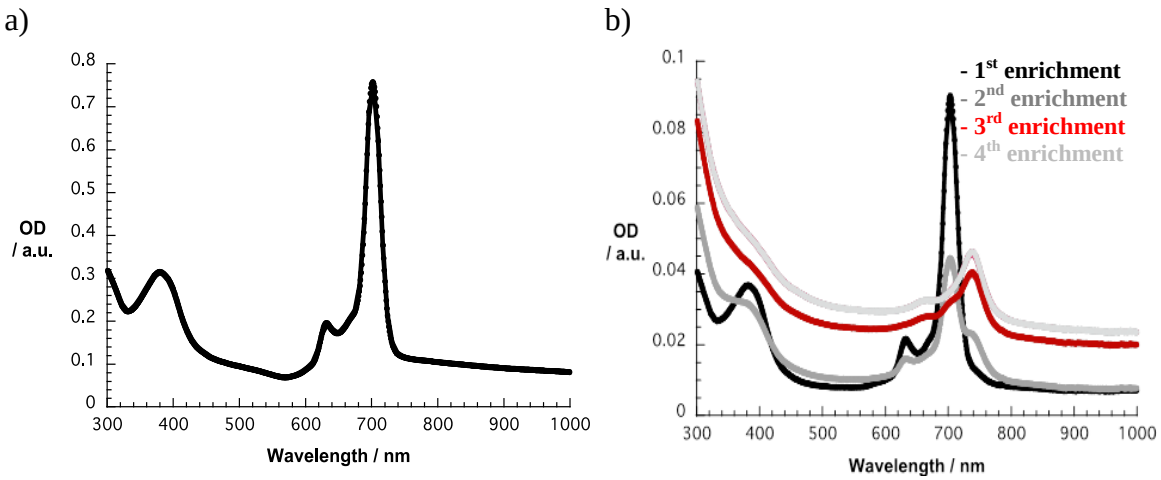

Figure 2.15 a) Absorption spectrum of **2.7**. b) Absorption spectra of **G2.7** after 1st, 2nd, 3rd and 4th enrichment.

The fluorescence spectra obtained after each enrichment cycle were also recorded, as it is exemplified in Figure 2.16 for **G2.7**. The results show that after four enrichment cycles the Pc centred fluorescence is nearly quantitatively quenched for **G2.7** (98.6%) and **G2.6** (99.4%); a quenching of 74.8% was observed for **G2.8**. These trends are in line with the absorption changes seen for **G2.6-G2.8** and indicate that in the end the Pcs are immobilized in graphene and no free Pcs is present in solution. The results obtained with **GZnPc** show a different situation: only a weak quenching was detected.

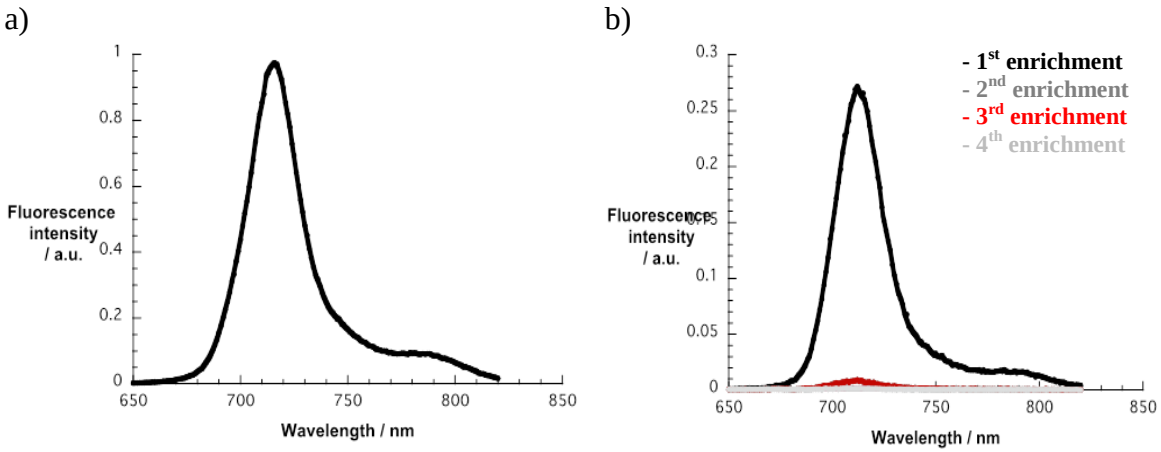

Figure 2.16 a) Fluorescence spectrum of **G2.7** before enrichment. b) Fluorescence spectra of **G2.7** after 1st, 2rd, 3rd and 4th enrichment.

2.3.6 Raman spectroscopy and transmission electron microscopy of nanographene/Pc nanohybrids

Further insights into the nature of **G2.7** came from Raman spectroscopy following laser excitation at 532 nm after drop casting the dispersion onto a Si/SiO_2 wafer. Raman spectroscopy is an important mean to characterize graphitic materials and identify single, bi- and few-layer graphene or turbostratic graphite. Typically, the D-band is discernable at around 1350 cm^{-1}, while the G- and 2D-bands are centred around 1580 and between 2650 and 2700 cm^{-1}, respectively. Figure 2.17 shows a selected Raman spectrum of **G2.7**. The I(2D)/I(G) intensity ratio of 6.3 and a single lorentzian fit of the 2D-band with a full width at half maximum (FWHM) of 34.6 cm^{-1} indicate monolayer graphene. In order to get a statistical overview over the sample, a Raman map with around 600 different spectra was evaluated (Figure 2.17).

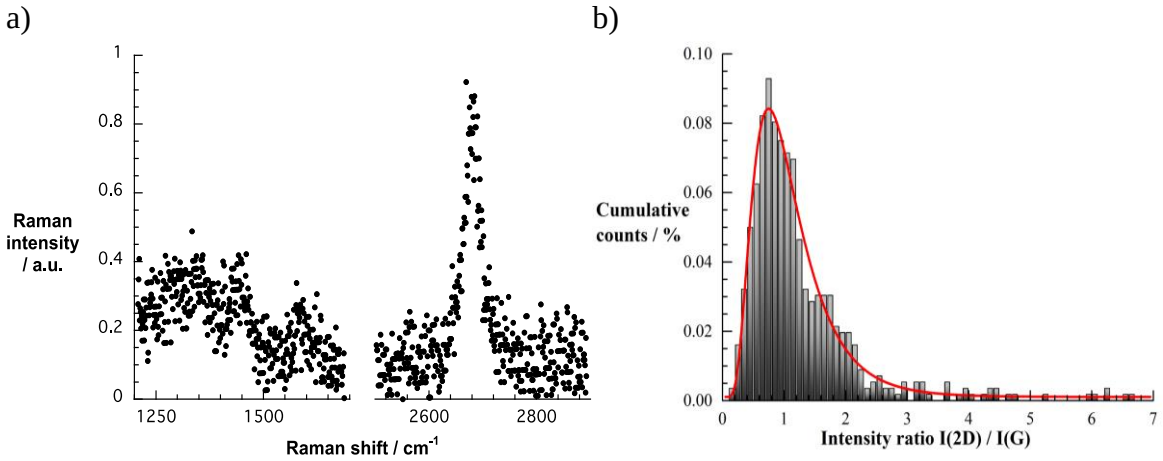

Figure 2.17 a) Selected Raman spectrum of **G2.7**. b) Histogram with relative counts *vs* I(2D) / I(G) ration and the corresponding log-normal distribution with a maximum at 0.97. The sample was drop casted from a DMF dispersion onto silicon oxide wafers and excited at 532 nm.

The resulting I(2D)/I(G) intensity ratios are best fit by a log-normal distribution function, which maximizes at a ratio of 0.97. From reference experiments we attribute any ratio of 0.7 or less to bulk graphite or few- to multilayer graphene. That means, in the current case, 25% of the collected spectra reveal bulk graphite / few- to multilayer graphene character, while 75% of the collected spectra correspond to turbostratic exfoliated graphite and monolayer graphene. For a further differentiation between the latter the FWHM of the 2D-band is decisive. Furthermore, a shape analysis of the 2D-band of the

spectra with a 2D/G intensity ratio above 1 was performed. In this case, the spectra could be fitted with a single lorentzian function, but differ in FWHM. On the one hand, 5% of the spectra display a FWHM between 25 and 45 cm^{-1} representing real monolayer graphene and 95% turbostratic graphite with a FWHM between 45 and 70 cm^{-1}, on the other hand. The high amount of turbostratic graphite is probably due to our preparation method of simply drop casting the dispersion onto the wafer. Hereby, the once exfoliated flakes tend to re-agglomerate upon the slow evaporation of the solvent DMF.[51]

This is also confirmed by transmission electron microscope images as it is exemplified for **G2.7** in Figure 2.18. In particular, small thin flakes as well as larger individual few-layer graphene flakes with lateral sizes up to 2 µm appear folded and intertwined to minimize surface energy. Furthermore, in atomic force microscopy (AFM) homogenous flakes can be found onto which smaller flakes as well as graphitic materials agglomerate. Specifically, height profiles of graphene flakes reveal sizes up to 1 µm that are around 1 nm in height, which still corresponds to a monolayer flake due to adsorbed water or stabilizer molecules.[52,53] Further agglomerated flakes are again 1 nm in height, whereas height profiles of graphitic materials reach 10 nm and beyond (Figure 2.18).

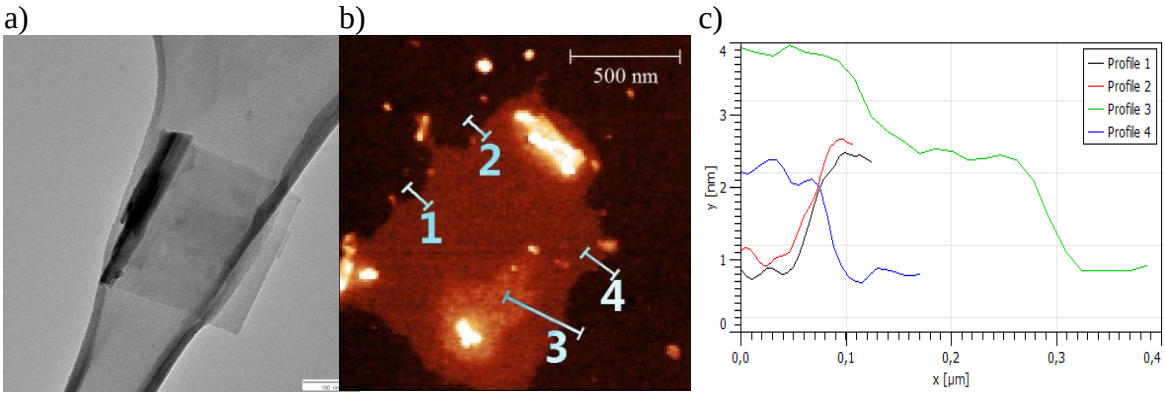

Figure 2.18 a) Transmission electron microscopy (TEM) images of **G2.7** on a lacey carbon grid – scale bar is 100 nm. b) Tapping mode AFM image of **G2.7** on a SiO_2 surface – scale bar is 500 nm. c) Height profiles at positions 1, 2, 3 and 4.

2.3.7 Femtosecond transient absorption spectroscopy of nanographene/Pc nanohybrids G2.6-G2.8

Finally, to characterize and to quantify the nature of the electronic interactions between graphene and the Pcs in terms of energy and / or electron transfer, it was

performed transient absorption experiments with **G2.6**-**G8** and **GZnPc** by means of exciting them at 387 nm. In order to obtain better results in the spectroscopic range between 700 and 800 nm, all measurements were carried out with optimized white light setting in this range of the spectrum and, additionally, the near-infrared (nIR) region is equally optimized in the range between 1000 to 1600 nm. In the case of **GZnPc**, the differential absorption spectrum lacks features in addition to those seen for the references, that is, graphene, on one hand, and **ZnPc**, on the other hand (data not shown). With regard to the earlier, a graphene related bleaching is discernable in the range from 900 to 1600 nm. With regard to the latter, the intensity of the phthalocyanines ground state bleaching, which is seen in the form of minima at 623 and 679 nm prompts to the presence of **ZnPc** that is free in solution and not immobilized onto graphene. Furthermore, the accordingly formed singlet-singlet absorption gives rise to maxima at 506, 592 and 856 nm, respectively, and, as such, identical to what is seen for the reference **ZnPc**.

In stark contrast, in the case of **G2.7**, within the first picoseconds following excitation broad minima evolve (Figures 2.19 and 2.20). It comprises graphene related bleaching in the visible and near infrared regions and Pc related ground state bleaching between 650 and 740 nm. Importantly, the Pc related ground state bleaching is 35 nm red-shifted in **G2.7** to 740 nm relative to the spectra recorded for **2.7**. In fact, the minima for **G2.7** are in excellent agreement with the shifted Q-band absorption seen in the absorption spectra. Both, that is, graphene and phthalocyanine related bleaching, decay rapidly – *vide infra*. For example, considering the bleaching of graphene at 1035 nm a lifetime of <1 ps evolves. Following the fast decays of these excited state features new features develop in the visible region at 462, 578 and, especially, at 763 nm. In line with the spectroelectrochemical investigations carried out with **2.7** in DMF (Figure 2.12a) the latter features suggest the formation of the one electron reduced form of the Pc following excited state electron transfer. The near infrared region is equally important. Here, new features were noted during the transient decay with a broad maximum ranging from 950 to 1300 nm. Implicit are new valence band holes in graphene – accepted from photoexcited **2.7**. Implicit is the formation of radical ion pair states, that is, reduced **2.7** and oxidized graphene. Analyses at the characteristic wavelengths give rise to three lifetimes, that were best fit by a multi-exponential fitting function affording for **G2.7** lifetimes of <1 and 330 ± 50 ps for charge separation and charge recombination, respectively. In addition, 1 ns component, which relates to Q-band ground state bleaching, is derived.

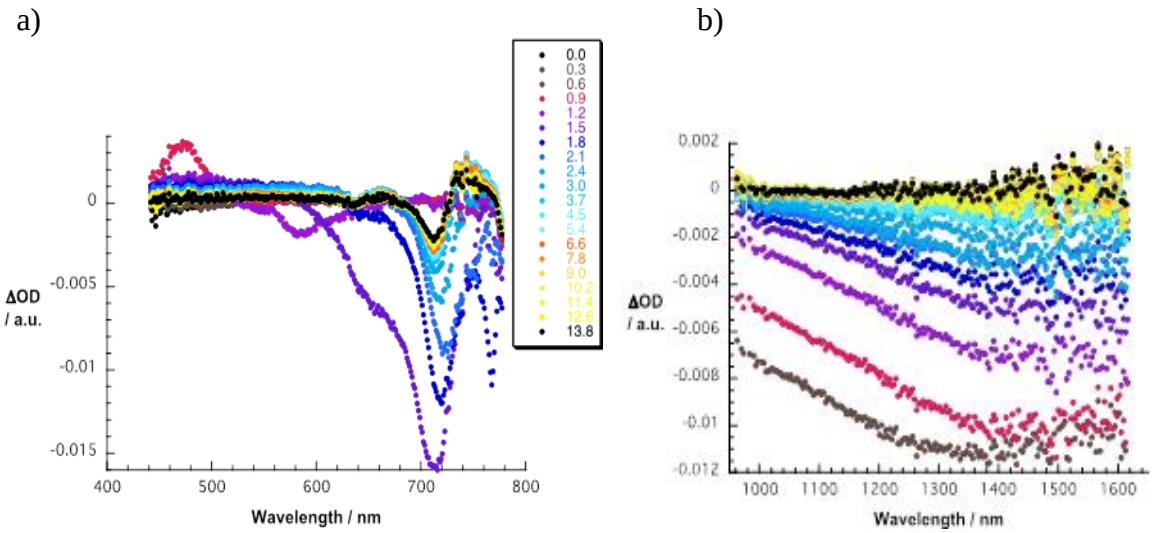

Figure 2.19 Differential absorption of a) visible and b) near infrared spectra obtained upon femtosecond pump probe experiments (387 nm) of **G2.7** in DMF with time delays between 0 and 13.8 ps at room temperature – for time delays see figure legend.

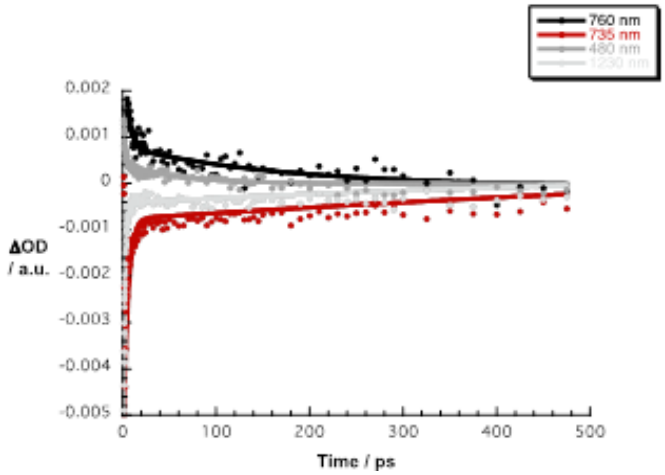

Figure 2.20 Time absorption profiles of the spectra shown at 480, 735, 760 and 1230 nm.

Overall, similar results with, however, slightly different spectral features and lifetimes came from complementary studies with **G2.6** and **G2.8** as shown in Figures 2.24 and 2.25, respectively. Please note that the new absorption features include signals red shifted to the Q-bands. In the case of **G2.6**, the maximum is found at 742 nm, while for **G2.8** it is expected to be around 780 nm. The latter is, however, masked by fundamental of the laser excitation at 775 nm. Interesting is the trend in terms of charge separation and charge recombination. The charge separation for **G2.6**-**G2.8** always occurs in less than 1 ps, but differs in terms of charge recombination: for **G2.7** the lifetime of the charge separated state is more than two times longer than for **G2.6** and **G2.8**.

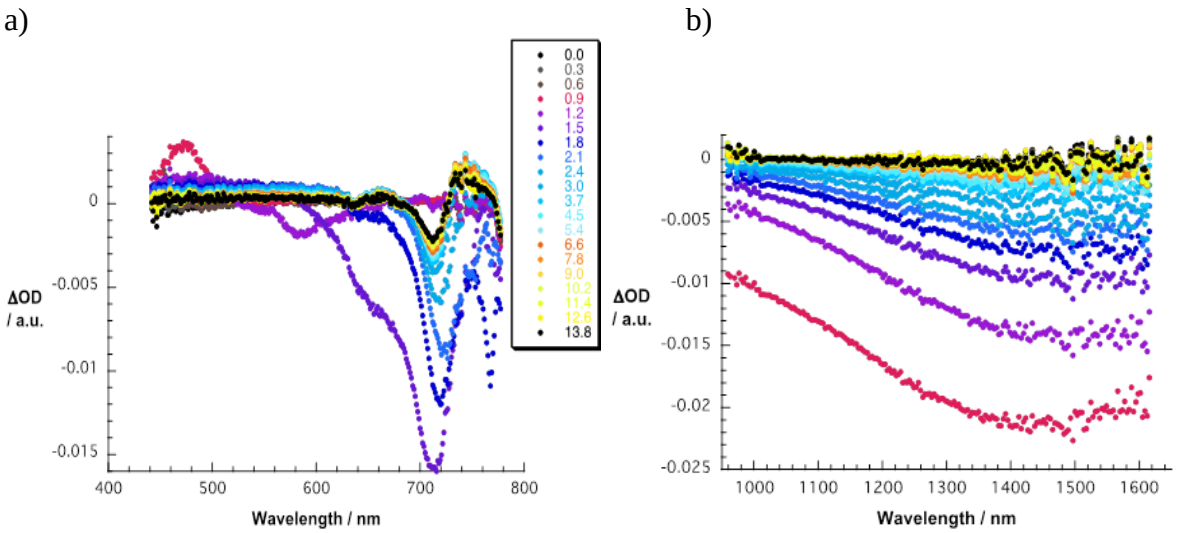

Figure 2.21 Differential absorption of a) visible and b) near infrared spectra obtained upon femtosecond pump probe experiments (387 nm) of **G2.6** in DMF with time delays between 0 and 13.8 ps at room temperature – for time delays see figure legend.

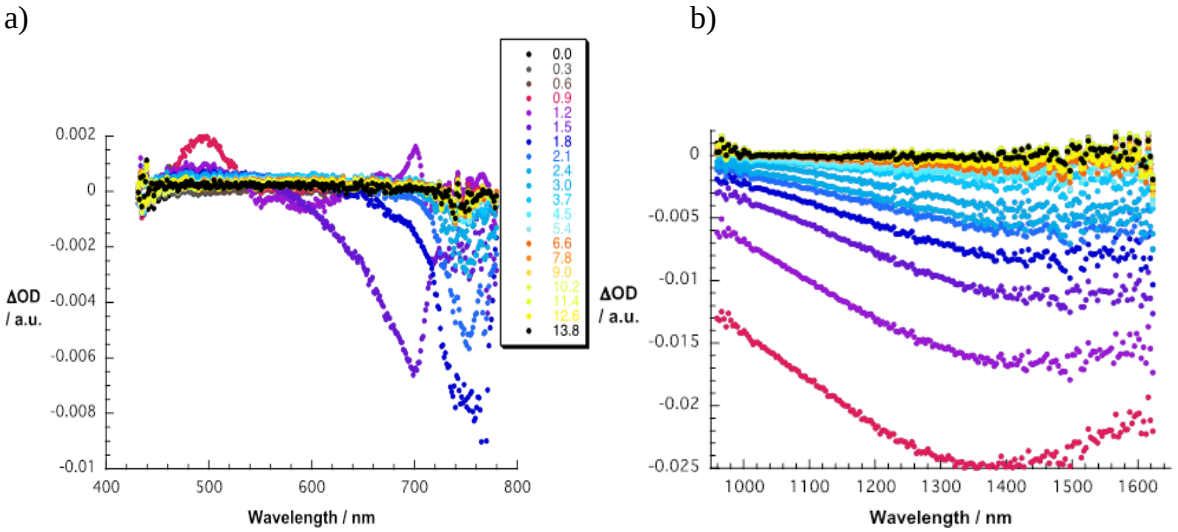

Figure 2.22 Differential absorption of a) visible and b) near infrared spectra obtained upon femtosecond pump probe experiments (387 nm) of **G2.8** in DMF with time delays between 0 and 13.8 ps room temperature – for time delays see figure legend.

2.4 Conclusions

Newly synthesized thiopyridylphthalocyanines **2.6**-**2.8** reveal low reduction potentials compared with the **ZnPc** reference. As such, they have evolved as interesting and promising building blocks to exfoliate graphite *via* their immobilization onto the basal plane of graphene. As a matter of fact, immobilization is enabled through electronic coupling as seen in newly developing absorption features and an almost complete

quenching of the Pc fluorescence in the case of the electron donor-acceptor nanohybrids **G2.6-G2.8**. The aforementioned was complemented by femtosecond pump probe spectroscopy, which corroborated that the electronic coupling between **G2.6-G2.8**, on one hand, and graphene, on the other hand, is indeed accompanied by charge transfer characteristics, yielding the one electron reduced phthalocyanine. In stark contrast, reference experiments with **ZnPc** completely lack any of the aforementioned new features. Therefore, in this case no immobilization occurs onto and/or electronic coupling with graphene compared to the graphene hybrids **G2.6-G2.8**. Raman, TEM and AFM analysis revealed that after drop casting the dispersion onto a Si/SiO_2 wafer, the exfoliated flakes tend to minimize surface energy by folding or reaggregating, thus forming turbostratic graphene.

2.5 Experimental section

2.5.1 General information

The organic solvents were dried according to standard methods by distillation over drying agents and stored under nitrogen or argon gas. Other solvents were used as commercial pure analytical. Deuterated solvents such as $CDCl_3$ and DMSO-d_6 were used for ^{1}H, ^{19}F and ^{13}C NMR spectra. The solvents used in this work were purchased from Fluka, Merck, TCI Europe and Acros.

The commercial reagents used from Sigma-Aldrich, Acros, TCI Europe and Merck have a purity $\geq$ 97 % protected of the air in dry conditions.

Preparative TLC was performed using aluminium plates coated with SiO_2 (Merck 60, F-254). TLC plates were viewed under UV light (λ = 254 nm). Flash column chromatography was performed using SiO_2 (0.040-0.063 mm). Gel column chromatography was done using Bio-Beads (BIO-RAD, 200-400 mesh).

NMR spectra were recorded on Brucker AC 300/500 instruments. Chemical shifts are reported as δ-values in ppm relative to tetramethylsilane (TMS).

Mass spectra were obtained using a Q-TOF (Q-TOF 2, Micromass, Manchester, UK) and a linear ion trap (LXQ, ThermoFinnigan, San Jose, CA, USA) mass spectrometer. ESI-HR mass spectra were acquired in Apex-Qe.

Steady-state absorption spectra were recorded with a Perkin-Elmer Lambda 35 and a Perkin-Elmer Lambda 2. Steady-state emission spectra were recorded with a Fluoromax-3-spectrometer from HORIBA Jobin Yvon. All samples were measured in a fused quartz glass cuvette with a diameter of 10 mm.

Femtosecond transient absorption spectra were obtained with a Ti:sapphire laser system CPA-2101 (Clark-MXR Inc.) in combination with a Helios TAPPS detection unit from Ultrafast Inc. The initial laser excitation wavelength is 775 nm with a pulse width of 150 fs. The used excitation wavelength was 387 nm, which was generated with a SHG crystal. For the generation of the white light a sapphire crystal of adequate thickness was used. The chirp-effect between 420 and 770 nm is approximately 350 fs. The detection was carried out with two CCD cameras, each for a specific measuring range. The spectral window is therefore 415 to 770 nm and 770 to 1600 nm. The delay line allows spectral acquisition up to time delays of 8000 ps. All samples were measured in a fused quartz glass cuvette with a thickness of 2 mm. Data was acquired with the software HELIOS Visible/nIR (Newport / Ultrafast Systems).

For electrochemistry, a Teflon coated Pt wire was used as working electrode, a Pt wire as counter electrode, and an Ag wire as quasi reference electrode. For better comparison the potentials were then converted to a ferrocene/ferrocenium redox couple. For spectroelectrochemistry, a Pt net was used as working electrode, a Pt sheet as counter electrode, and an Ag wire as quasi reference electrode. The potentials were applied with a METROHM PGSTAT 101 and the absorption spectra taken with a UV/nIR Cary5000 spectrometer.

Raman measurements were carried out with Renishaw in Via Reflex Confocal Raman Microscope using laser excitations of 532 nm. The sample was prepared by drop casting a dispersion on a Si substrate with a 300 nm oxide layer.

Sample preparation was performed by drop casting and drying the hybrids on lacey carbon coated copper grids. Bright-field TEM images were recorded with an 80 kV EM 900 from Carl Zeiss AG.

AFM images were obtained with a Nanoscope IIIa Multimode, Veeco in tapping mode. The sample was prepared by dip coating of onto a Si wafer.

2.5.2 Synthesis of thiopyridylphthalonitriles

*4-(thiopyridyl)phthalonitrile (**2.3**)*:

A mixture of 4-nitrophthalonitrile **2.1** (1.00 g, 5.78 mmol, 1 eq.) and 4-mercaptopyridine **2.2** (1.61 g, 14.4 mmol, 2.5 eq.) were stirred in 5 mL of DMF in the presence of using K_2CO_3 (2.14 g, 15.48 mmol, 2.7 eq.) for 5 h at 60 ºC. After this period of time it was added water and the obtained precipitate after being crystalized in MeOH/CH_2Cl_2 (1/1), afforded product **2.3** in 70% yield. ^{1}H NMR (300 MHz, DMSO-d_6): δ 7.35 (dd, J = 4.5, 1.6 Hz, 2H, H^d), 7.91 (dd, J = 8.4, 1.9 Hz, 1H, H^a), 8.15 (d, J = 8.4 Hz, 1H, H^c), 8.28 (s, 1H, H^b), 8.53 (dd, J = 4.5, 1.6 Hz, 2H, H^e). ^{13}C NMR (75 MHz, DMSO-d_6): δ 113.9, 115.4, 115.8, 116.1, 124.0, 134.9, 136.1, 136.2, 139.9, 143.8, 150.5. ESI-MS: *m/z* 237 $[M+H]^+$.

*4,5-(dithiopyridyl)phthalonitrile (**2.5**)*:

A mixture of 4-mercaptopyridine **2.2** (0.50 g, 4.50 mmol, 1 eq.) and 3,4-dichlorophthalonitrile **2.4** (1.71 g, 8.70 mmol, 1.9 eq.) in 10 ml of DMF was stirred at room temperature, in the presence of K_2CO_3 (2.01 g, 14.5 mmol, 3.2 eq.). After 2 h it was added water, and the solid obtained was filtered and washed with several additions of water and methanol. Product **2.5** was isolated in 50% yield after crystallization of the crude precipitate in a mixture of MeOH/CH_2Cl_2. ^{1}H NMR (300 MHz, $CDCl_3$): δ 7.25 (dd, J = 4.6, 1.6 Hz, 4H, H^b), 7.57 (s, 2H, H^a), 8.67 (dd, J = 4.6, 1.6 Hz, 4H, H^c). ^{13}C NMR (75 MHz, $CDCl_3$): δ 114.2, 114.8, 125.4, 135.0, 141.7, 142.6, 151.2. ESI-MS: *m/z* 347 $[M+H]^+$.

2.5.3 Synthesis of thiopyridylphthalocyanines

*2,9(10),16(17),23(24)-tetrakis(4-pyridylsulphanyl)phthalocyaninato zinc(II) (**2.6**)*:

The mono-substituted phthalonitrile **2.3** (400 mg, 1.69 mmol, 1 eq.) in 1.5 mL of DMAE was maintained overnight at reflux (140 ºC) in the presence of anhydrous $ZnCl_2$ (230 mg, 1.69 mmol, 1 eq.). Then, it was added methanol and the obtained crude was washed several times with methanol and water to remove the excess of $ZnCl_2$. Finally, the solid was dried under vacuum atmosphere during 2 h at 60 ºC, affording product **2.6** in 82% yield. ^{1}H NMR (300 MHz, DMSO-d_6 + TFA): δ 7.74 – 8.00 (br *m*, 8H, Ar-*o*-H^d), 8.26

– 8.48 (br *m*, 4H, β-H^{c}), 8.52 – 8.79 (br *m*, 8H, Ar-*m*-H^{e}), 8.88 – 9.45 (br *m*, 8H, α-$H^{a,b}$). UV–Vis (DMSO), λ_{max} (log ε): 347 (4.98), 617 (4.55), 684 (5.37) nm. MALDI-TOF-MS: *m/z* 1013 $[M+H]^+$.

*2,3,9,10,16,17,23,24-Octakis(4-pyridylsulphanyl)phthalocyaninato zinc(II) (**2.7**)*:

The synthesis of the octa-substituted Pc **2.7** was performed as it was described above but using the 4,5-dithiopyridylphthalonitrile (**2.5**). The Pc **2.7** was isolated in 85% yield.^{1}H NMR (300 MHz, DMSO-d_6 + TFA): δ 8.02 (d, J = 6.1 Hz, 16H, Ar-*o*-H^{b}), 8.70 (d, J = 6.1 Hz, 16H, Ar-*m*-H^{c}), 10.15 (s, 8H, Pc α-H^{a}). UV–Vis (DMSO), λ_{max} (log ε): 371 (4.59), 632 (4.47), 663 (4.68), 702 (5.03) nm. MALDI-TOF-MS: *m/z* 1448 $[M+H]^+$.

*1,4,8,11,15,18,22,25-Octafluoro-2,3,9,10,16,17,23,24-Octakis(4-pyridylsulphanyl)phthalocyaninato zinc(II) (**2.8**)*:

The reaction between commercial **$ZnPcF_{16}$** (200 mg, 0.23 mmol, 1 eq.) and 4-mercaptopyridine **2.2** (256.8 mg, 2.3 mmol, 10 eq.) was carried out in 50 mL of DMF and in the presence of 5 mL of diethylamine (DEA). The reaction mixture was maintained under stirring, at room temperature, overnight under nitrogen atmosphere. Then, it was added water and the green solid obtained by precipitation was filtered and washed with water and acetone. The Pc **2.8** was isolated in 89%, after drying the green solid during 2 h under vacuum atmosphere at 60 ºC. ^{1}H NMR (300 MHz, DMSO-d_6 + TFA): δ 7.28 (br s, 16H, Ar-*o*-H^{a}), 8.19 (br s, 16H, Ar-*m*-H^{b}). ^{19}F NMR (282 MHz, DMSO-d_6 + TFA): δ -126.91 (d, J = 173.5 Hz, 8F, α-F). UV–Vis (DMSO), λ_{max} (log ε): 384 (4.82), 690 (5.04), 720 (5.09) nm. MALDI-TOF-MS: *m/z* 1595 $[M+H]^+$.

2.5.4 Preparation of hybrids Pc/graphene

Natural graphite (1-2 mg) was added to a solution of thiopyridylphthalocyanines **2.6**-**2.8** in DMF (10^{-5} M), followed ultrasonication for 45 min and centrifugation at 20 G for 20 min. The supernatants were then extracted and again subjected to ultrasonication with newly added natural graphite.

2.6 References

1. Novoselov, K. S., Geim, A. K., Morozov, S. V., Jiang, D., Zhang, Y., Dubonos, S. V., Grigorieva, I. V., Firsov, A. A., *Science*, **2004**, 306, 666–669.
2. Geim, A. K., Novoselov, K. S., *Nat. Mater*., **2007**, 6, 183–191.
3. Lee, C., Wei, X., Kysar, J. W., Hone, J., *Science*, **2008**, 321, 385–388.
4. Bunch, J. S., Verbridge, S. S., Alden, J. S., van der Zande, A. M., Parpia, J. M., Craighead, H. G., McEuen, P. L., *Nano Lett*., **2008**, 8, 2458–2462.
5. Geim, A. K., *Science*, **2009**, 324, 1530–1534.
6. Ovid'ko, I. A., *Rev. Adv. Mater. Sci.*, **2013**, 34, 1–11.
7. Dorgan, V. E., Behnam, A., Conley, H. J., Bolotin, K. I., Pop, E., *Nano Lett*., **2013**, 13, 4581–4586.
8. Edwards, R. S., Coleman, K. S., *Nanoscale*, **2013**, 5, 38–51.
9. Subrahmanyam, K. S., Vivekchand, S. R. C., Govindaraj, A., Rao, C. N. R., *J. Mater. Chem*., **2008**, 18, 1517–1523.
10. Girit, Ç. Ö., Meyer, J. C., Erni, R., Rossell, M. D., Kisielowski, C., Yang, L., Park, C-H., Crommie, M. F., Cohen, M. L., Louie, S. G., Zettl, A., *Science*, **2009**, 323, 1705–1708.
11. Celik, V. O., Cahangirov, S., Ciraci, S., *Phys. Rev. B*, **2012**, 85, 235456 (1–7).
12. Zhang, Y., Zhang, L., Zhou, C., *Acc. Chem. Res*., **2013**, 46, 2329–2339.
13. Kobayashi, T., Bando, M., Kimura, N., Shimizu, K., Kadono, K., Umezu, N., Miyahara, K., Hayazaki, S., Nagai, S., Mizuguchi, Y., Murakami, Y., Hobara, D., *Appl. Phys. Lett*., **2013**, 102, 023112 (1–4).
14. Bonaccorso, F., Sun, Z., Hasan, T., Ferrari, A. C., *Nat. Photonics*, **2010**, 4, 611–622.
15. Hecht, D. S., Hu, L., Ir, G., *Adv. Mater*., **2011**, 23, 1482–1513.
16. Li, X., Cai, W., An, J., Kim, S., Nah, J., Yang, D., Piner, R., Velamakanni, A., Jung, I., Tutuc, E., Banerjee, S. K., Colombo, L., Ruoff, R. S., *Science*, **2009**, 324, 1312–1314.
17. Hernandez, Y., Nicolosi, V., Lotya, M., Blighe, F. M., Sun, Z., De, S., McGovern, I. T., Holland, B., Byrne, M., Gun'Ko, Y. K., Boland, J. J., Niraj, P.,

Duesberg, G., Krishnamurthy, S., Goodhue, R., Hutchison, J., Scardaci, V., Ferrari, A. C., Coleman, J. N., *Nat. Nanotechnol.*, **2008**, 3, 563–568.

18. Zhang, M., Ma, Y., Zhu, Y., Che, J., Xiao, Y., *Carbon*, **2013**, 63, 149–156.
19. Xu, L., McGraw, J. -W., Gao, F., Grundy, M., Ye, Z., Gu, Z., Shepherd, J. L., *J. Phys. Chem. C*, **2013**, 117, 10730–10742.
20. Torrisi, F., Hasan, T., Wu, W., Sun, Z., Lombardo, A., Kulmala, T. S., Hsieh, G.-W., Jung, S., Bonaccorso, F., Paul, P. J., Chu, D., Ferrari, A. C., *ACS Nano*, **2012**, 6, 2992–3006.
21. Li, X., Zhang, G., Bai, X., Sun, X., Wang, X., Wang, E., Dai, H., *Nat. Nanotechnol.*, **2008**, 3, 538–542.
22. Brownson, D. A. C., Kampouris, D. K., Banks, C. E., *J. Power Sources*, **2011**, 196, 4873–4885.
23. Buzaglo, M., Shtein, M., Kober, S., Lovrinčić, R., Vilan, A., Regev, O., *Phys.Chem.*, **2013**, 15, 4428–4435.
24. Liu, W. W., Wang, J. N., *Chem. Commun.*, **2011**, 47, 6888–6890.
25. Ragoussi, M.-E., Malig, J., Katsukis, G., Butz, B., Spiecker, E., de la Torre, G., Torres, T., Guldi, D. M., *Angew. Chem. Int. Ed.*, **2012**, 51, 6421–6425.
26. Englert, J. M., Dotzer, C., Yang, G., Schmid, M., Papp, C., Gottfried, J. M., Steinrück, H.-P., Spiecker, E., Hauke, F., Hirsch, A., *Nat. Chem.*, **2011**, 3, 279–286.
27. Malig, J., Romero-Nieto, C., Jux, N., Guldi, D. M., *Adv. Mater.*, **2012**, 24, 800–805.
28. Malig, J., Jux, N., Guldi, D. M., *Acc. Chem. Res.*, **2013**, 46, 53–64.
29. Brenner, W., Malig, J., Costa, R. D., Guldi, D. M., Jux, N., *Adv. Mater.*, **2013**, 25, 2314–2318.
30. Costa, R. D., Malig, J., Brenner, W., Jux, N., Guldi, D. M., *Adv. Mater.*, **2013**, 25, 2600–2605.
31. Malig, J., Jux, N., Kiessling, D., Cid, J.-J. Vázquez, P., Torres, T., Guldi, D. M., *Angew. Chem. Int. Ed.*, **2011**, 50, 3561–3565.
32. Guldi, D. M., Costa, R. D., *J. Phys. Chem. Lett.*, **2013**, 4, 1489–1501.
33. Zhang, X., Feng, Y., Tang, S., Feng, W., *Carbon*, **2010**, 48, 211–216.

34. Katsukis, G., Malig, J., Schulz-Drost, C., Leubner, S., Jux, N., Guldi, D. M., *ACS Nano*, **2012**, 6, 1915–1924.
35. Bikram K. C., C., Das, S. K., Ohkubo, K., Fukuzumi, S., D'Souza, F., *Chem. Commun*., **2012**, 48, 11859–11861.
36. Malig, J., Stephenson, A. W. I., Wagner, P., Wallace, G. G., Officer, D. L., Guldi, D. M., *Chem. Commun*., **2012**, 48, 8745–8747.
37. Brinkhaus, L., Katsukis, G., Malig, J., Costa, R. D., Garcia-Iglesias, M., Vázquez, P., Torres, T., Guldi, D. M., *Small*, **2013**, 9, 2348–2357.
38. Jiménez, A. J., Grimm, B., Gunderson, V. L., Vagnini, M. T., Calderon, S. K., Rodríguez-Morgade, M. S., Wasielewski, M. R., Guldi, D. M., Torres, T., *Chem. Eur. J*., **2011**, 17, 5024–5032.
39. Li, F., Yang, H., Shan, C., Zhang, Q., Han, D., Ivaska, A., Niu., L. J., *Mater. Chem*., **2009**, 19, 4022–4025.
40. Haddad, R., Cosnier, S., Maaref, F., Holzinger, M., *Analyst*., **2009**, 134, 2412–2418.
41. Bartelmess, J., Ehli, C., Cid, J-J., García-Iglesias, M., Vázquez, P., Torres, T., Guldi, D. M., *Chem. Sci*., **2011**, 2, 652–660.
42. Martínez-Díaz, M. V., Ince, M., Torres, T., *Monatsh Chem*., **2011**, 142, 699–707.
43. Wang, A., Long, L., Zhang, C., *J. Incl. Phenom. Macrocycl. Chem*., **2011**, 71, 1–24.
44. Pereira, J. B., Carvalho, E. F. A., Faustino, M. A., Neves, M. G. P. M. S., Cavaleiro, J. A. S., Gomes, N. C. M., Cunha, A., Almeida, A., Tomé, J. P. C., *Photochem. Photobiol*., **2012**, 88, 537–547.
45. Booysen, I., Matemadombo, F., Durmus¸ M., Nyokong, T., *Dyes Pigm.*, **2011**, 89, 111–119.
46. Tedesco, A. C., Rotta, J. C. G., Lunardi, C. N., *Curr. Org. Chem*., **2003**, 7, 187–196.
47. Durmus¸ M., Yaman, H., Göl, C., Ahsen, V., Nyokong, T., *Dyes Pigm.*, **2011**, 91, 153–163.
48. Bottari, G., Suanzes, J. A., Trukhina, O., Torres, T., *J. Phys. Chem. Lett*., **2011**, 2, 905–913.
49. Vincett, P. S., Voigt, E. M., Rieckhoff, K. E., *J. Chem. Phys*., **1971**, 55, 4131–4140.
50. Kiessling, D., Costa, R. D., Katsukis, G., Malig, J., Lodermeyer, F., Feihl, S., Roth, A., Wibmer, L., Kehrer, M., Volland, M., Wagner, P., Wallace, G. G., Officer, D. L., Guldi, D. M., *Chem. Sci*., **2013**, 4, 3085–3098.

51. O’Neill, A., Khan, U., Nirmalraj, P. N., Boland, J., Coleman, J. N., *J. Phys. Chem. C*, **2011**, 115, 5422–5428.
52. Wang, Q. H., Shih, C. -J., Paulus, G. L. C., Strano, M. S., *J. Am. Chem. Soc.*, **2013**, 135, 18866–18875.
53. Li, X., Zhang, G., Bai, X., Sun, X., Wang, X., Wang, E., Dai, H., *Nat. Nanotechnol.*, **2008**, 3, 538–542.

Chapter 3

Supramolecular interactions between pyridyl and pyridinium phthalocyanines with SWNTs

3.1 Overview

Carbon nanotubes (CNTs) have been considered attractive candidates for diverse nanotechnological applications due to their extraordinary properties, such as molecular tanks/deliveries,[1] "bio"-sensors,[2,3] electronics,[4] nanomagnetical particles,[5] structural materials,[6] and many others.[7-9] However, CNTs are practically insoluble or hardly dispersed in any solvent, due to the formation of big bundles held strongly together. This lack of solubility and the difficult manipulation have imposed great limitations to their use. For this, several ways of dispersion and solubilization have been tried and can be basically divided in two main approaches: covalent[10-12] and noncovalent[13-15] functionalization. Both methodologies have advantages and disadvantages, however on noncovalent interactions CNTs aromatic structure and their electronic characteristics are preserved.[16,17] This supramolecular way to render CNTs soluble in a wide range of solvents is based on their noncovalent hydrophobic and π-π stacking interactions with specific molecules. Indeed, this methodology has been widely used to prepare individual CNTs by wrapping on the tubular surface several organic molecules,[18] biomolecules,[20,21] polymers,[22,23] surfactants[24] and more recently, ionic liquids.[25] In this context, it is envisaged the use of phthalocyanine (Pc) derivatives with single-wall carbon nanotubes (SWNTs) due to their unique absorption features in a large range of the UV-Vis spectrum.[26,27]

Interactions between different photosensitizer macrocycle cores have interesting adsorption properties and play a significant role in supramolecular chemistry.[28] It has been well documented that different conjugated aromatic units have preferences to associate on the SWNT surface by host-guest interactions promoting aromatic association.[29-33] These macrocycles bearing flexible, rigid planar or non-planar frameworks[34] are considered to enhance a specific face-to-face orientation around the SWNT scaffold.[35] Depending on the molecule type it is possible to obtain electronic transitions between the aromatic macrocycle and SWNT establishing potential electronic donor-acceptor properties.[36] The association of SWNT with electron-donors or acceptors produces active materials, which are able to generate electrical energy when irradiated.[37] Indeed, the development of trustworthy and reproducible procedures to incorporate CNT into functional assemblies, like donor/acceptor hybrids to convert sunlight into electrical energy, has emerged as an interesting research area. In this way, Pcs as electron donors and SWNT as electron acceptors are promising building blocks in donor-acceptor devices for solar energy

conversion, which is nowadays an important research topic to produce innovative materials, composites, and electronic devices of greatly reduced size.[38]

Attending to their properties, it was envisaged that zinc complexes of Pcs bearing mercaptopyridine groups[39] could interact by coordinating the pyridine units with the metal of neighbour molecules. These non-covalent interactions can approach the zinc thiopyridyl Pcs around the SWNT providing a compact assembly. Moreover, the cationization of the pyridine units affording amphiphilic thiopyridinium Pc derivatives,[39] can allow a possible dispersion of the SWNTs though π-π stacking interactions in water media. The connection of photosensitizer-type compounds e.g. Pcs, may also employ some effect on solubility features and the formation of such a Pc/SWNT conjugate may be used in solar cells, nanodevices, nanosensors, nanoheaters, among others.[40]

Likewise, Nyokong have been developed interesting pyridyl Pcs due to their assembly properties with SWNTs.[41,42] In this work, host-guest supramolecular interactions of neutral and cationic thiopyridyl Pc derivatives with SWNTs were characterized by different spectroscopic techniques, namely steady-state absorption and fluorescence spectroscopy (analysing respectively the absorption shift – Δλ, optical difference – and the emission quenching), time correlated single photon counting (TCSPC), and femtosecond transient absorption spectroscopy.

3.2 Synthesis of the pyridinium phthalocyanine derivatives

The thiopyridyl Pcs **2.6**-**2.8** (Figure 3.1) were prepared according with the procedure described in Chapter 2. The posterior cationization of the pyridine with methyl iodide afforded the corresponding amphiphilic cationic Pcs **3.1**-**3.3**. These positively charged derivatives were prepared in order to study the formation of thiopyridinium Pcs/SWNT supramolecular assemblies in water media.

The cationization of the pyridyl units of the Pcs **2.6**-**2.8** were performed with an excess of methyl iodide at 40 ºC in dry DMF. After stirring overnight in a hermetic pressure flask, the reaction mixtures were cooled down in ice and then it was added diethyl ether. The precipitates were retaken in a mixture of methanol/acetone and re-precipitated again with diethyl ether, filtered and dry under reduced pressure at 60 ºC. The thiopyridinium Pcs **3.1**-**3.3** were obtained in almost quantitative yields.

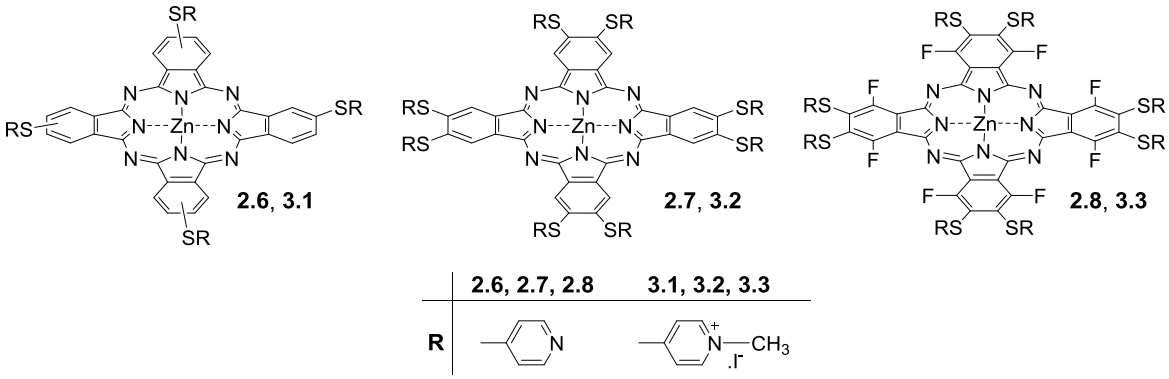

Figure 3.1 Thiopyridyl **2.6**-**2.8** and thiopyridinium **3.1**-**3.3** phthalocyanines.

The success of the cationization was confirmed by ^{1}H NMR spectroscopy; the spectra of **3.1**-**3.3** show in the aliphatic region at *ca* δ 4 ppm a peak or peaks (for **3.1** due to the presence of regioisomers) corresponding to the resonance of the methyl protons (Figures 3.2-3.4). In fact this is the main difference when these spectra are compared with the ones of the corresponding thiopyridyl Pcs **2.6**-**2.8**.

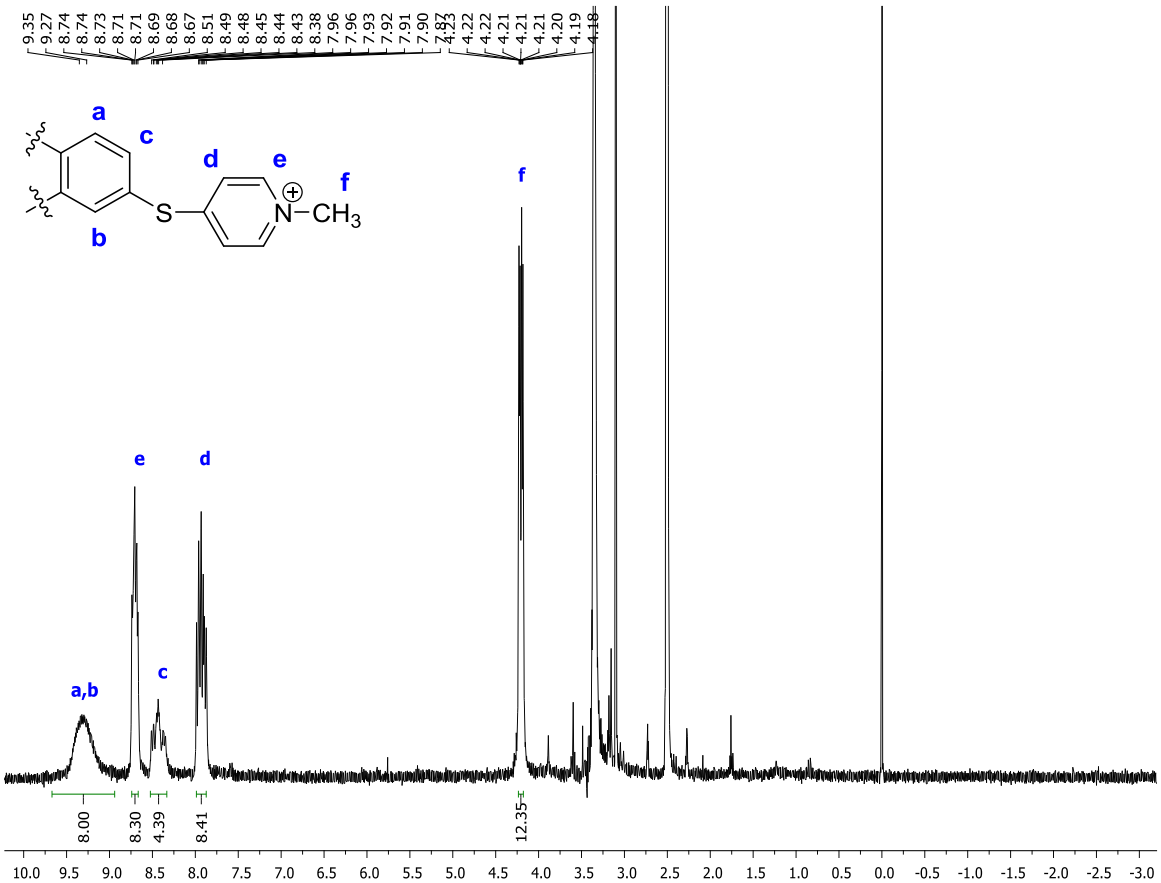

Figure 3.2 ^{1}H NMR spectrum of compound **3.1** in DMSO-d_6.

The resonances *ortho*- and *meta*-protons of the pyridinium moieties suffer a shift to lower fields due to the insertion of the methyl groups when compared with the corresponding neutral. Again, the resonances of the *ortho*- and *meta*-protons of the pyridinium moieties of **3.3** (δ 8.25 and 8.77 ppm, Figure 3.4) appear at slightly low field than the ones of the homologous Pc **3.2** (δ 8.10 and 8.72 ppm, Figure 3.3), due to presence of the electronegative fluorine atoms at the α-positions of the Pc **3.3**. Additionally, the α-proton resonances of **3.2** (δ 10.15 ppm, Figure 3.3) appear at lower fields when compared with the ones of **3.1** (δ 9.10–9.48 ppm, Figure 3.2) due to the presence of the two electron-withdrawing thiopyridinium units instead of one in the **3.1**.

The ^{19}F NMR spectrum of **3.3** confirmed also its high symmetry by showing the resonance of the α-fluorine atoms as a singlet at δ 127.25 (Figure 3.5).

The spectra of structures of compounds **3.1-3.3** confirmed also their structures by showing peaks at *m/z* at 1027 ($[M\text{-}3CH_3]^+$), 1463 ($[M\text{-}7CH_3]^+$) and 1608 ($[M\text{-}7CH_3]^+$) corresponding respectively to their base peak.

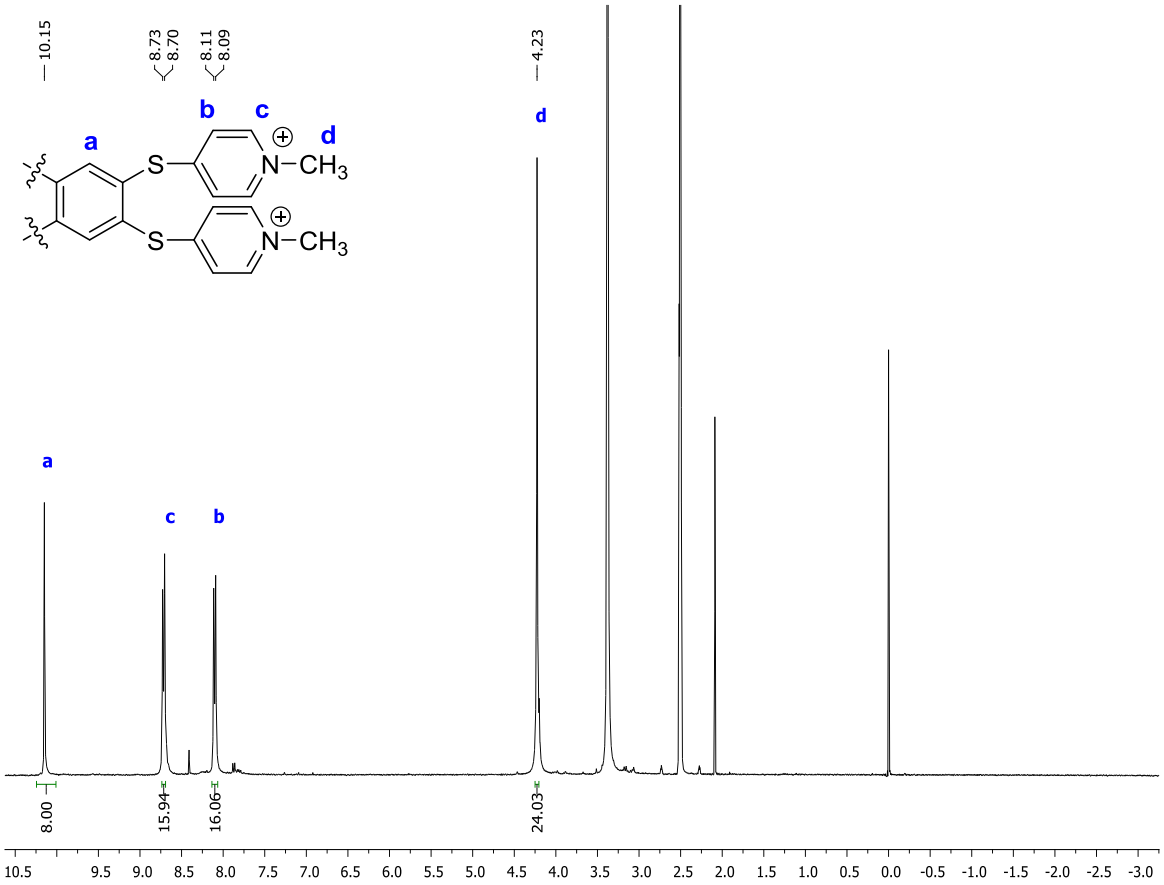

Figure 3.3 ^{1}H NMR spectrum of compound **3.2** in DMSO-d_6.

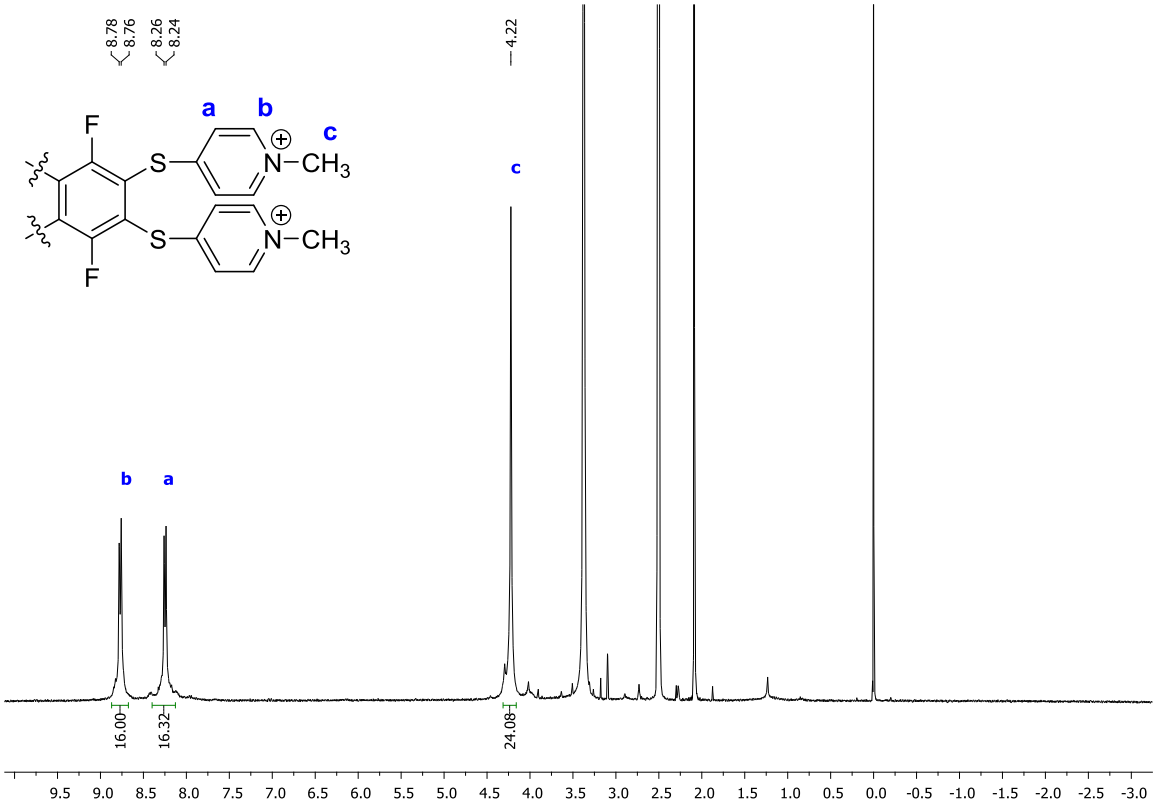

Figure 3.4 ^{1}H NMR spectrum of compound **3.3** in DMSO-d_6.

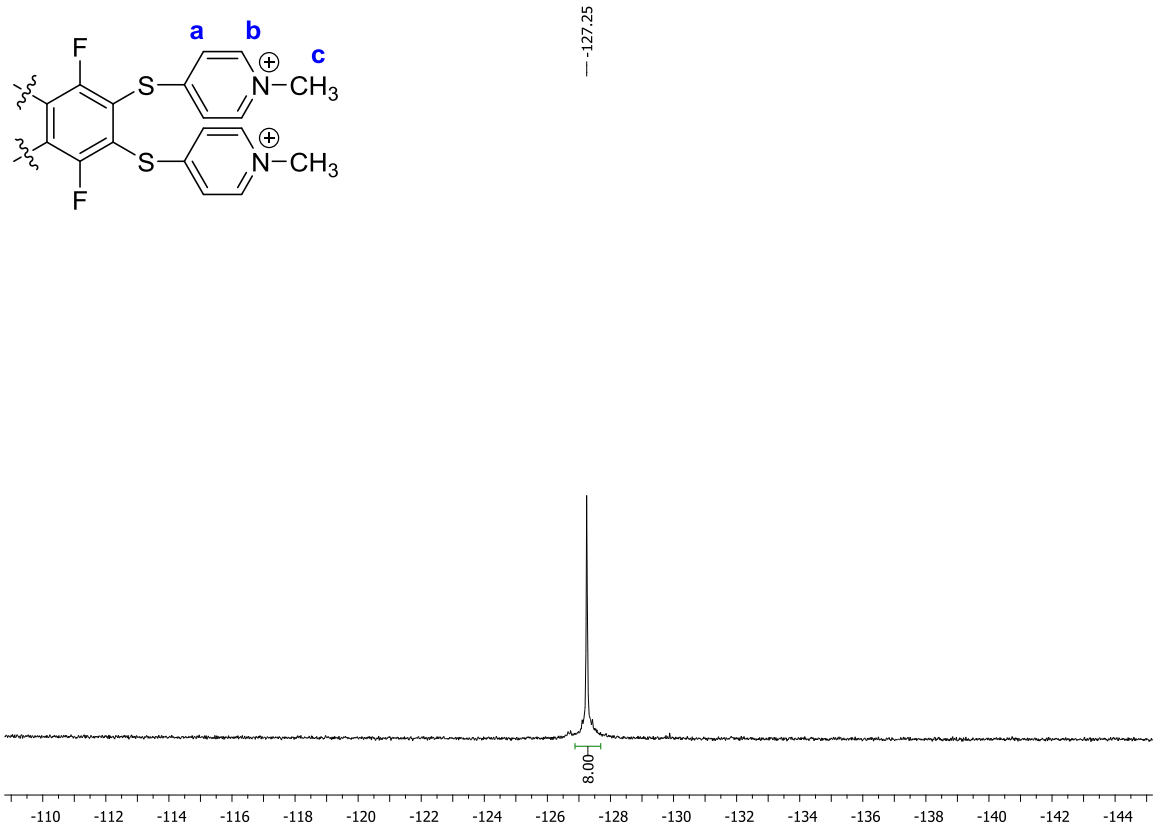

Figure 3.5 ^{19}F NMR spectrum of compound **3.3** in DMSO-d_6.

3.3 Photophysical properties of phthalocyanine/SWNT assemblies

As it was already mentioned, the host-guest supramolecular interactions between SWNTs and Pcs **2.6**-**2.8** and **3.1**-**3.3** were evaluated by different spectroscopic techniques, namely steady-state absorption and fluorescence spectroscopy (analysing respectively the absorption shift – $\Delta\lambda$, optical difference – and the emission quenching), TCSPC, and femtosecond transient absorption spectroscopy. However, in order to understand the type of interaction it is important to report previously the photophysical properties of the individual molecules.

3.3.1 Absorption and emission properties of the pyridinium phthalocyanines

The absorption and the emission properties of charged thiopyridinium Pcs **3.1**-**3.3** were evaluated in deuterium oxide (D_2O) with 0.1 wt% sodium dodecylbenzenesulfonate (SDBS), instead of DMF as it was reported for **2.6**-**2.8** in Chapter 2. These cationic Pcs **3.1**-**3.3** show absorption features similar to the ones described for **2.6**-**2.8** (Table 2.1 in Chapter 2), with the Q-band maxima at 683, 701 and 717 nm respectively (Figure 3.6a), and molar extinction coefficients (ε) of the same order of magnitude (Table 3.1). The fluorescence spectra of monomeric **3.1**-**3.3** in D_2O/SDBS (0.1 wt %) upon 620 nm excitation give rise to maxima at 689 nm for **3.1**, 704 nm for **3.2**, and 726 nm for **3.3** were gathered at concentrations below 10^{-5} M (Figure 3.6b). These Pcs show slightly lower fluorescence quantum yields, 0.031 for **3.1**, 0.056 for **3.2**, and 0.018 for **3.3** than **ZnPc** (0.30) used as reference[43] (Table 3.1).

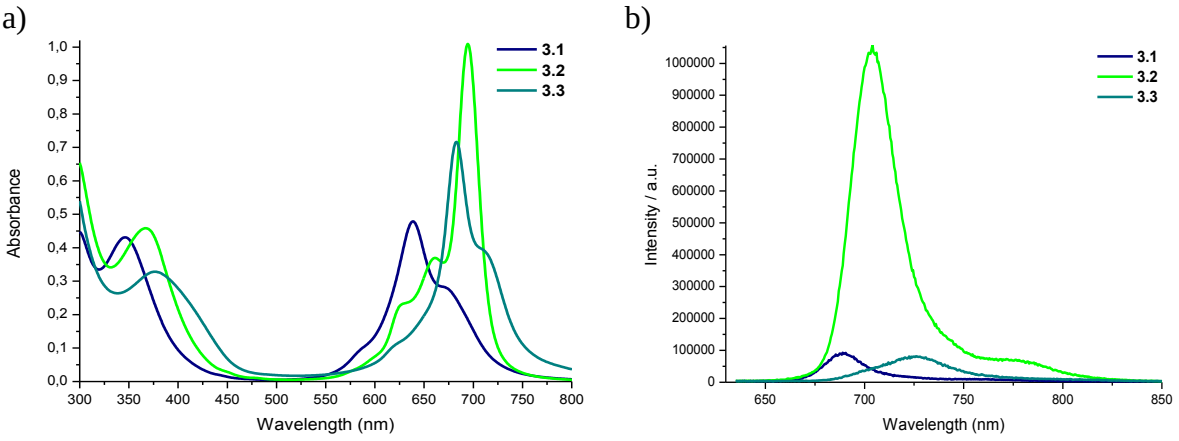

Figure 3.6 a) Absorption and b) emission, upon excitation wavelength at 620 nm, spectra of Pcs **3.1**-**3.3** in D_2O/SDBS (0.1 wt %) at concentrations of 10^{-6} M.

Table 3.1 The molar extinction coefficient (ε), fluorescence quantum yields (ϕ_F), and time correlated single photon counting (τ) in D_2O/SDBS (0.1 wt %).

Compounds	ε ($M^{-1}cm^{-1}$)	λ_{max} / nm	ϕ_F	τ_1 (ns)	τ_2 (ns)
3.1	1.84×10^4	689	0.031	1.42	2.97
3.2	2.58×10^4	704	0.056	0.18	1.53
3.3	1.83×10^4	726	0.018	0.08	1.90

Moreover, it was also studied the TCSPC using a $\lambda_{exc.}$ at 403 nm to analyse the relaxation of molecules from an excited state to a lower energy state. Since various molecules in a sample will emit photons at different times, despite their simultaneous excitation, the observed decay must be a certain rate of emission photons (Figure 3.7).

The resulting histograms are best fitted by biexponential functions yielding a short (τ_1) and a long lifetime (τ_2). The lifetimes values τ_1 and τ_2 along with the ratio of their relative amplitudes are 1.42 and 2.97 ns (0.075) for **3.1**, 0.18 and 1.53 ns (5.19) for **3.2** as well as 0.08 and 1.90 ns (0.13) for **3.3** (Table 3.1), respectively. Taking the aforementioned into concert, it was related the shorter lifetimes to those the aggregates, while the longer lifetimes are assigned to the fluorescing behaviour of the monomers.

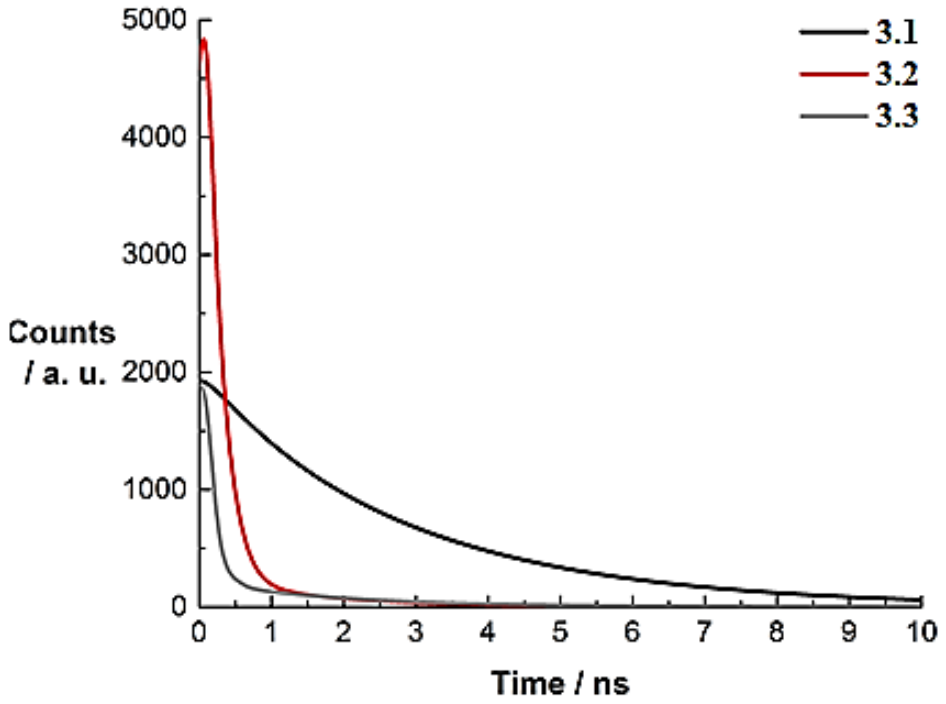

Figure 3.7 Emission time profiles of **3.1**-**3.3** in D_2O/SDBS (0.1 wt%) following 403 nm excitation wavelength and the corresponding emission maxima.

3.3.2 Absorption and emission properties of thiopyridylphthalocyanine/SWNT assemblies

The host-guest supramolecular interactions between the neutral Pcs **2.6-2.8** and SWNTs were performed by titrating SWNT suspensions in DMF with the Pcs dissolved also in DMF. The homogeneous and stable greyish suspensions of SWNT were obtained by ultrasonication (2×20 min, 100 W, 37 GHz), followed by centrifugation (10 min of at 5.000 RPM) in DMF.

The interactions were confirmed through the absorption wavelength alterations between the single Pcs **2.6**-**2.8** and the corresponding conjugates **2.6**-**2.8**/SWNT.

In the first set of titration assays (small additions of Pc solution to SWNT dispersion), the interactions between both species were probed unequivocally in all cases, by detection of an absorption red shift of the respectively Q-band (Figures 3.11a-3.13a). The maximum absorption wavelength of the Q-band for Pc **2.6**-**2.8** is respectively 683, 702 and 721 nm and their maximum absorption wavelength is modified after the interaction with the carbon allotrope. The optical difference between the corresponding single Pc **2.6**-**2.8** and the Pc **2.6**-**2.8**/SWNTs conjugates were: **2.6**/SWNT (Δλ = 17 nm), Pc **7**/SWNT (Δλ = 24 nm), and Pc **2.8**/SWNT (Δλ = 19 nm). On the other hand, the fluorescence measurements using an excitation wavelength (λ_{exc}) at 620 nm show, that after the first additions of Pc **2.6**-**2.8** to the SWNTs, the intensity of the prominent Q-band is substantially reduced, evidencing supramolecular interactions band (Figures 3.11b-3.13b).

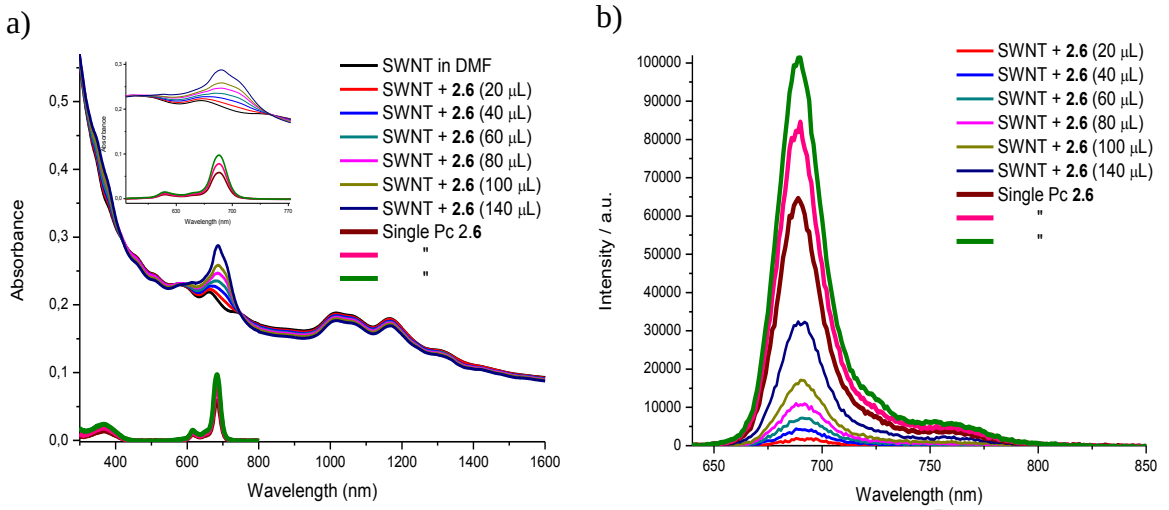

Figure 3.8 Titration of SWNT suspension with Pc **2.6** solution (10^{-5} M) in DMF. a) Absorption and b) emission spectra of the single Pc **2.6** and Pc **2.6**/SWNT (Δλ = 17 nm). Excitation wavelength at 620 nm. The insets show the expansion between 600-800 nm.

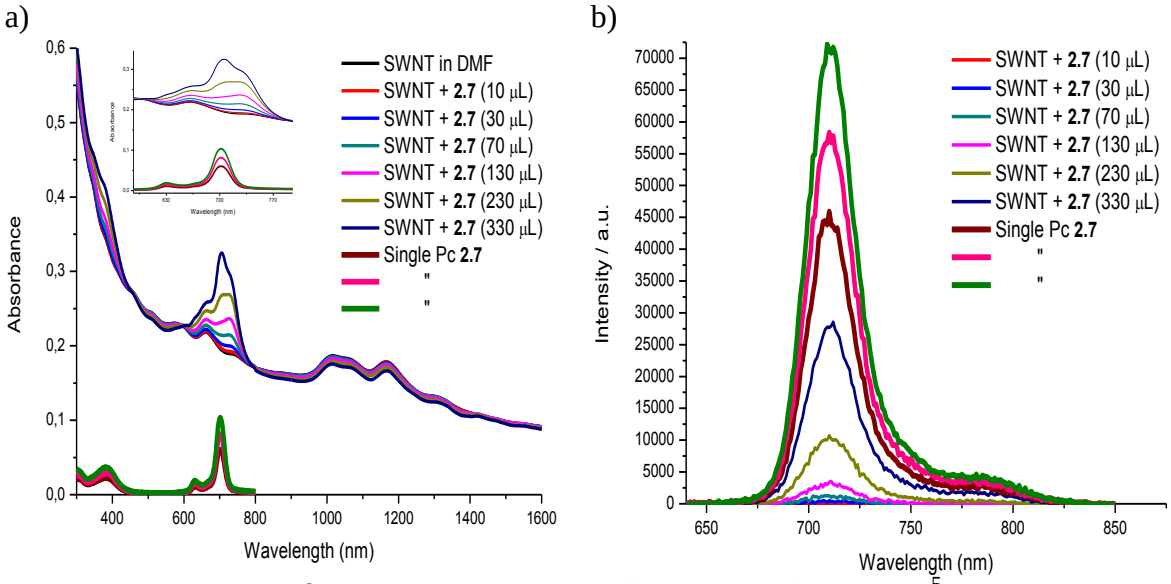

Figure 3.9 Titration of SWNT suspension with Pc **2.7** solution (10^{-5} M) in DMF. a) Absorption and b) emission spectra of the single Pc **2.7** and Pc **2.7**/SWNT ($\Delta\lambda$ = 24 nm). Excitation wavelength at 620 nm. The insets show the expansion between 600-800 nm.

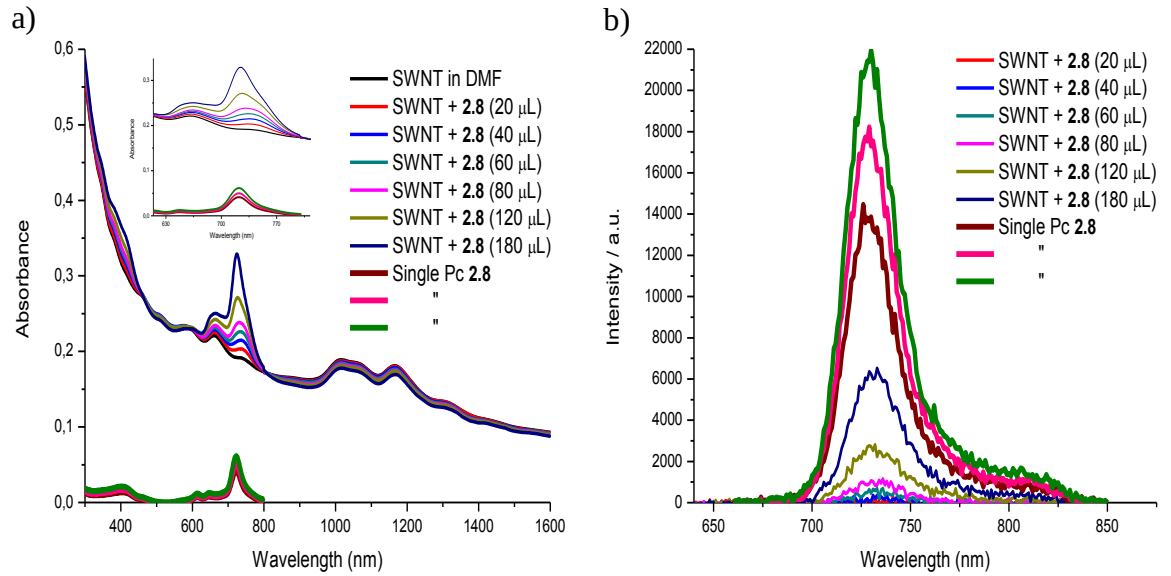

Figure 3.10 Titration of SWNT suspension with Pc **2.8** solution (10^{-5} M) in DMF. a) Absorption and b) emission spectra of the single Pc **2.8** and Pc **2.8**/SWNT ($\Delta\lambda$ = 19 nm). Excitation wavelength at 620 nm. The insets show the expansion between 600-800 nm.

The supramolecular assemblies most probably combine different interactions such as π-π and metal coordination between the inner zinc and the pyridyl groups (Figure 3.14).[44-47] These structures, even in the solution phase, may be associated *via* coordination around SWNTs as represented, for example, for the Pc **2.6**.

Most problably it is formed “nanocages”, because the multiple coordinated possibilities between the multiple pyridyl groups and the zinc metal ion of the neighbour molecules (Figure 3.15).

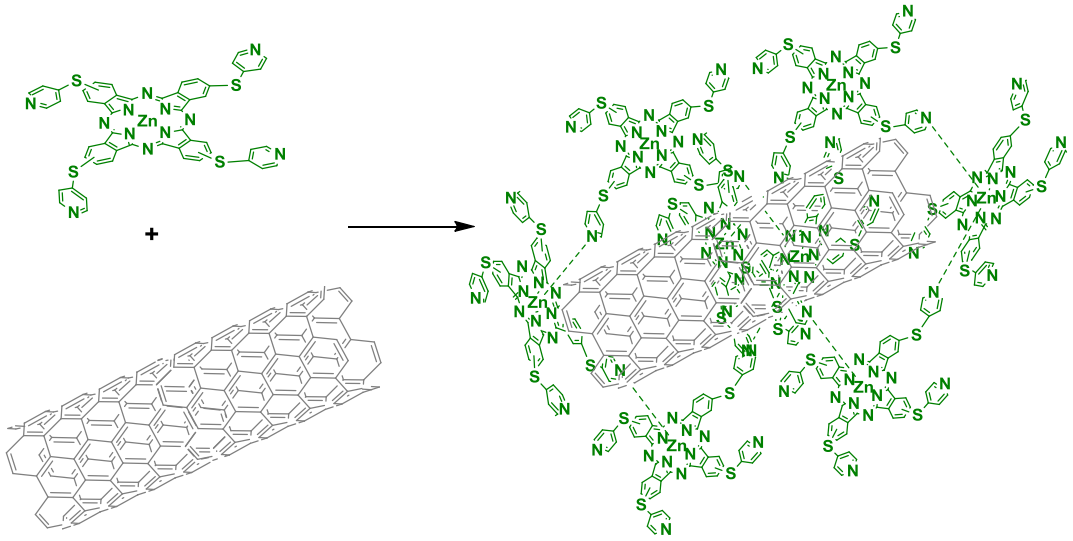

Figure 3.11 Possible noncovalent interactions of thiopyridyl Pcs **2.6**/SWNT assemblies.

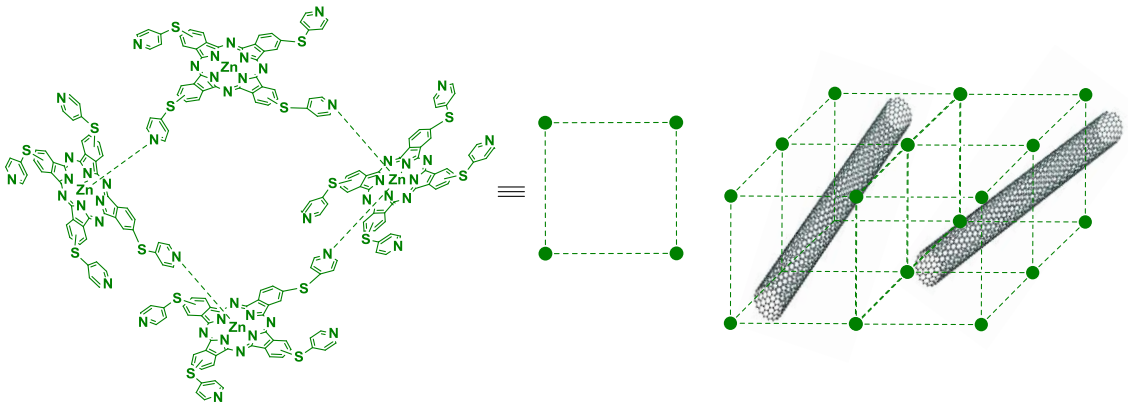

Figure 3.12 Randomly network performed with thiopyridyl Pcs **2.6** around SWNTs.

It was confirmed the supramolecular functionalization of SWNTs by the neutral thiopyridyl Pcs **2.6-2.8** by absorption and emission spectroscopic experiments explicitly referenced on the last Figures 3.11-3.13. However, it is important others photophysical studies, like transient absorption experiments, to prove the respective electronic

interactions of Pcs **2.6-2.8**/SWNTs, evidencing the donor-acceptor properties of these nanoconjugates.

3.3.3 Absorption and emission properties of thiopyridiniumphthalocyanine/SWNT assemblies

The supramolecular interactions between the single thiopyridinium Pcs **3.1-3.3** and the SWNTs suspensions were studied using a similar procedure to the one described for neutral Pc, but in this case the Pc were dissolved in D_2O/SDBS (0.1 wt%).

The single cationic Pcs **3.1-3.3** present the maximum Q-band absorption wavelength at respectively 689, 704 and 726 nm. The absorption shifts detected after the interaction of **3.1** and **3.2** with SWNTs were: Pc **3.1**/SWNT ($\Delta\lambda$ = 13 nm) and Pc **3.2**/SWNT ($\Delta\lambda$ = 7 nm). Despite the small values of the optical difference $\Delta\lambda$, the quenching of the emission intensity evidence host-guest interactions for both Pc **3.1**/SWNT and Pc **3.2**/SWNT nanoconjugates (Figures 3.16 and 3.17). A possible explanation of these lower shift values when compared with the shifts observed with the neutral Pc are probably due to repulsion between the positively charged Pc. Concerning the Pc **3.3**, it was not possible to obtain a decent spectrum for Pc **3.3**/SWNT maybe due to the aggregation of Pc **3.3** in D_2O/SDBS (0.1 wt%). Indeed, it will be necessary to perform more spectral measurements in different solvents to take unequivocal conclusions.

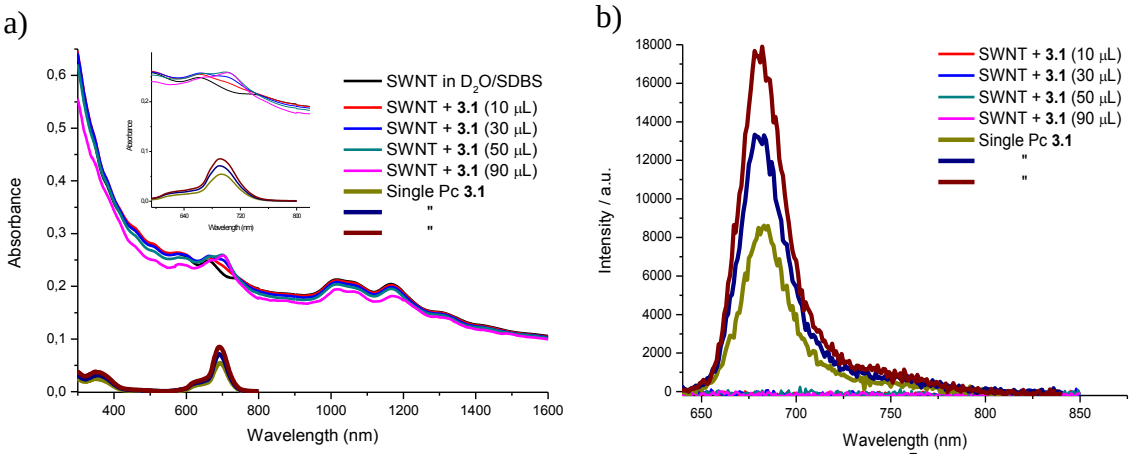

Figure 3.13 Titration of SWNTs suspension with Pc **3.1** solution (10^{-5} M) in D_2O/SDBS (0.1 wt%). a) Absorption and b) emission spectra of the single Pc **3.1** and Pc **3.1**/SWNT ($\Delta\lambda$ = 13 nm) in D_2O/SDBS (0.1 wt%). Excitation wavelength at 620 nm. The insets show the expansion between 600-800 nm.

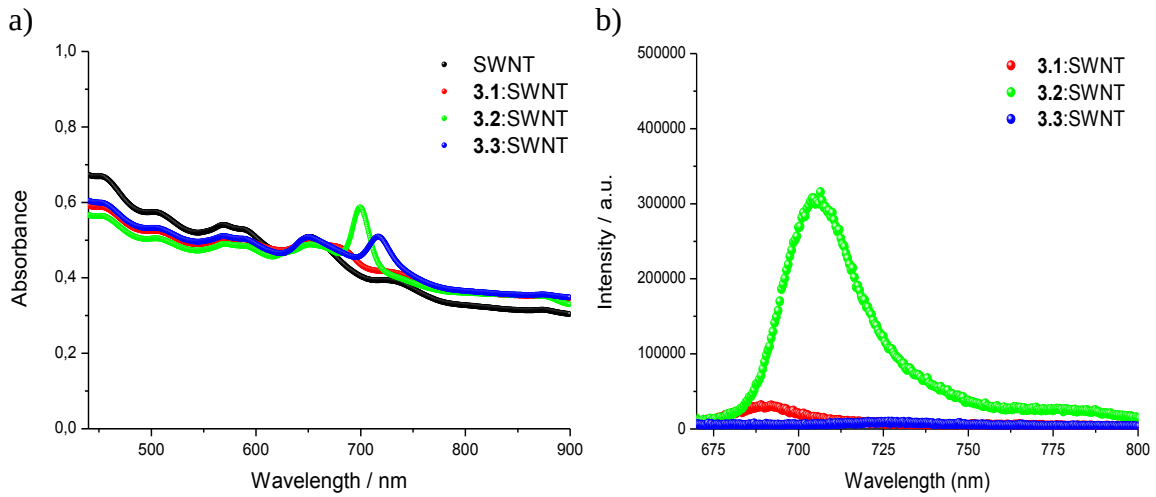

Figure 3.14 a) Absorption spectra of SWNT suspended in D_2O/SDBS (0.1 wt%) and titration of the SWNT with **3.1**-**3.3** (10^{-5} M) in D_2O/SDBS (0.1 wt%). Excitation wavelength at 620 nm. The insets show the expansion between 600-800 nm.

3.3.4 3D NIR fluorescence spectra of SWNT and Pc 3.1-3.3:SWNT

Motivated by absorption and emission properties of the hybrid materials Pc **3.1**-**3.3**/SWNT, it was mapped the 3D NIR fluorescence to detect the possibility of supramolecular interactions between both components. As a standard, was prepared a similar absorbing SWNT suspension in D_2O/SDBS (0.1 wt%). From Figures 3.18 and 3.19-3.21, which compare SWNT/D_2O/SDBS (0.1 wt%) and Pc **3.1**-**3.3**:SWNT/D_2O/SDBS (0.1 wt%), it is derived several trends with an excitation wavelength of 387 nm.

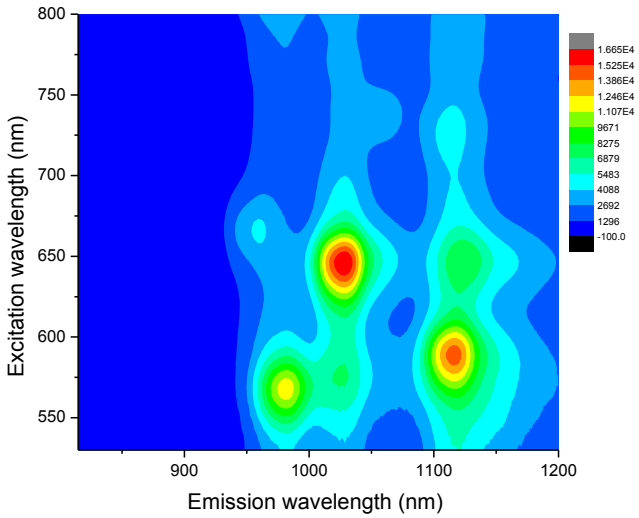

Figure 3.15 Steady-state 3D NIR fluorescence spectra of SWNT/D_2O/SDBS (0.1 wt%) – with increasing intensity from blue to green to yellow and to red.

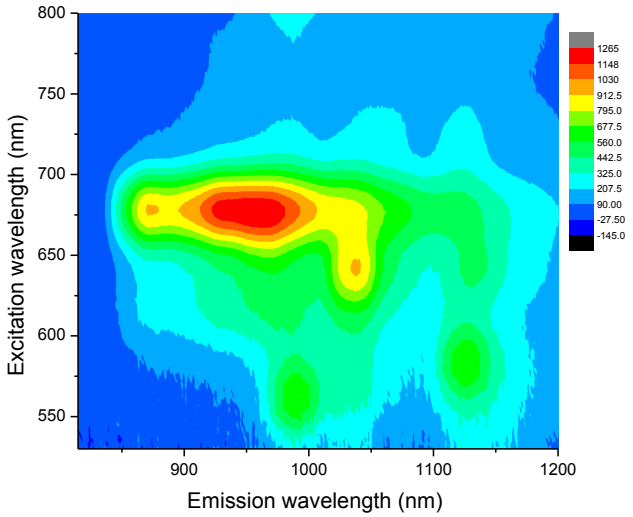

Figure 3.16 Steady-state 3D NIR fluorescence spectra of **3.1**:SWNT/D_2O/SDBS (0.1 wt%) – with increasing intensity from blue to green to yellow and to red.

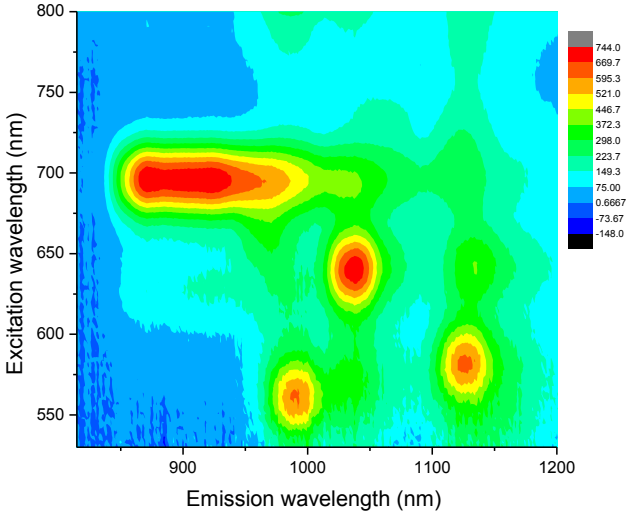

Figure 3.17 Steady-state 3D NIR fluorescence spectra of **3.2**:SWNT/D_2O/SDBS (0.1 wt%) – with increasing intensity from blue to green to yellow and to red.

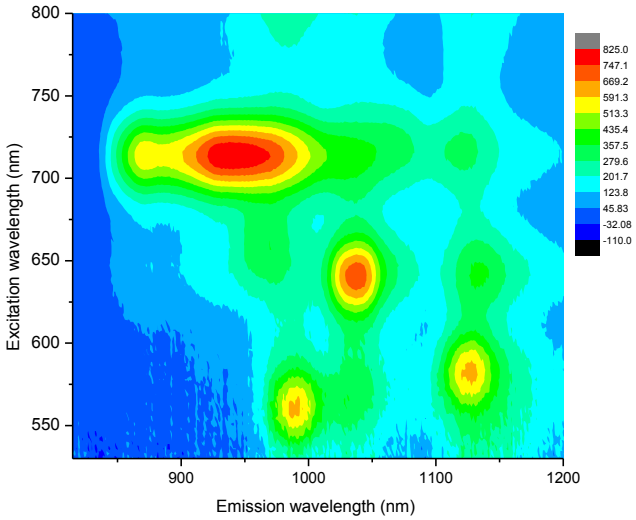

Figure 3.18 Steady-state 3D NIR fluorescence spectra of **3.3**:SWNT/D_2O/SDBS (0.1 wt%) – with increasing intensity from blue to green to yellow and to red.

The differences observed in steady-state 3D NIR fluorescence spectra of **3.1**-**3.3**:SWNT/D_2O/SDBS (0.1% wt) in comparison to NIR fluorescence spectra of SWNT/D_2O/SDBS (0.1% wt) are probably due to the electron-donor/acceptor interactions between them, while sizeable contributions from solvent effects were not ruled out (Figure 3.22).

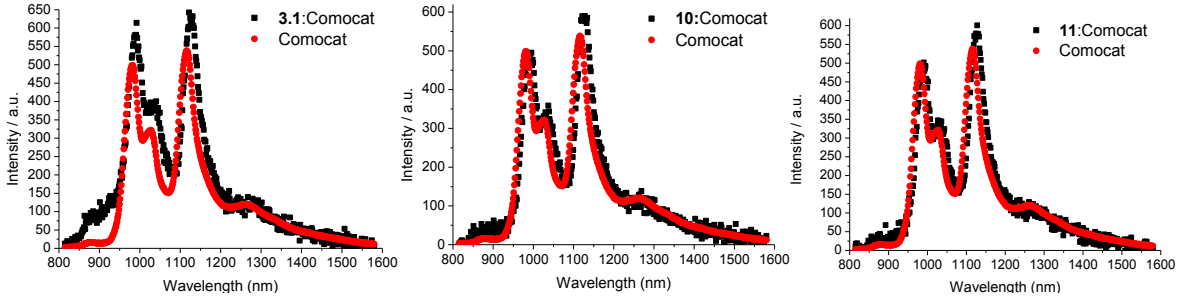

Figure 3.19 Comparison of the NIR fluorescence spectra of pristine SWNT/D_2O/SDBS (0.1 wt%) (black) and Pc **3.1**-**3.3**:SWNT/D_2O/SDBS (0.1 wt%) (red) upon lamp excitation at 575 nm.

3.3.5 Femtosecond Transient absorption spectroscopy

The differential absorption spectrum of **3.2**, which was probed in 0.1 wt% SDBS in D_2O, with minima at 631 and 701 nm arise as a consequence of 387 nm excitation (Figure 3.23). These are ascribed to ground state bleaching. The latter, together with rather broad maxima around 472, 596 and 1096 nm are assigned to singlet excited state features. Analyses of the absorption time profiles at these maxima reveal similar lifetimes, namely 15.5 ± 0.87 ps due to the presence of aggregates, 1.39 ± 0.06 ps for the transition from S_2 to S_1, and 440.1 ± 44.4 ps for intersystem crossing. As such, the intersystem crossing to the corresponding triplet excited state is nearly ten times faster for **3.2** than for **2.7**. In the latter case, maxima at 654 and 849 nm develop during the first picoseconds. Here, it is derived lifetimes of 2.72 ± 0.2 ps, 27.8 ± 1.5 ps, and 1.2 ± 0.08 ns at 849 nm. Again, similar trends are noted for **3.1** and **3.3** (Figures 3.24 and 3.25).

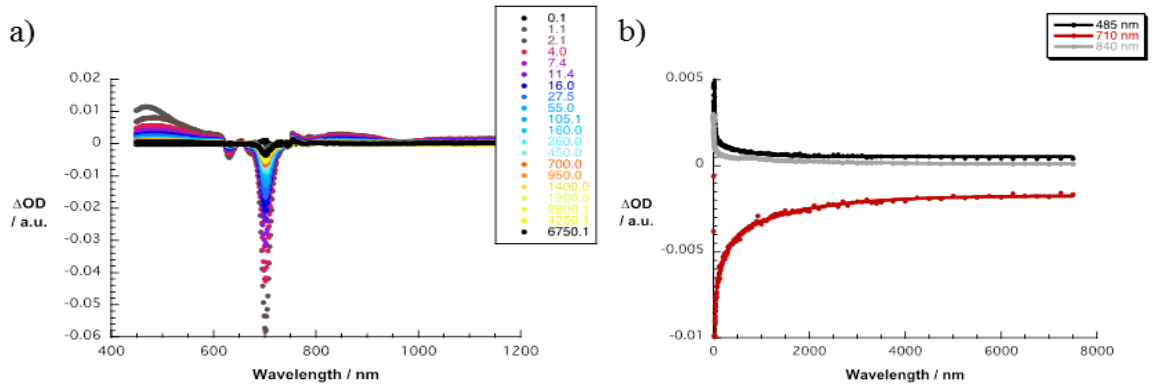

Figure 3.20 a) Differential absorption spectra (visible) obtained upon femtosecond pump probe experiments (387 nm) of **3.2** in D_2O/SDBS (0.1 wt %) with time delays between 0.1 and 6750.1 ps at room temperature. b) Time absorption profiles of the spectra shown at 485, 710 and 840 nm.

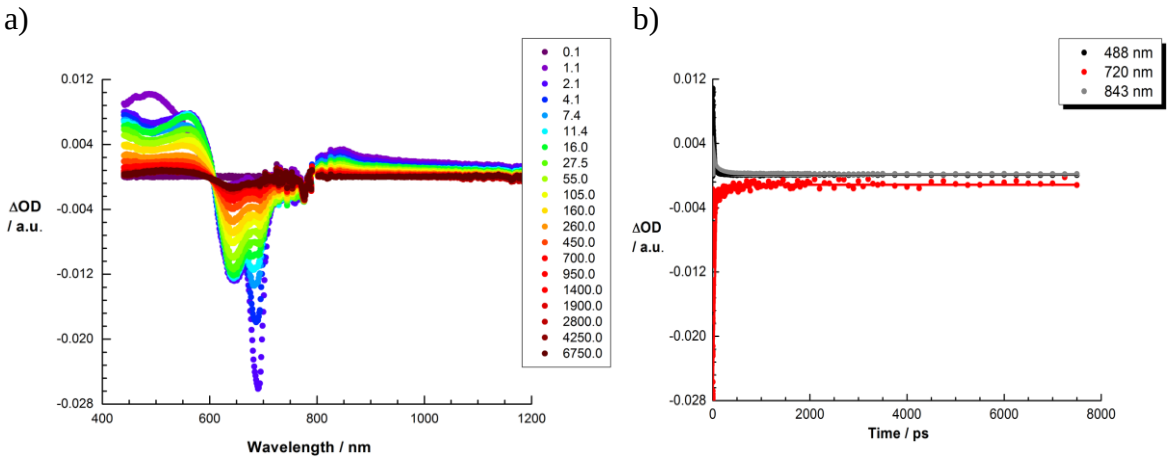

Figure 3.21 a) Differential absorption spectra (visible) obtained upon femtosecond pump probe experiments (387 nm) of **3.1** in D_2O/SDBS (0.1 wt%) with time delays between 0.1 and 6750.0 ps at room temperature. b) Time absorption profile of the spectra shown at 488, 720 and 843 nm.

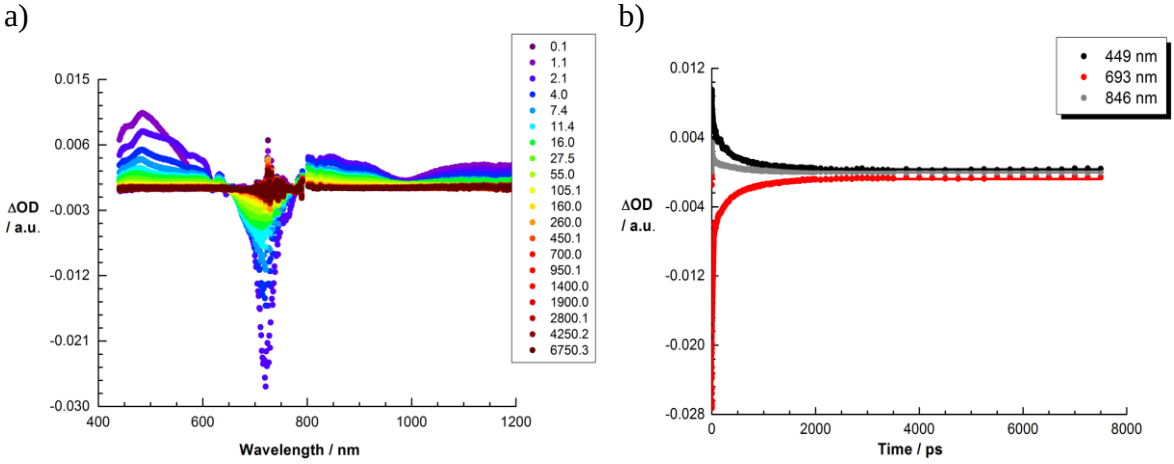

Figure 3.22 a) Differential absorption spectra (visible) obtained upon femtosecond pump probe experiments (387 nm) of **3.3** in D_2O/SDBS (0.1 wt%) with time delays between 0.1 and 6750.3 ps at room temperature. b) Time absorption profile of the spectra shown at 449, 693 and 846 nm.

Initially, upon photoexciting Pc **3.1**-**3.3**:SWNT/SDBS (0.1 wt%) at 387 nm, the Pc singlet excited state fingerprints – *vide supra* – are notable (Figures 3.26-3.28). At first glance, the visible range is dominated by transient maxima and transient minima ranges. These findings are important, since they attest to the successful formation of the ZnPc singlet excited state. At the end of the Pc **3.1**-**3.3** and SWNT excited state decays, characteristic changes occur in the differential absorption for Pc **3.1**-**3.3**:SWNT/SDBS (0.1 wt%). In the visible is appreciable a bleaching of the Q-bands (Figures 3.26-3.28). In the near infrared, on the other hand, we see a set of maxima and a set of minima that prove electronic communication in these assemblies.

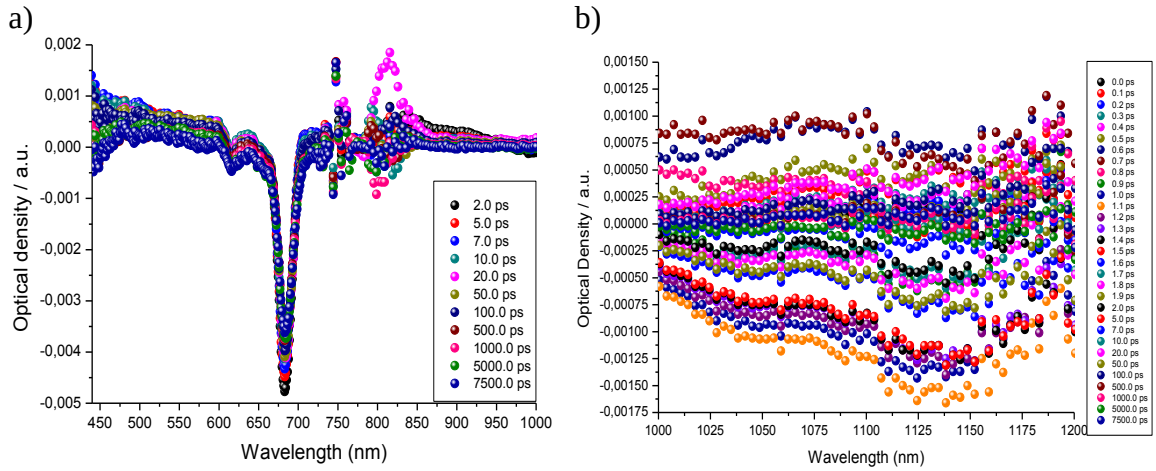

Figure 3.23 Transient absorption spectra of Pc **3.1**/SWNT in D_2O/SDBS (0.1 wt%) with time delays between 0.0 and 7500 ps at room temperature. Excitation at 387 nm, pulse width 150 fs, pump energy 200 nJ.

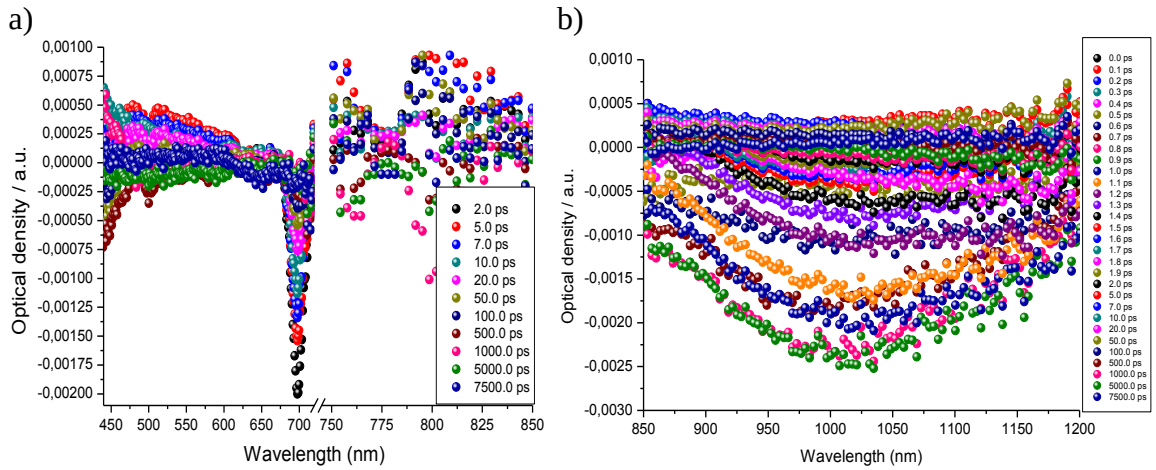

Figure 3.24 Transient absorption spectra of Pc **3.2**/SWNT in D_2O/SDBS (0.1 wt%) with time delays between 0.0 and 7500 ps at room temperature. Excitation at 387 nm, pulse width 150 fs, pump energy 200 nJ.

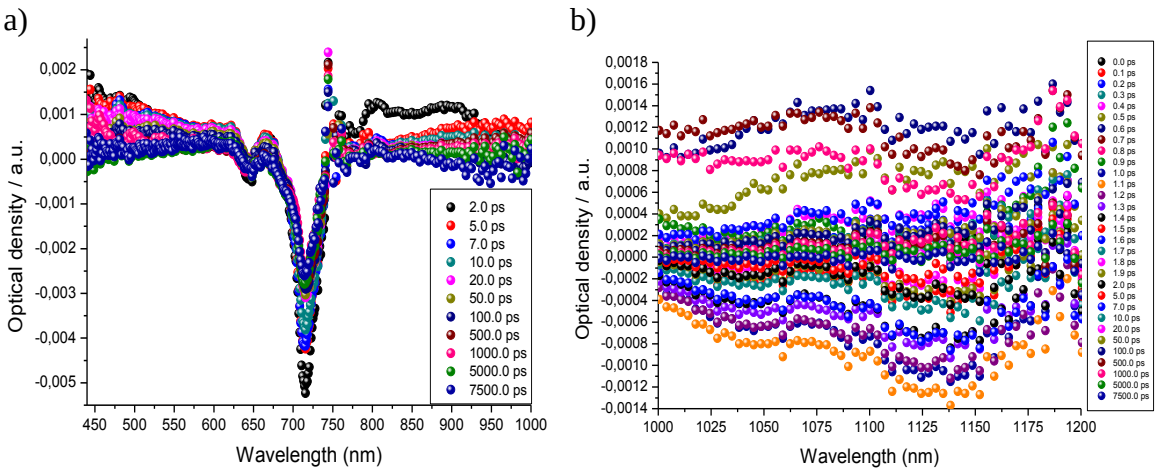

Figure 3.25 Transient absorption spectra of Pc **3.3**/SWNT in D_2O/SDBS (0.1 wt%) with time delays between 0.0 and 7500 ps at room temperature. Excitation at 387 nm, pulse width 150 fs, pump energy 200 nJ.

3.4 Final considerations

In conclusion, neutral Pcs **2.6**-**2.8** evidence π-π interactions with SWNTs (Δλ = 17–24 nm) in DMF, were the SPy groups have ability to coordinate the metal of the macrocycle core of the neighboring Pcs, around the SWNTs surface. Cationic Pcs **3.1** and **3.2** presents also noncovalent interactions but with smaller optical shift comparatively with the corresponding neutral Pcs **2.6** and **2.8**. With regards to the electron donor/acceptor character of these assemblies more studies will be necessary, in order to take final conclusions. However, the first photophysical properties of Pc **3.1**-**3.3**:SWNT nanoconjugates showed π–π stacking interactions by absorption and emission spectroscopy. We think that is essential more time-resolved studies to verify an electron transfer between the Pc to SWNT, upon photoexcitation, which will make this donor-acceptor hybrids promising for future electronic applications.

3.5 Experimental section

3.5.1 General information

The general information for this chapter is similar to the one described in Chapter 2 experimental. Steady-state absorption spectra were recorded with a Perkin-Elmer Lambda

35. Steady-state emission spectra were recorded with a Fluoromax-3-spectrometer from HORIBA Jobin Yvon. All samples were measured in a fused quartz glass cuvette with a diameter of 10 mm.

Femtosecond transient absorption spectra were obtained with a Ti:sapphire laser system CPA-2101 (Clark-MXR), Inc.) in combination with a Helios TAPPS detection unit from Ultrafast Inc. All samples were measured in a fused quartz glass cuvette with a thickness of 2 mm. Data was acquired with the software HELIOS Visible/nIR (Newport / Ultrafast Systems).

3.5.2 Syntheses of thiopyridiniumphthalocyanines 3.1-3.3

The methylation of Pcs **2.6**-**2.8** (150.0 mg) was performed in 10 mL of DMF using methyl iodide in excess (3.0 mL, 48.1 mmol). The reaction mixture was stirred for 24 h at 40 ºC. Then, the mixture was cooled down and the desired product was precipitated with diethyl ether. The solid was filtered and washed several times with diethyl ether. After that, the products were retaken in a mixture of methanol/acetone, re-precipitated from acetone, filtered and dry under reduced pressure at 60 ºC. Compounds **3.1**-**3.3** were obtained almost in quantitative yields.

*2,9(10),16(17),23(24)-tetrakis(4-methylpyridiniumsulfanyl)phthalocyaninato zinc(II) (**3.1**)*: ^{1}H NMR (300 MHz, DMSO-d_6): δ 4.18 – 4.23 (m, 12H, H^f), 7.87 – 7.96 (m, 8H, Ar-*o*-H^d), 8.33 – 8.52 (m, 4H, β-H^c), 8.67 – 8.74 (m, 8H, Ar-*m*-H^e), 9.10 – 9.48 (m, 8H, α-H^{a,b}). UV–Vis (DMSO), λ_{max} (log ε): 352 (4.60), 616 (4.39), 685 (5.20) nm. MALDI-TOF-MS: *m/z* 1027 [M-3CH_3]$^+$.

*2,3,9,10,16,17,23,24-Octakis(4-methylpyridiniumsulfanyl)phthalocyaninato zinc(II) (**3.2**)*: ^{1}H NMR (300 MHz, DMSO-d_6): δ 4.23 (s, 24H, H^d), 8.10 (d, *J* = 7.1 Hz, 16H, Ar-*o*-H^b), 8.72 (d, *J* = 7.1 Hz, 16H, Ar-*m*-H^c), 10.15 (s, 8H, Pc α-H^a). UV–Vis (DMSO), λ_{max} (log ε): 383 (4.55), 630 (4.38), 702 (5.03) nm. MALDI-TOF-MS: *m/z* 1463 [M-7CH_3]$^+$.

*1,4,8,11,15,18,22,25-Octafluoro-2,3,9,10,16,17,23,24-Octakis(4-methylpyridiniumsulfanyl)phthalocyaninato zinc(II) (**3.3**)*:
^{1}H NMR (300 MHz, DMSO-d_6): δ 4.22 (s, 24H, H^{c}), 8.25 (d, J = 7.1 Hz, 16H, Ar-*o*-H^{a}), 8.77 (d, J = 7.1 Hz, 16H, Ar-*m*-H^{b}). ^{19}F NMR (DMSO-d_6): δ -127.25 (s, 8F, Pc-α-F). UV–Vis (DMSO), λ_{max} (log ε): 407 (4.46), 647 (4.29), 722 (4.84) nm. MALDI-TOF-MS: *m/z* 1608 $[M\text{-}7CH_3]^+$.

3.5.3 Preparation of stable SWNT suspensions and the stock solutions of phthalocyanines

SWNTs (0.5 mg) were dispersed in DMF (10 mL) by ultrasonication (around 15 min), obtaining a dark gray suspension of SWNTs. Significantly, an excess of SWNTs was removed by centrifugation for 15 min at 9.6 kG. The resulting SWNT suspensions did not show appreciable SWNT-based fluorescence in the NIR, since most likely, debundling is incomplete. Nevertheless, their overall stability renders them an ideal starting point for further tests. The stock solutions of **2.6**-**2.8** and **3.1**-**3.3** were prepared in DMF and D_2O/SDBS (0.1 wt%), respectively, at concentrations of 10^{-5} M.

3.6 References

1. Liu, Q., Chen, B., Wang, Q., Shi, X., Xiao, Z., Lin, J., Fang, X., *Nano Lett.*, **2009**, 9, 1007–1010.
2. Wei, D., Bailey, M. J. A., Andrew, P., Ryhänen, T., *Lab Chip*., **2009**, 9, 2123–2131.
3. Jeykumari, D. R. S., Narayanan, S. S., *Analyst*., **2009**, 134, 1618–1622.
4. Cole, M. W., Crespi, V. H., Dresselhaus, M. S., Dresselhaus, G., Fischer, J. E., Gutierrez, H. R., Kojima, K.., Mahan, G. D., Rao, A. M., Sofo, J. O., Tachibana, M., Wako, K., Xiong, Q., *J. Phys. Condens. Matter.*, **2010**, 20, 334201–334225.
5. Ge, J., Hu, Y., Biasini, M., Beyermann, W. P., Yin, Y., *Angew. Chem. Int. Ed*., **2007**, 46, 4342–4345.
6. Ashrafi, B., Hubert, P., Vengallatore, V., *Nanotechnology*, **2006**, 174895–4903.
7. Robertson, N., McGowan, C. A., *Chem. Soc. Rev.*, **2003**, 32, 96–103.
8. Baughman, R. H., Zakhidov, A. A., de Heer, W. A., *Science*, **2002**, 297, 787–792.
9. Kauffman, D. R., Star, A., *Angew. Chem. Int. Ed*., **2008**, 47, 6550–6570.
10. Bahr, J. L., Tour, J. M., *J. Mater. Chem*., **2002**, 12, 1952–1958.
11. Burghard, M., *Surf. Sci. Rep*., **2005**, 58, 1–109.
12. Singh, P., Campidelli, S., Giordani, S., Bonifazi, D., Biancoa, A., Prato, M., *Chem. Soc. Rev*., **2009**, 38, 2214–2230.
13. Singh, P., Campidelli, S., Giordani, S., Bonifazi, D., Biancoa, A., Prato, M., *Chem. Soc. Rev*., **2009**, 38, 2214–2230.
14. Coleman, K. S., *Annu. Rep. Prog. Chem. Sect. A*, **2008**, 104, 379–393.
15. Sgobba, V., Guldi, D. M., *Chem. Soc. Rev*., **2009**, 38, 165–184.
16. Britz, D. A., Khlobystov, A. N., *Chem. Soc. Rev*., **2006**, 35, 637–659.
17. Liu, J. Q., Xiao, T., Liao, K., Wu, P., *Nanotechnology*, **2007**, 18, 165701–165706.
18. Chen, J., Collier, C. P., *J. Phys. Chem. B Letters*, **2005**, 109, 7605–7609.
19. Haddad, R., Cosnier, S., Maaref, F., Holzinger, M., *Analyst*., **2009**, 134, 2412–2418.
20. Gao, X. P. A., Zheng, G., Lieber, C. M., *Nano Lett.*, **2010**, 10, 547–552.
21. Zheng, G., Gao, X. P. A., Lieber, C. M., *Nano Lett.*, **2010**, 10, 3179–3183.
22. Ghosh, A., Rao, K. V., Voggu, R., George, S. J., *Chem. Phys. Lett*., **2010**, 488, 198–201.

23. Liu, Y., Wu, D.-C., Zhang, W.-D., Jiang, X., He, C.-B., Chung, T. S., Goh, S. H., Leong, K. W., *Angew. Chem. Int. Ed.*, **2005**, 44, 4782–4785.
24. Liu, L., Guo, L.-P., Bo, X.-J., Bai, J., Cui, X.-J., *Anal. Chim. Acta*, **2010**, 673, 88–94.
25. Carrión, F. J., Espejo, C., Sanes, J., Bermúdez, M. D., *Compos. Sci. Technol.*, **2010**, 70, 2160–2167.
26. Martínez-Díaz, M. V., Ince, M., Torres, T., *Monatsh. Chem.*, **2011**, 1–9.
27. Wang, A., Long, L., Zhang, C., *J. Incl. Phenom. Macrocycl. Chem*., **2011**, 71, 1–24.
28. Inokuma, Y., Osuka, A., *Dalton Trans.*, **2008**, 2517–2526.
29. Boul, P. J., Cho, D. G., Rahman, G. M. A., Marquez, M., Ou, Z., Kadish, K. M., Guldi, D. M., Sessler, J. L., *J. Am. Chem. Soc.*, **2007**, 129, 5683–5687.
30. Komatsu, N., in Heterocyclic Supramolecules, Topics in Heterocyclic Chemistry, *Heterocyclic Supramolecular Chemistry of Fullerenes and Carbon Nanotubes*, Matsumotovol, K., Ed., Springer, vol. 17, pp. 161–198, 2008.
31. Geng, J., Ko, Y. K., Youn, S. C., Kim, Y.-H., Kim, S. A., Jung, D.-H., Jung, H.-T., *J. Phys. Chem. C.*, **2008**, 112, 12264–12271.
32. Guo, Z., Mao, J., Ouyang, Q., Zhu, Y., He, L., Lv, X., Liang, L., Ren, D., Chen, Y., Zheng, J., *J. Dispersion Sci. Technol.*, **2010**, 31, 57–61.
33. Bartelmess, J., Soares, A. R. M., Martínez-Díaz, M. V., Neves, M. G. P. M. S., Tomé, A. C., Cavaleiro, J. A. S., Torres, T., Guldi, D. M., *Chem. Commun.*, **2011**, 47, 3490–3492.
34. Gros, C. P., Brisach, F., Meristoudi, A., Espinosa, E., Guilard, R., Harvey, P. D., *Inorg. Chem.*, **2009**, 48, 2571–2582.
35. Chichak, K. S., Star, A., Altoé, M. V. P., Stoddart, J. F., *Small*, **2005**, 1, 452–461.
36. Guldi, D. M., Menna, E., Maggini, M., Marcaccio, M., Paolucci, D., Paolucci, F., Campidelli, S., Prato, M., Rahman, G. M. A., Schergna, S., *Chem. Eur. J.*, **2006**, 12, 3975–3983.
37. Spänig, F., López-Duarte, I., Fischer, M. K. R., Martínez-Díaz, M. V., Bäuerle, P., Torres, T., Guldi, D. M., *J. Mater. Chem.*, **2011**, 21, 1395–1403.
38. Bartelmess, J., Ehli, C., Cid, J.-J., García-Iglesias, M., Vázquez, P., Torres, T., Guldi, D. M., *Chem. Sci.*, **2011**, 2, 652–660.

39. Pereira, J. B., Carvalho, E. F. A, Faustino, M. A., Neves, M. G. P. M. S., Cavaleiro, J. A. S., Gomes, N. C. M., Cunha, A., Almeida, A., Tomé, J. P. C., *Photochem. Photobiol*., **2012**, 88, 537–547.
40. Solladié, N., Nierengarten, J.-F., in Nanomaterials and Nanochemistry, *Supramolecular Chemistry: Applications and Prospects, Nanomaterials and Nanochemistry*, Bréchignac, C., Houdy, P., Lahmani, M., Eds., Springer, vol. 2, pp. 335–345, 2007.
41. Chidawanyika, W., Nyokong, T., Carbon, **2010**, 48, 2831–2838.
42. Moeno, S., Nyokong, T., *J. Photochem. Photobiol. A*, **2009**, 201, 228–236.
43. Vincett, P. S., Voigt, E. M., Rieckhoff, K. E., *J. Chem. Phys*., 1971, **55**, 4131–4140.
44. Kobuke, Y., *Eur. J. Inorg. Chem.*, **2006**, 2006, 2333–2351.
45. Moeno, S., Nyokong, T., *J. Photochem. Photobiol. A*, **2009**, 203, 204–210.
46. Ozoemena, K. I., Nyokong, T., *J. Electroanal. Chem.*, **2005**, 579, 283–289.
47. Sehlotho, N., Durmus, M., Ahsen, V., Nyokong, T., *Inorg. Chem. Commun.*, **2008**, 11, 479–483.

Chapter 4

Noncovalent assemblies based on thiopyridyl porphyrins and ruthenium phthalocyanines

4.1 Overview

Porphyrins (Pors) and phthalocyanines (Pcs) have been studied in different electronic applications,[1-15] namely in photoactive coordinated-systems due to their large range of UV-Vis absorption features and the ability to construct noncovalent assemblies, namely with carbon nanostructures, such as SWNTs and C_{60}.[16-22] In particular, Pors and Pcs with pyridyl units have been used to form supermolecules with ruthenium tetra-*tert*-butyl phthalocyanines (RuPcs), by noncovalent linkage involving the between pyridyl units and the ruthenium metal ion of the Pc.[23-26] In fact, RuPc derivatives are attractive, not only due to their application as photosensitising elements of photoelectrochemical cells but also due to their ability to coordinate neighbour molecules with pyridine units.[27,28,29,30] On the other hand, the selection of RuPcs with *tert*-butyl substituents can ensure a better solubility and a less tendency to form aggregates in solution.[31-35]

The crucial topic of synthetic photosynthesis is a line-up of light-induced energy- and electron-transfer reactions.[36] In this way, aromatic compounds evidencing light-harvesting and reactive processes should comprise light-absorbing chromophores, which arise as antenna molecules, excited-state electron donor and additionally electron acceptors.[37] Donor-acceptor ensembles also play key roles in molecular photovoltaic devices[38-40], where the prompt conversion of the energy is stored in the photogenerated radical ion pair states into electrical power. Supramolecular interactions between different dye molecules have interesting adsorption properties since they can cover a higher region of the visible spectrum.[41-45]

The potential in electronic supramolecular chemistry depends of the absorption and emission performance of the dyes that can be driven by self-assembly coordination processes. In this context, certain researchers have been constructed noncovalent multi-dye systems, such as the ones involving different pyridyl-dye derivatives and *tert*-butyl ruthenium phthalocyanines (RuPcs).[46,47] Due to the association properties, it is possible to obtain electronic transitions between both aromatic compounds. It has been well documented that different supramolecular electron donor-acceptor building blocks, such as perylenebisimide[28] or perylenediimide[27] with pyridyl units has been considered through axial coordination to the ruthenium(II) metal centres of two or four RuPc units, depending on the available pyridyl groups. Recently, a series of supramolecular Por-Pc assemblies have been prepared by D'Souza group presenting the axial coordination of (*ortho*-, *meta*-

or *para*-) imidozylphenyl-substituted free-base Pors to RuPc dyes.[48] On the other hand, pyridylporphyrins have been reported by Cook and co-workers to allow electron donor-acceptor hybrids with pronounced design flexibility.[49]

Zinc Pors are also known to successfully form self-assembled supramolecular dyads and triads *via* metal-ligand coordination with pyridyl-fullerene (C_{60}) derivatives, crown-ether inclusion, ion pairing, hydrogen-bonding, or π-π stacking interactions.[50] The supramolecular heterochromophore ensembles presented an energy transfer from the periphery to the central core of these multichromophore systems. The interesting properties brought to synthesise and study Por-Pc electron donor/acceptor assemblies as promising candidates for solar energy conversion, based on noncovalent linkage. Indeed, it is reported here the mono- and tetra-thiopyridylporphyrins, previously reported by our research group,[52] coordinated with one or four RuPc unit(s) to perform the supramolecular assemblies **4.10**-**4.12** (Figure 4.10, pg. 133). It is noteworthy that the synthesis involves rigorous control conditions due to the possibility of incomplete axial derivatization of the RuPc by pyridyl groups of the Por derivatives.[51,52] It is established a versatile platform to functionalize pyridyl porphyrins and present the synthesis of porphyrin dyes peripherally supramolecular-substituted with ruthenium chromophores. Herein, it is reported a notable redistribution of electron density of new heterochromophore structures, evidencing the electron-donating/-accepting communication between both dyes in the supramolecular hybrids. Photophysical investigation by time-resolved transient absorption, mainly fluorescence and femtosecond spectroscopy, evidenced efficient intermolecular energy transfer from the photoexcited central porphyrin to the peripheral phthalocyanines in the supramolecular multichromophore ensembles. The outcome forms the source to architect interesting materials in solar light converting systems.

4.2 Synthesis of the ruthenium(II) *tert*-butylphthalocyanine

The synthesis of the supramolecular assemblies **4.10**-**4.12** (Figure 4.10) requires the previous preparation of the **RuPc 4.3**. Generally, metallated Pcs can be synthesised by two different methods.[53] One of them consists on the cyclotetramerization of a phthalonitrile derivative in the presence of the adequate metal salt, and the other involves the direct insertion of a metal into the macrocycle core of a pre-synthesised metal-free Pc. In this

study, the access to **RuPc 4.3** was based on the cyclotetramerisation of the precursor 4-(*tert*-butyl)phthalonitrile **4.1** affording the corresponding metal free **H_2Pc 4.2**, followed by insertion of the ruthenium metal ion with triruthenium dodecacarbonyl, $Ru_3(CO)_{12}$ (Scheme 4.1).[54] It is noteworthy that the synthesis requires a rigorous control on the experimental conditions in order to obtain the metal with only one axial ligand; in this way, the second ligand, the thiopyridylporphyrins **4.7**-**4.9** (Schemes 4.3 and 4.4) can be successfully incorporated to develop the multichromophoric clusters. This is a well-known procedure used to prepare ruthenium complexes of Pcs bearing two different ligands.[51]

The tetramerization of 4-*tert*-butylphthalonitrile **4.1** was performed in 1-pentanol at 150 ºC in the presence of lithium (Scheme 4.1).[55]

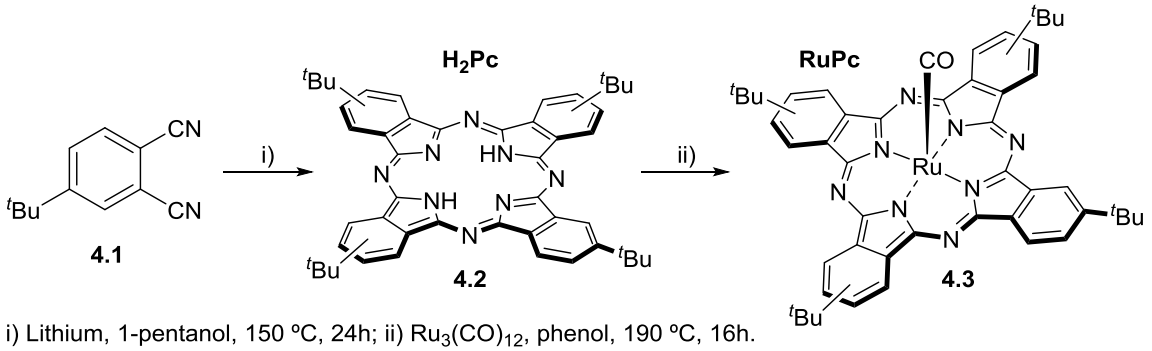

i) Lithium, 1-pentanol, 150 ºC, 24h; ii) $Ru_3(CO)_{12}$, phenol, 190 ºC, 16h.

Scheme 4.1

After 12 h under stirring, the reaction was finished by adding a mixture of methanol/water (1:1). The obtained precipitate was filtrated and washed several times with the same mixture of methanol/water to remove the lithium residues. Then, the solid after being purified in a silica gel chromatography column, using dichloromethane/hexane (3:1) as eluent, afforded the pure metal-free **H_2Pc 4.2** as a deep blue solid in 84% yield.

The structure of **4.2** was confirmed by NMR spectroscopy and mass spectrometry. The ^{1}H NMR spectrum of **4.2** (Figure 4.1) shows the resonances corresponding to the aromatic protons β-H^c and α-$H^{a,b}$, as two multiplets at δ 8.27-8.39 and 9.14-9.58 ppm, respectively. The resonances of the 36 *tert*-butyl protons (H^d) appear as a singlet at δ 1.90 ppm. The multiplet between δ -1.20 and -0.98 ppm corresponds to the resonance of the internal -NH protons. In the mass spectrum of **4.2**, the presence of a peak at *m/z* 739, corresponding to the molecular ion is also in agreement with the expected structure.

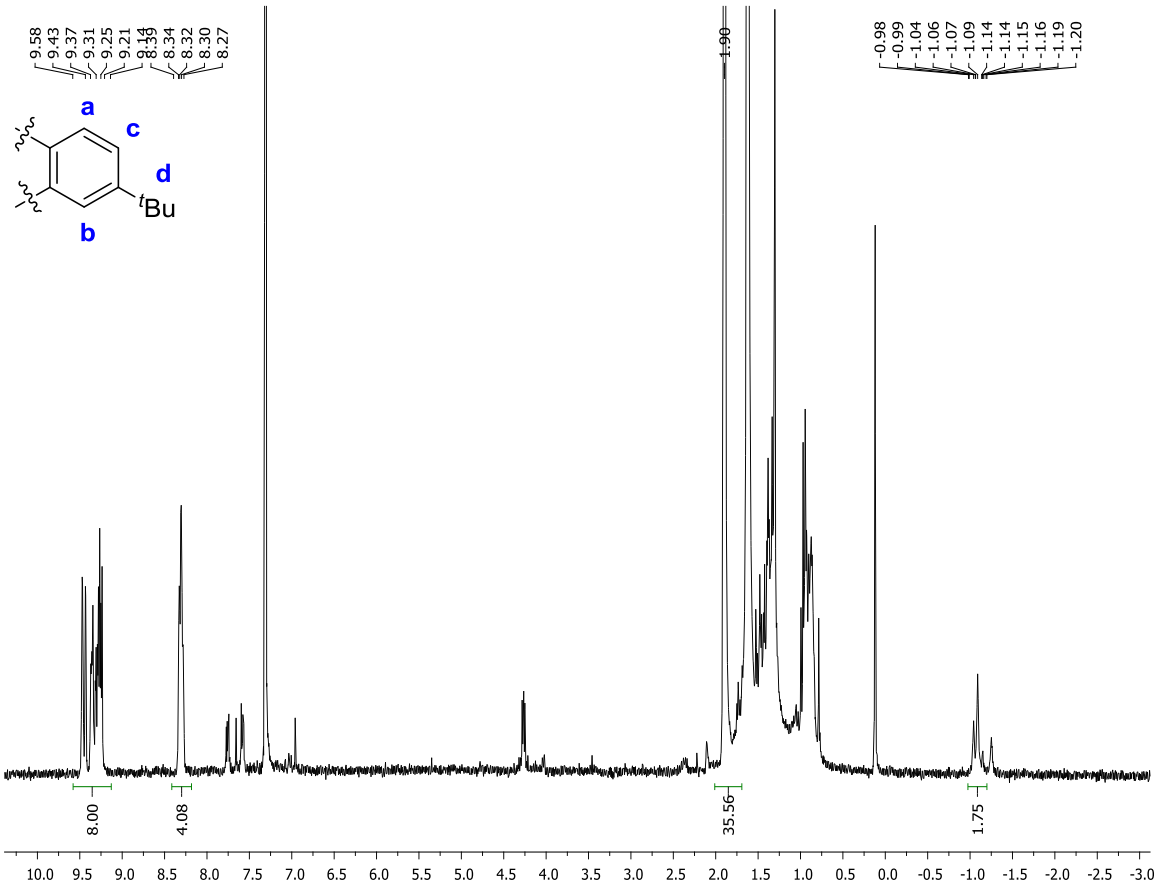

Figure 4.1 ^{1}H NMR spectrum of compound **4.2** in $CDCl_3$.

The metallation of the tetra-*tert*-butyl phthalocyanine **4.2** was carried out using $Ru_3(CO)_{12}$ in refluxing phenol (190 ºC). After 16 h, the control by TLC showed the complete consumption of the starting material **4.2**. After the usual work up and purification by column chromatography, the Pc **4.3** was obtained in 82% yield as a mixture of regioisomers (Scheme 4.1).

The ^{1}H NMR spectrum of **4.3** in deuterated chloroform shows the β-H^{c} and α-H^{a,b} aromatic protons of the isoindole units as broad multiplets at δ 8.01-8.14 and 9.14-9.40 ppm, respectively. The resonances of the aliphatic *tert*-butyl protons H^{d} appear as a singlet at δ 1.71 ppm and the absence of the multiplet at high field due to the inner -NH protons of the macrocycle core confirmed the success of the ruthenium complexation (Figure 4.2).

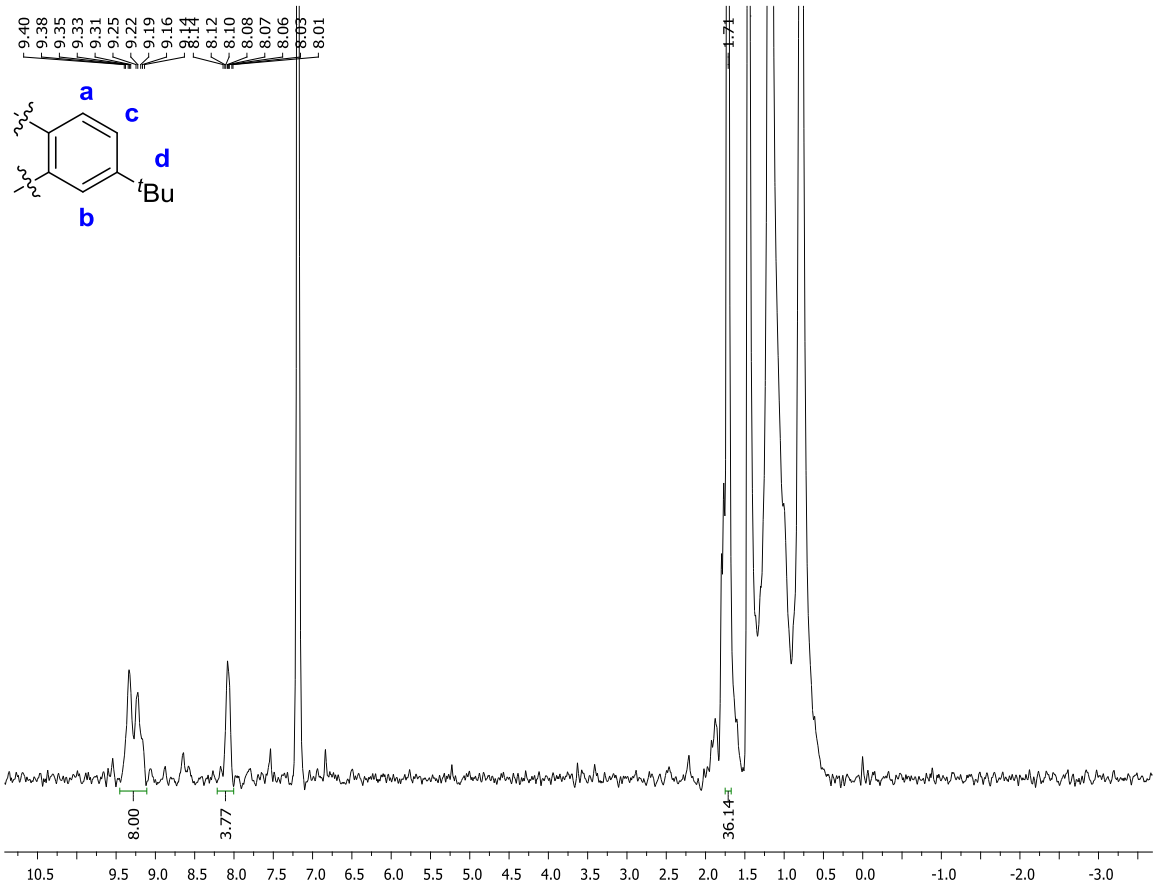

Figure 4.2 ^{1}H NMR spectrum of compound **4.3** in $CDCl_3$.

The UV-Vis spectrum of **4.3** displays Soret- and Q-band absorptions at 296 and 652 nm, respectively. Finally, the ESI-MS spectrum of **4.3** confirmed also the success of the metal insertion by showing the peak corresponding to the molecular ion at *m*/*z* 866.[27]

In this way, the potential noncovalent access between **RuPcs** and pyridyl dyes provides a high interest to study new examples of supermolecules.[56,57] In this sense, it is reported here the noncovalent functionalization of the free and complexed thiopyridylporphyrins, which promote association with **RuPcs 4.3** owing the intermolecular affinity between the pyridyl substituents and the ruthenium-Pc metal ions.

4.3 Syntheses of the thiopyridylporphyrins

The 5,10,15,20-tetraquis(pentafluorphenyl)porphyrin **4.6** (**$TPPF_{20}$**) (Scheme 4.2) required to prepare the thiopyridylporphyrins **4.7** (Scheme 4.3) and **4.8** (Scheme 4.4) was synthesised using a modified Rothemund condition.[58,59] The simple one-step reaction

involved the equimolar condensation of pyrrole with pentafluorobenzaldehyde in a mixture of acetic acid/nitrobenzene under refluxing conditions. The expected porphyrin, was obtained after removing the mixture of acetic acid/nitrobenzene under reduced pressure and purification of the crude residue by silica gel chromatography.[60-63]

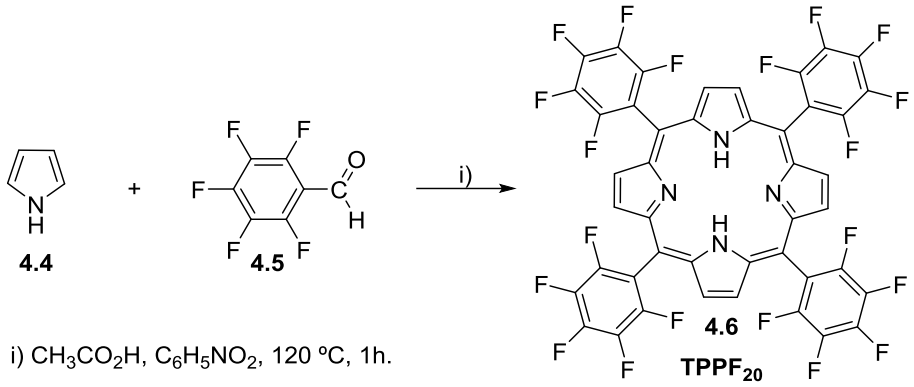

Scheme 4.2

The ^{1}H NMR spectrum of **4.6** in $CDCl_3$ is in agreement with the structure. The proton resonances of the inner -NH appears at δ -3.19 ppm and the signal due to the β-protons at δ 9.45 ppm. The ^{19}F NMR spectrum of **4.6** shows the resonances due to the *ortho*-, *para*-, and *meta*-fluorine atoms, respectively at δ -184.92 to -184.70, -174.70, and -160.04 ppm as a multiplet, triplet and doublet of doublets (Figure 4.3).

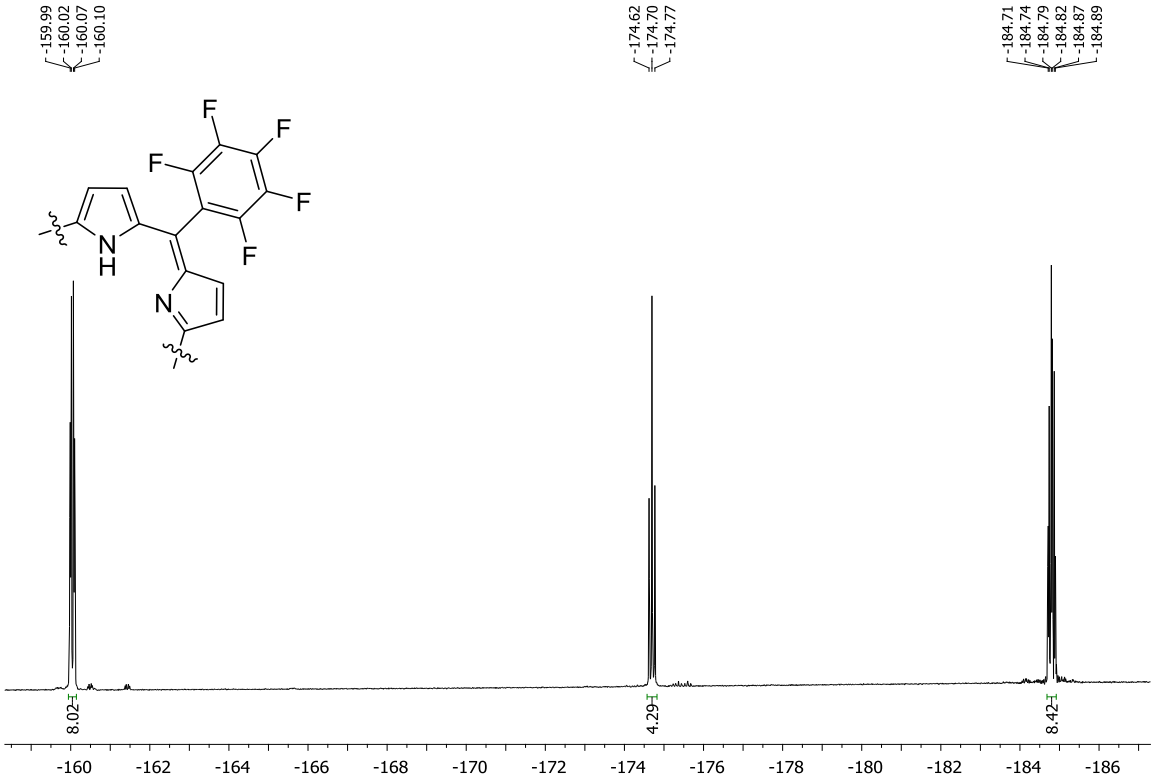

Figure 4.3 ^{19}F NMR spectrum of compound **4.6** in $CDCl_3$.

The nucleophilic substitution reactions of the four *para*-fluorine atoms on **$TPPF_{20}$** (**4.6**) are already well documented.[64-68] The reactivity of the *para*-fluorine atoms on the pentafluorophenyl moiety varies significantly with the specific nucleophile used and several studies about nucleophile reactivity can be found in literature.[69] The synthesis of the mono- and tetra-thiopyridylporphyrins **4.7** and **4.8** (Schemes 4.3 and 4.4) required the selection of 4-mercaptopyridine **2.2** to be used as nucleophile. Although both reactions were accomplished in DMF and in the presence of diethylamine (DEA) the experimental conditions were different in order to favour the mono- or the tetra-substitution of the fluorine atoms.

The synthesis of the mono-thiopyridylporphyrin **4.7** (Scheme 4.3) required the presence of an excess of **$TPPF_{20}$** comparatively to the 4-mercaptopyridine (1:0.7) and it was carried out at room temperature under nitrogen atmosphere. This is an important aspect in order to avoid the oxidation of the 4-mercaptopyridine. After 1 h, the solvent was removed under reduced pressure and the residue after purification and crystallization, afforded compound **4.7** in 22% of yield.

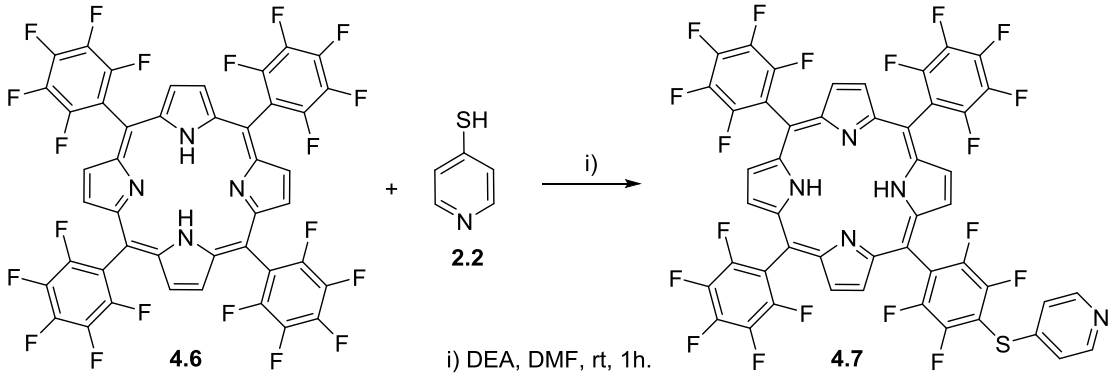

Scheme 4.3

The structure of **4.7** was confirmed by NMR and mass spectrometry. The ^{1}H NMR spectrum shows the typical internal aromatic -NH protons as a singlet at δ -2.97 ppm and the resonances of the aromatic β-pyrrolic protons (β-H) appear between δ 8.87 and 8.89 ppm (Figure 4.4).

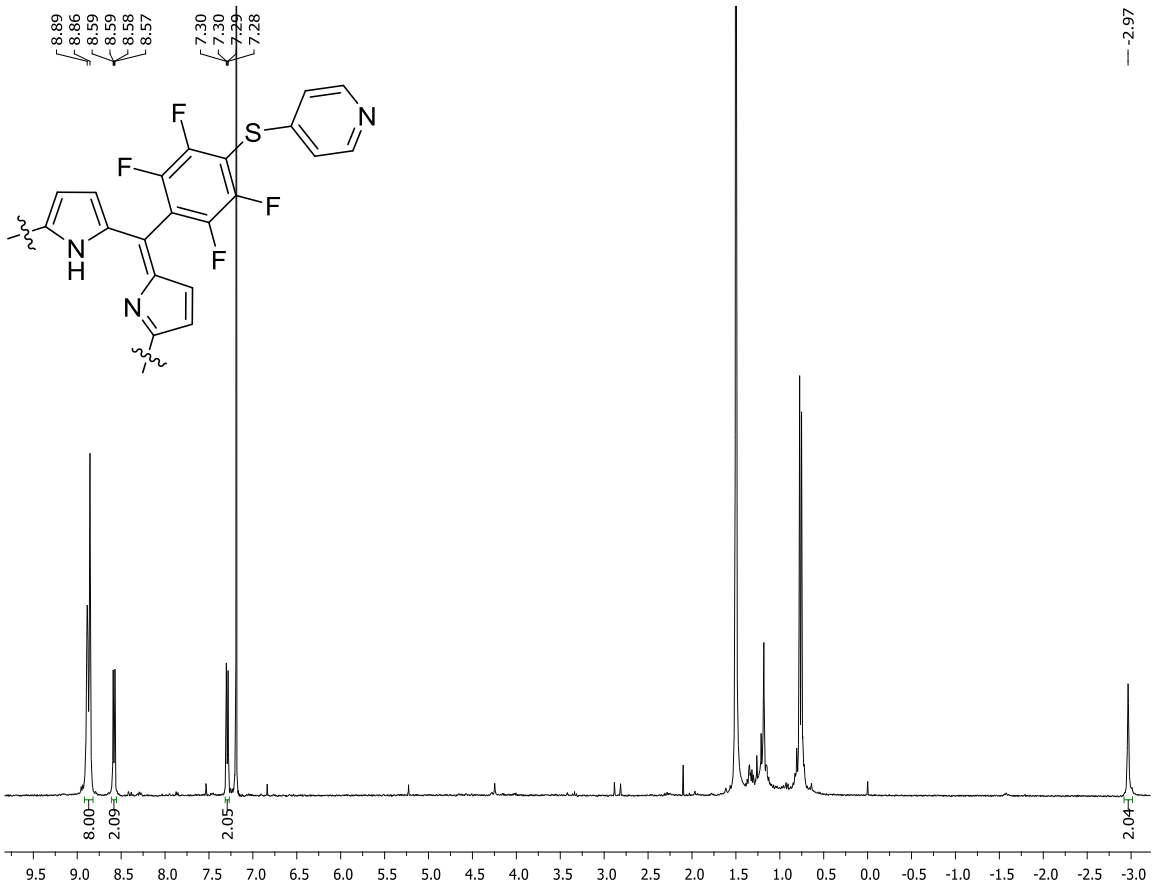

Figure 4.4 ^{1}H NMR spectrum of compound **4.7** in $CDCl_3$.

The resonances of the four *ortho*- and *meta*-protons of the extra pyridyl unit appear as doublet of doublets at δ 7.29 and 8.58 ppm, respectively. The ^{19}F NMR spectrum of **4.7** is also in agreement with the mono-substitution (Figure 4.5). The two multiplets and the doublet of doublets at δ -184.87 to -184.67, -174.75 to -174.51 and -160.02 ppm correspond to the 6 *ortho*-F, 3 *para*-F and 6 *meta*-F resonances of the unsubstituted rings. The doublet of doublets at δ -158.15 and -154.30 ppm correspond to the 2 *ortho*-F and 2 *meta*-F atoms of the substituted fluorophenyl unit. The MALDI-MS spectrum of **4.7** shows a peak at *m/z* 1066 corresponding to the protonated molecular ion $[M+H]^+$.

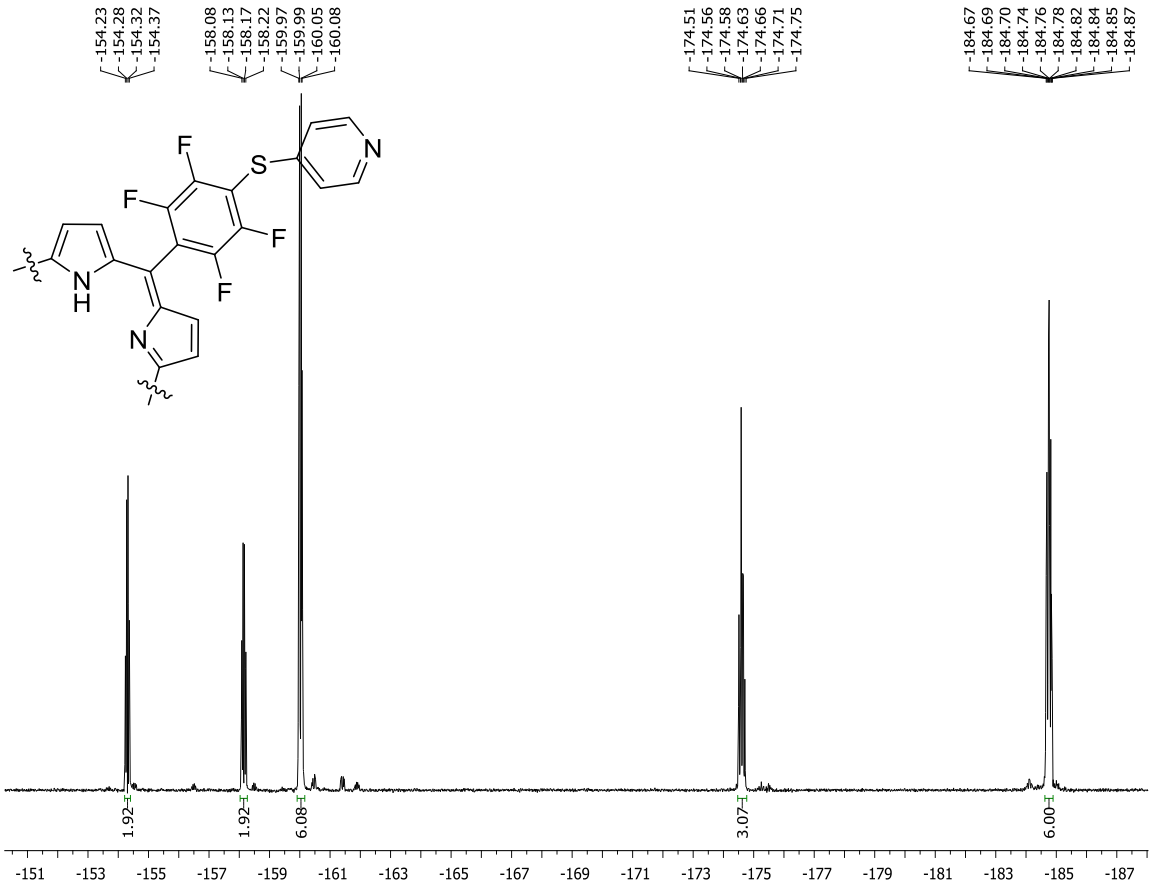

Figure 4.5 ^{19}F NMR spectrum of compound **4.7** in $CDCl_3$.

The synthesis of the tetra-thiopyridylporphyrin **4.8** required more drastic conditions when compared with the previous synthesis (Scheme 4.4). The nucleophilic substitution was performed in the presence of an excess of 4-mercaptopyridine **2.2** and in DMF at reflux

The Zn(II) complex **4.9** was prepared by metallation of **4.8** using an excess of $Zn(AcO)_2$ in a mixture of $CHCl_3$/MeOH (9/1) (Scheme 4.4). After refluxing for 3 h it was added a mixture of $CHCl_3$/MeOH (98:2)/hexane; the resulting precipitate afforded compound **4.9** in 96% yield, after a careful elimination of the excess of zinc(II) salt with water.

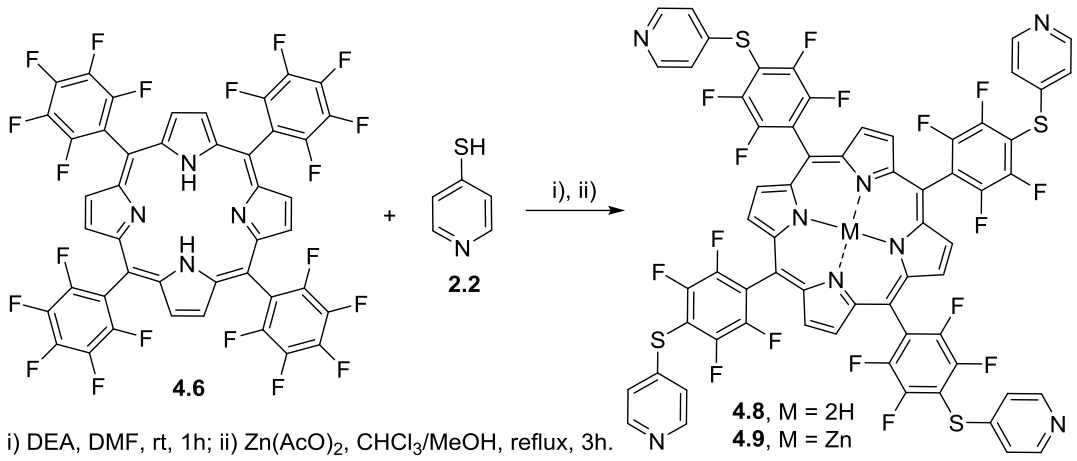

Scheme 4.4

The NMR, UV-Vis and mass spectrometry confirm the structures of **4.8** and **4.9**. The ^{1}H NMR spectrum of **4.8** (Figure 4.6) indicates clearly the presence of two distinct regions: a singlet at higher field (δ -3.12 ppm) due to the resonances of the inner -NH protons of Por core and signals at lower field due to the aromatic β-pyrrolic (singlet at δ 9.61 ppm) and pyridyl protons.

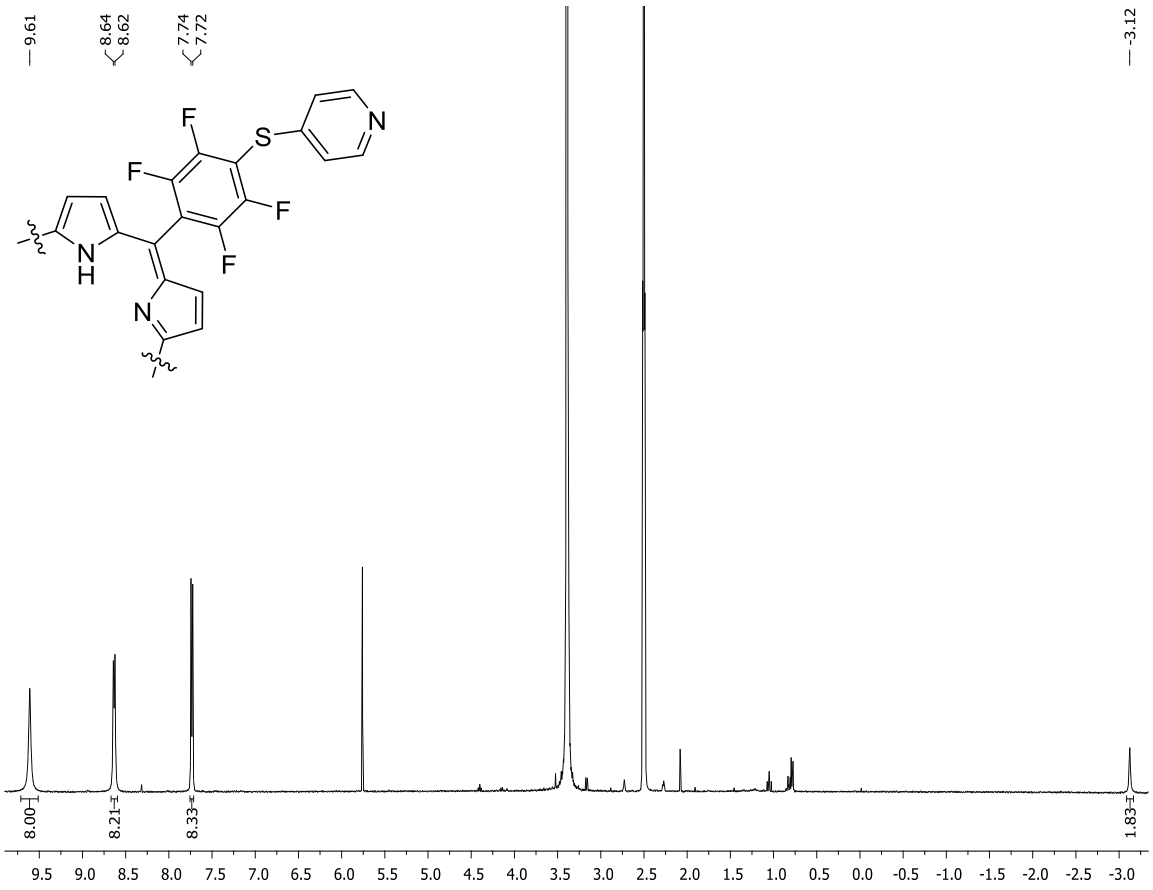

Figure 4.6 ^{1}H NMR spectrum of compound **4.8** in DMSO-d_6.

The resonances of the *ortho*- and *meta*-protons of the pyridyl moieties appear as doublets at δ 7.73 and 8.63 ppm, respectively. The ^{19}F NMR spectrum of **4.8** confirmed also the complete nucleophilic substitution of the four *para*-fluorine atoms by the 4-mercaptopyridine units by the disappearance of the corresponding resonance signals in the spectrum. The resonances of the *ortho*- and *meta*-fluorine atoms appear as two doublet doublets (J = 11.9 and 26.3 Hz) at δ -161.11 and -156.14 ppm, respectively (Figure 4.7). The MALDI-TOF-MS spectrum of **4.8** confirmed the molecular ion peak at *m/z* 1339 $[M+H]^+$.

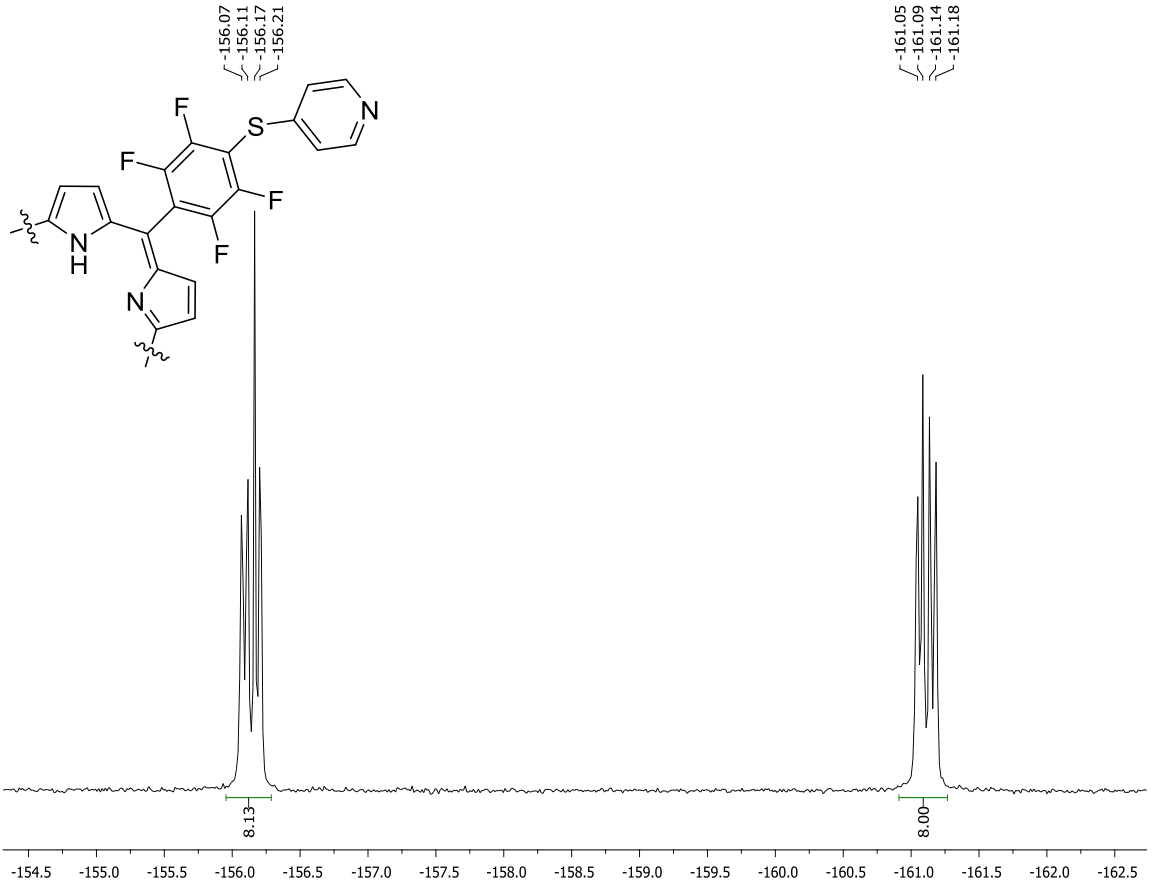

Figure 4.7 ^{19}F NMR spectrum of compound **4.8** in DMSO-d_6.

The structure of compound **4.9** was also confirmed by the same spectroscopic data (^{1}H and ^{19}F NMR and mass spectrometry). The ^{1}H NMR spectrum (Figure 4.8) shows the expected disappearance of the resonance of inner -NH protons due to inclusion of the zinc metal ion. The signals of the *ortho*- and *meta*-protons of the pyridyl groups and of the aromatic β-pyrrolic protons suffer a slight high field shift (δ 7.23, 8.07 and 8.95 ppm) when compared with the signals of the free-base analogues. The presence of a peak

corresponding to the protonated molecular ion $[M+H]^+$ at *m/z* 1401 in the MALDI-MS spectrum of **4.9** is also in agreement with the structure.

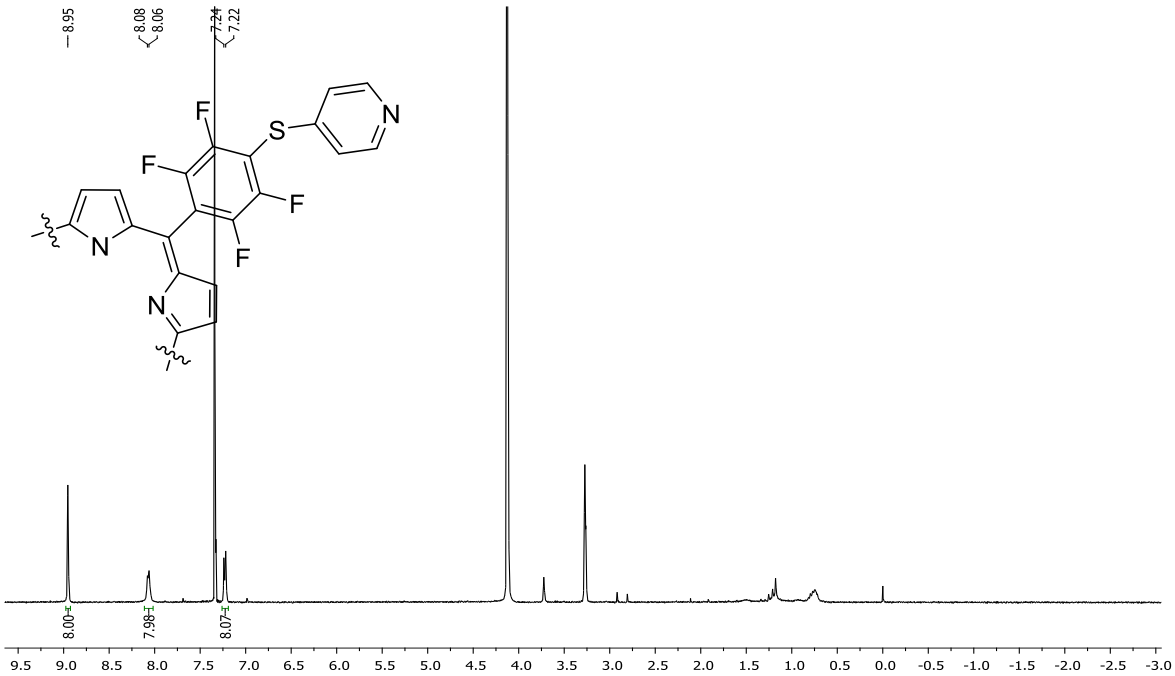

Figure 4.8 ^{1}H NMR spectrum of compound **4.9** in $CDCl_3$.

In the ^{19}F NMR spectrum of **4.9** (Figure 4.9) the resonances of the fluorine atoms appear as two doublet doublets at δ -154.93 and -151.46 ppm.

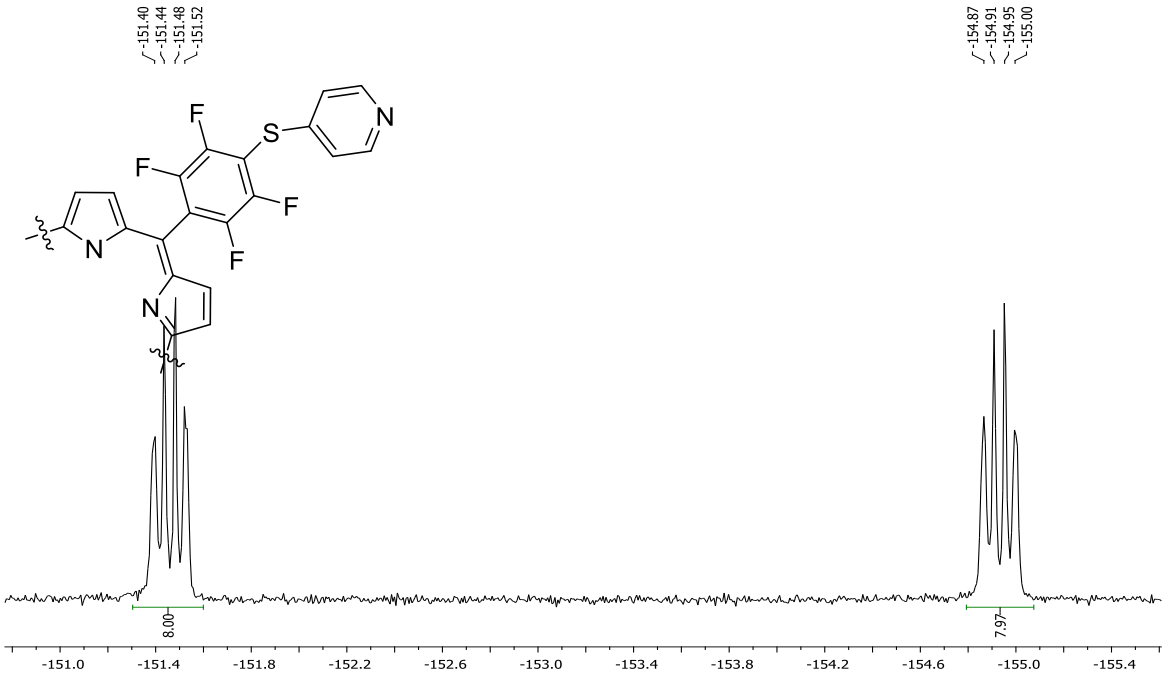

Figure 4.9 ^{19}F NMR spectrum of compound **4.9** in $CDCl_3$.

4.4 Supramolecular arrays based on thiopyridylporphyrins and ruthenium phthalocyanines

Torres *et al*. showed that the appropriate peripheral substitution of the aromatic perylene core with strongly ruthenium-coordinating pyridyl ligands afforded highly-ordered supramolecular arrays with electron donor-acceptor features.[28] Analogously, the novel supramolecular assemblies **4.10**-**4.12** were developed through axial coordination of the thiopyridylporphyrins **4.7**-**4.9**, bearing one or four pyridyl substituents to the ruthenium(II) metal centre of one or four **RuPcs 4.3** (Figure 4.10). It is noticeable, that the coupling of the **RuPcs** to the thiopyridylporphyrin improves the solubility of the assembly in organic solvents without altering significantly the electron-donor features[27] of the Por backbone; this fact was confirmed by transient photophysical experiments (see discussion below in subtopic 4.4).

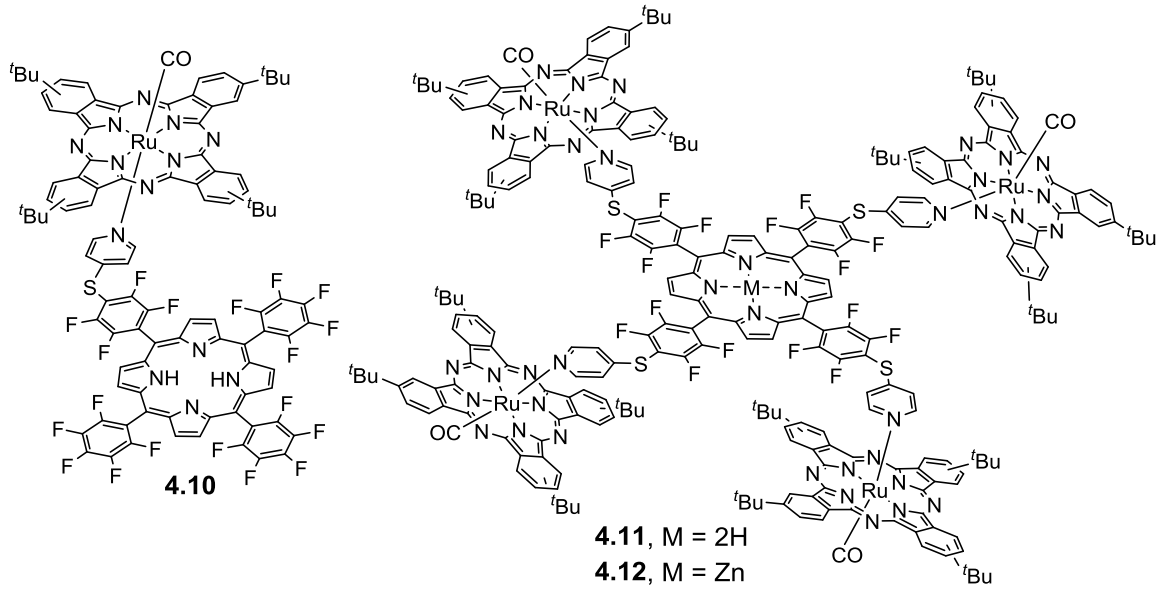

Figure 4.10 Supramolecular arrays of **4.10**-**4.12**.

The supramolecular arrays of **4.10**-**4.12** (Figure 4.10) were obtained by just adding porphyrin **4.7**-**4.9** to the adequate number of **RuPc 4.3** equivalents in dichloromethane. The mixtures were maintained under stirring at room temperature overnight. After this period, the TLC control confirmed the formation of the new Por-RuPc clusters **4.10**-**4.12** and the solvent was then evaporated. The crude mixtures, after being purified by molecular exclusion Bio-Beads gel chromatography using $CHCl_3$ as eluent, afforded the Por-RuPc clusters **4.10**-**4.12** in 71, 91 and 90% yields, respectively. The new assemblies were characterised by ^{1}H, ^{19}F NMR, UV-Vis spectroscopy and mass spectrometry.

The ^{1}H NMR spectrum of **4.10** (Figure 4.11) shows the resonances of -NH protons of the porphyrin macrocycle as a singlet at high field (δ -3.02 ppm), and of the **RuPc** *tert*-butyl protons as a singlet at δ 1.79 ppm. Moreover, the *ortho*- and *meta*-proton resonances of the pyridine unit appear as doublets at δ 8.62 and 8.80 ppm (J = 4.6 Hz). The signals of the β- and α-proton resonances of the **RuPc** are distributed at δ 8.18 and 9.30-9.47 ppm, respectively. Finally, the signals at δ 6.99-7.13 and 8.90 ppm are probably due to the β-pyrrolic protons of the porphyrin unit. The ^{19}F NMR spectrum of **4.10** presents the resonances of the fluorine atoms in the unsubstituted rings as three multiplets between δ -184.89 and -184.68, δ -174.74 and -174.51 and δ -160.09 and -159.91 ppm; these signals correspond respectively to the 6 *ortho*-F, 3 *para*-F and 6 *meta*-F atoms (Figure 4.12). The resonances of the fluorine atoms in the substituted ring emerge as doublet of doublets at δ -157.62 (2 *ortho*-F) and -153.97 ppm (2 *meta*-F). The ESI-MS spectrum of **4.10** (Figure 4.13) is also in agreement with the proposed assembly, by showing a peak corresponding to the molecular ion at *m/z* 1931 $[M]^{+\cdot}$.

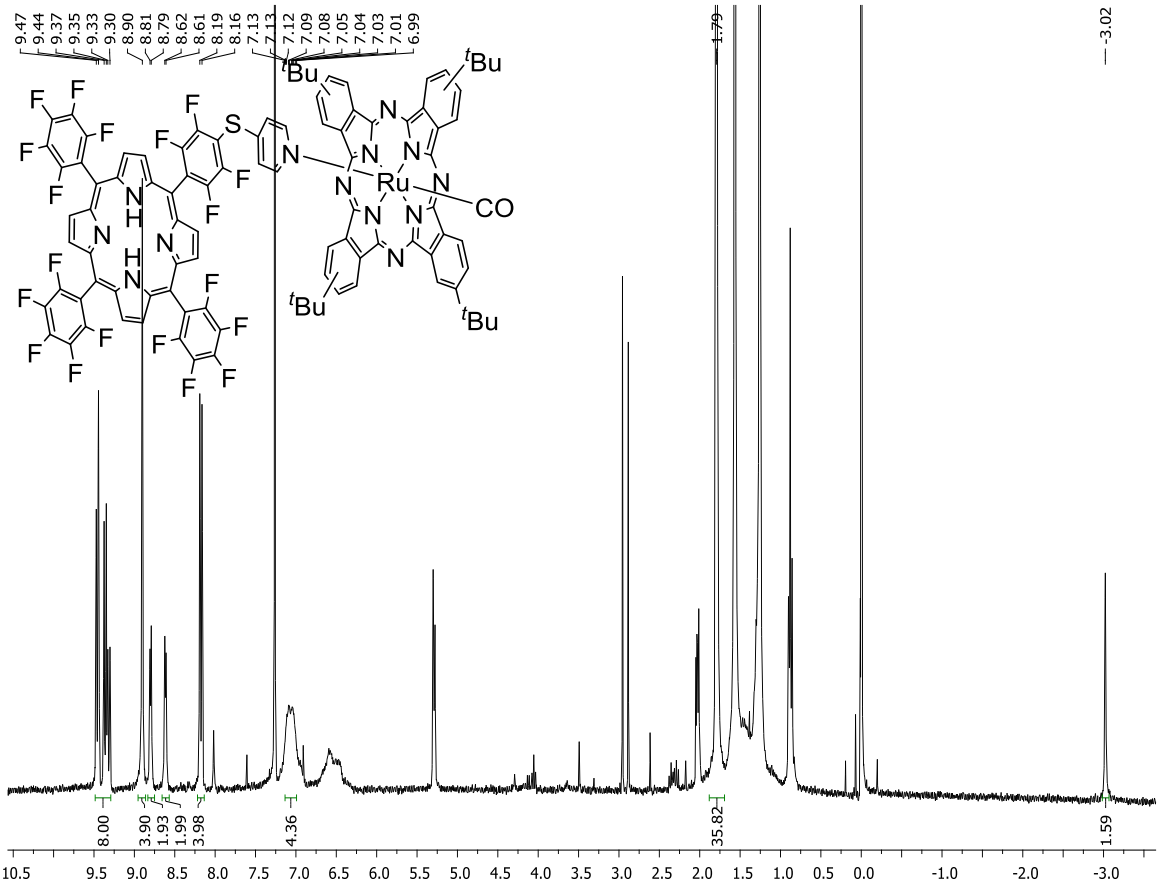

Figure 4.11 ^{1}H NMR spectrum of compound **4.10** in $CDCl_3$.

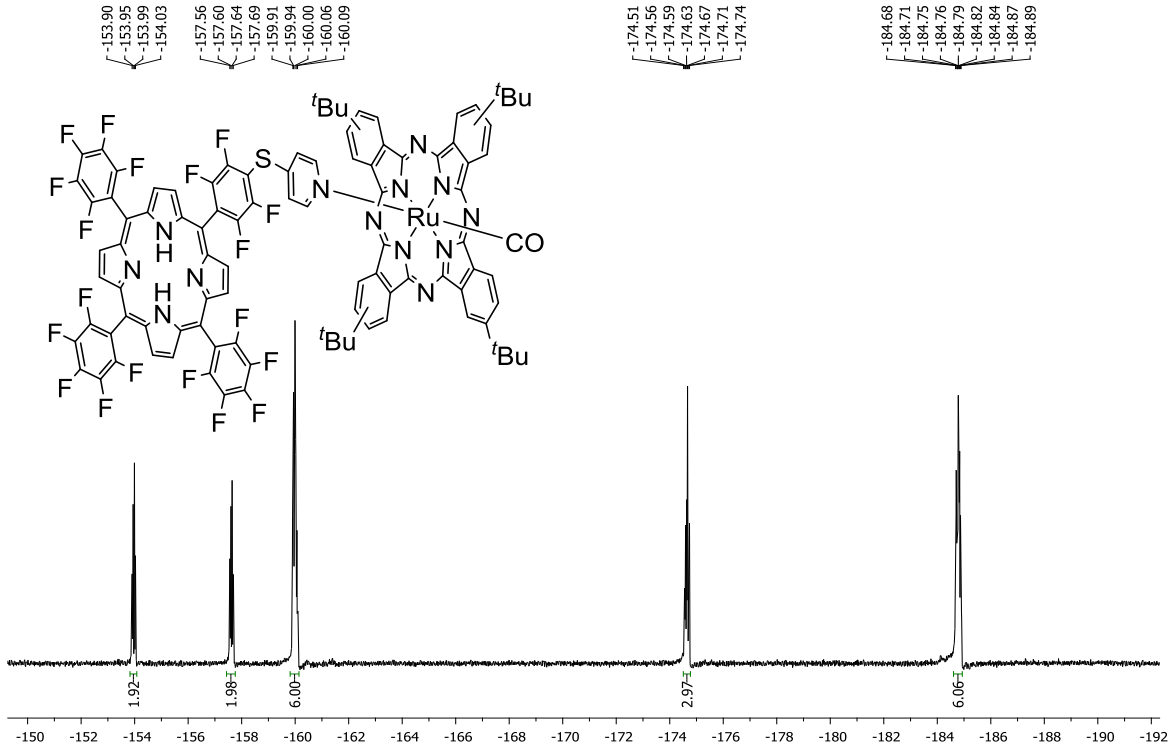

Figure 4.12 ^{19}F NMR spectrum of compound **4.10** in $CDCl_3$.

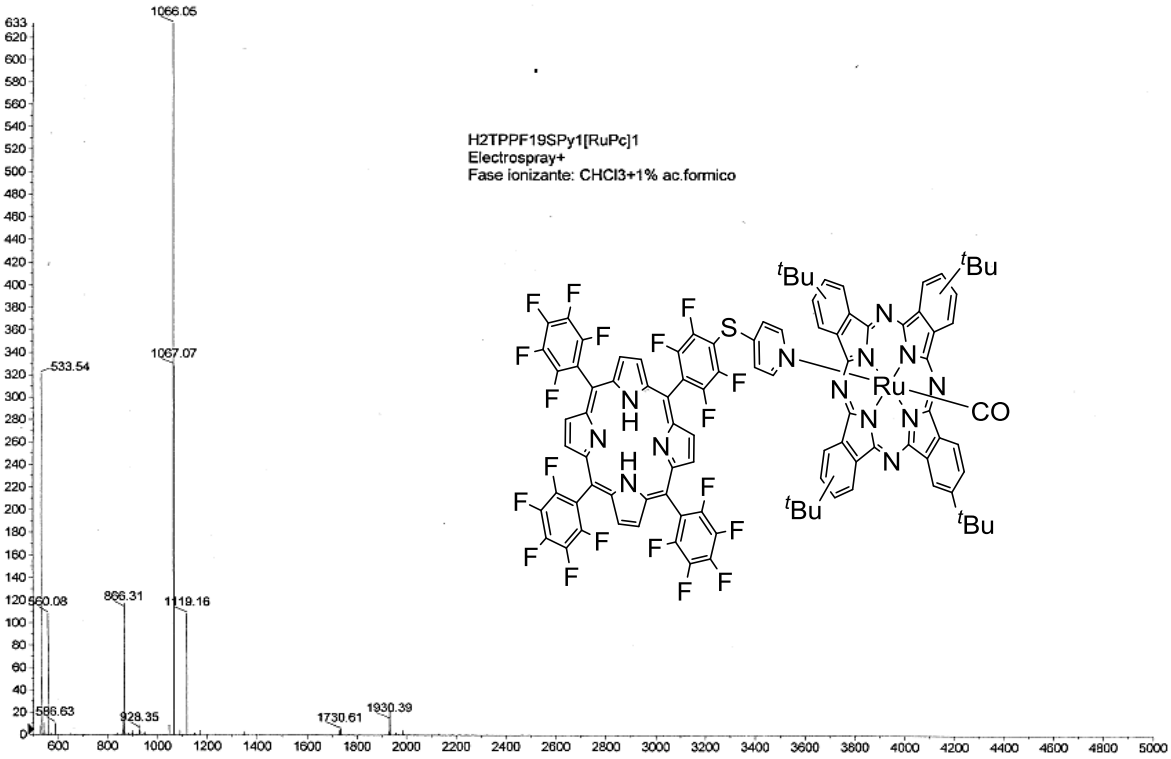

Figure 4.13 ESI-MS/MS spectrum of compound **4.10**.

As a complement it was also analyzed the results obtained in the ESI-MS/MS spectrum of the $[M]^{+\cdot}$ ion of **4.10** and the results are summarized in Table 4.1. The MS/MS

spectrum shows a product ion at *m/z* 1066, corresponding to the loss of the **RuPc** residue (-865 Da, loss of ≈$RuPc_{res}$), and another one at *m/z* 866 due to the loss of the thiopyridylporphyrin unit (-1065 Da, loss of ≈$PorSPy_{res}$). This pattern of fragmentation confirms the presence of the **RuPc** moiety linked supramolecularly to the Por **4.7**.

Table 4.1 Results of ESI-MS experiments performed for **4.10**.

Produced ions from	**Neutral loss (Da)**	***m/z***
$\mathbf{[M]^{+\cdot}}$		1931
$\mathbf{[M\text{-}RuPc_{res}]^{+}}$	-865	1066
$\mathbf{[M\text{-}PorSPy_{res}]^{+}}$	-1065	866

The ^{1}H NMR spectrum of **4.11** indicates unequivocally all the resonance signals (Figure 4.14). Definitely, the proton resonances of the Por core are located as a multiplet at high field (δ -3.39 to -3.35 ppm). On the high field of the spectrum are also situated the *tert*-butyl proton resonances which appear as a singlet at δ 1.60 ppm. On the other side of the spectrum, it is detected the pyridyl *ortho*-H and Por β-H proton resonances respectively as a doublet (δ 5.27 ppm) and singlet (δ 8.36 ppm). On the middle of these signals are positioned the β-H proton resonances of the **RuPc** at δ 8.06 ppm, integrating for 16 protons. Finally, in the cluster **4.11** it was detected as multiplet the overlapping signals α-H protons of the **RuPc** and pyridyl *meta*-H protons of Por among δ 9.25-9.39 ppm, integrating for 40 protons. However, the ^{19}F NMR spectrum of **4.11** showed the *ortho*- and *meta*-fluorine atoms as two multiplets respectively between δ -134.18 and -133.96 and between δ -130.45 and -130.29 ppm (Figure 4.15).

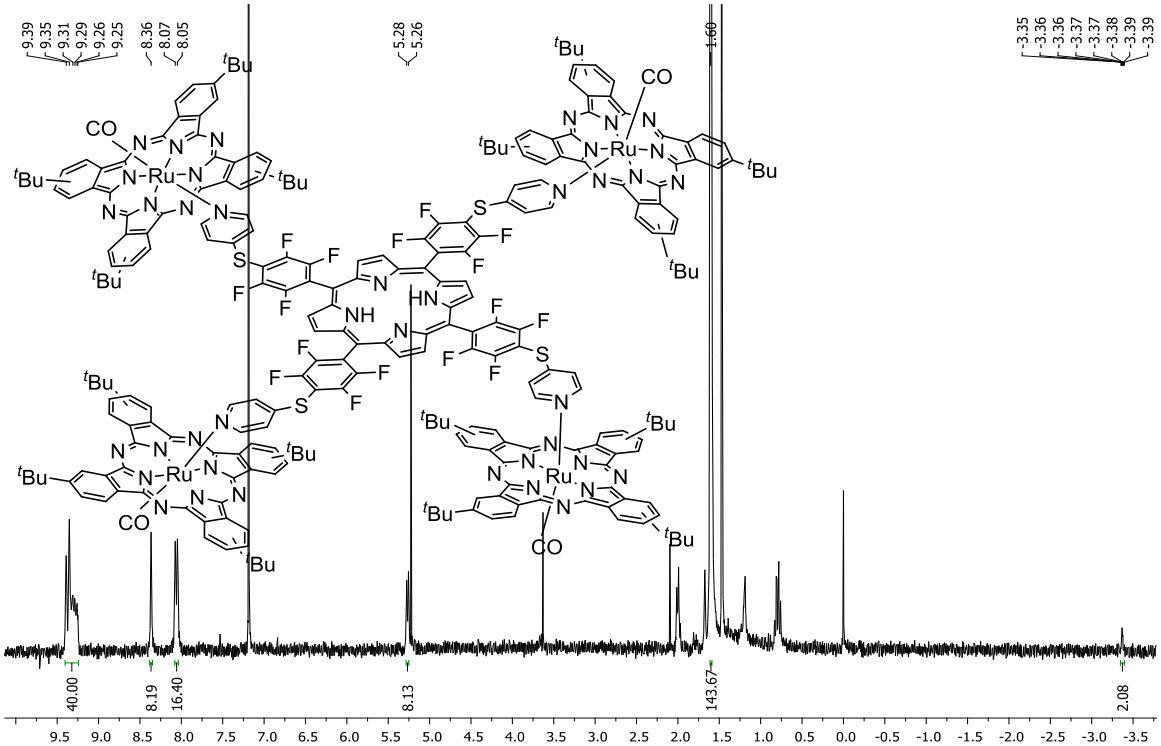

Figure 4.14 ^{1}H NMR spectrum of compound **4.11** in $CDCl_3$.

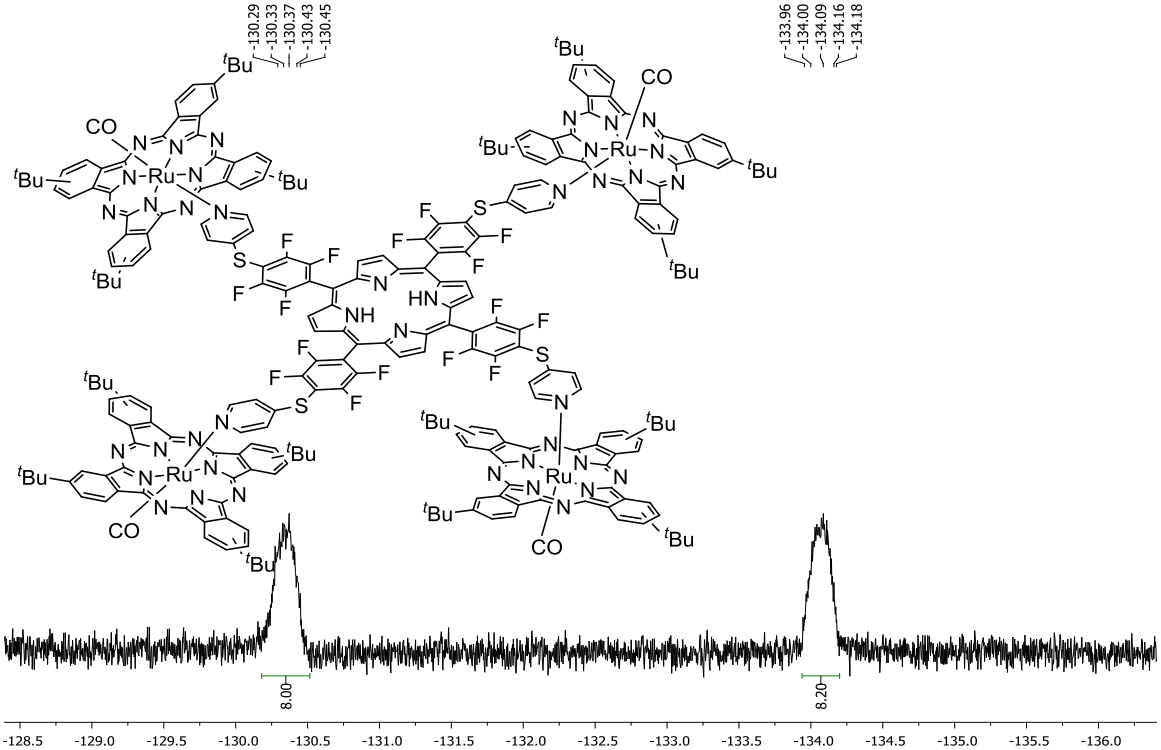

Figure 4.15 ^{19}F NMR spectrum of compound **4.11** in $CDCl_3$.

The structure of **4.11** was also confirmed by electrospray ionisation tandem mass spectrometry ESI-MS/MS (Figure 4.16), which is a very fast and sensitive technique that

provided clearly the molecular ion peak of **4.11** at *m/z* 4803 $[M]^{+\cdot}$ (Figure 4.16 and Table 4.2) and consequently the gradual fragmentation of each **RuPc 4.3**.

The obtained results are summarized in Table 4.2, demonstrating losses of one to *n*-**RuPc** residues (-865 Da, loss of ≈$RuPc_{res}$) with maximum sequential losses of 4 $RuPc_{res}$ units for $[\mathbf{M}\text{-}RuPc_{res}]^+$ (*m/z* 3938), $[\mathbf{M}\text{-}2RuPc_{res}]^+$ (*m/z* 3070), $[\mathbf{M}\text{-}3RuPc_{res}]^+$ (*m/z* 2598) and $[\mathbf{M}\text{-}4RuPc_{res}]^+$ (*m/z* 1339), respectively. This pattern of fragmentation confirms the presence of 4 **RuPc** moiety linked to the free-base Por **4.8**. These fragmentations are rather interesting, since the maximum number of lost $RuPc_{res}$ is equal to the coordination number of pyridyl units of the porphyrin. This information confirms the structural identification of the Por-RuPc complex which it is easy to observe the gradual elimination of the Pc units linked noncovalently to the thiopyridylporphyrin.

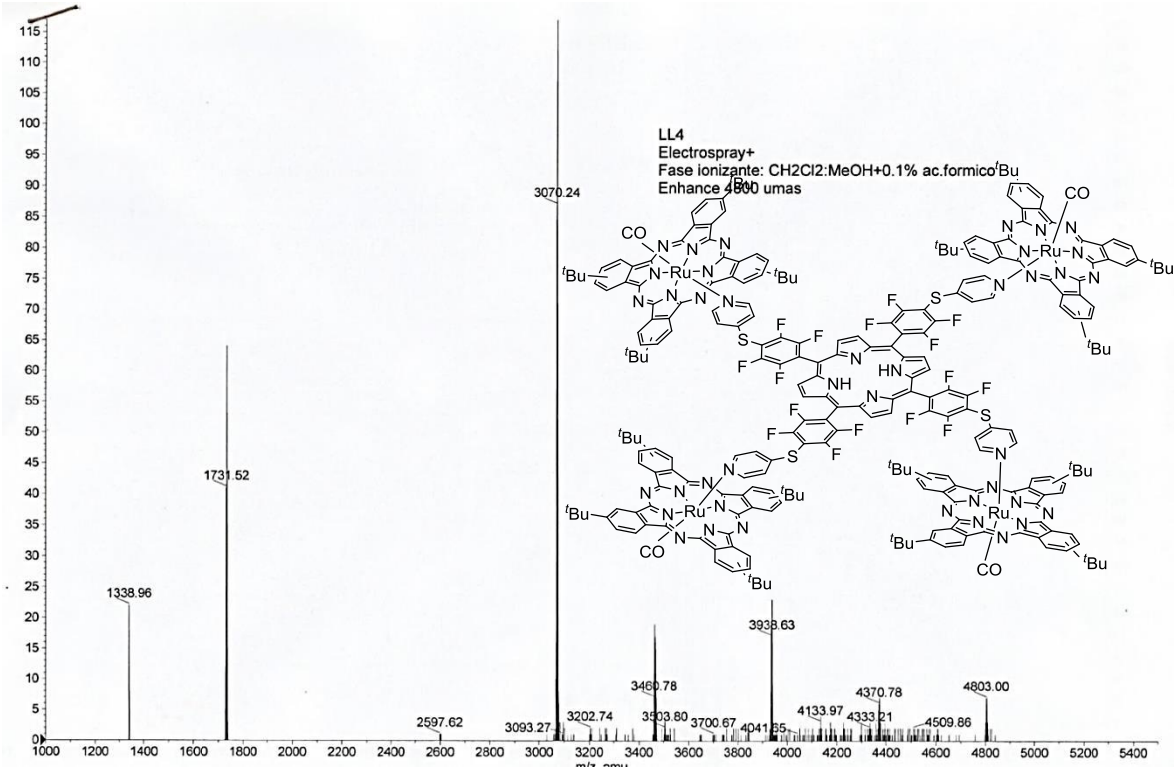

Figure 4.16 ESI-MS/MS spectrum of compound **4.11**.

Table 4.2 Results of ESI-MS experiments performed for **4.11**.

Produced ions from	Neutral loss (Da)	*m/z*
$\mathbf{[M]^{+\cdot}}$		4803
$\mathbf{[M\text{-}1RuPc_{res}]^+}$	-865	3938
$\mathbf{[M\text{-}2RuPc_{res}]^+}$	-1733	3070
$\mathbf{[M\text{-}3RuPc_{res}]^+}$	-2205	2598
$\mathbf{[M\text{-}4RuPc_{res}]^+}$	-3464	1339

The hybrid **4.11** and zinc acetate were stirred in a mixture of CH_2Cl_2/MeOH (9:1, 5 mL) for 3 h refluxing under nitrogen atmosphere. After that, the product was purified by molecular exclusion to obtain the corresponding zinc complex **4.12** in 90% of yield, isolated as a deep blue solid. The ^{1}H NMR spectrum of **4.12** shows a more complex and broad pattern than the spectrum of the corresponding free-base **4.11** (Figure 4.17). As expected no signal was detected at high field region due to the absence of the internal -NH protons. On the other hand, ^{19}F NMR spectrum of **4.12** shows two distinct multiplets at δ -157.95 to -157.15 and at δ -155.07 to -153.31 ppm referent to the integration of the 16 fluorine atoms (Figure 4.18).

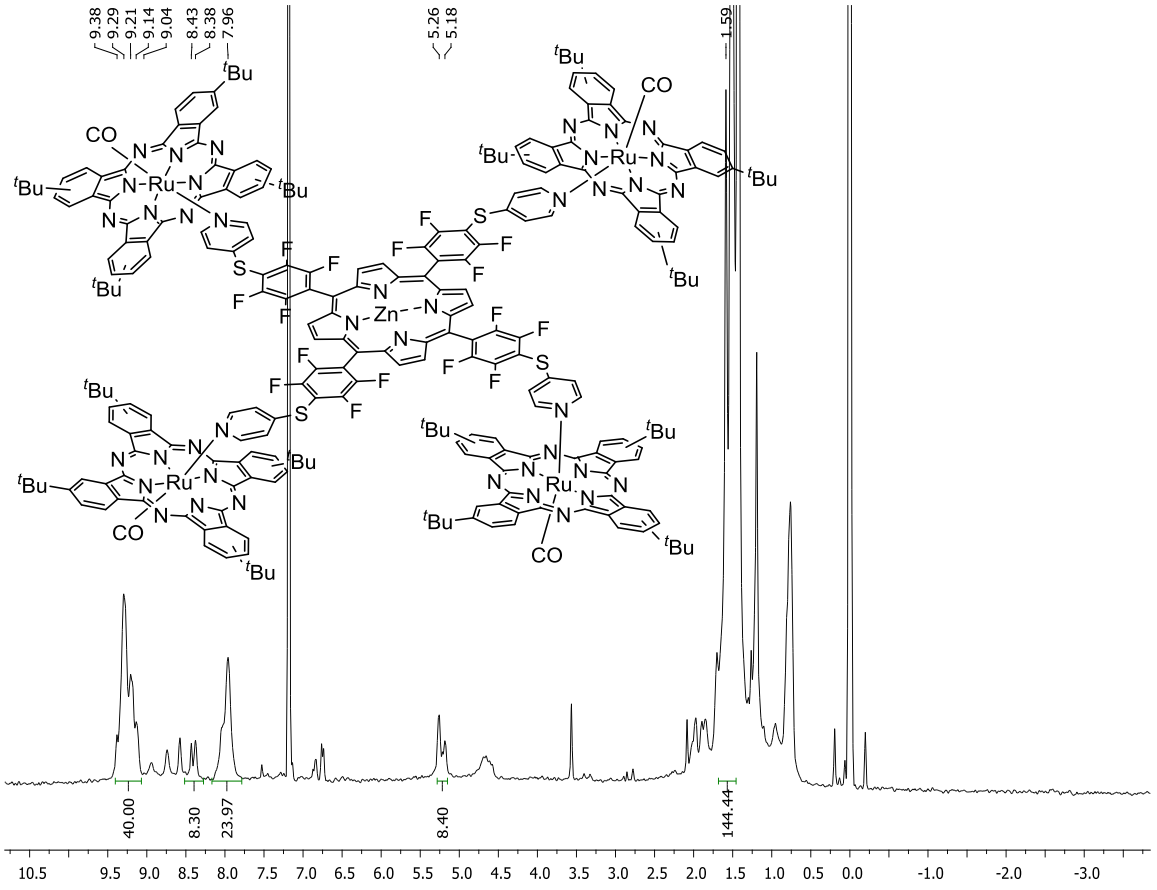

Figure 4.17 ^{1}H NMR spectrum of compound **4.12** in $CDCl_3$.

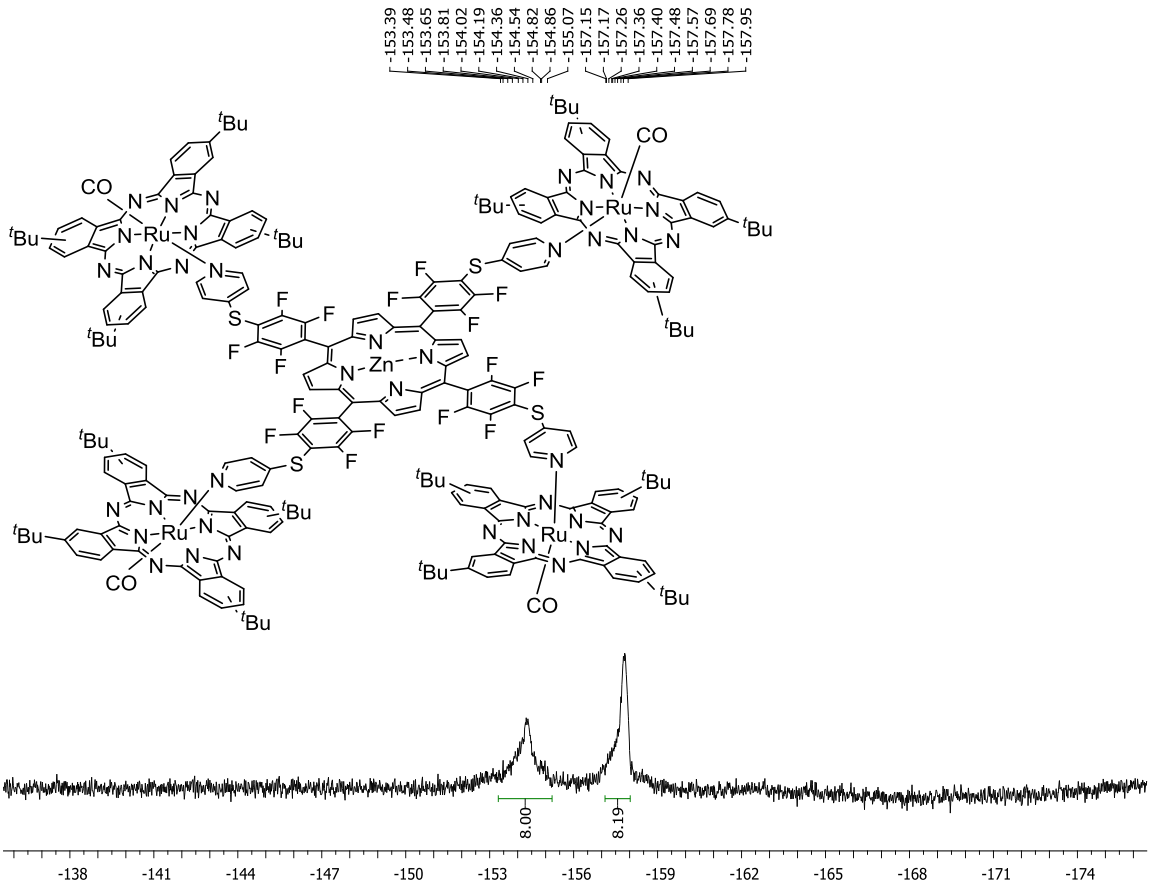

Figure 4.18 ^{19}F NMR spectrum of compound **4.12** in $CDCl_3$.

4.5 Photophysical properties*

Considering the remarkable photochemical and photophysical properties of Pors and Pcs to act as electron carriers and the simple access to obtain the new supramolecular conjugates **4.10**-**4.12** (Figure 4.10), in this section it will be discussed the photophysical characterization of the supramolecular hybrids. In fact, the procedure that proved to be an efficient methodology to prepare the desired supramolecular ensembles **4.10**-**4.12** *via* noncovalent interaction of Pors **4.7** or **4.8**[52] with the adequate number of **RuPc 4.3** units allowed us to study the type of photoinduced energy and electronic communication involving the dyes present.

The absorption spectra of **4.10**-**4.12** are summarised in Figure 4.19 and their profile were compared with the profile of the individual components. The absorption spectra of

*These compounds were tested by **Anita Hausmann** and **Christina Schubert**, who kindly provided their results for a comprehensive analysis of the photophysical values of these supramolecular arrays.

4.7 and **4.8** show a dominating Soret-band absorption that maximizes at *ca* 415 nm and a series of weaker Q-band absorptions in the region between 500 and 650 nm, which are in agreement with the spectrum of 5,10,15,20-tetraphenylporphyrin (**H_2P**) reference[70] (Table 4.3). Similarly, the absorption spectrum of zinc tetra-thiopyridylporphyrin **4.9** is a good resemblance of the absorption spectrum of zinc(II) complex of 5,10,15,20-tetraphenylporphyrin (**ZnP**)[70] comprising a dominant Soret-band absorption that maximizes at 423 nm and weak Q-band absorptions in the region of 500 – 600 nm (Table 4.3). On the other hand, the optical absorption spectrum of **RuPc 4.3** shows a weak Soret-band, in the region of 300 – 400 nm and a strong Q-band maximum at 650 nm, which matches quite well with the absorption features seen for metallated phthalocyanines.

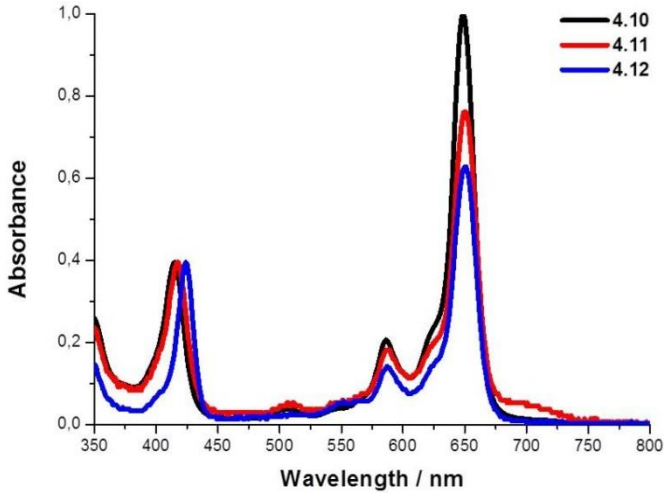

Figure 4.19 Room temperature absorption spectra of **4.10**-**4.12** in toluene.

Table 4.3 Soret-band wavelengths, maxima of fluorescence wavelength ($\lambda_{max.\ emission}$), fluorescence quantum yields (φ_F) and life times of **4.7**-**4.12**.

Compound	Soret-band (nm)	Q-bands (nm)	Emission[a] ($\lambda_{max.}$ nm)	φ_F[b]	τ
4.7	412	505, 536, 581, 634	---	---	---
4.8	415	507, 537, 581, 633	705	0.06	---
4.9	423	552, 586	655	0.03	2.1 ns
4.10	418	587, 650	663	0.01	---
4.11	422	587, 650	655	0.003	< 100 ps
4.12	430	586, 650	658	0.0002	112 ± 10 ps

[a]excited at 420 nm; [b]using **H_2P** and **ZnP** as reference.

The UV-vis spectra of **4.10** and **4.11**, show the characteristic absorption features of the corresponding individual constituents **4.7** and **4.8** and of **RuPc 4.3** (Figure 4.19 and Table 4.3). In particular, the spectra show the Soret-bands at 418 and 422 nm for **4.10** and

4.11, respectively, as well as the characteristic Q-band of the metallated Pc or Pcs at 650 nm. By the same token, **4.12** features the absorption characteristics of **4.9**, with a Soret-band that maximizes at 430 nm and of the **RuPc** with a strong Q-band at 650 nm that remained unchanged. Finally, considering the Soret- and Q-bands intensity of hybrids **4.10** and **4.11**, it was expected that absorption intensity of Q-band of **4.11** would be amplified by the contribution of the four **RuPc** units comparatively to the dyad **4.10** (Figure 4.19). Interesting it was observed a less intense Q-band absorption for the pentamer.

In Table 4.3 are also summarized the fluorescence maxima, fluorescence quantum yields, and fluorescence lifetimes obtained from the steady state and time resolved fluorescence studies. Porphyrins **4.8** and **4.9** and the references **H_2P** and **ZnP** were all photoexcited at 420 nm, while **RuPc 4.3** was photoexcited at 610 nm. In Figure 4.20, the fluorescence spectra of **4.8** and **H_2P**[71] are shown featuring maxima at 640 and 705 nm and quantum yields of 0.06 and 0.1, respectively. In contrast, **4.9** and **ZnP**[71] reveal maxima at 600 and 655 nm and quantum yields of 0.03 and 0.04, respectively. The energy of the triplet excited states of **H_2P** and **ZnP** are known from the literature as 1.43 and 1.53 eV, respectively.[71] For **4.8** and **4.9** we expect the same energetic levels of their triplet excited states. Finally, for **RuPc** a maximum at 670 nm and a quantum yield of 0.01 evolves. Furthermore, the phosphorescence spectrum of **RuPc** features a maximum at 968 nm. For the latter, the energy of the triplet excited state is estimated in 1.33 ± 0.01 eV.

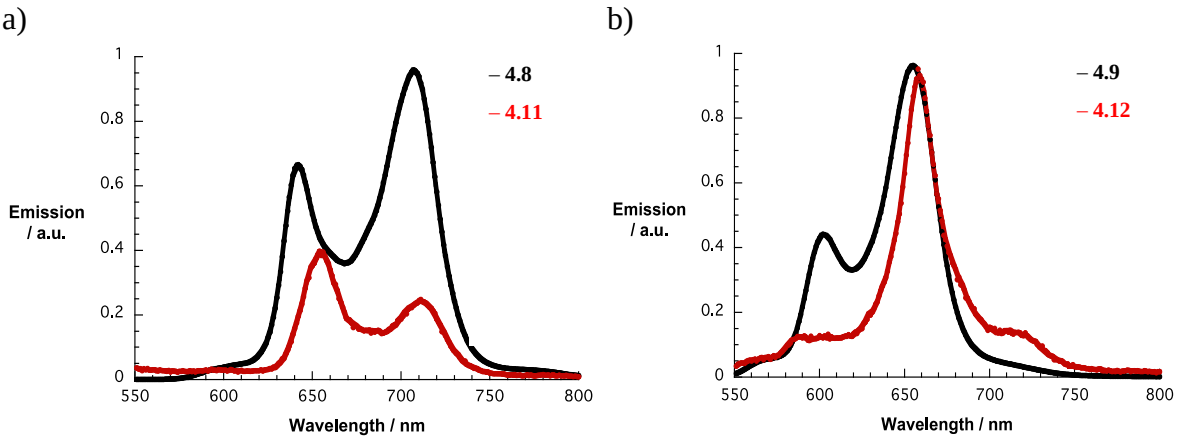

Figure 4.20 Room temperature fluorescence spectra of a) **4.8** in dichloromethane and **4.11** in toluene and b) **4.9** in dichloromethane and **4.12** in toluene with identical absorption at the 420 nm excitation wavelength.

In case of **4.12**, the Por **4.9** centred fluorescence is notably quenched when photoexcited at 420 nm with a value of around 0.007 (Figure 4.20). Similarly, the Por **4.9**

fluorescence lifetime is in **4.12** much shorter (112 ps ± 10 ps) relative to that seen in the absence of **RuPc** (2.1 ns). These are considered as first evidences for electronic communication either in the form of energy or electron transfer between the light harvesting **4.9** and **RuPc**. Despite the exclusive excitation of **4.9**, **RuPc** centred fluorescence emerges at 657 nm with a quantum yield of 0.0002. Implicit in such a finding is a thermodynamically driven transduction of singlet excited state energy from the higher lying singlet exited state of **4.9** (2.05 eV) to the lower lying singlet excited state of **RuPc** (1.85 eV). Important is the confirmation of the energy transfer hypothesis by means of measuring an excitation spectrum for **4.9** at the newly evolving **RuPc** fluorescence. It resembles the ground state absorption, that is, giving rise to the absorption features of **4.9** (430, 500 – 600 nm), on one hand, and of **RuPc** (300 – 400, 650 nm), on the other hand.

All of the aforementioned effects are even more pronounced when photoexciting **4.11** and **4.8** at 420 nm and comparing their fluorescence features it is observed a fluorescence quenching (Figure 4.20). In fact, the fluorescence quantum yield of **4.11** is much lower (0.003) than that of **4.8** (0.06) and **H_2P** (0.1). Also in the case of **4.11**, **RuPc** fluorescence evolved at 658 nm, which, again, came at the expense of the **4.8** fluorescence. A complementary performed excitation spectrum of the **RuPc** fluorescence corroborates with the **4.8** and **RuPc** sensitised fluorescence with maxima at 422, 500 – 600 and 300 – 400 / 650 nm, respectively. More importantly, it also confirms the energy transfer between the **4.8** singlet exited state (1.95 eV) and the **RuPc** singlet excited state (1.85 eV). Like what has been seen before for **4.12**, the **4.8** fluorescence lifetime is in **4.11** very short with a value below the time resolution of 100 ps. Interesting is the fact that in **4.10** the fluorescence quenching is weaker than in **4.11** with a quantum yield of nearly 0.01. Notably, besides the **4.9** (2.05 eV), **4.8** / **4.7** (1.95 eV) and **RuPc** (1.85 eV) fluorescence no additional features are seen.

In additional experiments, all of the **RuPc** containing systems **4.10**-**4.12** were excited at 610 nm. Here, the exclusive **RuPc** excitation results only in the fluorescence of the latter without giving rise to any appreciable **4.9** or **4.8** / **4.7** fluorescence and without any notable **RuPc** fluorescence quenching. Moreover, the corresponding maxima match in these 610 nm excitation experiments those seen for **4.10** (663 nm), **4.11** (655 nm), and **4.12** (658 nm) in 420 nm excitation experiments.

In order to shed more light onto the mutual interactions in the excited state of **4.10**-**4.12** and of their references, the femtosecond transient absorptions were probed. Here,

either excitation of **4.9** / **4.8** at 420 nm or excitation of **RuPc** at 656 nm stood at the forefront of the investigations.

The excitation of **4.9** at 420 nm gives rise to the direct formation of the singlet excited state with maxima at 531, 575 and 623 nm and minima at 552, 595 and 652 nm; a similar excitation of **4.8** affords maxima at 494, 535, 571 and 622 nm and minima at 515, 550, 592 and 648 nm (Figure 4.21).

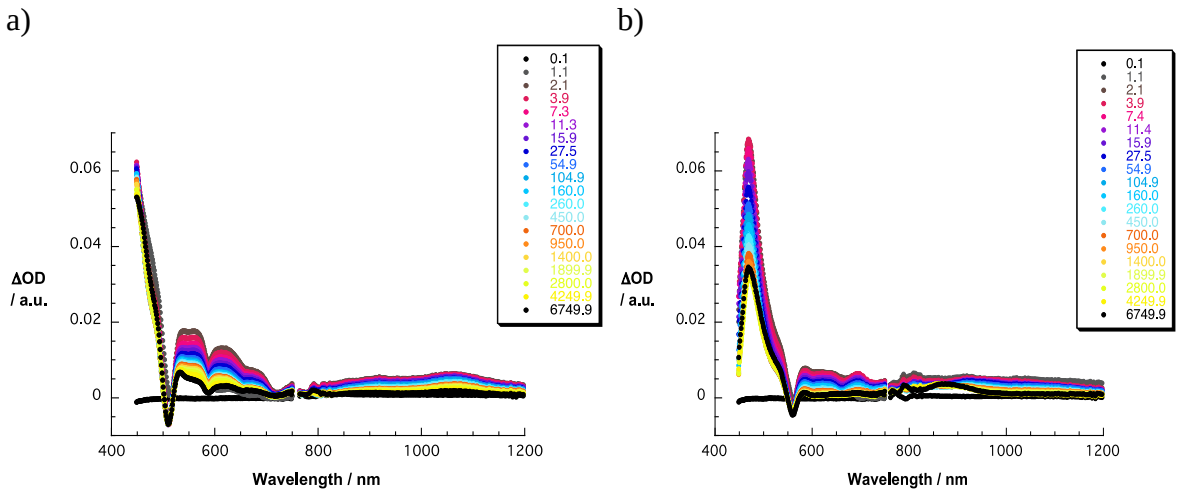

Figure 4.21 Differential absorption spectra (visible and near-infrared) obtained upon femtosecond pump probe experiments (420 nm) of a) **4.8** and b) **4.9** in dichloromethane with several time delays between 0.1 and 6749.9 ps at room temperature.

Via intersystem crossing (ISC) corresponding to the triplet manifolds evidence latter decay with lifetimes about 2.1 ± 0.5 and 9.8 ± 0.5 ns for **4.9** and **4.8**, respectively, featuring maxima at 840 nm (**4.9**) as well as 780 nm (**4.8**). The triplet lifetimes are 80 µs for **4.9** and 1 µs for **4.8**. Immediately after exciting **RuPc** at 656 nm its singlet excited state features are formed in the form of a bleaching at around 590 and 650 nm (Figure 4.22). The latter features a lifetime of 7.5 ± 2.5 ps. Owing to the presence of ruthenium the intersystem crossing to the corresponding triplet excited state is fast and efficient yielding a 1 µs lived transient maximum at 515 nm.

In case of **4.12**, which was also excited at 420 nm, the spectral features of the **4.9** singlet excited state – *vide supra* – are seen. Most notably, are the minimum at 560 nm and the maxima at 465, 605 and 695 nm (Figure 4.23).

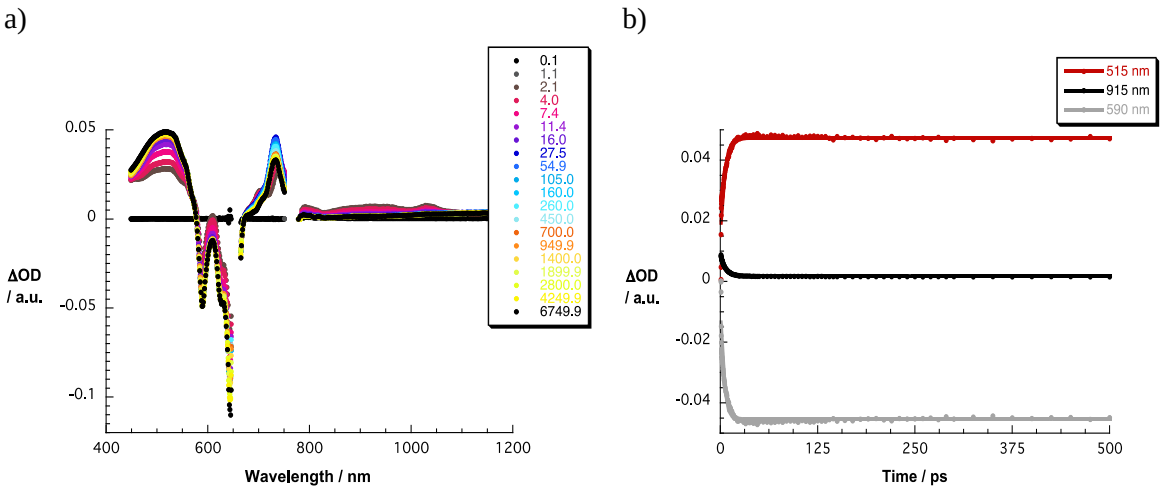

Figure 4.22 a) Differential absorption spectra (visible and near-infrared) obtained upon femtosecond pump probe experiments (656 nm) of **RuPc** in toluene with several time delays between 0.1 and 6749.9 ps at room temperature. b) Time absorption profiles of the spectra shown in the upper part at 515 (red spectrum), 915 (black spectrum) and 590 nm (grey spectrum) monitoring the excited state decay.

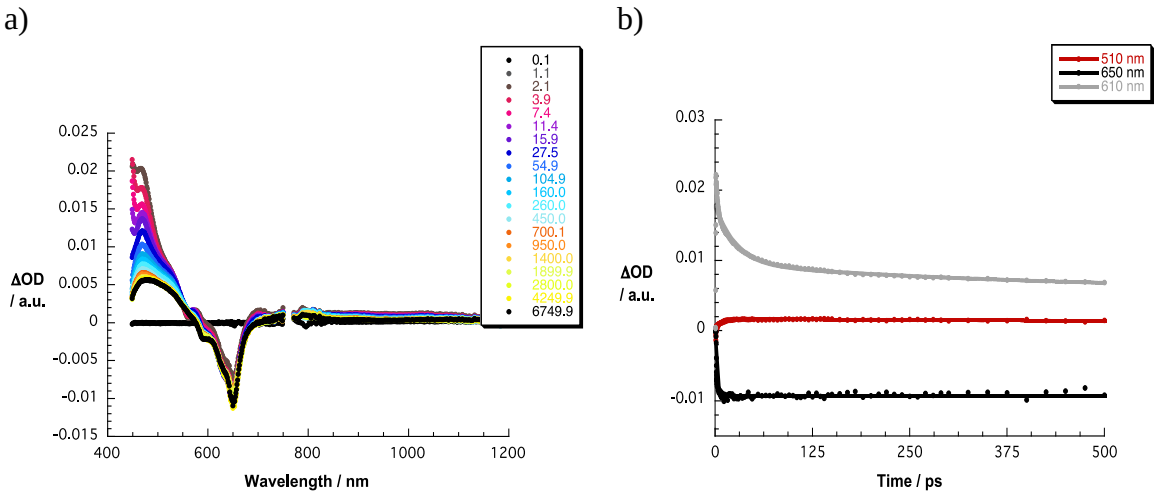

Figure 4.23 a) Differential absorption spectra (visible and near-infrared) obtained upon femtosecond pump probe experiments (420 nm) of **4.12** in toluene with several time delays between 0.1 and 6749.9 ps at room temperature. b) Time absorption profiles of the spectra shown in the upper part at 510 (red spectrum), 650 (black spectrum) and 610 nm (grey spectrum) monitoring the excited state energy transfer.

The presence of the **RuPc** evokes a significant shortening of the **4.9** singlet excited state lifetimes, namely 130 ± 20 ps. Concomitant with the latter decay it was noted the formation of a new transient state. The new transient features a characteristic words minima at 590 and 650 nm, which resembles that seen for **RuPc**. In other, in case of **4.12** an intramolecular energy transfer transduces singlet excited state energy from the initially

excited **4.9** to **RuPc**. As a matter of fact, the current finding compares well with the conclusions from the steady-state and time-resolved fluorescence experiments. On the nanosecond time scale the decay of the triplet excited state features of **RuPc** leads to a lifetime of 8.3 ± 1 µs.

Turning again to **4.11**, right after the 420 nm excitation of the **4.8** singlet ground states, its singlet excited state is formed (Figure 4.24). Evidence for the latter stems from monitoring ground state bleaching at 510 nm and transient maxima at 460, 615 and 690 nm. In analogy to the observation made with **4.12** – *vide supra* – an intramolecular energy transfer sets in shortly after the formation of the **4.8** singlet excited state. In fact, the **RuPc** singlet excited minima at 590 and 650 nm grown in with 21 ± 7 ps, which matches the decay of the **4.8** singlet excited state. On the nanosecond time scale, the decay of the triplet excited state features of **RuPc** are discernible, which give rise to lifetimes of 4.0 ± 0.5 µs. A quantitatively similar picture evolves for **4.10** with an intramolecular energy transfer that takes 150 ± 50 ps (Figure 4.25).

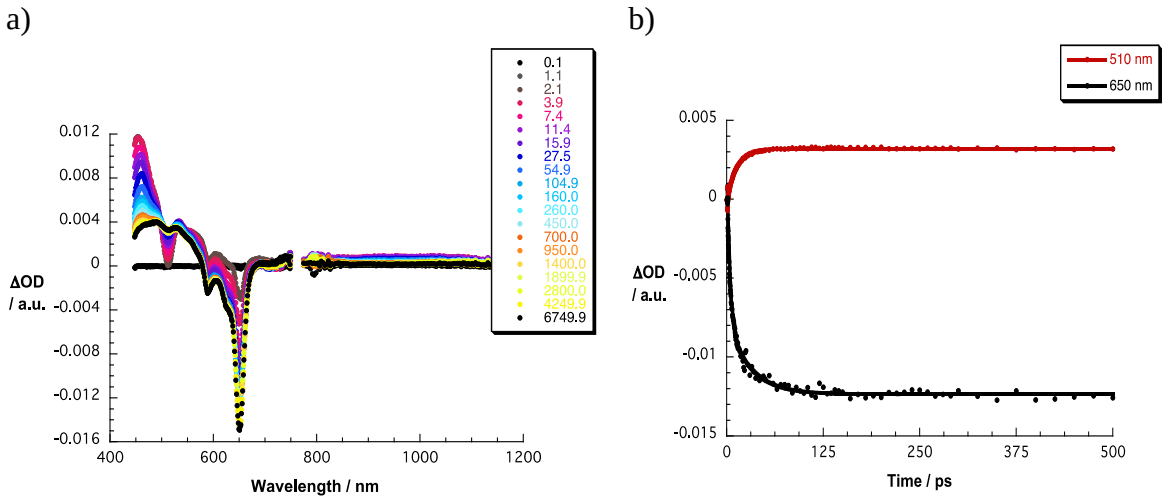

Figure 4.24 a) Differential absorption spectra (visible and near-infrared) obtained upon femtosecond pump probe experiments (420 nm) of **4.11** in toluene with several time delays between 0.1 and 6749.9 ps at room temperature. b) Time absorption profiles of the spectra shown in the upper part at 510 (red spectrum) and 650 nm (black spectrum) monitoring the excited state energy transfer.

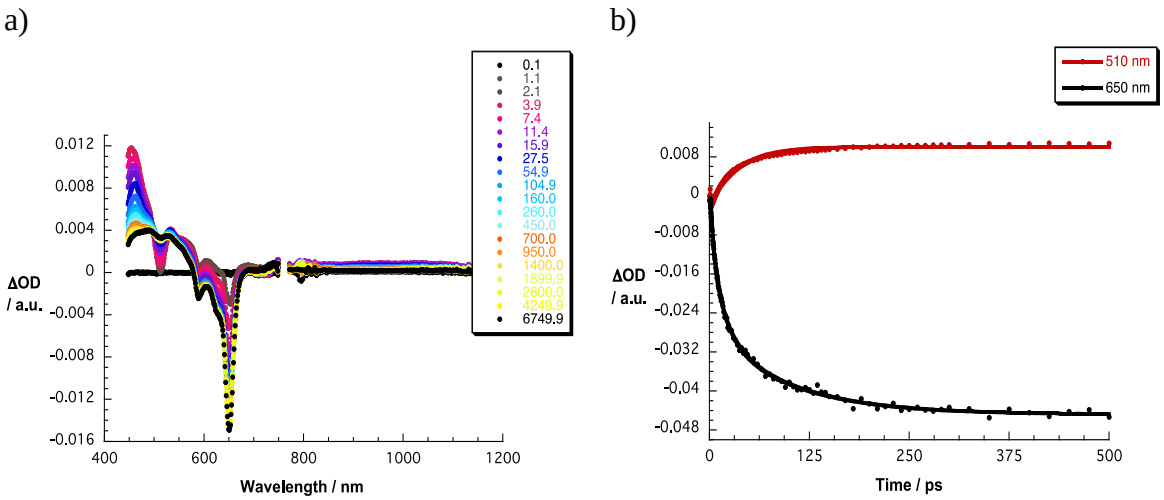

Figure 4.25 a) Differential absorption spectra (visible and near-infrared) obtained upon femtosecond pump probe experiments (420 nm) of **4.10** in toluene with several time delays between 0.1 and 6749.9 ps at room temperature. b) Time absorption profiles of the spectra shown in the upper part at 510 (red spectrum) and 650 nm (black spectrum) monitoring the excited state energy transfer.

In complementary experiments, when **4.10**-**4.12** are excited at 656 nm only the features of **RuPc** are observed. No appreciable **4.7**, **4.8**, and **4.9** based features are seen at any time during the time evolution due to the dominating absorptions of **RuPc**.

The thiopyridylporphyrins **4.10**-**4.12** and the ruthenium phthalocyanine proved to be versatile building blocks of novel supramolecular Por-Pc hybrid systems by axial ruthenium coordination. The thiopyridyl groups placed at the bay region of the porphyrins coordinate the **RuPc** dye, showing a notable redistribution of electron density of new heterochromophore structures evidencing the electron-donating/-accepting communication between both dyes in the supramolecular hybrids. These structural hybrids were projected to promote electronic coupling between the electron donor-acceptors and were physicochemical investigated by the ground and excited state reactivities.

4.6 Final considerations

In summary, we have unequivocally demonstrated herein the preparation of three novel heterochromophore structures **4.10**-**4.12** based on noncovalent linkage, to study photoinduced energy- and/or electron-transfer processes. Pyridyl substituted Pors were coordinated with **RuPc** to promote electronic communication between these electron donor

/ acceptor moieties. It is noteworthy, that an energy transfer from the thiopyridylporphyrins to the **RuPcs** was found. However, in case of the hybrid **4.10** occurs an unidirectional energy transfer, and for hybrids **4.11** and **4.12** energy transfer sets are noted. This was demonstrated by **RuPc** centred fluorescence features, evolved upon photoexcitation of the Por, which show lower fluorescence quantum yields and shorter fluorescence lifetimes than the corresponding references. Excitation spectra as well as transient absorption measurements help to confirm that hypothesis, while the latter reveals a significant shortening of the porphyrin´s singlet excited state lifetimes. In this circumstance, we corroborate the electronic communication of the supramolecular building blocks by energy transfer. Photophysical investigation by means of time-resolved transient absorption, namely fluorescence and femtosecond spectroscopy, revealed in the supramolecular multichromophore ensembles efficient intermolecular energy transfer from the photoexcited central thiopyridylporphyrin to the peripheral **RuPcs**. These results prove to be important for the future design of new Por-Pc electron donor / acceptor hybrids to be used as building blocks in solar light converting systems.

4.7 Experimental Section

4.7.1 General information

^{1}H and ^{19}F NMR spectra were recorded in a *Bruker Avance-300* spectrometer at 300.13 and 282.38 MHz, respectively. Tetramethylsilane was used as internal reference. Steady-state absorption spectra were recorded with a Perkin-Elmer Lambda 35. Steady-state emission spectra were recorded in a Fluoromax-3-spectrometer from HORIBA Jobin Yvon. All samples were measured in a fused quartz glass cuvette with a 10 mm of light path. Analytical TLC was carried out on precoated silica gel sheets (Merck, 60, 0.2 mm). Column chromatography was carried out over silica gel (Merck, 63–200 mesh). Molecular exclusion column chromatography was carried out over Bio-beads^{TM} S-X1 Beads (200-400 Mesh, 100 g), Bio-Rad Laboratories, Inc. MALDI-MS mass spectra were acquired using a MALDI-TOF/TOF Applied Biosystems 4800 Proteomics Analyzer (Applied Biosystems, Framingham, MA, USA) instrument equipped with a nitrogen laser emitting at 337 nm. Prior to MALDI-MS analysis, 4 µL of matrix, dithranol (10 mg mL^{-1} in methanol / 0.1% TFA) were mixed with 2 µL of the dye solution in CH_2Cl_2/MeOH (≈10 $\mu g.mL^{-1}$), and 1 µL

of this mixture was deposited on the MALDI plate and let to dry. MALDI-MS spectra were acquired in the positive ion reflector mode using delayed extraction in the mass range between 600 and 4500 Da with ca. 1500 laser shots. For the following acquisition of tandem mass spectra collision energy of 2 keV was used to induce fragmentation, and air was used as collision gas.

Femtosecond transient absorption spectra were obtained with a Ti:sapphire laser system CPA-2101 (Clark-MXR), Inc.) in combination with a Helios TAPPS detection unit from Ultrafast Inc. The initial laser excitation wavelength is 775 nm with a pulse width of 150 fs. The used excitation wavelength was 387 nm, which was generated with a SHG crystal. For the generation of the white light a sapphire crystal of adequate thickness was used. The chirp-effect between 420 and 770 nm is approximately 350 fs. The detection was carried out with two CCD cameras, each for a specific measuring range. The spectral window is therefore 415 to 770 nm and 770 to 1200 nm. The delay line allows spectral acquisition up to time delays of 6750 ps. All samples were measured in a fused quartz glass cuvette with a thickness of 2 mm. Data was acquired with the software HELIOS Visible/nIR (Newport / Ultrafast Systems).

4.7.2 Synthesis and characterization of the free *tert*-butylphthalocyanine

*2(3),9(10),16(17),23(24)-tetrakis-tert-butylphthalocyanine (**4.2**)*:

A mixture of phthalonitrile 4-(*tert*-butyl)phthalonitrile **4.1** (2.74 mmol, 1 eq.) and lithium (53.0 mg, 7.64 mmol, 3 eq.) was carried out overnight at 140 ºC in 5 mL of 1-pentanol as solvent.[55] The crude of reaction was precipitated from a mixture of MeOH/H_2O (1/1), filtrated and washed several times with the same mixture. The obtained blue solid was redissolved in CH_2Cl_2 and purified over silica gel chromatography column using CH_2Cl_2/C_6H_{14} (3:1) as eluent. The main fraction was dry under reduce pressure and the pure product **4.2** was obtained in 84% yield. ^{1}H NMR (300 MHz, $CDCl_3$): δ -1.20 – -0.98 (m, 2H, NH), 1.90 (s, 36H, ^{t}Bu-H^d), 8.27–8.39 (m, 4H, β-H^c), 9.14–9.58 (m, 8H, α-H^{a,b}). MALDI-TOF-MS: *m/z* 739 $[M+H]^+$.

4.7.3 Synthesis and characterization of the ruthenium *tert*-butylphthalocyanine 4.3

*[Carbonyl-2(3),9(10),16(17),23(24)-tetrakis-tert-butylphthalocyaninato] ruthenium(II) (**4.3**)*:

A mixture of **H_2Pc 4.2** (100 mg, 0.13 mmol), $Ru_3(CO)_{12}$ (173 mg, 0.27 mmol) and phenol (6 g) was heated at reflux temperature (190 ºC) under argon during 16 h. The solution was cooled to room temperature, and then dissolved in 50 mL of ethanol. After addition of 200 mL of water, the resulting blue precipitate was filtered, washed with a mixture of water/methanol (4/1), and dry under reduce pressure. The crude was redissolved and purified by column chromatography on silica gel using toluene as eluent.[27,28] The product was dry and the blue solid **4.3** was determined in 82% of yield. H^1 NMR (300 MHz, $CDCl_3$): δ 1.71 (s, 36H, ^{t}Bu-H^d), 8.01-8.14 (m, 4H, RuPc β-H^c), 9.14-9.40 (m, 8H, RuPc α-H^{a,b}). UV-Vis ($CHCl_3$), $\lambda_{max.}$ nm (ε): 296 (5.01), 330 (4.56), 590 (4.42), 627 (4.81), 650 nm (5.18). ESI-MS: *m/z* 866 $[M]^{+\cdot}$.

4.7.4 Synthesis of the *meso*-pentafluorophenyl porphyrin, $TPPF_{20}$ 4.6

*5,10,15,20-tetrakis(2,3,4,5,6-pentafluorophenyl)porphyrin, **$TPPF_{20}$ (4.6)***:

A mixture of pyrrole (5 mL, 72.0 mmol) and pentafluorobenzaldehyde (8 mL, 65.0 mmol) was stirring in a mixture of acetic acid (400 mL) and nitrobenzene (300 mL) refluxing at 120 ºC. The reaction was followed by TCL and after 1 h was concluded. After that, the mixture of solvents was distillate under reduce pressure. The obtained residue was dissolved in petroleum ether and purified by silica gel chromatography column using a mixture of petroleum ether/CH_2Cl_2 (3:1) as eluent. The first fraction was identified by **$TPPF_{20}$**. The ^{1}H and ^{19}F NMR spectra confirmed the corresponding **$TPPF_{20}$** (**4.6**). ^{1}H NMR (300 MHz, $CDCl_3$): δ -3.19 (s, 2H, NH), 9.45 (s, 8H, β-H). ^{19}F NMR (282 MHz, $CDCl_3$): δ -184.92 – -184.70 (m, 8F, Ar-*o*-F), -174.70 (t, J = 20.9 Hz, 4F, Ar-*p*-F), -160.04 (dd, J = 22.8, 7.7 Hz, 8F, Ar-*m*-F).

4.7.5 Synthesis and characterization of thiopyridylporphyrins 4.7-4.9

*5-[2,3,5,6-tetrafluoro-4-(pyridylsulphanyl)phenyl]-10,15,20-tris(pentafluorophenyl)porphyrin (**4.7**)*:

The reaction of 5,10,15,20-tetrakis(pentafluorophenyl)porphyrin (**$TPPF_{20}$**, 222.1 mg, 0.228 mmol) and 4-mercaptopyridine (17.1 mg, 0.154 mmol, 0.7 eq.) using 1 mL of DEA was accomplished in 3 mL of DMF during 1 h at room temperature. After reaction, DMF was evaporated under reduced pressure and the residue was subjected to flash chromatography, using CH_2Cl_2 and CH_2Cl_2/MeOH (98/2) as eluents. The product was crystallised from CH_2Cl_2/MeOH (98:2)/hexane as purple solid in 22% yield. ^{1}H NMR (300 MHz, $CDCl_3$): δ -2.97 (s, 2H, NH), 7.29 (dd, *J* = 4.6, 1.5 Hz, 2H, SPy-*o*-H), 8.58 (dd, *J* = 4.6, 1.5 Hz, 2H, SPy-*m*-H), 8.87–8.89 (m, 8H, β-H). ^{19}F NMR (282 MHz, $CDCl_3$): δ -184.87 – -184.67 (m, 6F, Ar-*o*-F), -174.75 – -174.51 (m, 3F, Ar-*p*-F), -160.02 (dd, *J* = 23.1, 7.8 Hz, 6F, Ar-*m*-F), -158.15 (dd, *J* = 24.8, 12.5 Hz, 2F, SPyAr-F), -154.30 (dd, *J* = 24.8, 12.5 Hz, 2F, SPyAr-F). MALDI-TOF-MS: *m/z* 1066 $[M+H]^+$.

*5,10,15,20-Tetrakis[2,3,5,6-tetrafluoro-4-(pyridylsulphanyl)-phenyl]porphyrin (**4.8**)*:

4-Mercaptopyridine (47.0 mg, 4 eq.) and DEA (1 mL) were added to a solution of **$TPPF_{20}$** (100.0 mg, 0.1 mmol) in dry DMF (5 mL). This mixture was kept under stirring for 1 h, under a nitrogen atmosphere, at room temperature. After reaction, the DMF was evaporated under reduced pressure and the residue was subjected to flash chromatography, using dichloromethane and CH_2Cl_2/MeOH (98/2) as eluents. The fraction containing Por **4.8** (120 mg, 90%) was concentrated and crystallised from a mixture of CH_2Cl_2/MeOH (98:2)/hexane. ^{1}H NMR (300 MHz, DMSO-d_6): δ -3.12 (s, 2H, NH), 7.73 (d, *J* = 5.9 Hz, 8H, SPy-*o*-H), 8.63 (d, *J* = 5.9 Hz, 8H, SPy-*m*-H), 9.61 (s, 8H, β-H). ^{19}F NMR (282 MHz, DMSO-d_6): δ -161.11 (dd, *J* = 11.9 and 26.3 Hz, 8F, Ar-*o*-F), -156.14 (dd, *J* = 11.9 and 26.3 Hz, 8F, Ar-*m*-F). UV-Vis (CH_2Cl_2), $\lambda_{max.}$ nm (ε): 415 (5.48), 507 (4.34), 581 (3.87), 633 (3.59). MALDI-TOF-MS: *m/z* 1339 $[M+H]^+$.

*5,10,15,20-Tetrakis[2,3,5,6-tetrafluoro-4-(pyridylsulphanyl)-phenyl]porphyrinato zinc(II) (**4.9**)*:

A mixture of Por **4.8** (31.6 mg, 0.024 mmol) and zinc acetate (23.7 mg, 0.13 mmol, 5 equiv.) were carried out in 5 mL of $CHCl_3$/MeOH (9:1) at reflux. The reaction was

followed by TCL and completed after stirring during 3 h under nitrogen atmosphere. By precipitation from a mixture of $CHCl_3$/MeOH (98:2)/hexane, it was obtained a purple solid and washed several times with water in order to remove the excess of zinc acetate. Compound **4.9** was obtained in 96% yield. ^{1}H NMR (300 MHz, $CDCl_3$): δ 7.23 (d, J = 5.7 Hz, 8H, SPy-*o*-H), 8.07 (d, J = 5.7 Hz, 8H, SPy-*m*-H), 8.95 (s, 8H, β-H). ^{19}F NMR (282 MHz, $CDCl_3$): δ -154.93 (dd, J = 24.5, 11.8 Hz, 8F, Ar-*o*-F), -151.46 (dd, J = 24.5, 11.8 Hz, 8F, Ar-*m*-F). UV-Vis (CH_2Cl_2), $\lambda_{max.}$ nm (ε): 423 (5.63), 552 (4.31), 586 (3.40). MALDI-TOF-MS: *m/z* 1401 $[M+H]^+$.

4.7.6 Synthesis of the supramolecular arrays 4.10-4.12

*Compound **4.10***:

A mixture of Por **4.7** (14.8 mg, 0.014 mmol) and **RuPc** (13.2 mg, 0.015 mmol, 1.1 equiv.) was stirred in 5 mL of CH_2Cl_2 overnight at room temperature. After concentration under reduce pressure, the products was purified by molecular exclusion chromatography column (Bio-Beads S-X1) using CH_2Cl_2 as eluent. The main fraction was dry and the solid product **4.10** afforded in 71% yield. ^{1}H NMR (300 MHz, $CDCl_3$): δ -3.02 (s, 2H, NH), 1.79 (s, 36H, ^{t}Bu-H), 6.99 – 7.13 (m, 4H, Por β-H), 8.18 (d, J = 8.1 Hz, 4H, RuPc β-H), 8.62 (d, J = 4.6 Hz, 2H, SPy-*o*-H), 8.80 (d, J = 4.6 Hz, 2H, SPy-*m*-H), 8.90 (s, 4H, Por β-H), 9.30 – 9.47 (m, 8H, RuPc α-H). ^{19}F NMR (282 MHz, $CDCl_3$): δ -184.89 – -184.68 (m, 6 F, Ar-*o*-F), -174.74 – -174.51 (m, 3 F, Ar-*p*-F), -160.09 – -159.91 (m, 6 F, Ar-*m*-F), -157.62 (dd, J = 24.3, 11.9 Hz, 2F, SPyAr-F), -153.97 (dd, J = 24.3, 11.9 Hz, 2F, SPyAr-F). ESI-MS: *m/z* 1931 $[M]^{+\cdot}$.

*Compound **4.11***:

A mixture of **4.8** (15.0 mg, 0.011 mmol) and **RuPc** (51.3 mg, 0.056 mmol, 5 equiv.) was stirred in 5 mL of CH_2Cl_2 overnight at room temperature. After reaction, the products were purified by molecular exclusion chromatography column (Bio-Beads S-X_1) using CH_2Cl_2 as eluent. The main fraction was dry and the obtained blue solid **4.11** afforded in 91% yield. ^{1}H NMR (300 MHz, $CDCl_3$): δ -3.39 – -3.35 (m, 2H, NH), 1.60 (s, 144H, ^{t}Bu-H), 5.27 (d, J = 6.6 Hz, 8H, SPy-*o*-H), 8.06 (d, J = 8.0 Hz, 16H, RuPc β-H), 8.36 (s, 8H, Por β-H), 9.25 – 9.39 (m, 40H, RuPc α-H and SPy-*m*-H). ^{19}F NMR (282 MHz,

$CDCl_3$): δ -134.18 – -133.96 (m, 8F, Ar-*o*-F), -130.45 – -130.29 (m, 8F, Ar-*m*-F). ESI-MS: *m/z* 4803 $[M]^{+\cdot}$.

*Compound **4.12***:

A mixture of **4.11** (15.0 mg, 0.003 mmol) and zinc acetate (0.57 mg, 0.003 mmol, 1 equiv.) was stirred in 5 mL of CH_2Cl_2/MeOH (9:1) during 3 h at reflux. After that, the products of reaction werer purified by molecular exclusion to obtain the corresponding zinc complex **4.12** in 90% yield, isolated as a deep blue solid. ^{1}H NMR (300 MHz, $CDCl_3$): δ 1.59 (s, 144H, ^{t}Bu-H), 5.22 (d, J = 18.9 Hz, 8H, SPy-*o*-H), 7.96 (br s, 24H, RuPc β-H and Por β-H), 8.40 (d, J= 18.9 Hz, 8H, Ar-*m*-H), 9.04 – 9.38 (m, 40H, Por β-H and RuPc α-H). ^{19}F NMR (282 MHz, $CDCl_3$): δ -157.95 – -157.15 (m, 8F, Ar-*o*-F), -155.07 – -153.39 (m, 8F, Ar-*m*-F). UV-Vis ($C_6H_5CH_3$), $\lambda_{max.}$ nm (ε): 430 (5.93), 552 (5.06), 587 (5.48), 650 (6.14).

4.8 References

1. Oswald, F., Islam, D.-M. S., El-Khouly, M. E., Araki, Y., Caballero, R., Cruz, P., Ito, O., Langa, F., *Phys. Chem. Chem. Phys.*, **2014**, 16, 2443–2451.
2. Martínez-Díaz, M. V., Torre, G., Torres, T., *Chem. Commun.*, **2010**, 46, 7090–7108.
3. Melomedov, J., Ochsmann, J. R., Meister, M., Laquai, F., Heinze, K., *Eur. J. Inorg. Chem.*, **2014**, 1984–2001.
4. Pereshivko, L. Y., Grishina, A. D., Gorbunova, Y. G., Zolotarevskii, V. I., Enakieva, Y. Y., Nekrasov, A. A., Krivenko, T. V., Savel'ev, V. V., Vannikov, A. V., Tsivadze, A. Y., *High Energy Chem.*, **2009**, 43, 7, 543–551.
5. D'Souza, F., Ito, O., *Chem. Soc. Rev.*, **2012**, 41, 86–96.
6. Das, S. K., Song, B., Mahler, A., Nesterov, V. N., Wilson, A. K., Ito, O., D'Souza, F., *J. Phys. Chem. C*, **2014**, 118, 3994–4006.
7. Ragoussi, M.-E., Katsukis, G., Roth, A., Malig, J., Torre, G., Guldi, D. M., Torres, T., *J. Am. Chem. Soc*., **2014**, 136, 4593−4598.
8. Vinodh, M., Alipour, F. H., Mohamod, A. A., Al-Azemi, T. F., *Molecules*, **2012**, 17, 11763–11799.
9. Zeng, J., Chen, K.-Q., *J. Mater. Chem. C*, **2013**, 1, 4014–4019.
10. Kiessling, D., Costa, R. D., Katsukis, G., Malig, J., Lodermeyer, F., Feihl, S., Roth, A., Wibmer, L., Kehrer, M., Volland, M., Wagner, P., Wallace, G. G., Officer, D. L., Guldi, D. M., *Chem. Sci*., **2013**, 4, 3085–3098.
11. Walter, M. G., Rudine, A. B., Wamser, C. C., *J. Porphyrins Phthalocyanines*, **2010**, 14, 759–792.
12. Tanaka, T., Osuka, A., *Chem. Soc. Rev*., **2014**, DOI: 10.1039/C3CS60443H.
13. González-Rodríguez, D., Bottari, G., *J. Porphyrins Phthalocyanines*, **2009**, 13, 624–636.
14 Giribabu, L., Kanaparthi, K., *Current Science*, **2013**, 104, 847 – 855.
15. Guldi, D. M., Rahman, G. M. A., Sgobba, V., Ehli, C., *Chem. Soc. Rev*., **2006**, 35, 471–487.
16. Yedukondalu, M., Ravikanth, M., *Coord. Chem. Rev.*, **2011**, 255, 547–573.
17. Megiatto, J. D., Schuster, D. I., Abwandner, S., Miguel, G., Guldi, D. M., *J. Am. Chem. Soc*., **2010**, 132, 3847–3861.

18. Varotto, A., Nam, C.-Y., Radivojevic, I., Tomé, J. P. C., Cavaleiro, J. A. S., Black, C. T., Drain, C. M., *J. Am. Chem. Soc.*, **2010**, 132, 2552–2554.
19. Maligaspe, F., Sandanayaka, A. S. D., Hasobe, T., Ito, O., D'Souza, F., *J. Am. Chem. Soc*., **2010**, 132, 8158–8164.
20. D'Souza, F., Sandanayaka, A. S. D., Ito, O., *J. Phys. Chem. Lett*., **2010**, 1, 2586–2593.
21. Pereira, A. M. V. M., Hausmann, A., Tomé, J. P. C., Trukhina, O., Urbani, M., Neves, M. G. P. M. S., Cavaleiro, J. A. S., *Chem. Eur. J.*, **2012**, 18, 3210–3219.
22. Bottari, G., Torre, G., Guldi, D. M., *Chem. Rev.*, **2010**, 110, 6768–6816.
23. Rawling, T., Austin, C., Buchholz, F., Colbran, S. B., McDonagh, A. M., *Inorg. Chem*., **2009**, 48, 3215–3227.
24. Berber, B., Cammidge, A. N., Chambrier, I., Cook, M. J.., Hough, P. W., *Tetrahedron. Lett*., **2003**, 44, 5527–5529.
25. Georgiades, S. N., Karim, N. H. A, Suntharalingam, K., Vilar, R., *Angew. Chem. Int. Ed*., **2010**, 49, 4020–4034.
26. Cammidge, A. N., Berber, G., Chambrier, I., Hough, P. W., Cook, M. J., *Tetrahedron*, **2005**, 61, 4067–4074.
27. Rodríguez-Morgade, M. S., Torres, T., Atienza-Castellanos, C., Guldi, D. M., *J. Am. Chem. Soc*., **2006**, 128, 15145–15154.
28. Jiménez, A. J., Grimm, B., Gunderson, V. L., Vagnini, M. T., Calderon, S. K., Rodríguez-Morgade, M. S., Wasielewski, M. R., Guldi, D. M., Torres, T., *Chem. Eur. J*., **2011**, 17, 5024–5032.
29. Torre, G., Claessens, C. G., Torres, T., *Chem. Commun*., **2007**, 20, 2000–2015.
30. Dreyse, P., Isaacs, M., Calfumán, K., Cáceres, C., Aliaga, A., Aguirre, M. J., Villagra, D., *Electrochim. Acta*, **2011**, 56, 5230–5237.
31. González-Cabello, A., Vázquez, P., Torres, T., Guldi, D. M., *J. Org. Chem*., **2003**, 68, 8635–8642.
32. González-Rodríguez, D., Claessens, C. G., Torres, T., Liu, S., Echegoyen, L., Vila, N., Nonell, S., *Chem. Eur. J.*, **2005**, 11, 3881–3893.
33. Doyle, J. J., Ballesteros, B., Torre, G., Torres, T., Blau, W. J., *Chem. Phys. Lett.*, **2006**, 428, 307–311.

34. Ballesteros, B., Torre, G., Torres, T., Hug, G. L., Rahmanc, G. M. A., Guldi, D. M., *Tetrahedron lett*., **2006**, 62, 2097–2101.
35. Rodríguez-Morgade, M. S., Plonska-Brzezinska, M. E., Athans, A. J., Carbonell, E., Miguel, G., Guldi, D. M., Echegoyen, L., Torres, T., *J. Am. Chem. Soc*., **2009**, 131, 10484–10496.
36. McEvoy, J. P., Brudvig, G. W., *Chem. Rev*., **2006**, 106, 4455–4483.
37. Scholes, G. D., Fleming, G. R., Olaya-Castro, A., Grondelle, R., *Nat. Chem.*, **2011**, 3, 763–774.
38. O'Regan, B., Grätzel, M., *Nature* (London), **1991**, 353, 737–739.
39. Meyer, G., *J. Inorg. Chem*., **2005**, 44, 6852–6854.
40. Grätzel, M., *Inorg. Chem*., **2005**, 44, 6841–6851.
41. Wasielewski, M. R., *Acc. Chem. Res*., **2009**, 42, 1910–1921.
42. Fukuzumi, S., *Phys. Chem. Chem. Phys*., **2008**, 10, 2283–2297.
43. Flamigni, L., Collin, J. P., Sauvage, J. P., *J. Acc. Chem. Res*., **2008**, 41, 857–871.
44. Gust, D., Moore, T. A., Moore, A. L., *Acc. Chem. Res*., **2009**, 42, 1890–1898.
45. Berber, G., Cammidge, A. N., Chambrier, I., Cook, M. J., Hough, P. W., *Tetrahedron Lett.*, **2003**, 44, 5527–5529.
46. Torre, G., Bottari, G., Sekita, M., Hausmann, A., Guldi, D. M., Torres, T., *Chem. Soc. Rev*., **2013**, 42, 8049–8105.
47. Frischmann, P. D., Mahata, K., Würthner, F., *Chem. Soc. Rev*., **2013**, 42, 1847–1870.
48. Jacobs, R., Stranius, K., Maligaspe, E., Lemmetyinen, H., Tkachenko, N. V., Zandler, M. E., D'Souza, F., *Inorg. Chem.*, **2012**, 51, 3656–3665.
49. Cammidge, A. N., Berber, G., Chambrier, I., Hough, P. W., Cook, M. J., *Tetrahedron*, **2005**, 61, 4067–4074.
50. D'Souza, F., Ito, O., *Chem. Commun*., **2009**, 146, 4913–4928.
51. Fischer, M. K. R., López-Duarte, I., Wienk, M. M., Martínez-Díaz, M. V., Janssen, R. A. J., Bäuerle, P., Torres, T., *J. Am. Chem. Soc*., **2009**, 131, 8669–8676.
52. Gomes, M. C., Woranovicz-Barreira, S. M., Faustino, M. A. F., Fernandes, R., Neves, M. G. P. M. S., Tomé, A. C., Gomes, N. C. M., Almeida, A., Cavaleiro, J. A. S., Cunha, Â., Tomé, J. P. C., *Photochem. Photobiol. Sci*., **2011**, 10, 1735–1743.

53. McKeown, N. B., *Phthalocyanine Materials*: *Synthesis, Structure and Function*, Cambridge University Press: Cambridge, 1998.
54. Rihter, B. D., Kenney, M. E., Ford, W. E., Rodgers, M. A. J., *J. Am. Chem. Soc*., **1990**, 112, 8064–8070.
55. Abrams, M. J., *Platinum Metals Rev.*, **1995**, 39, 14–18.
56. Iengo, E., Pantos, G. D., Sanders, J. K. M., Orlandi, M., Chiorboli, C., Fracasso, S., Scandola, F., *Chem. Sci*., **2011**, 2, 676–685.
57. Elliott, P. I. P., *Annu. Rep. Prog. Chem. Sect. A*, **2010**, 106, 526–552.
58. Rothemund, P., *J. Am. Chem. Soc*., **1935**, 57, 2010–2011.
59. Rothemund, P., *J. Am. Chem. Soc*., **1939**, 61, 2912–2915.
60. Gonsalves, A. M. d'A. R., Varejão, J. M. T. B., Pereira, M. M., *J. Heterocyclic Chem.*, **1991**, 28, 635–640.
61. Nascimento, B. F. O., Pineiro, M., Gonsalves, A. M. d'A. R., Silva, M. R., Beja, A. M., Paixão, J. A., *J. Porphyrins Phthalocyanines*, **2007**, 11, 77–84.
62. De Paula, R., Faustino, M. A. F., Pinto, D. C. G. A., Neves, M. G. P. M. S., Cavaleiro, J. A. S., *J. Heterocyclic Chem.*, **2008**, 45, 453–459.
63. Adler, A., Longo, F., Kampus, F., Kim, J., *J. Inorg. Nucl. Chem*., **1970**, 32, 2443–2445.
64. Chen, X., Hui, L., Foster, D. A., Drain, C. M., *Biochemistry*, **2004**, 43, 10918–10929.
65. Samaroo, D., Soll, C. E., Todaro, L. J., Drain, C. M., *Org. Lett*., **2006**, 8, 4985–4988.
66. Pasetto, P., Chen, X., Drain, C. M., Franck, R. W., *Chem. Commun*., **2001**, 81–82.
67. Costa, J. I. T., Tomé, A. C., Neves, M. G. P. M. S., Cavaleiro, J. A. S., *J. Porphyrins Phthalocyanines*, **2011**, 15, 1116–1133.
68. Battioni, P., Brigaud, O., Desvaux, H., Mansuy, D., Traylor, T. G., *Tetrahedron Lett*., **1991**, 32, 2893–2896.
69. Samaroo, D., Vinodu, M., Chen, X., Drain, C. M., *J. Comb. Chem*., **2007**, 9, 998–1011.
70. Guldi, D. M., Imahori, H., Tamaki, K., Kashiwagi, Y., Yamada, H., Sakata, Y., Fukuzumi, S., *J. Phys. Chem. A*, **2004**, 108, 541–548.
71. Schlundt, S., Kuzmanich, G., Spänig, F., Rojas, G. M., Kovacs, C., Garcia-Garibay, M. A., Guldi, D. M., Hirsch, A., *Chem. Eur. J*., **2009**, 15, 12223–12233.

Chapter 5

Inverted pyridinium phthalocyanines as PDI agents against pathogenic bacteria

5.1 Overview

Phthalocyanines (Pcs),[1,2] and the corresponding naphthalocyanine analogues,[3,4] are well-known aromatic compounds, which have being intensively studied for different applications due to their excellent physicochemical properties (absorb light in the red and near-infrared regions of the electromagnetic spectrum, 600-800 nm).[5-7] In particular, Pc derivatives have been exploited as photosensitizers (PSs) for photodynamic therapy (PDT), evidencing a high potential in cancer treatment[8-17] and in the photodynamic inactivation (PDI) of microorganisms in infectious diseases[18-23] and/or in contaminated environments[5,24,25] All these applications are based on cell death induced by reactive oxygen species (ROS), mainly singlet oxygen ($^1O_2$), generated by the combined action of visible light, molecular oxygen and a PS.[26-28] Since the chemical structure is a key factor in the physicochemical properties of the PSs, different approaches have been used to introduce particular functionalities on the phthalocyanine structures[29] in order to obtain certain physicochemical features, namely desired levels of hydrophobicity or hydrophilicity. The molecular structure of unsubstituted phthalocyanines can be modified by the incorporation of substituents in the peripheral positions of the macrocycle to improve their amphiphilicity,[10,30] or by metallation of the Pc core with different metal ions in the macrocycle.[31] Pcs modifications are an important factor for an efficient generation of ROS. In fact, the introduction of diamagnetic metal ions (Zn, Si, Al, Ga or In) into the cavity of the Pc core can results in an enhancement of triplet state parameters (triplet quantum yields and lifetimes) and $^1O_2$ quantum yields.[32-34] The addition of axial ligands in coordinative positions of such metal centres can also improve the efficiency of these compounds as PSs.[35-42] These modifications can unequivocally modulate the photophysical and photochemical characteristics of Pc derivatives and affect their interaction with cells, providing different photobiological effects.[5,6,43]

The emergent antibiotic resistance of pathogenic bacteria has prompted several research groups, namely our, to explore the principle of PDT as an alternative antibacterial therapy. In this way, it is recognised that some metallated Pcs upon photoexcitation with light, photoinactivate efficiently different pathogenic microorganisms and could be an excellent approach to inactivate bacteria.[18,44,45] The two photodynamic mechanisms that can justify the cell death through the interaction of light-excited PS with the cellular substrate are known as type I (initial formation of radicals by direct reaction of the excited

PS with cellular substrates, followed by reaction with molecular oxygen) and type II (interaction of the excited PS with molecular oxygen originates singlet oxygen).[46,47] The ability of Pcs to interact with bacteria and their capability to generate ROS has been related with the cell death mediated by the concerted action of cellular oxidative stress.[48]

It is well established that in general, for an efficient photoinactivation of Gram-negative bacteria, it is required the use of photoactive cationic PSs.[18,49,50,51] The positive charged PS derivatives can interact electrostatically with the negative charged parts of the outer wall (lipoproteins, lipopolysaccharides), which simplifies the binding and relative entrance, mainly in the Gram-negative bacteria.[52] The presence of cationic moieties promotes a strait electrostatic interaction with negatively charged sites at the outer membrane surface of the Gram-negative bacteria, increasing the efficiency of the photodynamic activity. On the other hand, inactivation of Gram-positive bacteria is ensured by neutral, anionic and cationic PSs which promptly cross the relatively porous cell wall.[52,53] However, the set of damages involved in the bacterial PDI is not fully clarified yet.

As already highlighted, Gram-negative bacteria are resistant to the photodynamic action of mostly neutral and anionic PSs;[54] so the presence of positively charged functional groups in the Pc dyes allows an extensive photoinduced killing of these pathogenic microorganisms.[18] In that way, considering that PDI of microorganisms can be a promising methodology for the treatment of infectious diseases[18-23] or contaminated media, and following our undoubtedly interest in this subject, we describe here the relationship between the chemical structure of innovative inverted pyridinium Pc derivatives and their efficiency as PSs in the inactivation of microbial strains. For that, a bioluminescent *Escherichia coli* (*E. coli*) strain was used as a model of Gram-negative pathogenic bacteria.

Knowing that 4-hydroxypyridine exists under many conditions preferably as pyridine, that results from a tautomerization of the enolic phenol form, previous results showed that the tetra-substitution of **$TPPF_{20}$** results in a 4-pyridinone derivate.[55] So, in this chapter, it is described the synthesis and characterization of pyridinone and pyridinium Pc derivatives **5.6**-**5.9** (Schemes 5.2 and 5.3). It is also reported the photophysical, photochemical and photobiological properties of these inverted pyridinium Pcs **5.8** and **5.9** and compared then with the thiopyridiniumphthalocyanine ones, previously reported by our research group.[18] The later ones already had exhibited a number of interesting features for a prospective phototherapeutic application and a notable phototoxicity against bacteria.

5.2 Syntheses of pyridinone phthalonitrile and phthalocyanine derivatives

Considering the remarkable photochemical and photophysical properties of Pc derivatives and the excellent features of pyridinium groups to act as PDI drugs, it was envisaged a simple access to obtain the new amphiphilic pyridinium Pc conjugates **5.8** and **5.9** (Scheme 5.3). The synthetic strategy required the previous preparation of the new pyridinone phthalonitrile derivatives **5.4** and **5.5** (Scheme 5.1) and the corresponding pyridinone Pc dyes **5.6** and **5.7** (Scheme 5.2).

The phthalonitriles **5.4** and **5.5** were obtained from commercially available reagents, 4-hydroxypyridine (**5.1**) and the adequate 4-fluorophthalonitrile (**5.2**) and 4,5-difluorophthalonitrile (**5.3**) (Scheme 5.1). Both reactions were performed at 80 ºC in dry DMF (3 mL) under nitrogen atmosphere. After 5 h, the total consumption of the starting fluorophthalonitriles was confirmed by analytical TLC. The products were then directly purified by column chromatography (silica gel) using a mixture of $CHCl_3$/MeOH as eluent. After precipitation with $CHCl_3$, the desired products were filtered and washed with $CHCl_3$. Recrystallization from MeOH/$CHCl_3$ gave products **5.4** and **5.5,** as light yellow solids, with yields above 92%. Both products were characterized by ^{1}H, COSY 2D ^{1}H-^{1}H, ^{13}C NMR, and mass spectroscopy (MS) using electrospray (ESI) in positive mode.

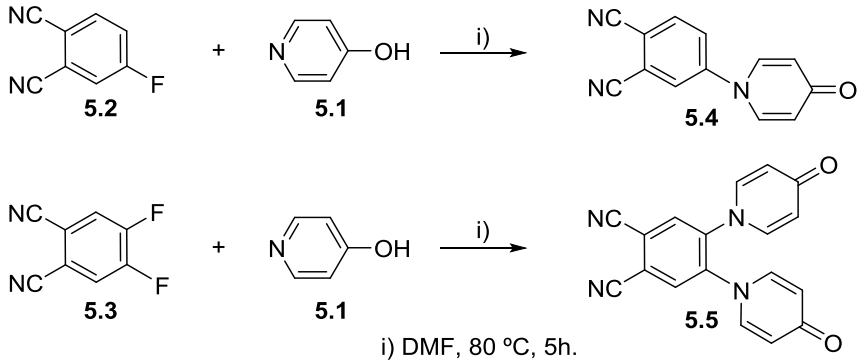

Scheme 5.1

In particular, the ^{1}H NMR spectrum of the phthalonitrile **5.4** (Figure 5.1), show the resonances of all protons at δ 6.31, 8.14–8.17, 8.33 and 8.50 ppm. The doublet and multiplet at δ 6.31 and 8.14–8.17 ppm were attributed respectively to the protons H^e and $H^{c,d}$ (confirmed by the COSY 2D ^{1}H-^{1}H spectrum, Figure 5.2). The resonance of H^d at lower fields comparatively to H^e can be justified by the electron-withdrawing character of

the carbonyl group and the nitrogen atom. The 2 protons of the phthalonitrile moiety H^a and H^b appear as two doublets respectively at δ 8.33 and 8.50 ppm. The structure **5.4** was also confirmed by ESI-MS spectrum that showed the presence of the molecular ion peak $[M+H]^+$ at *m/z* 222.

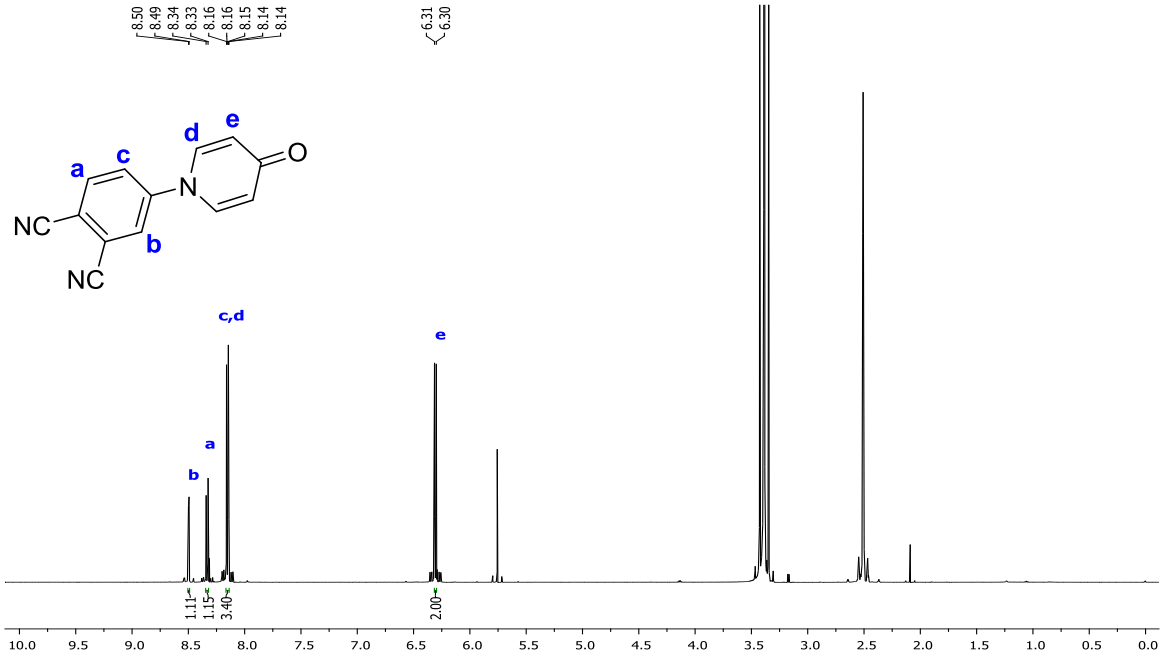

Figure 5.1 ^{1}H NMR spectrum of compound **5.4** in DMSO-d_6.

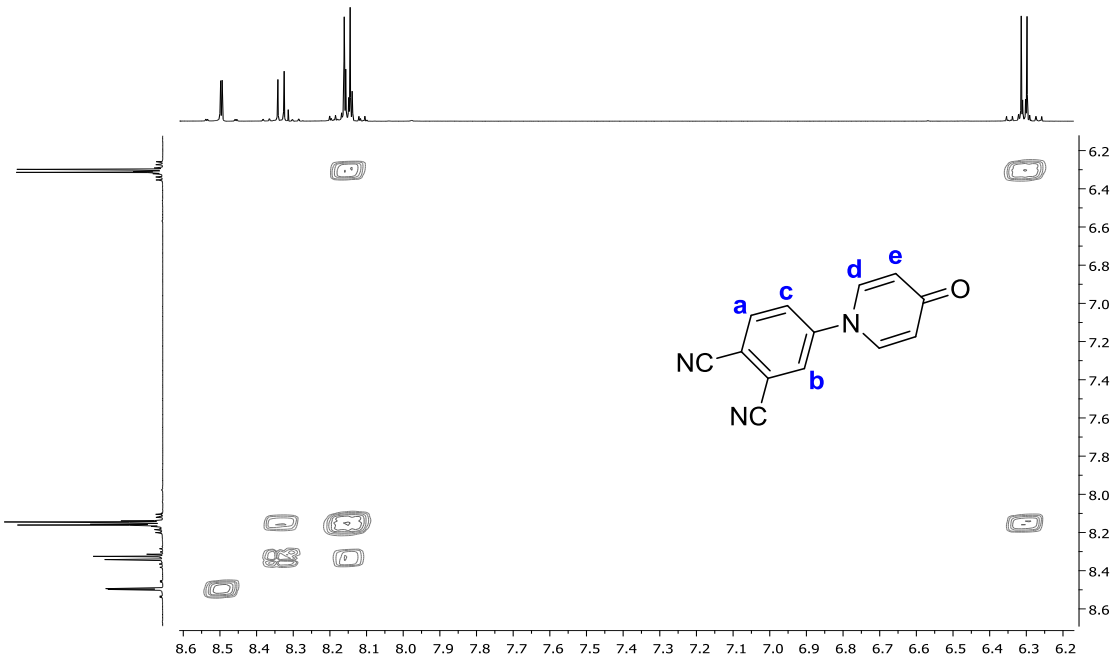

Figure 5.2 COSY 2D ^{1}H-^{1}H NMR spectrum of compound **5.4** in DMSO-d_6.

The ^{1}H NMR spectrum of the pyridinone phthalonitrile derivative **5.5** (Figure 5.3) show the resonances of the 10 protons at δ 6.21, 7.64 and 8.70 ppm. The two doublets at δ

6.21 and 7.64 ppm were attributed to the 8 pyridinone protons H^c and H^b (see also the COSY 2D ^{1}H-^{1}H spectrum, in Figure 5.4). The two phthalonitrile protons H^a appear at lower fields as a singlet at 8.70 ppm. The structure of **5.5** was also confirmed by ESI-MS spectrum that showed the presence of protonated molecular ion peak $[M+H]^+$ at *m/z* 315.

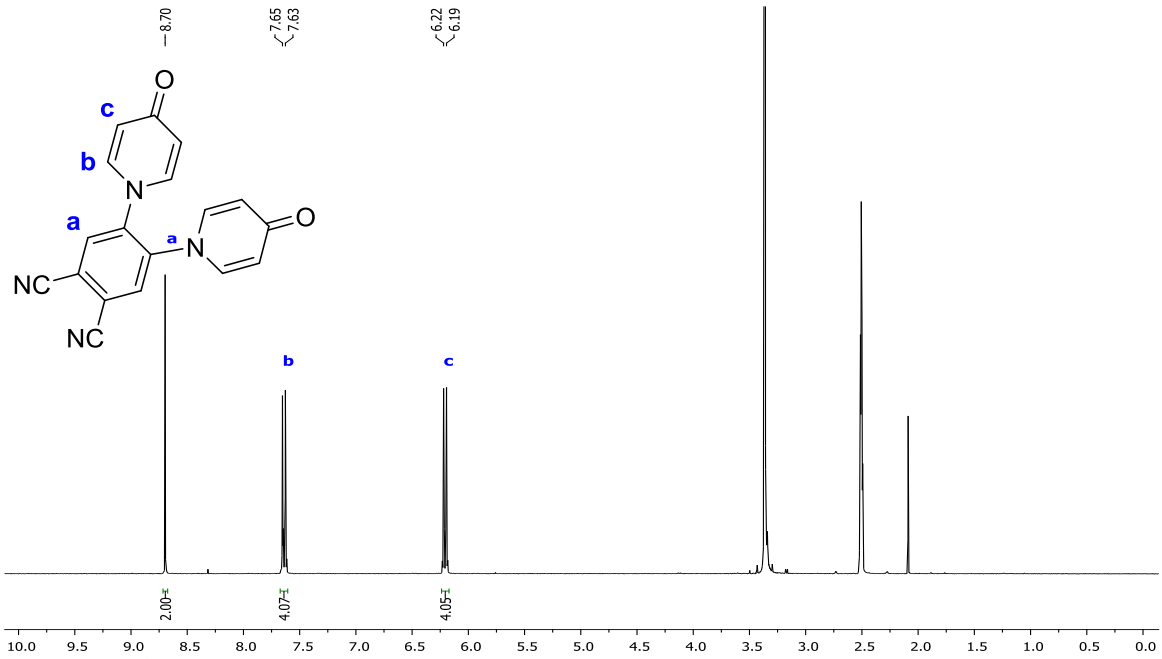

Figure 5.3 ^{1}H NMR spectrum of compound **5.5** in DMSO-d_6.

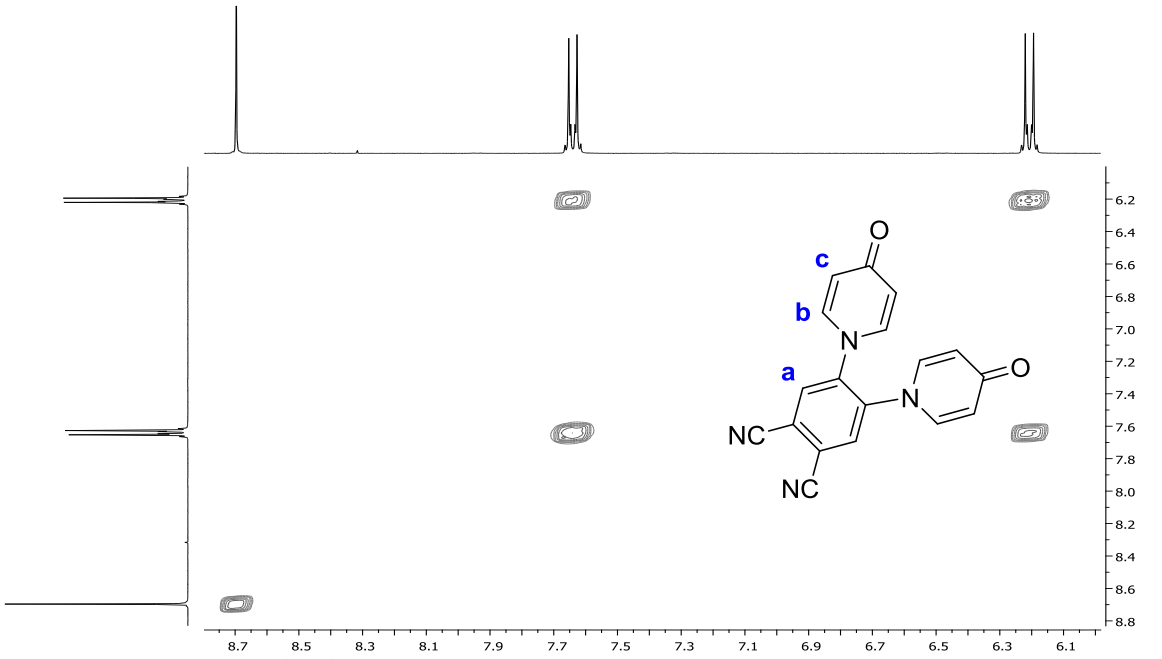

Figure 5.4 COSY 2D ^{1}H-^{1}H NMR spectrum of compound **5.5** in DMSO-d_6.

The pyridinone phthalocyanines **5.6** and **5.7** were obtained by tetramerization of the adequate pyridinone phthalonitrile derivatives **5.4** and **5.5**, respectively, in the presence of

anhydrous zinc chloride (Scheme 5.2). Both reactions were performed in 1-pentanol at reflux under N_2 atmosphere. After 16 h (overnight), the reaction mixtures were allowed to cool down and then chloroform was added. The obtained crude solids were purified by molecular exclusion column chromatography (Bio-beadsTM S-X1) using pure DMF as eluent. After the elimination of the solvent, the desired products were washed several times with chloroform and dried under vacuum. Compounds **5.6** and **5.7** were isolated as dark green solids with yields above 58%.

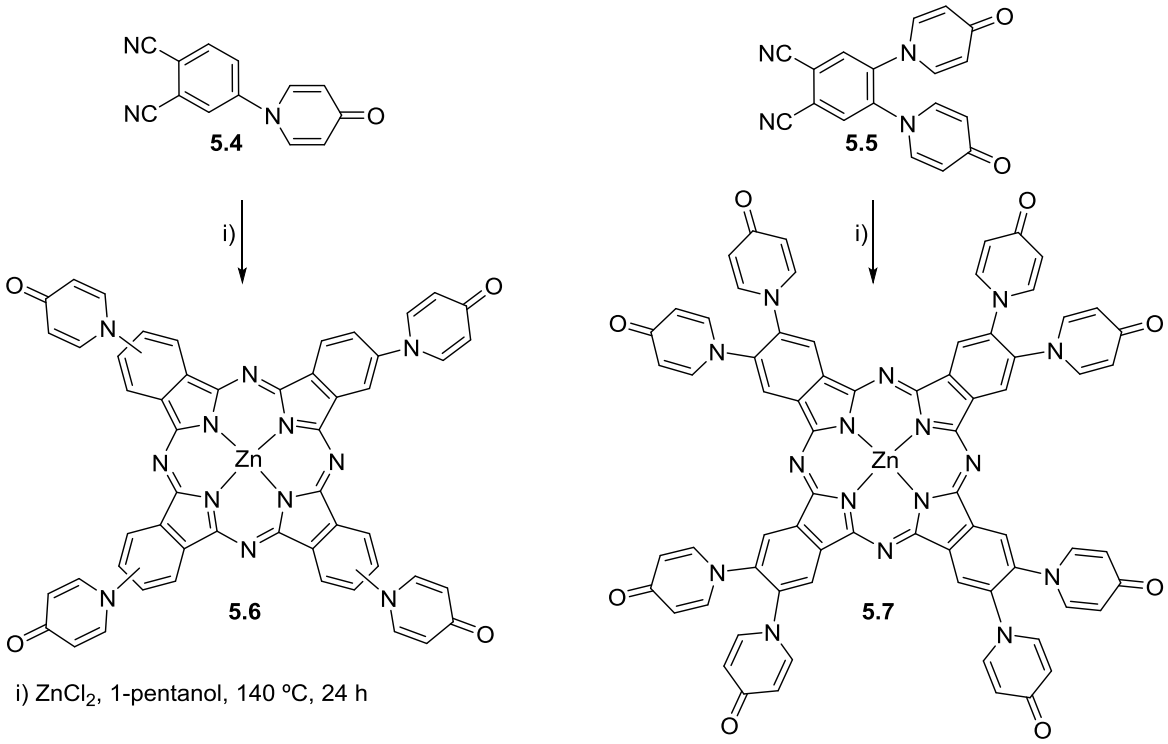

Scheme 5.2

The ^{1}H NMR spectrum of **5.6** (Figure 5.5) showed all proton resonances as multiplets due to the obtained mixture of regioisomer compounds and the corresponding attribution was also confirmed by COSY ^{1}H-^{1}H NMR. The signals between δ 6.58–6.66 and 8.54-8.58 ppm correspond to the resonances 16 pyridinone protons H^e and H^d, respectively. The 8 α-protons $H^{a,b}$ are distributed at lower fields as a multiplet at δ 8.96–9.05 ppm, and the resonance of the 4 β-protons H^c are the ones between δ 8.21 and 8.24 ppm. The structure of **5.6** was also confirmed by the ESI-HRMS, which shows the protonated molecular ion peak $[M+H]^+$ at *m/z* 949.

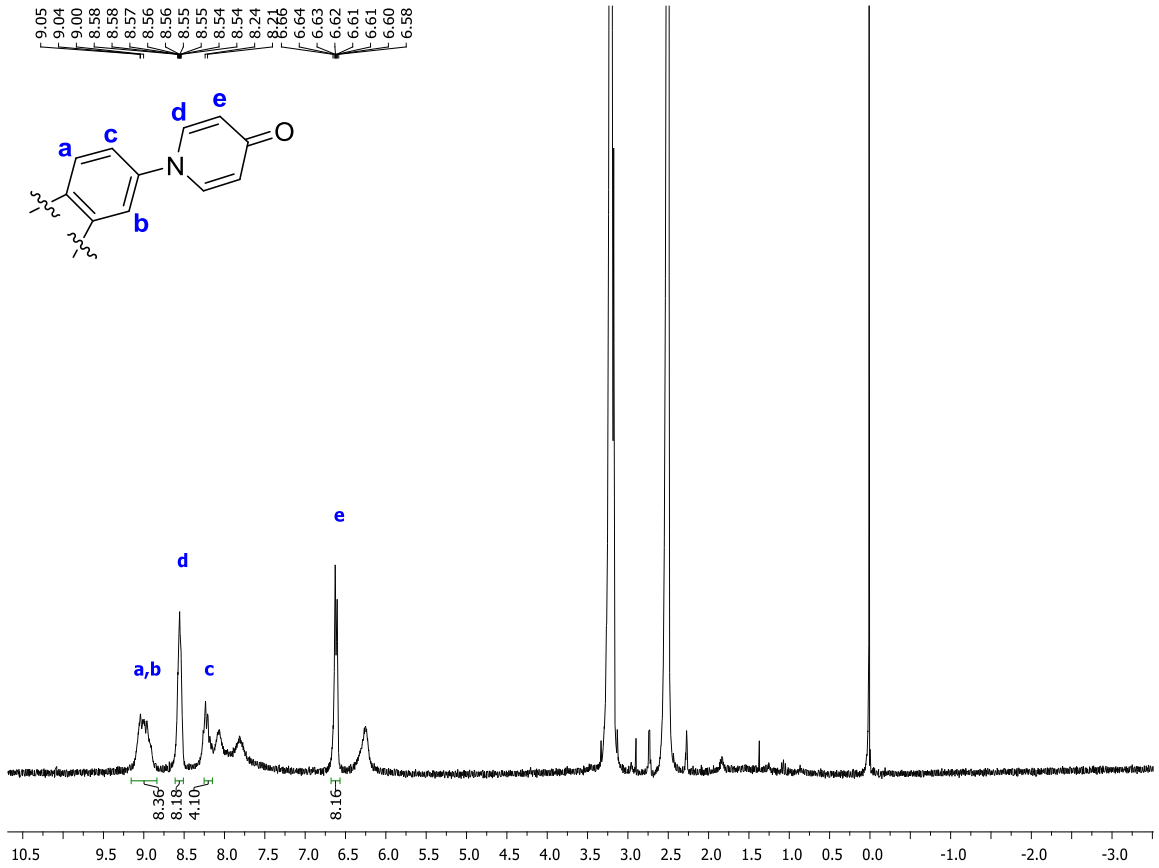

Figure 5.5 ^{1}H NMR spectrum of compound **5.6** (with some impurities) in DMSO-d_6.

Considering the characterization of the Pc **5.7**, the ^{1}H NMR spectrum (Figure 5.6) show the resonances of the 32 pyridinone-protons H^{c} and H^{b} as two doublets (each integrating for 16 protons) at δ 6.36 and 8.13 ppm. Interesting is a higher field shift of the pyridinone proton resonances H^{c} and H^{b} comparatively with the analogous ones of the tetra-substituted Pc **5.6** (δ 6.58–6.66 and 8.54–8.58 ppm, Figure 5.5), confirming the undoubtable resonance influence of the eight pyridinone groups on the Pc β-positions. Moreover, it was observed a singlet at δ 9.63 ppm that was attributed to the 8 α-protons H^{a} of the Pc ring, evidencing a single symmetric compound when compared with the analogue signal of the tetra-substituted **5.6**. The structure of **5.7** was also confirmed by ESI-HRMS, showing in the spectrum the protonated molecular ion peak $[M+H]^{+}$ at *m/z* 1321.

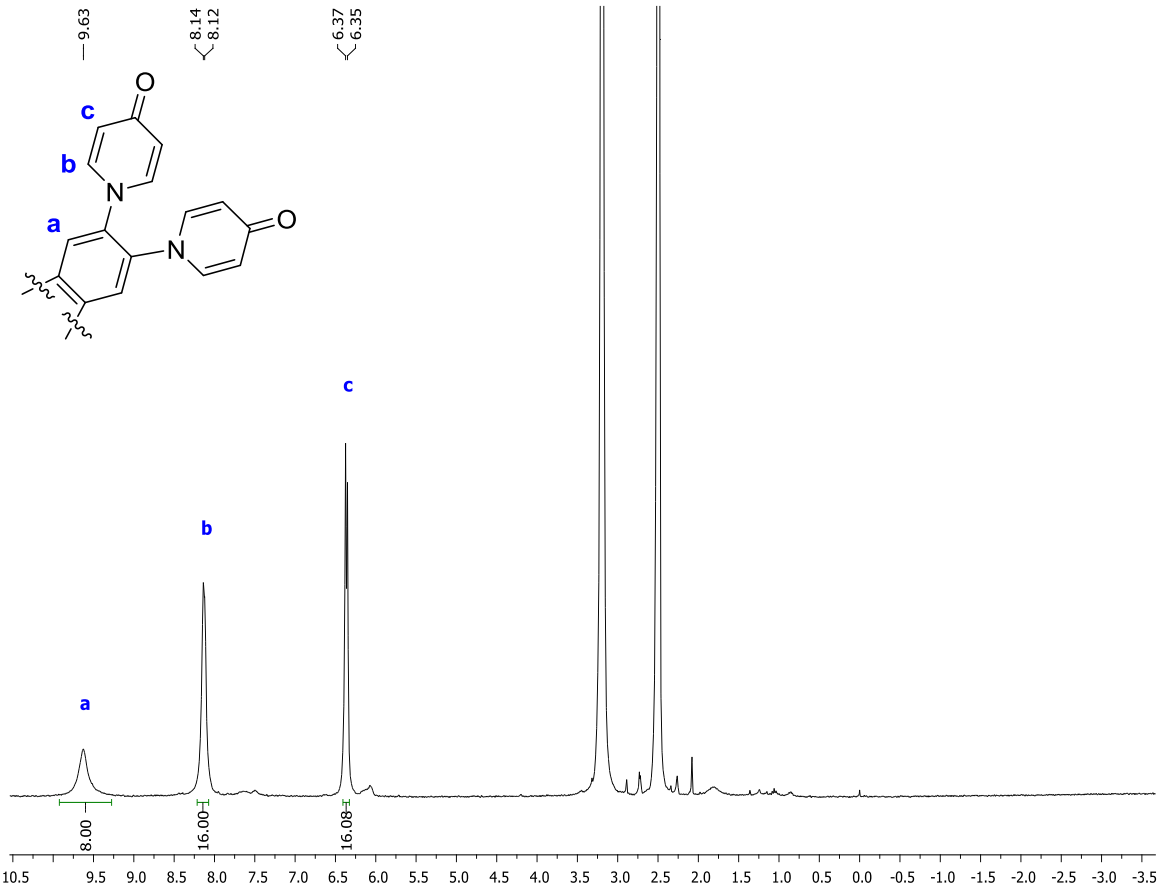

Figure 5.6 ^{1}H NMR spectrum of compound **5.7** in DMSO-d_6.

5.3 Synthesis of inverted pyridinium phthalocyanines

The inverted pyridinium Pcs **5.8** and **5.9** were obtained by cationization of the corresponding pyridinone phthalocyanines **5.6** and **5.7** using the experimental conditions shown in (Scheme 5.3). The reactions were performed by adding to a suspension of the pyridinone phthalocyanines **5.6** and **5.7** in dry DMF a large excess of dimethyl sulphate. Then, the reaction mixtures were kept under stirring overnight at 80 ºC in a sealed pressure flask. After this period the mixtures were cooled down and precipitated in acetone/dichloromethane. The residues were filtered, taken up in MeOH/H_2O (2:1) and reprecipitated by addition of dichloromethane. The desired products were filtered, washed with dichloromethane and dried under vacuum. The products **5.8** and **5.9** (Scheme 5.3) were obtained as dark green solids with yields above 85%.

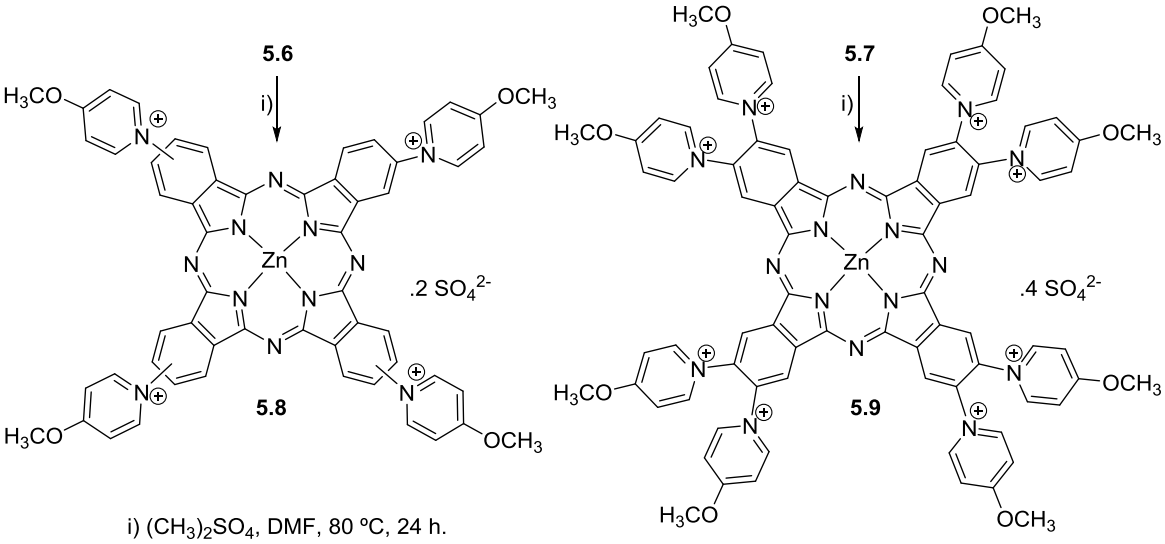

Scheme 5.3

The ^{1}H NMR spectrum of **5.8** (Figure 5.7), using also COSY ^{1}H-^{1}H NMR, present all proton resonances as multiplets at δ 4.29–4.54, 6.69–6.75, 7.99–8.15, 8.62–8.70, and 9.62–9.73 ppm corresponding to the aliphatic protons H^{f}, pyridinium protons H^{e}, β-aromatic proton atoms β-H^{c}, pyridinium protons H^{d}, α-aromatic proton H^{a,b}, respectively.

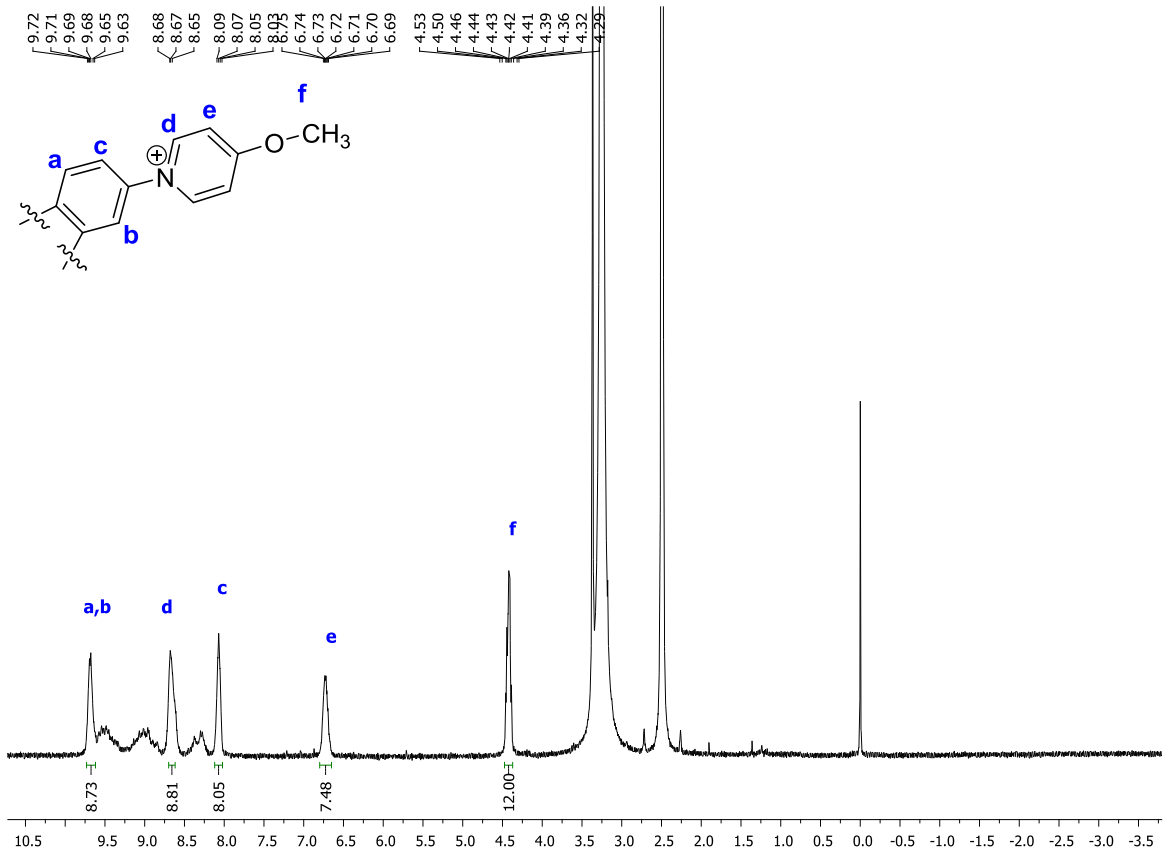

Figure 5.7 ^{1}H NMR spectrum of compound **5.8** (with some impurities) in DMSO-d_6.

As expected, a shift of the pyridinium protons H^e and H^d to lower fields was observed when compared with the analogous proton resonances of the corresponding noncationic tetra-substituted Pc **5.6** (δ 6.17–6.36 and 8.54-8.58 ppm). In case of the α-aromatic proton resonances $H^{a,b}$ of Pc **5.8** also occur a lower field shift. In this way, the presence of the methoxy group changes considerably the electronic distribution of the phthalocyanine **5.8**. The structure of **5.8** was also confirmed by MALDI-MS, showing in the spectrum the molecular ion peak *m/*z 963 $[M\text{-}CH_3]^{+\cdot}$.

The ^{1}H NMR spectrum of **5.9** (Figure 5.8) presents two singlets at δ 4.31 and 10.12 ppm corresponding to the resonances of the 24 aliphatic protons H^d and of the 8 α-aromatic protons H^a, respectively. Moreover, the resonance of methoxypyridinium protons H^c and H^b appears as two doublets at δ 7.93 and 9.43 ppm, respectively. The presence of the methoxy groups and the aromatic structure of the derivative **5.9** induces entirely the methoxypyridium proton resonances to lower fields when compared with the proton resonances of the analogous signals of the corresponding noncationic Pc **5.7** (δ 6.36 and 8.13 ppm). The structure of **5.9** was confirmed by MALDI-MS, showing in their spectrum the molecular ion peak at *m/*z 1335 $[M\text{-}7CH_3]^{+\cdot}$.

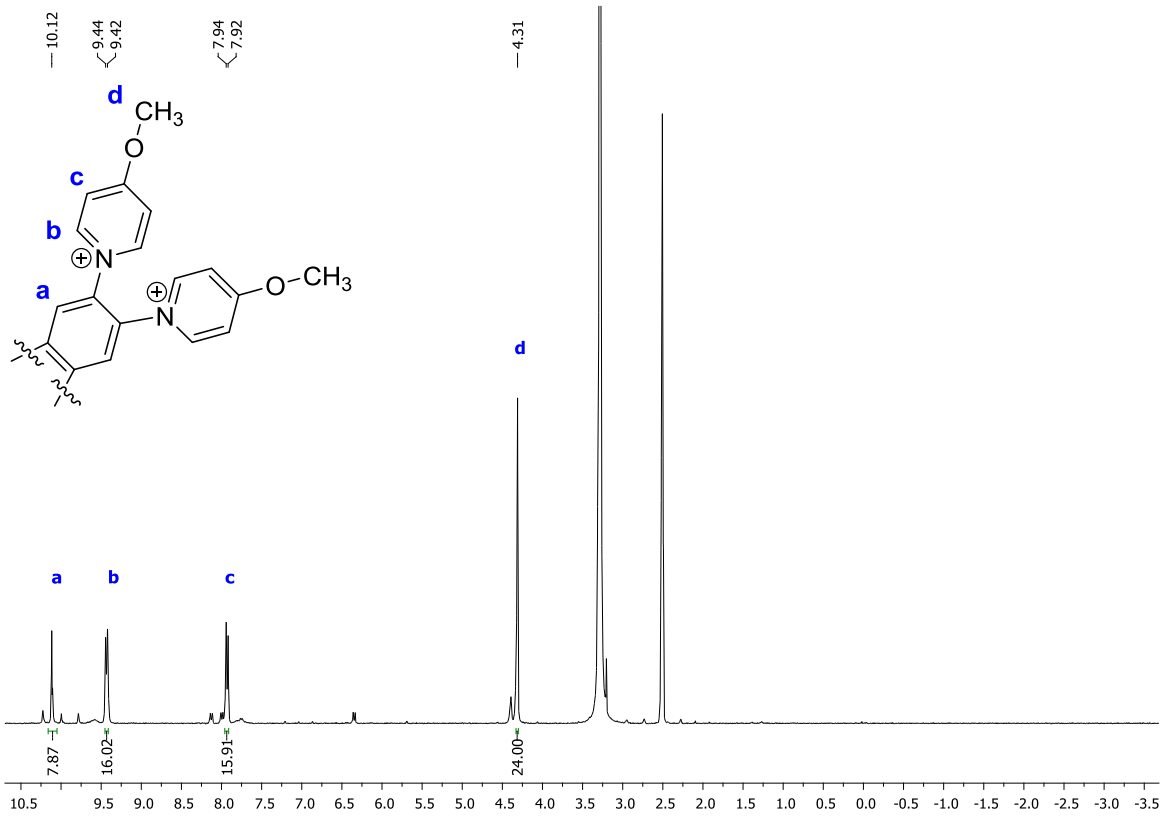

Figure 5.8 ^{1}H NMR spectrum of compound **5.9** in DMSO-d_6.

5.4 Optical properties

Phthalocyanine dyes are well-known optical absorbers, with high chemical stability and tailorability, and possess unequivocally strong absorption bands in the UV-Vis region.[56] The characteristic absorption features of metallic phthalocyanines are seen for Pcs **5.6**-**5.9** in the form of a rather weak absorption Soret-band in the region of 300 – 425 nm and a strong Q-band maximum at 680 – 684 nm (Figure 5.9). Figure 5.9 also shows the fluorescence spectra of Pc derivatives **5.6**-**5.9** upon excitation at 400 nm in DMF. All the fluorescence spectra show a maximum at 688 nm and the main photophysical features – Q-band wavelengths, molar extinction coefficients (ε), fluorescence emission wavelength ($\lambda_{emission}$), Stokes shift and fluorescence quantum yields (Φ_F) – are gathered in Table 5.1. The values of the quantum yields, which vary between 0.05-0.14, are slight lower than the one of **ZnPc** (0.3) used as reference.

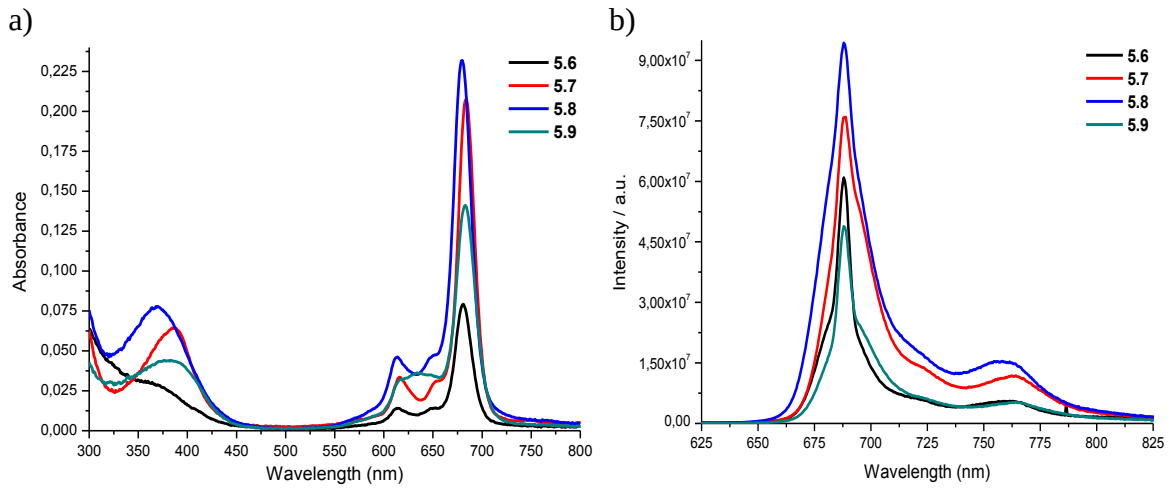

Figure 5.9 a) absorption and b) emission spectra of Pc derivatives **5.6**-**5.9** (C = 1 × 10^{-6} M) in DMF.

Table 5.1 Photophysical properties of phthalocyanine derivatives **5.6**-**5.9**.

Compound	Q-band λ_{max} (nm)	log ε	$\lambda_{emission}$ (nm)[a)]	Stokes shift (nm)	Φ_F[b)]
5.6	681	4.90	688	7	0,10
5.7	684	5.31	688	4	0,18
5.8	680	5.36	688	8	0,24
5.9	683	4.56	688	5	0,09

[a)]excited at 400 nm; [b)]using **ZnPc** in DMF as reference (Φ_F = 0.30)[65].

5.5 Inverted pyridinium phthalocyanine derivatives as PDI agents*

Solubility

UV-Vis absorption spectra acquire in phosphate buffered saline (PBS) and DMSO are displayed in Figure 5.10. Both cationic tetra-Pc **5.8** and octa-Pc **5.9** showed typical absorption spectra in DMSO, with two well-defined Q-bands at 605 and 677 nm. However, a visible change is observed in the UV-Vis spectra when PBS was used as solvent. In case of PS **5.8**, the two Q-bands became a broad brand with absorbance maximum at 610 nm and an intense Soret-band, signal of high aggregation in PBS. The PS **5.9** shows slight blue shift of both bands but still sharp, evidence of good solubility in PBS.

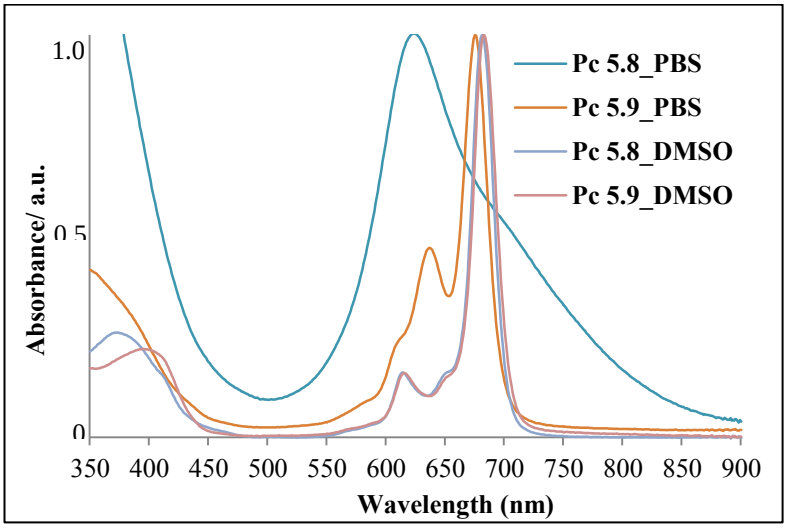

Figure 5.10 Normalized UV–Vis absorption spectra of phthalocyanines **5.8** and **5.9** in DMSO and PBS ($\times 10^{-6}$ M).

Solubility studies relying on Beer-Lambert law, determined in DMSO and PBS (Figure 5.11), did not show aggregation behaviour for concentrations bellow 20 and 5 μM, respectively. However, **5.8** exhibited visible signs of aggregation after being at the same conditions as in the pre-incubation period used in PDI assays (15 min stirring in PBS and covered with aluminium foil), Figure 5.12.

*These compounds were tested by **Andreína Sousa** and **Clara Gomes**, who kindly provided their results for a comprehensive analysis of the photophysical and photodynamic activity values of the Pc derivatives.

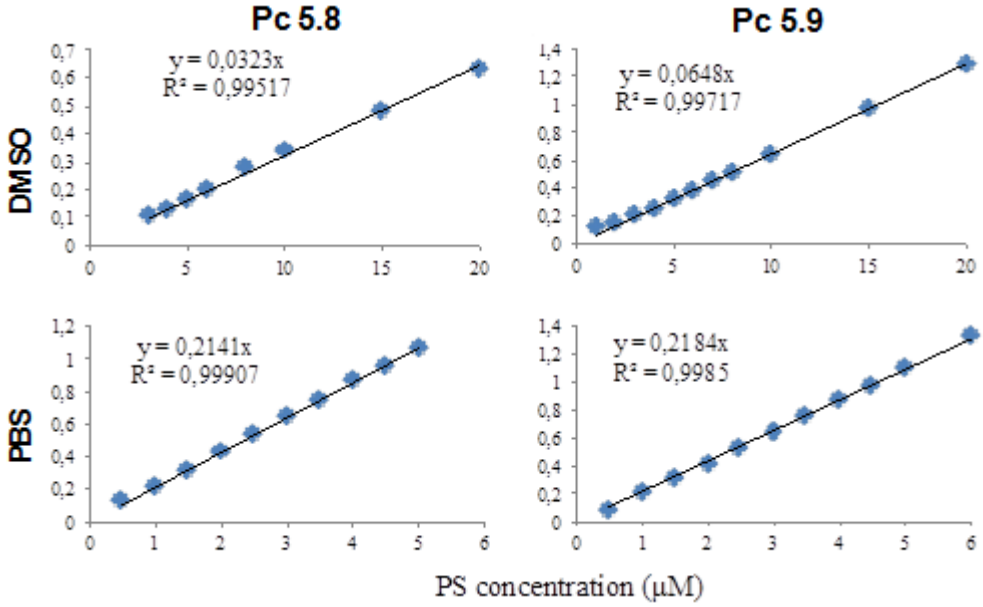

Figure 5.11 Linear regression graphics of Pcs **5.8** and **5.9** plotted the Q-band absorbance *vs* the concentrations in PBS and DMSO.

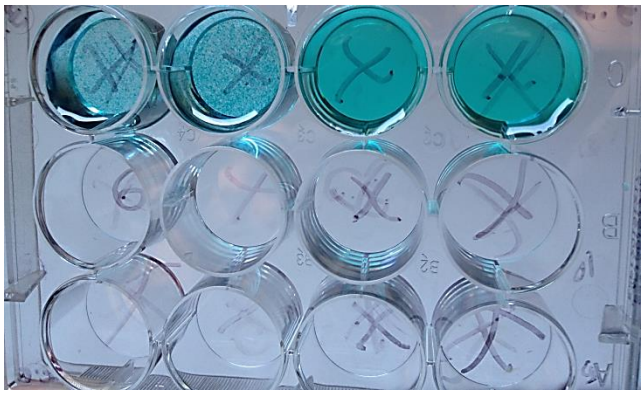

Figure 5.12 12-well plate prepared for PDI studies with 20 μM of **5.8**, two left wells, and **5.9**, two right wells, after 15 min of pre-incubation in the dark, under gentle shaking conditions.

Ability to generate $^1O_2$

The photodegradation of 1,3-diphenylisobenzofuran (DPBF) allowed qualitative evaluation of the ability of these cationic pyridinone (**5.8** and **5.9**) and thiopyridiniumphthalocyanines (**3.1** and **3.2**) to generate singlet oxygen ($^1O_2$). According to the results (Figure 5.13), both pyridinium Pcs **5.8** and **5.9** and thiopyridiniumphthalocyanine **3.1** proved to be efficient $^1O_2$ generators (92, 37 and 76% of DPBF decay, respectively) in DMF/H_2O (9:1). In turn, Pc **3.2**, under the same

experimental conditions, only presented 9% of DPBF decay, being the less efficient one at least in this mixture of solvents.

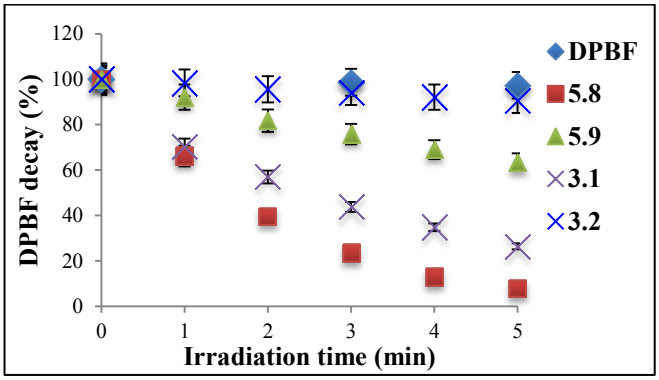

Figure 5.13 Time-dependent decomposition of DPBF (50 μM) photosensitized by Pc **5.8**, **5.9**, **3.1** and **3.2**, in DMF/H_2O (9:1) upon irradiation with a LED array system (640 nm ± 20 nm) at a fluence rate of 6.0 mW.cm^{-2} with or without PS (0.5 μM).

5.5.1 Photodynamic inactivation of bioluminescent *Escherichia coli*

The inactivation kinetics of *E. coli* during the irradiation assays with artificial white and red lights, in the presence of PSs **5.8**, **5.9**, **3.1** and **3.2** are represented in Figure 5.14. Two different controls, light and dark control (L.C. and D.C., respectively) were performed, in order to ensure that the obtained PDI results were exclusively due to the PS effect. Both controls showed that the viability of bioluminescent *E. coli* are not affected neither by irradiation itself (L.C.), nor by any of the PSs tested in the dark (D.C.) using the same concentration studied. Looking to white light condition (Figure 5.14a) it is clear that PS **5.9**, **3.1** and **3.2** produced significantly higher inactivation rate (2.8, 2.3 and 2.5 log of inactivation, respectively; ANOVA, $p < 0.05$) than PS **5.8** (0.8 log of inactivation; ANOVA, $p > 0.05$), after 20 min of irradiation with white light. Concerning to red light (Figure 5.14b), three distinct profiles were observed. Once again, PS **5.8** showed lower inactivation results (0.9 log of reduction; ANOVA, $p < 0.05$) followed by PS **3.2** (2.3 log of reduction) (ANOVA, $p < 0.05$). With respect of PSs **5.9** and **3.1**, their photoinactivation profile is very similar during the initial 15 min of irradiation (3.2 log of reduction). However, during the last 5 min of irradiation PS **3.1** inactivation stagnate, while PS **5.9** photoinactivation increases to 4.3 log of reduction. Comparing the PDI efficiency of both light conditions, red one presents significantly better photoinactivation results for PS **5.9**

and **3.1** (ANOVA, $p < 0.05$), while for PS **3.2** the wavelength of the irradiation light seems to have no effect in terms of bacterial photoinactivation.

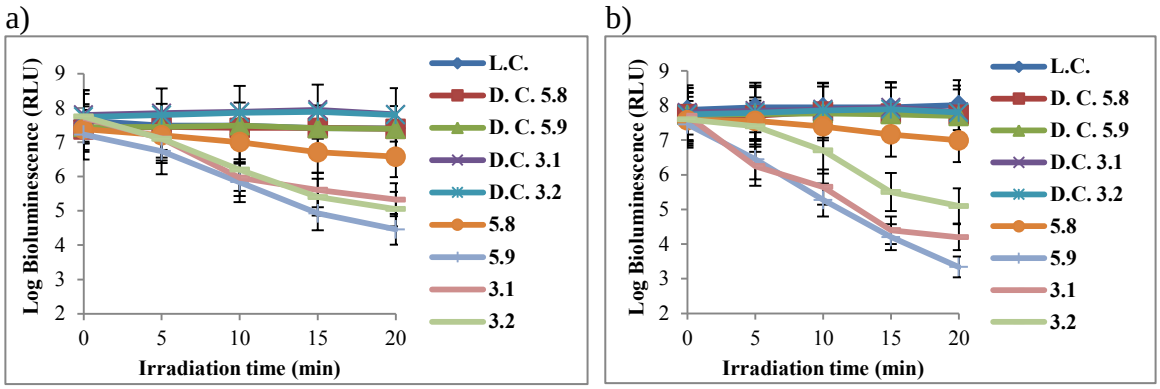

Figure 5.14 Survival of bioluminescent *E. coli* during PDI experiments with 20 μM of PSs **5.8**, **5.9**, **3.1** and **3.2**, after irradiation with a) white light (400–800 nm) and b) red light (620-750 nm) at a fluence rate of 150 mW.cm^{-2}, during 20 min. Values correspond to the average of 3 independent experiments in duplicate. Error bars represent standard deviation.

Photosensitizer uptake by the bioluminescent E. coli cells

The amount of PSs adsorbed by the bioluminescent *E. coli* in presence of the cationic PSs (20 μM), after 15 min of incubation in dark conditions, are summarized in Figure 5.15. PS **5.8** showed significantly higher adsorption values (5.98×10^7 molecules (PS) CFU.mL^{-1}, ANOVA, $p < 0.05$) when compared to PS **5.9** (3.95×10^6 PS molecules CFU.mL^{-1}). However, these values are most probably related to the aggregation tendency of **5.8** on the cells than related to uptake.

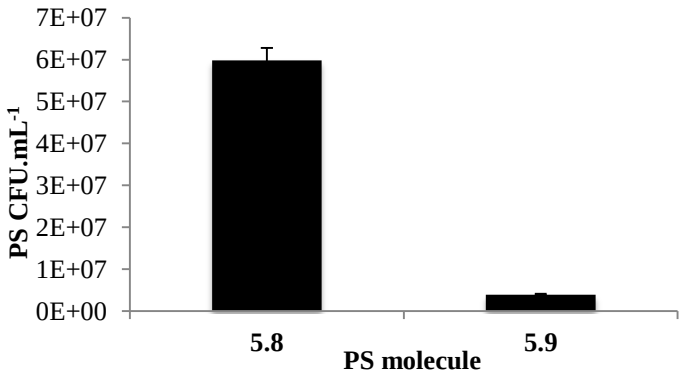

Figure 5.15 Uptake of cationic pyridinone Pc **5.8** and **5.9** (20 μM) by the bioluminescent *E. coli* cells after 15 min of incubation in dark at room temperature. Values correspond to the average of 3 independent experiments. Error bars represent standard deviation.

Photodynamic activities of pyridinium phthalocyanines

Based on the interaction of the Gram-negative membranes with the cationic charges, new tetra- and octa-pyridinium Pcs were synthesized, being evaluated their photophysical, photochemical and photoinactivation efficiency. The use of cationic Pcs as antimicrobial agents has already been described in the literature using trimethylammonium[57,58] or even pyridinium groups.[18] The photodynamic inactivation (PDI) studies showed two clearly behaviours between the tetra- (**5.8**) and octa-cationic (**5.9**) PSs. PS **5.9** showed to be more efficient PS against bioluminescent *E. coli* (3.6 and 4.4 log of reduction under white and red light, respectively) comparing the PS **5.8** (1.3 and 1.0 log of reduction under white and red light, respectively). Charge number is an essential role in driving the PS toward sites that are critical for the stability of cell organization and/or the cell functions.[59,60] According to previous studies where this matter has been emphasized, high number of positive charges hypothesized to be the reason of PS efficiency decreasing.[61,62] However, other factors like PS binding, substitution type or even photophysical features can be related to PS efficiency against bacterial cells.[63] Having this in mind, parallel studies such as singlet oxygen ($^1O_2$) production, aggregation and PS adsorption studies were conducted. The evaluation of these studies allowed us to understand the photosensitization behaviour of these tetra- and octa-cationic PSs. It has been already discussed by several researchers that $^1O_2$ is the major ROS produced by this kind of macrocycles during PDI, being the intermediate for cell damage and subsequently death. In the present case, PS **5.8** shows significantly higher $^1O_2$ production (92%) when compared to PS **5.9** (36%), however their PDI efficiency cannot be correlated just with the production of $^1O_2$. The behaviour of PS **5.8** in PBS may be the reason of these results. In fact, PS **5.8** showed aggregation behaviour in the buffer solution used in the PDI assays, even when 5% of additional DMSO was added. This performance can also be the reason why PS **5.8** presented these particular values in terms of PS uptake/internalization (5.98×10^7 *vs* 3.95×10^6 for PS **5.9**). The addition of positive charges, besides the interaction with the negative bacteria membrane, should confer hydrophilicity to the molecule, making them amphiphilic. However, the way that hydroxypyridine is bound to the Pc core should, in some way, influence their behaviour. Indeed, the substitution by the nitrogen instead of the thiol in case of **3.1** and **3.2**, make the first ones, most probably less flexible. In addition, the position of the positive charge may also contribute to the aggregation behaviour in

water, once it is more protected from the surrounding environment. This can make the molecule less water-soluble.

Phthalocyanines are suitable PS due to their high absorbance in the red region of visible light. The significant difference between both lights (≈2 more log of reduction under red light) can also be explained by the overlap of the red light (620-750 nm) and the second Q-band of PS **5.9**. As a matter of fact, the light wavelength necessary to induce microorganism photoinactivation depends on the electronic absorption spectrum of the PS and the emission spectrum of the light source.[64] In case of PS **5.8**, the aggregation performance overlapped the effect of light in terms of bacterial photoinactivation.

Based on the studies conducted in parallel with PS **5.9**, **3.1** and **3.2**, the differences observed in the inactivation profiles can be mainly justified by aggregation phenomenon presented by **5.8** in PBS. In this context, the number and position of the positive charged groups play a key role in the physicochemical and biological behaviours. The $^1O_2$ production by **5.8** is higher than by **5.9** and **3.1**, its aggregation behaviour overlaps this verdict. In fact, the method used to evaluate the $^1O_2$ production (qualitatively) uses only a small percentage of water (10%). Moreover, PSs **5.9**, **3.1** and **3.2** have equal photoinactivation performance, under white light, although **5.8** present higher $^1O_2$ production justified eventually by the overlapping absorbance spectra between PSs tested and white and red light used in biological assays (Figure 5.15).

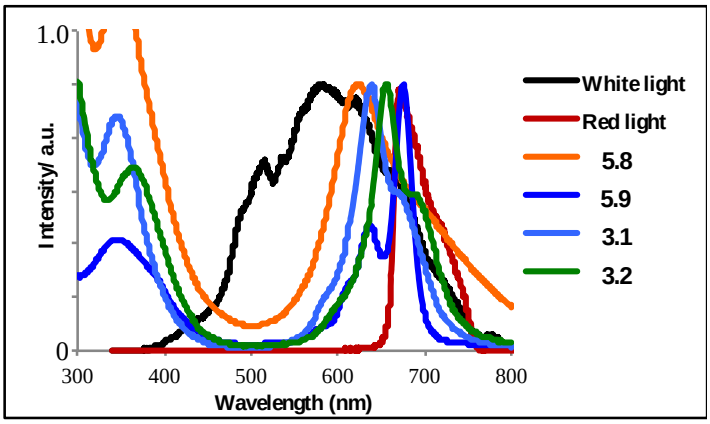

Figure 5.16 Normalized UV–Vis spectra of **5.8**, **5.9**, **3.1** and **3.2**, in PBS, with white and red light source emission.

Indeed, PSs **3.1** and **3.2** have higher absorbance in the wavelengths where white light also absorbs compared with **5.9**. The better performance of **5.9** under red light may be due to the conjunction of several features, such as: better solubility, higher $^1O_2$ production,

higher overlap with the absorbance spectrum of the red light, comparing to the thiopyridinium PSs previously studied.

5.6 Final considerations and outlook

In summary, it was reported here an efficient synthetic strategy that can be used to access phthalocyanines bearing pyridinium units. The approach requires the synthesis of adequate pyridinone phthalonitriles to obtain inverted tetra- or octa-substituted pyridinone Pcs that after cationization afford the corresponding pyridinium Pc derivatives.

The new pyridinone and pyridinium Pc derivatives **5.6**-**5.9** were structurally characterized by NMR spectroscopy and mass spectrometry, in which the observed data were therefore relevant for the identification of such pyridinone and/or pyridinium Pc derivatives. Moreover, derivative **5.9** proved to be an efficient photosensitizer against bioluminescent *E. coli*. Interestingly, PS **3.1** and **3.2** have higher absorbance in the wavelengths where white light system emits compared with Pc **5.9**; and the better performance of **5.9** under red light system can be due to its higher production of $^1O_2$ and/or higher overlap with the absorbance spectrum of the red light, comparing to thiopyridiniumphthalocyanines.

5.7 Experimental section

General information

All reagents were purchased from Sigma-Aldrich and used analytical TLC was carried out on precoated silica gel sheets (Merck, 60, 0.2 mm). Molecular extrusion column chromatography was carried out over Bio-beadsTM S-X1 Beads (200-400 Mesh, 100 g), Bio-Rad Laboratories, Inc.

^{1}H and ^{13}C NMR spectra were recorded on a *Bruker Avance-300* spectrometer at 300.13 and 75.47 MHz, respectively, or on a *Bruker Avance-500* spectrometer at 125.77 MHz for ^{1}H and ^{13}C. Tetramethylsilane was used as internal reference. The chemical shifts are expressed in δ (ppm) and the coupling constants (*J*) in Hz. Absorption and fluorescence spectra were recorded in DMF using a *Shimadzu UV-2501-PC* and FluoroMax3 (excitation

wavelengths of 400 nm, emission range 625–825 nm, slit 2 nm), respectively. The fluorescence emission spectra of Pc derivatives **5.6-5.9** (C = 1 × 10^{-6} M) were measured in DMF in 1 cm × 1 cm quartz optical cells under normal air conditions on a computer controlled Horiba Jobin Yvon FluoroMax-3 spectrofluorimeter. The widths of both excitation and emission slits were set at 2.0 nm. The fluorescence quantum yields (Φ_F) of **5.6**-**5.9** were calculated in DMF by comparison of the area below the corrected emission spectra (between 600 nm to 800 nm) using **ZnPc** as standard ($\lambda_{excitation}$ at 400 nm, Φ_f = 0.17 in DMF).[65] For that, the following equation was used:

$$\Phi_f^{sample} = \Phi_f^{standard} \frac{AUC^{sample}(1-10^{-Abs_{standard}})}{AUC^{standard}(1-10^{-Abs_{sample}})},$$

where *AUC* is the integrated area under the fluorescence curves for each sample and standard, and *Abs* is the absorbance of the samples and the standard at the excitation wavelength ($\lambda_{excitation}$ at 400 nm). The acquisition of the electrospray high resolution mass spectra (ESI-HRMS) was obtained in an *Apex-Qe*.

Synthesis and characterization of pyridinone phthalonitriles 5.4 and 5.5

*4-(4-oxopyridin-1(4H)-yl)phthalonitrile (**5.4**)*:

In a 25 mL round-bottom flask, 4-fluorophthalonitrile (512.5 mg, 3.5 mmol) and 4-hydroxypyridine (352.9 mg, 3.7 mmol, 1.1 equiv.) were dissolved in 3 mL of dry DMF, and then it was added some drops of triethylamine and keep under N_2 atmosphere. The reaction mixture was maintained under stirring for 5 h at 80 ºC, when the TLC control confirmed the consumption of the starting phthalonitrile. Then the reaction mixture was purified by silica gel column chromatography using a mixture of $CHCl_3$/MeOH (95/5) as eluent. The phthalonitrile **5.4** (712.3 mg, 3.2 mmol) was obtained in 92% yield, after recrystallization from $CHCl_3$/MeOH. ^{1}H NMR (500 MHz, DMSO-d_6): δ 6.31 (d, J = 7.9 Hz, 2H, H^e), 8.14 – 8.17 (m, 3H, $H^{c,d}$), 8.33 (d, J = 8.6 Hz, 1H, H^a), 8.50 (d, J = 2.4 Hz, 1H, H^b). ^{13}C NMR (75 MHz, DMSO-d_6): δ 112.8, 115.3, 115.5, 116.2, 118.3, 127.1, 127.6, 135.6, 139.0, 145.5, 177.7. ESI-MS: *m/*z 222 $[M+H]^+$.

*4,5-bis(4-oxopyridin-1(4H)-yl)phthalonitrile (**5.5**)*:

In a 25 mL round-bottom flask, 4,5-difluorophthalonitrile (300.1 mg, 1.8 mmol) and 4-hydroxypyridine (356.5 mg, 3.7 mmol, 2.1 equiv.) were dissolved in 3 mL of DMF, and then it was added some drops of triethylamine. The reaction mixture was maintained under stirring during 5 h at 80 ºC, when the TLC control confirmed the consumption of the starting phthalonitrile. Then, the reaction mixture was purified by silica gel column chromatograph using a mixture of $CHCl_3$/MeOH (90/10) as eluent. After evaporation of the solvent, the residue was crystallized from the same mixture and phthalonitrile **5.5** (569.3 mg, 1.8 mmol) afforded in 99% yield. ^{1}H NMR (500 MHz, DMSO-d_6): δ 6.21 (d, J = 7.9 Hz, 4H, H^c), 7.64 (d, J = 7.9 Hz, 4H, H^b), 8.70 (s, 2H, H^a). ^{13}C NMR (75 MHz, DMSO-d_6): δ 114.6, 115.4, 118.3, 133.7, 140.0, 141.2, 177.2. ESI-MS: *m/*z 315 $[M+H]^+$.

5.7.1 Synthesis and characterization of pyridinone phthalocyanines 5.6 and 5.7

*2,9(10),16(17),23(24)-tetrakis(4-oxopyridin-1(4H)-yl)phthalocyaninato zinc(II) (**5.6**)*:

In a 25 mL round-bottom flask, a solution containing phthalonitrile **5.4** (207.5 mg, 0.9 mmol) and anhydrous zinc chloride (138.9 mg, 1.0 mmol) in 2 mL of 1-pentanol was heated at 140 ºC under nitrogen atmosphere. After 16 h, the reaction was considered complete since no starting phthalonitrile **5.4** could be detected by analytic TLC. Then, it was added chloroform and the precipitate washed several times with the same solvent. The obtained solid was subsequently washed with water in order to remove the excess of zinc chloride. After being dried under vacuum, the crude product was purified by Bio-beadsTM S-X1 column molecular exclusion chromatography using DMF as eluent. The desired product was precipitated from chloroform, filtrated and washed with the same solvent. The Pc **5.6** (129.5 mg, 0.14 mmol) was isolated in 58% yield. ^{1}H NMR (300 MHz, DMSO-d_6): δ 8.21 – 8.24 (m, 4H, β-H^c), 6.58 – 6.66 (m, 8H, H^e), 8.54 – 8.58 (m, 8H, H^d), 8.96 – 9.05 (m, 8H, α-$H^{a,b}$). ^{13}C NMR (126 MHz, DMSO-d_6): δ 41.3, 118.1, 118.6, 123.7, 139.8, 140.3, 143.4, 177.8. ESI-HRMS: *m/*z 949.17293 $[M+H]^+$. UV–Vis (DMF), λ_{max} (log ε): 613 (4.14), 681 (4.90).

*2,3,9,10,16,17,23,24-Octakis(4-oxopyridin-1(4H)-yl)phthalocyaninato zinc(II) (**5.7**)*:

In a 25 mL round-bottom flask, a solution containing phthalonitrile **5.5** (310.4 mg, 1.0 mmol) and anhydrous zinc chloride (128.4 mg, 0.9 mmol, 0.9 equiv.) in 2 mL of 1-pentanol was heated at 140 ºC under nitrogen atmosphere. After 16 h, the TLC control confirmed the reaction was complete. The reaction mixture was then precipitated with chloroform, and the solid obtained was washed several times with the same solvent and with water in order to remove the excess of zinc chloride. After being dried under vacuum, the crude product was purified by Bio-beadsTM S-X1 column molecular exclusion chromatography using DMF as eluent. The desired product was obtained from precipitation with chloroform, filtration and after washing with the same solvent. Pc **5.7** (262.2 mg, 0.2 mmol) was obtained in 80% yield. ^{1}H NMR (300 MHz, DMSO-d_6): δ 6.36 (d, J = 7.2 Hz, 16H, H^{c}), 8.13 (d, J = 5.0 Hz, 16H, H^{b}), 9.63 (s, 8H, α-H^{a}). ^{13}C NMR (75 MHz, DMSO-d_6): δ 118.0, 121.9, 138.3, 139.6, 141.0, 152.3, 176.9. ESI-HRMS: *m/*z 1323.25865 $[M+3H]^{+}$. UV–Vis (DMF), λ_{max} (log ε): 616 (4.52), 684 (5.31).

5.7.2 Synthesis and characterization of pyridinium phthalocyanines 5.8 and 5.9

*2,9(10),16(17),23(24)-tetrakis(4-methoxypyridinium)phthalocyaninato zinc(II) (**5.8**)*:

The pyridinone Pc **5.6** (103.3 mg, 0.11 mmol) after being dissolved in 20 mL of dry DMF was added to a large excess of dimethyl sulphate (4 mL, 37.5 mmol, 341 equiv.). The reaction mixture was kept under stirring overnight at 80 ºC in a sealed tube. After this period of time, the mixture was allowed to cool down and then it was precipitated with a mixture of acetone/CH_2Cl_2 (1:1). The obtained residue was filtrated and after being taken up in MeOH/H_2O (2:1) was re-precipitated by addition of dichloromethane. The desired product was filtrated, washed with dichloromethane and dried under vacuum. The dark green solid identified as Pc **5.8** (110.7 mg, 0.09 mmol) was isolated in 85% yield. ^{1}H NMR (300 MHz, DMSO-d_6): δ 4.29 – 4.54 (m, 12H, H^{f}), 6.69 – 6.75 (m, 4H, β-H^{e}), 7.99 – 8.15 (m, 8H, H^{c}), 8.62 – 8.70 (m, 8H, H^{d}), 9.62 – 9.73 (m, 8H, α-H^{a,b}). ^{13}C NMR (126 MHz, DMSO-d_6): δ 41.4, 48.6, 52.9, 58.9, 114.0, 117.9, 146.8, 172.1. UV–Vis (DMF), λ_{max} (log ε): 614 (4.66), 680 (5.36); UV–Vis (DMSO), λ_{max} (log ε): 615 (4.70), 682 (5.40); UV–Vis (PBS), λ_{max} (log ε): 624 (4.49). MALDI-TOF-MS: *m/*z 963 $[M-CH_3]^{+\cdot}$.

*2,3,9,10,16,17,23,24-Octakis(4-methoxypyridinium)phthalocyaninato zinc(II) (**5.9**)*:

The pyridinone Pc **5.7** (106.9 mg, 0.08 mmol) after being dissolved in 20 mL of dry DMF was added to a large excess of dimethyl sulphate (4 mL, 37.5 mmol, 469 equiv.). The reaction mixture was kept under stirring overnight at 80 ºC in a sealed tube. After this period, the mixture was cooled down and then it was precipitated using a mixture of acetone/dichloromethane (1/1). The residue obtained was filtrated and after being taken up in MeOH/H_2O (2:1) was re-precipitated by addition of dichloromethane. The desired product was filtrated, washed with dichloromethane and dried under vacuum. The dark green solid identified as Pc **5.9** (130.6 mg, 0.07 mmol) was obtained in 88% yield. ^{1}H NMR (300 MHz, DMSO-d_6): δ 4.31 (s, 24H, H^d), 7.93 (d, J = 7.1 Hz, 16H, H^c), 9.43 (d, J = 7.1 Hz, 16H, H^b), 10.12 (s, 8H, α-H^a). ^{13}C NMR (126 MHz, DMSO-d_6): δ 41.4., 48.6, 52.9, 59.1, 114.3, 137.6, 139.5, 147.6, 153.0, 172.8. UV–Vis (DMF), λ_{max} (log ε): 634 (4.56), 683 (5.15); UV–Vis (DMSO), λ_{max} (log ε): 616 (4.55), 683 (5.35); UV–Vis (PBS), λ_{max} (log ε): 637 (4.10), 675 (5.13). MALDI-TOF-MS: *m/*z 1335 $[M\text{-}7CH_3]^{+\cdot}$.

Photosensitizer stock solution

Stock solutions of the photosensitizers used in the photophysical and biological studies were prepared in dimethyl sulfoxide (DMSO) at a concentration of 500 μM, and diluted in DMF/H_2O (9:1), PBS or sodium dodecyl sulphate (SDS).

Light source

All the photoinactivation assays were performed under white and red light from a compatible optic fibre probe (400–800 nm and 620–750 nm, respectively) attached to a illumination system (LumaCare®, USA, model LC122, with halogen⁄quartz 250 W lamp) with a fluence rate of 150 mW.cm^{-2}.

Singlet oxygen generation

An aliquot of 3 mL of a solution of the Pc (0.5 μM) and 1,3-diphenylisobenzofuran (DPBF, 50 μM) in DMF/H_2O (9:1) was transferred to a glass cuvette and irradiated with a red LED array, in order to prevent the photodegradation of DPBF, at a fluence rate of 6.0

$mW.cm^{-2}$, at room temperature and under gentle magnetic stirring. The LED array is composed of a matrix of 5 Å~ 5 LED that makes a total of 25 light sources with an emission peak at 640 nm and a bandwidth at half maximum of ± 20 nm. The absorption of DPBF at 415 nm was measured at defined time intervals during 15 min. The percentage of the DPBF absorption decay, proportional to the production of $^1O_2$, was assessed by the difference between the initial absorbance and the absorbance of DPBF after a given period of irradiation.[66]

Solubility studies

The solubility of new cationic phthalocyanines **5.8** and **5.9** in DMSO and PBS was assessed by UV–Visible spectroscopy. Concentrations, between 1 and 20 μM, obtained by the addition of aliquots of each Pc stock solution (500 μM), were analysed. The intensity of the Q-band *versus* Pc concentration was plotted in a graphic for linear regression to determine if these concentrations follow the Beer–Lambert law.

Bacterial strains, growth conditions and preparation of stock-suspensions

The used bioluminescent *E. coli* was collected from a sample previously transformed and storage at -80 ºC in 10% glycerol. Before the photoinactivation assay, a fresh culture of *E. coli* was growth in Tripic Soy Agar (TSA) with the antibiotics ampicillin (100 $mg.mL^{-1}$) and chloramphenicol (25 $mg.mL^{-1}$) and grown for 24 h at 37 ºC. One isolated colony was aseptically inoculated on Tripic Soy Broth (TSB) (30 mL) with both the antibiotics and grown overnight at 26 ºC under stirring (120 rpm). An aliquot (240 μL) of this culture was subcultured in TSB (30 mL) with antibiotics and grown during 20 h at 26 ºC.

PDI experimental setup

Bacterial suspensions prepared from overnight cultures ($\approx 10^9$ $CFU.mL^{-1}$) were ten-fold diluted in PBS to a final concentration of $\approx 10^8$ $CFU.mL^{-1}$. For the experiments, 450 μL of bacterial suspension was aseptically transferred to sterilized 12-well plates and the PS was added from the stock solution to achieve final concentrations of 20 μM. PBS was

added to the suspension in order to obtain a final volume of 4.5 mL. After the addition of the PS, wells were protected from accidental light exposure with an aluminium foil and pre-incubated for 15 min in the dark, under 100 rpm stirring at room temperature, to promote PS binding to *E. coli* cells. After this period, the irradiation was conducted under white and red light during 30 min. Light and dark controls were included in the experiments. The light control was irradiated without Pc. The dark control contained (20 μM**)** of Ps, but was protected from light with aluminium foil. Three independent assays were conducted for each condition.

Bioluminescence monitoring

In all experiments, aliquots (500 μL) of treated and control samples were collected at time 0, 5, 10, 15, 20, 25 and 30 min of irradiation for bioluminescence measurement in a luminometer (TD-20/20 Luminometer; Turner Designs, Inc.).

Photosensitizer uptake

Three replicate bioluminescent *E. coli* (10^8 cells mL^{-1}) suspensions were prepared in PBS and incubated in the dark at room temperature in the presence of 20 μM of each PS. After 15 min of incubation, unbound PS was removed out of the suspension by centrifugation for 5 min, at 13000 *G* (Hettich Mikro 120). Pellets were further washed with PBS + 5% DMSO, digested in 1 mL of a solution containing 2% SDS (Merck) and 0.1 M of NaOH and incubated at room temperature for 24 h or until a clear solution. The fluorescence of the extracts was measured on a FluoroMax3 spectrofluorimeter with a slit of 2 nm. The excitation wavelengths for all compounds were 400 nm. The range for emission was 625 to 825 nm. The measured fluorescence intensity allowed the determination of the corresponding PS concentration by interpolation with a calibration plot built with known concentrations of each PS, using the digestion solution as solvent. Parallel aliquots of cell suspensions incubated in the presence of the PS were read and log luminescence (RLU) was assessed. The adsorption value (PS $CFU.mL^{-1}$) was calculated according to the literature.[67] Three independent assays were performed for each combination of bacterial strain PS.

Statistical analysis

Statistical analysis was performed in SPSS 15.0 for Windows (SPSS Inc., USA). The significance of the PDI effect of each PS and of the irradiation time on bacterial cells viability was assessed by an unvaried analysis of variance (ANOVA) model with the Bonferroni post hoc test. Normal distributions were assessed by the Kolmogorov–Smirnov test and homogeneity of variances was assessed by the Levene test. A value of $p < 0.05$ was considered significant.

5.8 References

1. McKeown, N. B., in The Porphyrin Handbook, *The synthesis of symmetrical phthalocyanines*, Kadish, K. M., Smith, K. M., Guilard, R., Eds., Academic Press, New York, NY, USA, vol. 15, cap. 98, pp. 61–124, 2003.
2. Lyubimtsev, A., Iqbal, Z., Crucius, G., Syrbua, S., Ziegler, T., Hanack, T., *J. Porphyrins Phthalocyanines*, **2012**, 16, 434–463.
3. Luan, L., Ding, L., Zhang, W., Shi, J., Yu, X., Liu, W., *Bioorg. Med. Chem. Lett*., **2013**, 23, 3775–3779.
4. Camerin, M., Rello-Varona, S., Villanueva, A., Rodgers, M. A. J., Jori, G., *Laser. Surger. Med*., **2009**, 41, 665–673.
5. Lourenço, L. M. O., Neves, M. G. P. M. S., Cavaleiro, J. A. S., Tomé, J. P. C., *Tetrahedron,* **2014**, 70, 2681–2698.
6. Lyubimtsev, A., Iqbal, Z., Crucius, G., Syrbu, S., Ziegler, T., Hanack, M., *J. Porphyrins Phthalocyanines*, **2012**, 16, 434–463.
7. Berthold, H. J., Franke, S., Thiem, J., Schotten, T., *J. Org. Chem*., **2010**, 75, 3859–3862.
8. Lourenço, L. M. O., Pereira, P. M. R., Maciel, E., Domingues, M. R. M., Fernandes, R., Neves, M. G. P. M. S., Cavaleiro, J. A. S., Tomé, J. P. C., *Chem. Comm*., **2014**, *submitted*.
9. Soares, A. R., Neves, M. G. P. M. S., Tomé, A. C., Iglesias-de la Cruz, M. C., Zamarron, A., Carrasco, E., Gonzalez, S., Cavaleiro, J. A. S., Torres, T., Guldi, D. M., Juarranz, A., *Chem. Res. Toxicol.*, **2012**, 25, 940–951.
10. Silva, S., Pereira, P. M. R., Silva, P., Paz, F. A. A., Faustino, M. A. F., Cavaleiro, J. A. S., Tomé, J. P. C., *Chem. Commun.*, **2012**, 48, 3608–3610.
11. Bolfarini, G. C., Siqueira-Moura, M. P., Demets, G. J. F., Morais, P. C., Tedesco, A. C., *J. Photochem. Photobiol., B*, **2012**, 115, 1–4.
12. Bolfarini, G. C., Siqueira-Moura, M. P., Demets, G. J. F., Tedesco, A. C., *Dyes Pigm.*, **2014**, 100, 162–167.
13. Huang, J.-D., Wang, S., Lo, P.-C., Fong, W.-P., Kod, W.-H., Ng, D. K. P., *New J. Chem*., **2004**, 28, 348–354.

14. Lo, P.-C., Huang, J.-D., Cheng, D. Y. Y., Chan, E. Y. M., Fong, W.-P., Ko, W.-H., Ng, D. K. P., *Chem. Eur. J.*, **2004**, 10, 4831–4838.
15. Allen, C. M., Sharman, W. M., Van Lier, J. E., *J. Porphyrins Phthalocyanines*, **2001**, 5, 161–169.
16. Josefsen, L. B., Boyle, R. W., *Met. Based Drugs*, **2008**, 2008, 1–24.
17. Liu, J.-Y., Jiang, X.-J., Fong, W.-P., Ng, D. K. P., *Org. Biomol. Chem.*, **2008**, 6, 4560–4566.
18. Pereira, J. B., Carvalho, E. F. A., Faustino, M. A., Neves, M. G. P. M. S., Cavaleiro, J. A. S., Gomes, N. C. M., Cunha, Â., Almeida, A., Tomé, J. P. C., *Photochem. Photobiol.*, **2012**, 88, 537–547.
19. Almeida, A., Cunha, Â., Faustino, M. A. F., Tomé, A. C., Neves, M. G. P. M. S., in Photodynamic Inactivation of Microbial Pathogens, Medical and Environmental Applications, *Porphyrins as Antimicrobial Photosensitizing Agents*, Hamblin, M. R., Jori, G., Eds., RSC Publishing: Cambridge, England, Chapter 5, pp. 83–160, 2011.
20. Gad, F., Zahra, T., Hasan, T., Hamblin, M. R., *Antimicrob. Agents Chemother.*, **2004**, 48, 2173–2178.
21. Tomé, J. P. C., Neves, M. G. P. M. S., Tomé, A. C., Cavaleiro, J. A. S., Soncin, M., Magaraggia, M., Ferro, S., Jori, G., *J. Med. Chem.*, **2004**, 47, 6649–6652.
22. Nagata, J. Y., Hioka, N., Kimura, E., Batistela, V. R., Terada, R. S. S., Graciano, A. X., Baesso, M. L., Hayacibara, M. F., *Photodiagn. Photodyn. Ther.*, **2012**, 9, 122–131.
23. CIBA Foundation Symposium, Photosensitizing Compounds: Their Chemistry, Biology and Clinical Use; Bock, G., Harnett, S., Eds., John Wiley: Chichester, UK, vol. 727, pp. 1–32 and 60–130, 2008.
24. Dumoulin, F., Durmuş, M., Ahsen, V., Nyokong, T., *Coord. Chem. Rev.*, **2010**, 254, 2792–2847.
25. Kussovski, V., Mantareva, V., Angelov, I., Orozova, P., Wöhrle, D., Schnurpfeil, G., Borisova, E., Avramov, L., *FEMS Microbiol. Lett.*, **2009**, 294, 133–140.
26. Alves, E., Faustino, M. A. F., Tomé, J. P. C., Neves, M. G. P. M. S., Tomé, A. C., Cavaleiro, J. A. S., Cunha, Â., Gomes, N. C. M., Almeida, A., *Bioorg. Med. Chem.*, **2013**, 21, 4311–4318.

27. Senge, M. O., Radomski, M. K., *Photodiagn. Photodyn. Ther.*, **2013**, 10, 1–16.
28. Gomes, M. C., Woranovicz-Barreira, S. M., Faustino, M. A. F., Fernandes, R., Neves, M. G. P. M. S., Tomé, A. C., Gomes, N. C. M., Almeida, A., Cavaleiro, J. A. S., Cunha, Â., Tomé, J. P. C., *Photochem. Photobiol. Sci*., **2011**, 10, 1735–1743.
29. Moser, F. H., Thomas, A. L., in Phthalocyanine Compounds, American Chemical Society, Reinhold Publishing, New York, NY, USA, 1963.
30. Soares, A. R. M., Neves, M. G. P. M. S., Santos, S. M., Tomé, J. P. C., Tomé, A. C., Cavaleiro, J. A. S., Torres, T., Domingues, M. R. M., *Rapid Commun. Mass Spectrom*., **2013**, 27, 1019–1026.
31. Ghani, F., Kristen, J., Riegler, H., *J. Chem. Eng. Data*., **2012**, 57, 439−449.
32. McKeown, N. B., in An introduction to the phthalocyanines. Phthalocyanine Materials: Synthesis, Structure and Function, McKeown, N. B., Ed., Cambridge University Press, Cambridge, UK, Chapters 1 and 2, pp. 1-31, 1998.
33. Masilela, N., Nyokong, T., *J. Lumin*., **2010**, 130, 1787–1793.
34. Durmus, M., Nyokong, T., *Tetrahedron*, **2007**, 63, 1385–1394.
35. Oleinick, N. L., Antunez, A. R., Clay, M. E., Rihter, B. D., Kenney, M. E., *Photochem. Photobiol*., **1993**, 57, 242–247.
36. Zamora-León, S. P., Golde, D. W., Concha, I. I., Rivas, C. I., Delgado-Lopez, F., Baselga, J., Nualart, F., Vera, J. C., *Proc. Natl. Acad. Sci. U.S.A*., **1996**, 93, 1847–1852.
37. Kumamoto, K., Goto, Y., Sekikawa, K., Takenoshita, S., Ishida, N., Kawakita, M., Kannagi, R., *Cancer Res*., **2001**, 61, 4620–4627.
38. Chandler, J. D., Williams, E. D., Slavin, J. L., Best, J. D., Rogers, S., *Cancer*, **2003**, 97, 2035–2042.
39. Lo, P.-C., Huang, J.-D., Cheng, D. Y. Y., Chan, E. Y. M., Fong, W.-P., Ko, W.-H., Ng, D. K. P., *Chem. Eur. J*., **2004**, 10, 4831–4838.
40. Leng, X., Choi, C.-F., Lo, P.-C., Ng, D. K. P., *Org. Lett*., **2007**, 9, 231–234.
41. Hofman, J.-W., Zeeland, F. V., Turker, S., Talsma, H., Lambrechts, S. A. G., Sakharov, D. V., Hennink, W. E., Nostrum, C. F. V., *J. Med. Chem*., **2007**, 50, 1485–1494.

42. Lee, P. P. S., Lo, P. C., Chan, E. Y. M., Fong, W. P., Ko, W. H., Ng, D. K. P., *Tetrahedron Lett*., **2005**, 46, 1551–1554.
43. Peng, Q., in Photodynamic Therapy and Fluorescence Diagnosis in Dermatology, *Correlation of intracellular and intratumoural photosensitizer distribution with photodynamic effect*, Calzavara-Pinton, P. G., Szeimies, R. M., Ortel, B., Eds., Elsevier, Amsterdam, pp. 55–66, 2001.
44. Mantareva, V., Kussovski, V., Angelov, I., Borisova, E., Avramov, L., Schnurpfeil, G., Wöhrle, D., *Bioorg. Med. Chem.*, **2007**, 15, 4829–4835.
45. Fu, X.-J., Fang, Y., Yao, M., *BioMed Research International*, **2013**, 2013, 1–9.
46. Donnelly, R., Cassidy, C., Tunney, M., in Photodynamic Inactivation of Microbial Pathogens: Medical and Environmental Applications, Jori, G., Hamblin, M., Eds., Royal Society of Chemistry, pp. 185–216, 2011.
47. Sharma, S. K., Mroz, P., Dai, T., Huang, Y. Y., Denis, T. G., St., Hamblin, M. R., *Isr. J. Chem*., **2012**, 52, 691–705.
48. Chen, J., Chen, Z., Zheng, Y., Zhou, S., Wang, J., Chen, N., Huang, J., Yan, F., Huang, M., *J. Porphyrins Phthalocyanines*, **2011**, 15, 293–299.
49. Spesia, M. B., Rovera, M., Durantini, E. N., *Eur. J. Med. Chem*., **2010**, 45, 2198–2205.
50. Junqueira, J. C., Jorge, A. O. C., Barbosa, J. O., Rossoni, R. D., Vilela, S. F. G., Costa, F. A. C. B. P., Primo, L., Gonçalves, J. M., Tedesco, A. C., Suleiman, J. M. A. H., *Lasers Med. Sci.*, **2012**, 27, 1205–1212.
51. Spesia, M. B., Durantini, E. N., *J. Photochem. Photobiol., B*, **2013**, 125, 179–187.
52. Malik, Z., Ladan, H., Nitzan, Y., *J. Photochem. Photobiol. B*, **1992**, 14, 262–266.
53. Kuznetsova, N. A., Makarov, D. A., Kaliya, O. L., Vorozhtsov, G. N., *J. Hazard. Mater*., **2007**, 146, 487–491.
54. Taraszkiewicz, A., Grinholc, M., Bielawski, K. P., Kawiak, A., Nakonieczna, J., *Appl. Environ. Microbiol*., **2013**, 79, 3692–3702.
55. Costa, D. C. S., Gomes, M. C., Faustino, M. A. F., Neves, M. G. P. M. S., Cunha, A., Cavaleiro, J. A. S., Almeida, A., Tomé, J. P. C., *Photochem. Photobiol. Sci*., **2012**, 11, 1905–1913.

56. Leeuwen, M. v., Beeby, A., Fernandes, I., Ashworth, S. H., *Photochem. Photobiol. Sci*., **2014**, 13, 62–69.
57. Segalla, A., Borsarelli, C. D, Braslavsky, S. E., Spikes, J. D., Roncucci, G., Dei, D., Chiti, G., Jori, G., Reddi, E., *Photochem. Photobiol. Sci.*, **2002,** 1, 641–648.
58. Soncin, M., Fabris, C., Busetti, A., Dei, D., Nistri, D., Roncucci, G., Jori, G., *Photochem. Photobiol. Sci.*, **2002**, 1, 815–819.
59. Merchat, M., Bertolini, G., Giacomini, P., Villanueva, A., Jori, G., *J. Photochem. Photobiol., B,* **1996**, 32, 153–157.
60. Lazzeri, D., Rovera, M., Pascual, L., Durantin, E. N., *Photochem. Photobiol.*, **2004**, 80, 286–293.
61. Spesia, M., Rovera, M., Durantini, E., *Eur. J. Med. Chem.*, **2010**, 45, 2198–2205.
62. Segalla, A., Borsarelli, C. D., Braslavsky, S. E., Spikes, J. D., Roncucci, G., Dei, D., Chiti, G., Jori, G., Reddi, E., *Photochem. Photobiol. Sci.*, **2002**, 1, 641–648.
63. Gomes M. C., Silva S., Faustino, M. A. F., Neves, M. G. P. M. S., Almeida, A., Cavaleiro, J. A. S., Tomé, J. P. C., Cunha, Â., *Photochem. Photobiol. Sci*., **2013**, 12, 262–271.
64. Costa, L., Carvalho, C. M. B., Faustino, M. A. F., Neves, M. G. P. M. S., Tomé, J. P. C., Tomé, A. C., Cavaleiro, J. A. S., Cunha, A., Almeida, A., *Photochem. Photobiol. Sci.,* **2010**, 9, 1126–1133.
65. Ogunsipe, A., Maree, D., Nyokong, T., *J. Mol. Struct*., **2003**, 650, 131–140.
66. Pereira, P. M. R., Carvalho, J. J., Silva, S., Cavaleiro, J. A. S., Schneider, R. J., Fernandes, R., Tomé, J. P. C., *Org. Biomol. Chem.*, **2014**, 12, 1804–1811.
67. Demidova, T. N., Hamblin, M. R., *Appl. Environ. Microbiol.*, **2005**, 71, 6918–6925.

Chapter 6

Synthesis, photophysical and photodynamic activities of amphiphilic phthalocyanine-cyclodextrin conjugates

6.1 Overview

Phthalocyanines (Pcs) and cyclodextrins (CDs) have been intensively studied due to their applications in many scientific areas, namely in medicinal and supramolecular chemistry.[1-5] Pcs are well-known aromatic macrocycles with excellent photophysical properties to be used as photosensitizers (PSs) in photodynamic therapy (PDT) for the treatment of cancer.[6,7] This therapy combines visible light, molecular oxygen and a PS that after irradiation with light are able to generate reactive oxygen species (ROS), like singlet oxygen ($^1O_2$), which can induce cell death pathways resulting in tumour tissues destruction.[8] Pcs, besides their high efficiency in generating of $^1O_2$, have the advantage to absorb light in the red and near-infrared regions (600-800 nm) of the electromagnetic spectrum.[7] The conjugation of Pcs with biochemical motifs is of utmost importance in the development of promising PSs, since it improves their solubility in water and are able to act as Pcs carriers, delivering them into cancer cells. CDs offer unique features towards this goal allowing the design and synthesis of compounds perfectly defined with specific structural characteristics. The most common natural CDs are the α-, β- and γ-CDs, constituted respectively by six (α-CD), seven (β-CD) and eight (γ-CD) glucopyranose units, bound *via* α-1,4-glycosidic linkages. Moreover, these non-toxic molecules can encapsulate several hydrophobic PSs within their truncated cone-shaped hydrophobic cavity, conferring amphiphilicity, biocompatibility and availability at the surface of cancer cell membranes.[9,10] In spite of the high potential of CDs as PS carriers, conjugates involving Pcs and CDs covalently linked are rare and only few works report their application as new PDT agents.[2,3,11-13] Moreover, as far as we know, there are no reports comparing the PDT efficacy of Pcs conjugated with α-, β- and γ-CDs.

Herein, it is reported the preparation, characterization and *in vitro* evaluation of photodynamic efficacy of the new phthalocyanine-cyclodextrin (Pc-CD) conjugates **6.1**-**6.3** (Figure 6.1). The effect of different CDs (α-, β- and γ-CDs) in Pc solubility, $^1O_2$ production, photostability, ability to interact with human serum albumin (HSA) and phototoxicity against human bladder cancer cells were studied.

6.2 Synthesis and characterization of phthalocyanine-cyclodextrin (Pc-CD) conjugates

Considering the remarkable photo-chemical and -physical properties of Pcs and the excellent features of CDs to act as the Pc carrier, it is envisaged a simple access to obtain new amphiphilic Pc-CD conjugates *via* post-modification of the commercial available hexadecafluorophthalocyaninatozinc(II) (**PcF_{16}**). The reaction involved the nucleophilic substitution of two β-fluorine atoms, one each adjacent isoindole unit, by cyclo-maltohexaose (α-CD), cyclo-maltoheptaose (β-CD) and cyclo-maltooctaose (γ-CD) – Figure 6.1. A nucleophilic substitution in the same isoindole unit of the Pc is improbable due to the structural hindrance. It is noteworthy that the hydrophilic properties of the CDs[14] allow the solubilization of this Pc in water and proves to be an exceptional methodology to prepare the water-soluble conjugates **6.1-6.3**.[15]

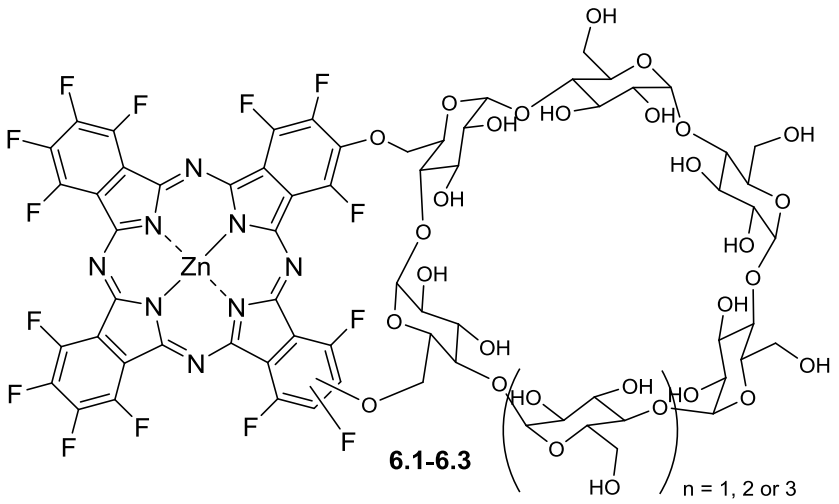

6.1, **Pc-α-CD** (n=1); **6.2**, **Pc-β-CD** (n=2); **6.3**, **Pc-γ-CD** (n=3)

Figure 6.1 Representation of the Pc-CD conjugates **6.1-6.3**.

The reactions between **PcF_{16}** and the adequate equimolar quantity of CDs (α-, β- and γ-CD) were performed in 10 mL of dimethyl sulfoxide (DMSO) in the presence of excess potassium carbonate (8 equiv.) at 50 ºC. These reactions were finished after stirring for 16 h and the reactions mixtures were precipitated in chloroform. The corresponding Pc-CD conjugates were purified by silica gel and reverse phase column chromatography, using a gradient of tetrahydrofuran/water as eluent; and finally by molecular exclusion column chromatography using DMF as solvent. The purified Pc-CDs were reprecipitated in chloroform. The structures of conjugates **6.1-6.3** were confirmed by UV–Vis

spectroscopy, ^{19}F NMR spectroscopy (Figures 6.2-6.4) and MALDI-TOF mass spectrometry (Figures 6.5-6.7). The degree of homogeneity of the sample was assayed by high-performance liquid chromatography (HPLC) analysis (Figures 6.9-6.11).

The low resolution observed in the ^{1}H and ^{19}F NMR spectra and the overlap of signals did not allow the adequate assignment of the protons and fluorine atoms, respectively. However, the ^{19}F NMR spectra of Pc-CDs **6.1**-**6.3** in DMSO-d_6 show the presence of two multiplets around δ -167.16 to -164.15 and -179.92 to -175.51 ppm, corresponding to the six and eight β- and α-fluorine atoms of the Pc moiety (Figures 6.2-6.4), respectively.

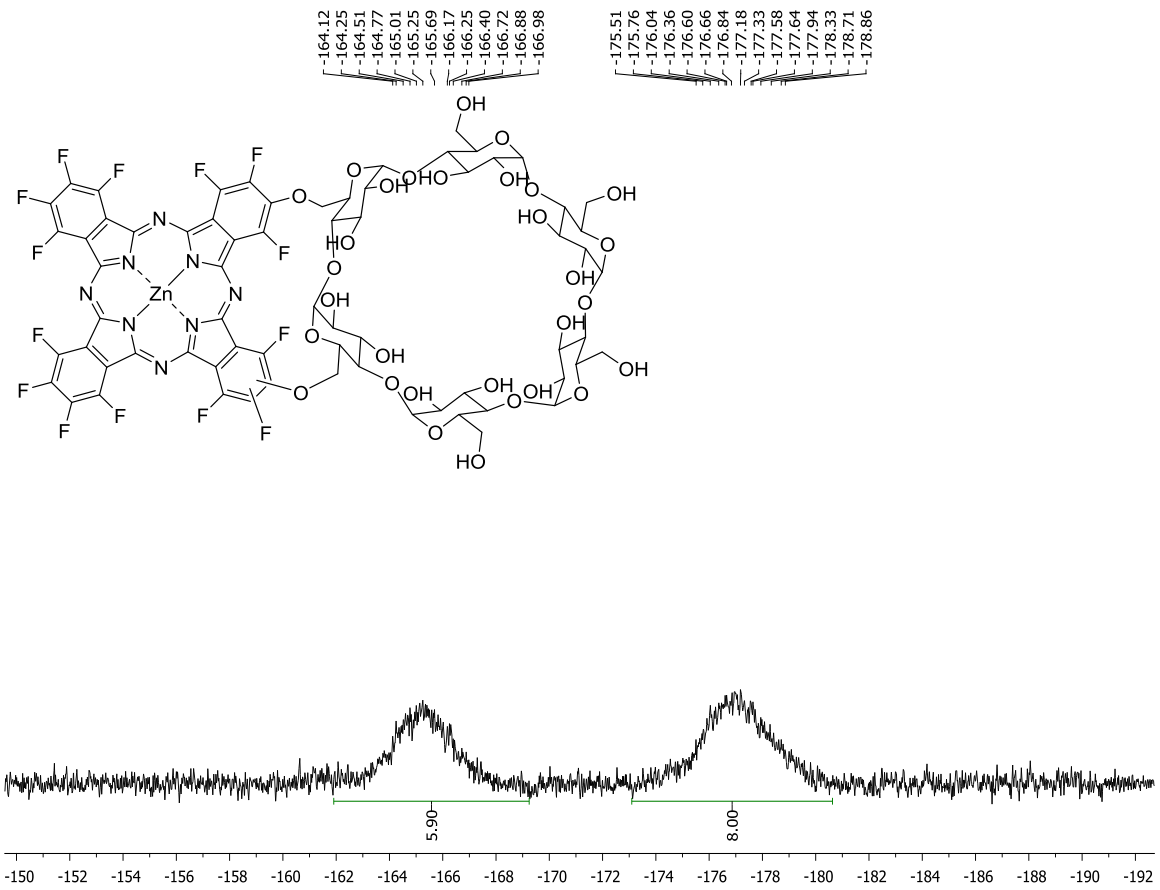

Figure 6.2 ^{19}F NMR spectrum of compound **6.1**, **Pc-α-CD** in DMSO-d_6.

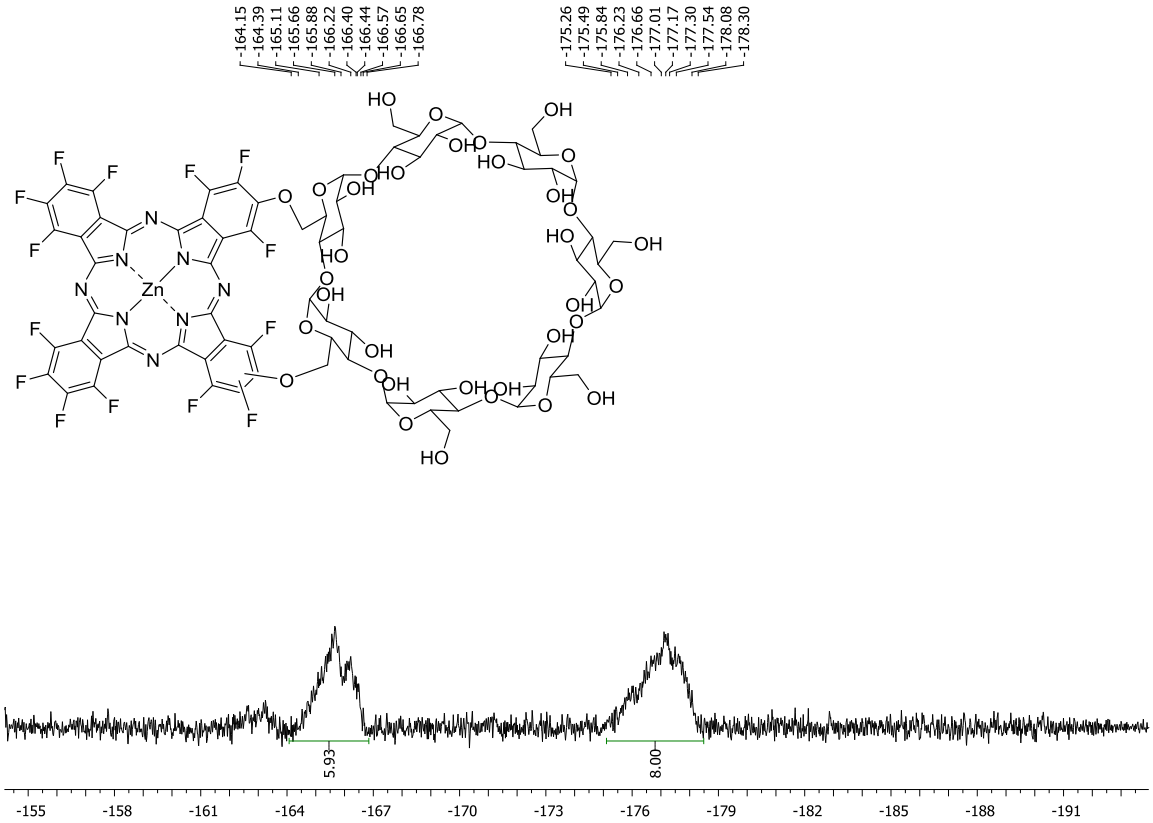

Figure 6.3 ^{19}F NMR spectrum of compound **6.2**, **Pc-β-CD** in DMSO-d_6.

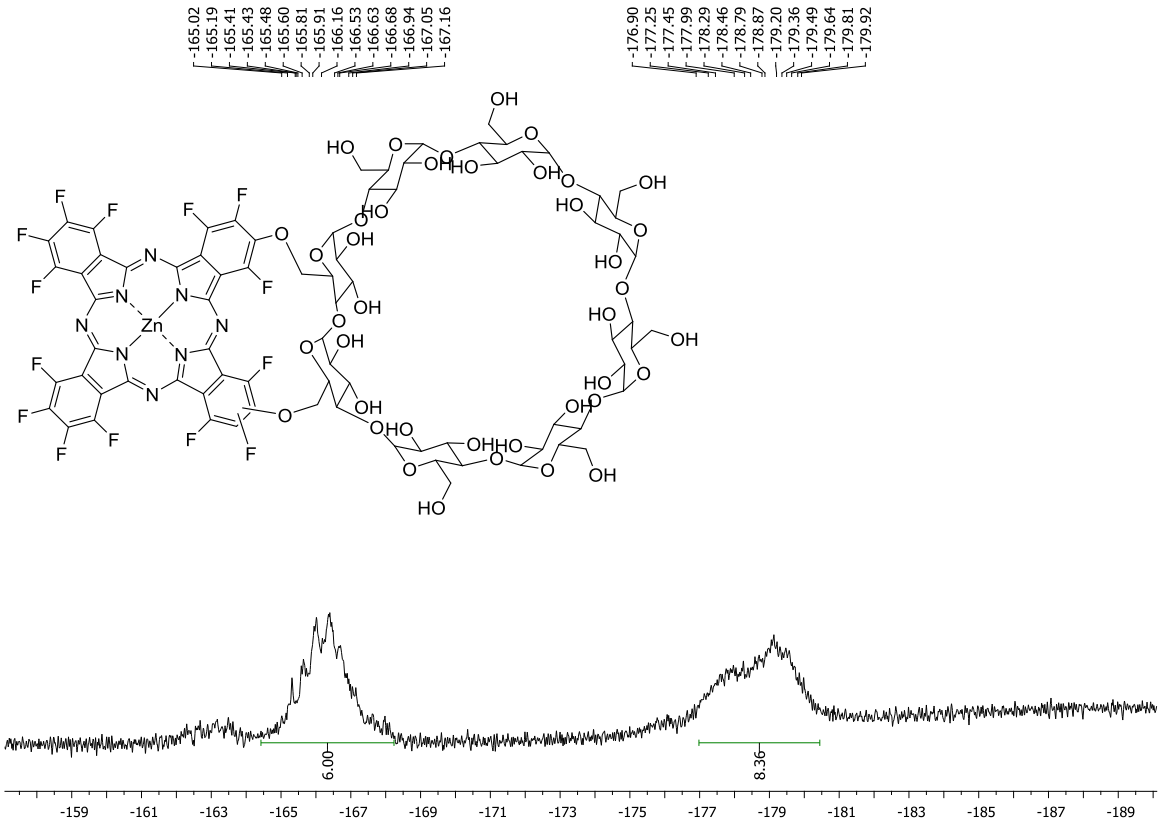

Figure 6.4 ^{19}F NMR spectrum of compound **6.3**, Pc-γ-CD in DMSO-d_6.

6.2.1 MALDI-TOF mass spectrometry of Pc-CD conjugates

Amongst the techniques used for the characterization of the Pc-CDs **6.1**-**6.3**, the most appropriate one was MALDI-TOF-MS, which is very useful for sequencing and structurally analyzing saccharide and oligosaccharide derivatives,[16,17] namely CDs[18] and glycophthalocyanines.[19] Moreover, the study by MS/MS can also be an excellent and valuable tool to assess structural characterization. The MALDI-TOF-MS spectra of the Pc-CDs showed the molecular ion peak $[M+Na]^+$ at *m/z* 1821, 1981 and 2143 for **Pc-α-CD**, **Pc-β-CD** and **Pc-γ-CD**, respectively. These $[M+Na]^+$ ions confirmed the nucleophilic substitution of two β-fluorine atoms of Pc by the corresponding α-, β- and **γ**-CDs, accompanied by elimination of two molecules of hydrofluoric acid.[20] The formation of $[M+Na]^+$ ions are typical of glycoderivatives[21,22] and it was previously observed in other glycophthalocyanines.[19] MALDI-TOF-MS/MS spectra were acquired to confirm the structural assignment of each $[M+Na]^+$ ion of **Pc-α-CD**, **Pc-β-CD** and **Pc-γ-CD**, and the spectra are displayed respectively in Figures 6.5-6.7. The MS/MS spectra of Pcs **6.1**-**6.3** showed a characteristic fragmentation owing to the preferential cleavage, whose the sequential loss number depends on the CD type coupled to the β-position of Pcs macrocycle.

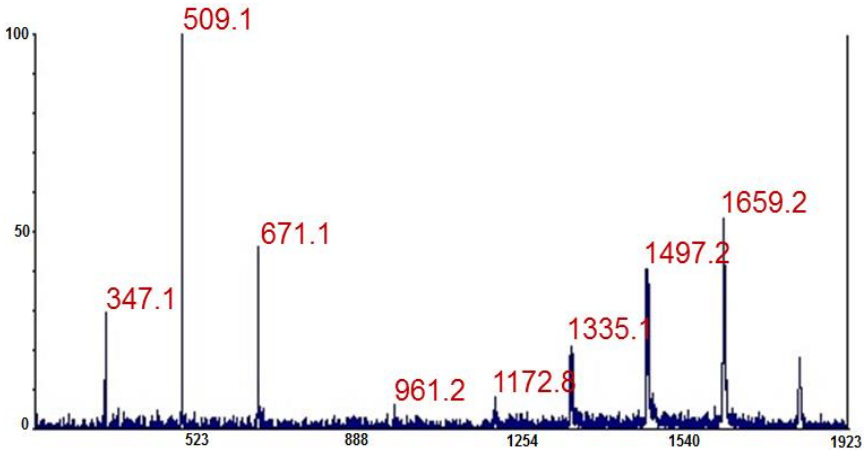

Figure 6.5 MALDI-TOF-MS/MS of the ion $[M+Na]^+$ at *m/z* 1821.2 of **6.1** (**Pc-α-CD**).

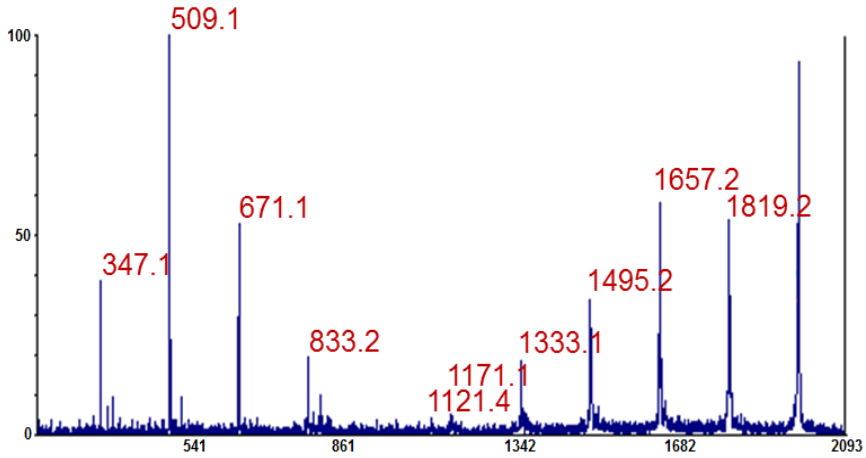

Figure 6.6 MALDI-TOF-MS/MS of the ion $[M+Na]^+$ at *m/z* 1981.2 of **6.2** (**Pc-β-CD**).

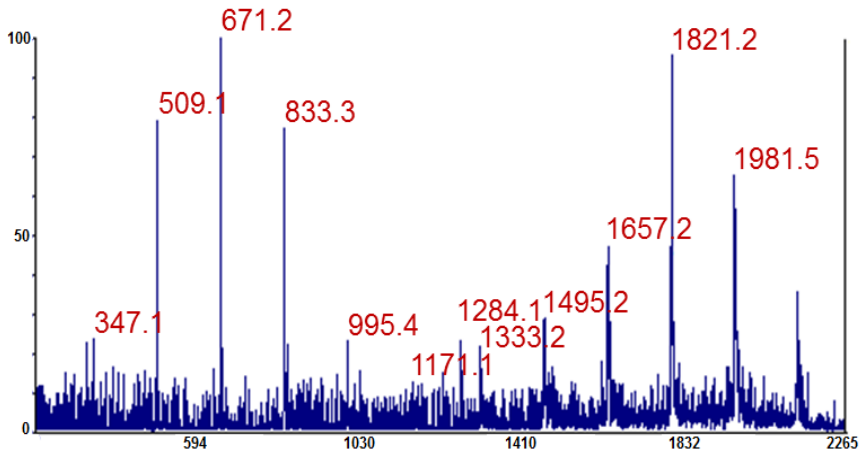

Figure 6.7 MALDI-TOF-MS/MS of the ion $[M+Na]^+$ at *m/z* 2143.3 of **6.3** (**Pc-γ-CD**).

The results obtained in the MALDI-TOF-MS/MS spectra of Pc-CDs **6.1-6.3** are summarized in Table 6.1. All MS/MS spectra demonstrated losses of one to *n*-hexose residues (-162 Da, loss of $C_5H_{10}O_5 \approx Hex_{res}$) with maximum sequential losses of 4, 5 and 6 hexose units for [**Pc-α-CD**+Na-4Hex_{res}]$^+$ (*m/z* 1173), [**Pc-β-CD**+Na-5Hex_{res}]$^+$ (*m/z* 1171) and [**Pc-γ-CD**+Na-6Hex_{res}]$^+$ (*m/z* 1171), respectively. This pattern of fragmentation confirms the presence of the CD moiety linked to the Pc. These fragmentations are rather interesting, since the maximum number of lost hexoses is equal to the number of hexose residues present in the CD (6, 7 and 8 Hex_{res} for **α-**, **β-** and **γ-CDs**, respectively) minus 2. This information confirms a scission of the structure for the Pc-CD derivatives since the two sugar units linked to the Pc core are more difficult to be eliminated. Other fragmentation pathways owing to the cleavage between the Pc and CD units lead to the formation of the product ions correspondent to the CD moiety at *m/z* 961, 1121 and 1284 for **Pc-α-CD**, **Pc-β-CD** and **Pc-γ-CD**, respectively, but with minus two water molecules

([CD-2H_2O+Na]$^+$) which confirms the size of the CD linked to Pc (Figure 6.8). The formation of these product ions rather the total CD is due to the favored cleavage in the sugar units between the C6 and the O that occurs in both sides. This leads to a product ion, with a mass equal to the mass of the sugar minus 18 (sugar-H_2O). Since this type of cleavages occur twice in these Pc-CDs, the product ion obtained in the MS/MS spectra was identified as [CD-2H_2O+Na]$^+$. In addition, the formation of sodium adducts of oligosaccharides [$Hex_{res}n$+Na]$^+$ (*n* = 2-4, 5 or 6 for **Pc-α-CD**, **Pc-β-CD** and **Pc-γ-CD**, respectively) also confirms the structural identification of these Pc derivatives. This fragmentation pattern occur at every acetal connection of the opened CD concerning to *n* (*n* = 1-6) monomeric units respectively.[23]

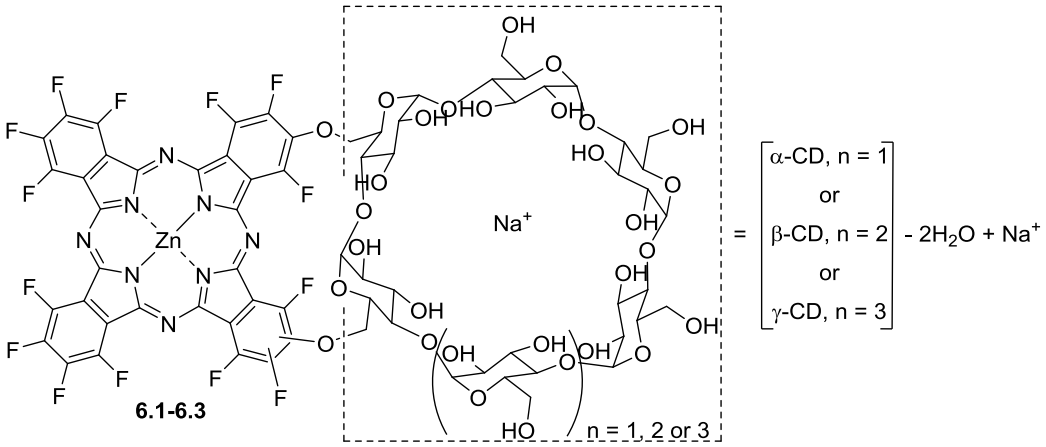

6.1, **Pc**-α-**CD** (n=1); **6.2**, **Pc**-β-**CD** (n=2); **6.3**, **Pc**-γ-**CD** (n=3)

Figure 6.8 Representation of the cleavage between Pc and CD for Pc-CDs **6.1-6.3**.

Table 6.1 Results of MS/MS experiments performed for **Pc-α-CD**, **Pc-β-CD** and **Pc-γ-CD** (**6.1-6.3**) ionized by MALDI-TOF-MS.

Produced ions from	**Neutral loss (Da)**	**6.1, Pc-α-CD** ***m/z*** **(%RA$^{Q\text{-}TOF}$)**	**6.2, Pc-β-CD** ***m/z*** **(%RA$^{Q\text{-}TOF}$)**	**6.3, Pc-γ-CD** ***m/z*** **(%RA$^{Q\text{-}TOF}$)**
[PcCD+Na]$^+$		1821	1981	2143
[PcCD+Na-1Hex_{res}]$^+$	-162	1659 (55)	1819 (55)	1981 (65)
[PcCD+Na-2Hex_{res}]$^+$	-324	1497 (40)	1657 (60)	1821 (100)
[PcCD+Na-3Hex_{res}]$^+$	-486	1335 (20)	1495 (35)	1657 (48)
[PcCD+Na-4Hex_{res}]$^+$	-648	1173 (10)	1333 (20)	1495 (30)
[PcCD+Na-5Hex_{res}]$^+$	-810	-----	1171 (7)	1333 (20)
[PcCD+Na-6Hex_{res}]$^+$	-972	-----	-----	1171 (12)
[CD+Na-2H_2O]$^+$	-860	961 (5)	1121 (5)	1284 (22)
[Hex_{res6}+Na]$^+$	-1148	-----	-----	995 (22)
[Hex_{res5}+Na]$^+$	----- /-1148/-1310	-----	833 (20)	833 (78)
[Hex_{res4}+Na]$^+$	-1150/-1310/-1472	671 (45)	671 (55)	671 (100)
[Hex_{res3}+Na]$^+$	-1312/-1472/-1634	509 (100)	509 (100)	509 (80)
[Hex_{res2}+Na]$^+$	-1474/-1634/-1796	347 (30)	347 (38)	347 (25)

In summary, MALDI-TOF-MS/MS proved to be an excellent tool to distinguish the Pc-CD dyads **6.1**-**6.3**, requiring very low quantities of sample without the need of sample manipulation. The MS/MS spectra of these samples allow differentiation of gradual loss of sugar units and confirm the structure of all three derivatives.

6.2.2 HPLC analysis of Pc-CD conjugates*

The degree of homogeneity of the Pc-CD conjugates was analysed by HPLC using the following experimental conditions: solvent A – water (33%), solvent B – methanol (20%), and Solvent C – tetrahydrofuran (47%); chromatograph column – waters spherisorb C8, 54.6 × 250 mm; flow of 0.5 mL/min; and chart speed of 1.25 mm/min.

The **Pc-β-CD 6.2** conjugate (Figure 6.9b) was found to elute as a reasonably sharp band at 20 min (uncorrected retention time) in a recently conditioned column (1/1 methanol, THF). Retention times drop down to about 18 min after a series of six injections.

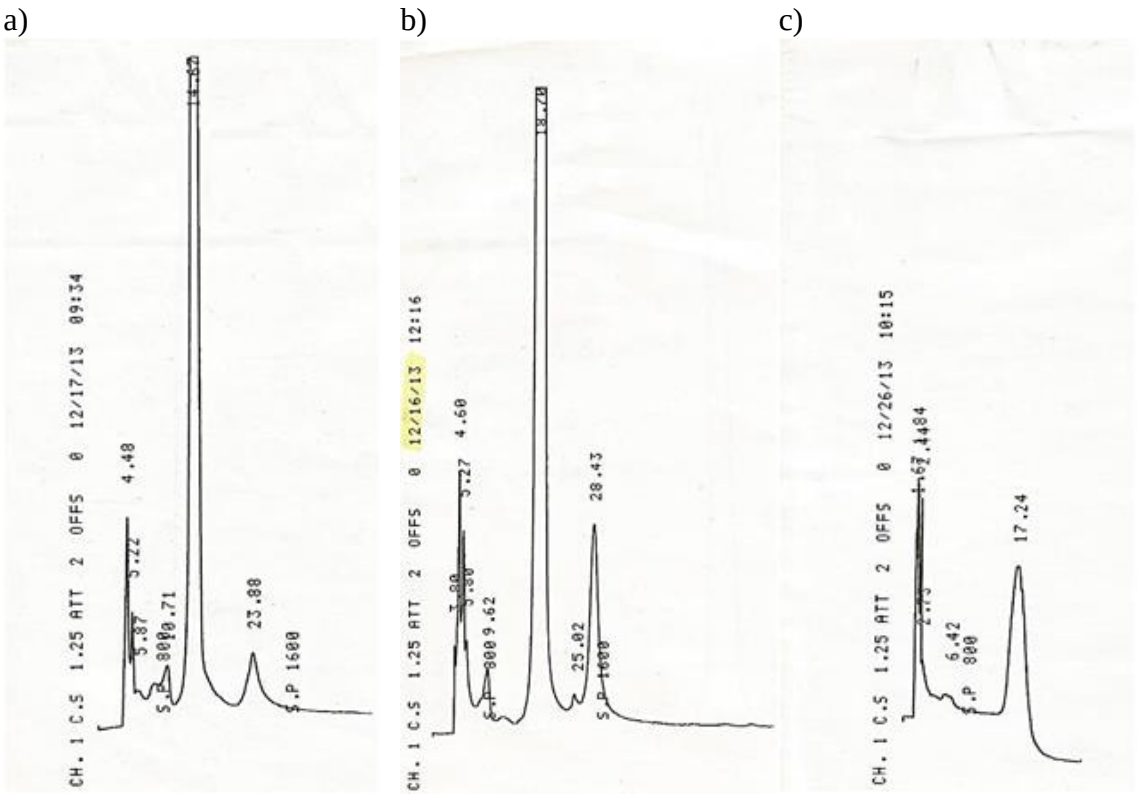

Figure 6.9 HPLC chromatogram of a) **Pc-α-CD 6.1**, b) **Pc-β-CD 6.2** and c) **Pc-γ-CD 6.3** after elution at 15, 18 and 17 min, respectively.

*These compounds were analyzed by **Prof. Fernando Domingues** and **Dr. Mónica Válega**, which kindly provided their results for a comprehensive analysis of the homogeneity of these Pc-CD conjugates.

At higher concentrations a small peak elutes at 30 min, which accounts for less than 4.5% of the area. Visible spectra were obtained for these peaks, using the built in facilities of the detector.

Under similar conditions the **Pc-α-CD 6.1** (Figure 6.9a) conjugate elutes at 15 min as a sharp band, with a small peak at 23 min, accounting for less than 2.5% of the area.

Best conditions for the elution of the **Pc-γ-CD 6.3** (Figure 6.9c) conjugate were as follows: water/methanol/THF (40/20/40) for 10 min, increasing to 0/20/80 during 5 min, with a 1.5 mL/min flow. The compound elutes at 17 min as a broad band.

6.3 Photochemical and photophysical properties of Pc-CD conjugates*

Absorption and emission spectra of Pc-CDs **6.1-6.3** were recorded on a UV-2501 PC Shimadzu and FluoroMax3 spectrophotometers, respectively, and the spectroscopic properties of the novel Pc-CDs in DMSO are summarized in Table 6.2.

6.3.1 Absorption and emission features

In DMSO and in phosphate buffered saline (PBS) buffer, the compounds exhibited very similar absorption spectra with strong Q absorption bands at the red visible region (694-699 nm, Figures 6.10A and 6.11).

It is noteworthy that the stock solutions of the conjugates were prepared at a concentration of 20 mM in DMSO and stored in the dark at room temperature (rt). The working solutions were freshly prepared prior to use by diluting the stock solutions in DMSO (Figure 6.12), phosphate buffered saline (PBS) (10 mM NaH_2PO_4, 70 mM Na_2HPO_4 and 145 mM NaCl at pH 7.6, Figure 6.13) with the concentration of DMSO being always below 1% (v/v), or DMF/H_2O (9:1 v/v, Figure 6.14).

*These compounds were tested by **Patrícia Pereira**, who kindly provided their results for a comprehensive analysis of the photophysical and photodynamic activity values of the Pc-CD conjugates.

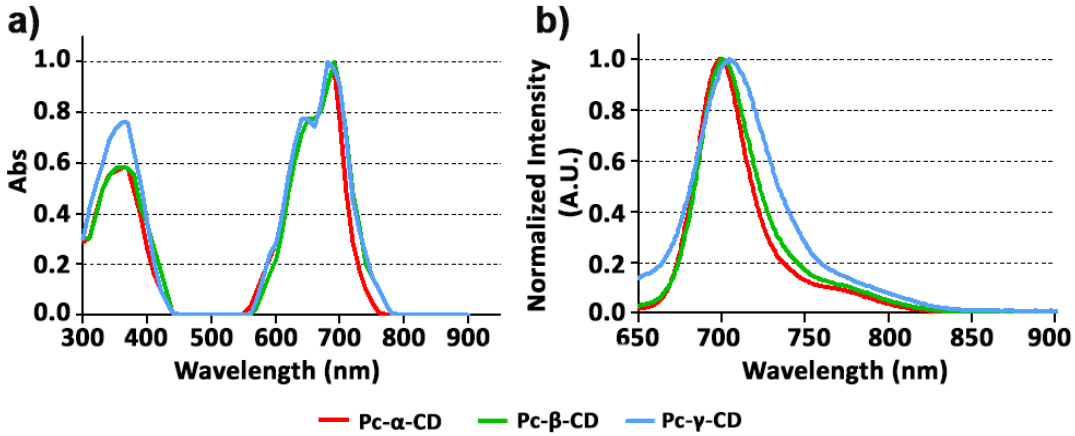

Figure 6.10 Normalized electronic a) absorption and b) emission ($\lambda_{exc.}$ = 610 nm) spectra of **Pc-α-CD**, **Pc-β-CD** and **Pc-γ-CD** in DMSO.

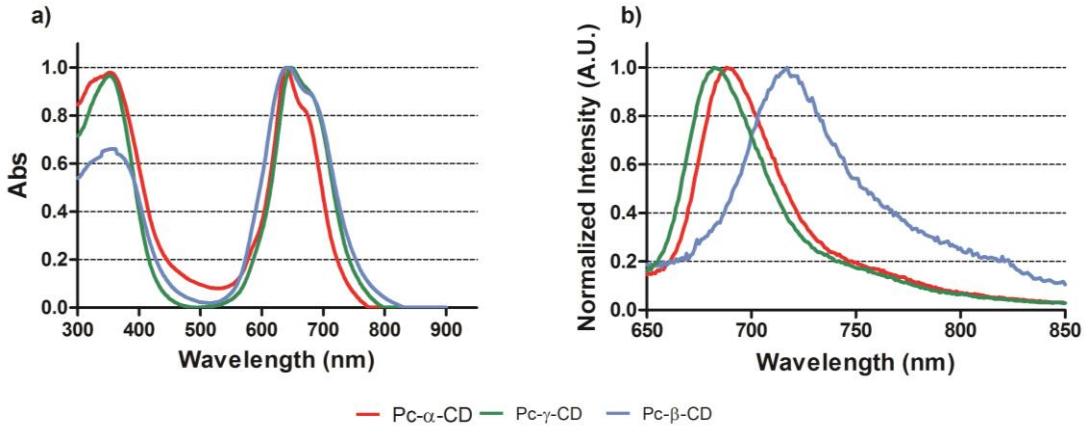

Figure 6.11 Normalized electronic a) absorption and b) emission ($\lambda_{exc.}$ = 610 nm) spectra of **Pc-α-CD**, **Pc-β-CD** and **Pc-γ-CD** in PBS.

Table 6.2 Photophysical data of Pc-CDs **6.1**-**6.3** in DMSO.

Compound	**Q-band λ_{max} (nm)**	**log ε**	**$\lambda_{emission}$ (nm)[a)]**	**Stokes Shift (nm)**	**Φ_F[b)]**
Pc-α-CD (6.1)	694	3.67	698	4	0.28 ± 0.02
Pc-β-CD (6.2)	696	3.03	700	4	0.10 ± 0.02
Pc-γ-CD (6.3)	699	3.91	705	6	0.18 ± 0.02

[a)]OD = 0.03-0.05; excited at 610 nm; [b)]using **ZnPc** in DMSO as reference (Φ_F = 0.20)[24].

The Pc-CDs in DMSO followed the Lambert-Beer's law (Figure 6.12), suggesting that solubility of these conjugates was not compromised for concentrations ranging from 0 to 50 μM. Upon excitation at 610 nm, all conjugates showed in DMSO the same emission behaviour, with a emission band in the red spectral region at 698-705 nm (Figure 6.10B)

and fluorescence quantum yields (Φ_F) of 0.10-0.28 (Table 6.2), relative to the unsubstituted phthalocyaninato zinc(II) (**Pc**, Φ_F = 0.20 in DMSO).[24] The fluorescence quantum yields of the Pc-CDs decrease in the order **Pc-α-CD** > **Pc-γ-CD** > **Pc-β-CD**.

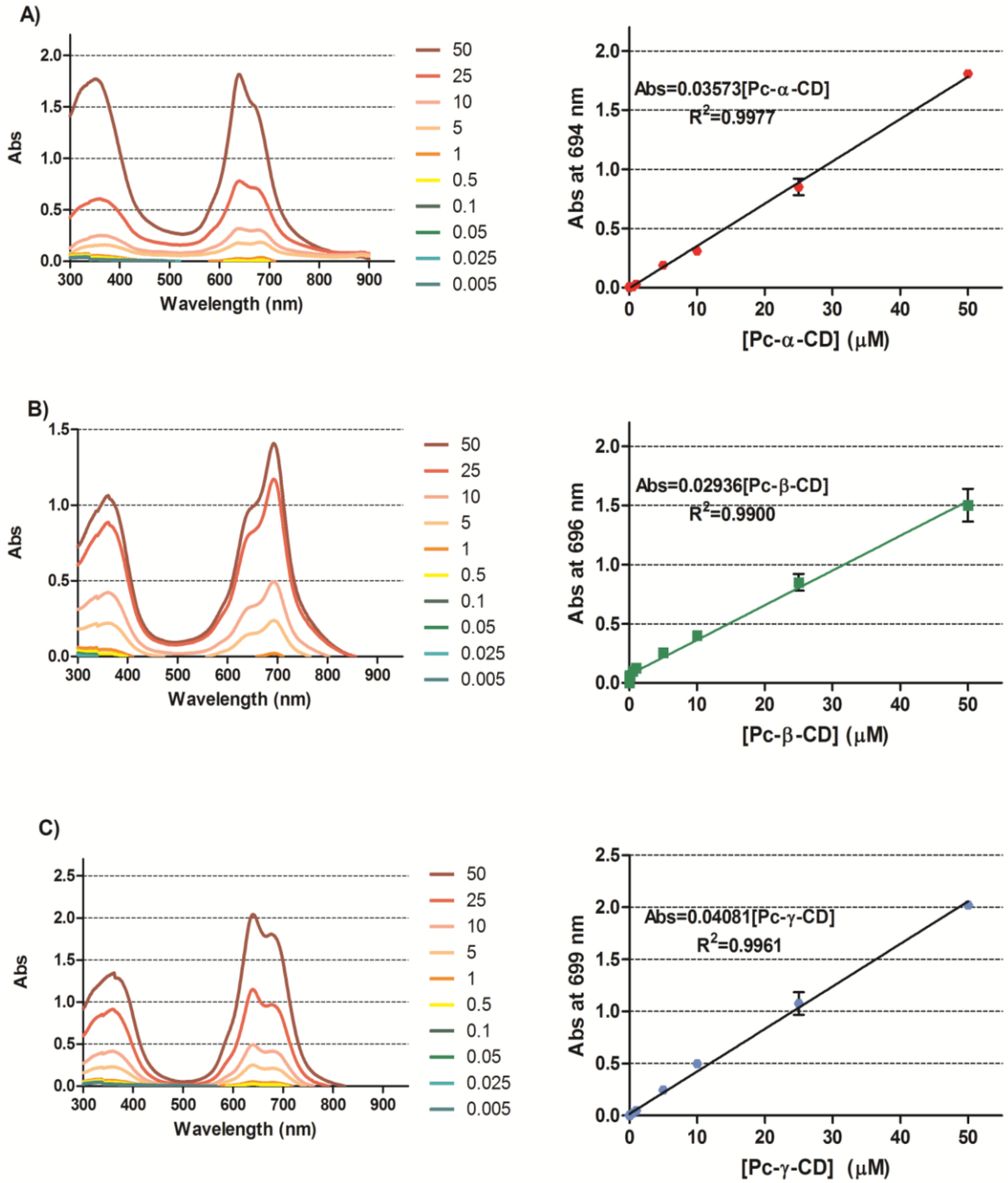

Figure 6.12 UV-Vis spectra of A) **Pc-α-CD 6.1**, B) **Pc-β-CD 6.2** and C) **Pc-γ-CD 6.3** in DMSO at different concentrations 0 to 50 μM. The inset of each spectrum plots the Q-band absorbance *versus* the concentration of the Pc-CD in DMSO, and the line represents the best-fitted straight line.

In PBS the emission spectra of **Pc-α-CD** and **Pc-γ-CDs** demonstrated similar shapes with maximum emission bands respectively at 688 and 682 nm (Figure 6.11). In the same medium **Pc-β-CD** demonstrated a bathochromic shift with a maximum emission band at 717 nm. The spectral shape of the emission excitation spectra of all conjugates, in DMSO and in PBS, closely resemble the absorption spectra and therefore confirm the existence of single chemical species (data not shown).

6.3.2 Solubility of the Pc-CD dyads

The water solubility of the new PSs is a critical parameter for the photodynamic effect, as low solubility compromises their bio-distribution, uptake by the cells and ROS production.[25,26] The solubility of Pc-CDs **6.1-6.3** in PBS (with <1% v/v DMSO) was investigated for different concentrations (Figure 6.13), in close resemblance conditions to those used in the *in vitro* PDT assays.

The solubility of the Pc-CDs decreased in the order **Pc-γ-CD** ≈ **Pc-α-CD** > **Pc-β-CD** in PBS buffer (<1% v/v DMSO). The Q absorption bands of **Pc-α-CD** and **Pc-γ-CD** were significantly broadened, but still followed the Lambert-Beer's law, suggesting that solubility of these conjugates was not compromised under these conditions. However, the absorption spectra of **Pc-β-CD** indicated that the solubility of this compound is lower in PBS buffer (Figure 6.13) than in DMSO (Figure 6.12). The self-aggregation of **Pc-β-CD** can be a possible explanation for its lower water solubility when compared with **Pc-α-CD** and **Pc-γ-CD**. In fact, the self-aggregation of drug-loaded CDs in water is a well-known phenomenon,[27] which can be caused by the self-aggregation tendency of β-CD native structure,[28] since its molecular dimensions are optimal for the formation of an intramolecular hydrogen bond within the CD molecule, preventing its hydrogen bond formation with surrounding water molecules and reducing its solubility.[28]

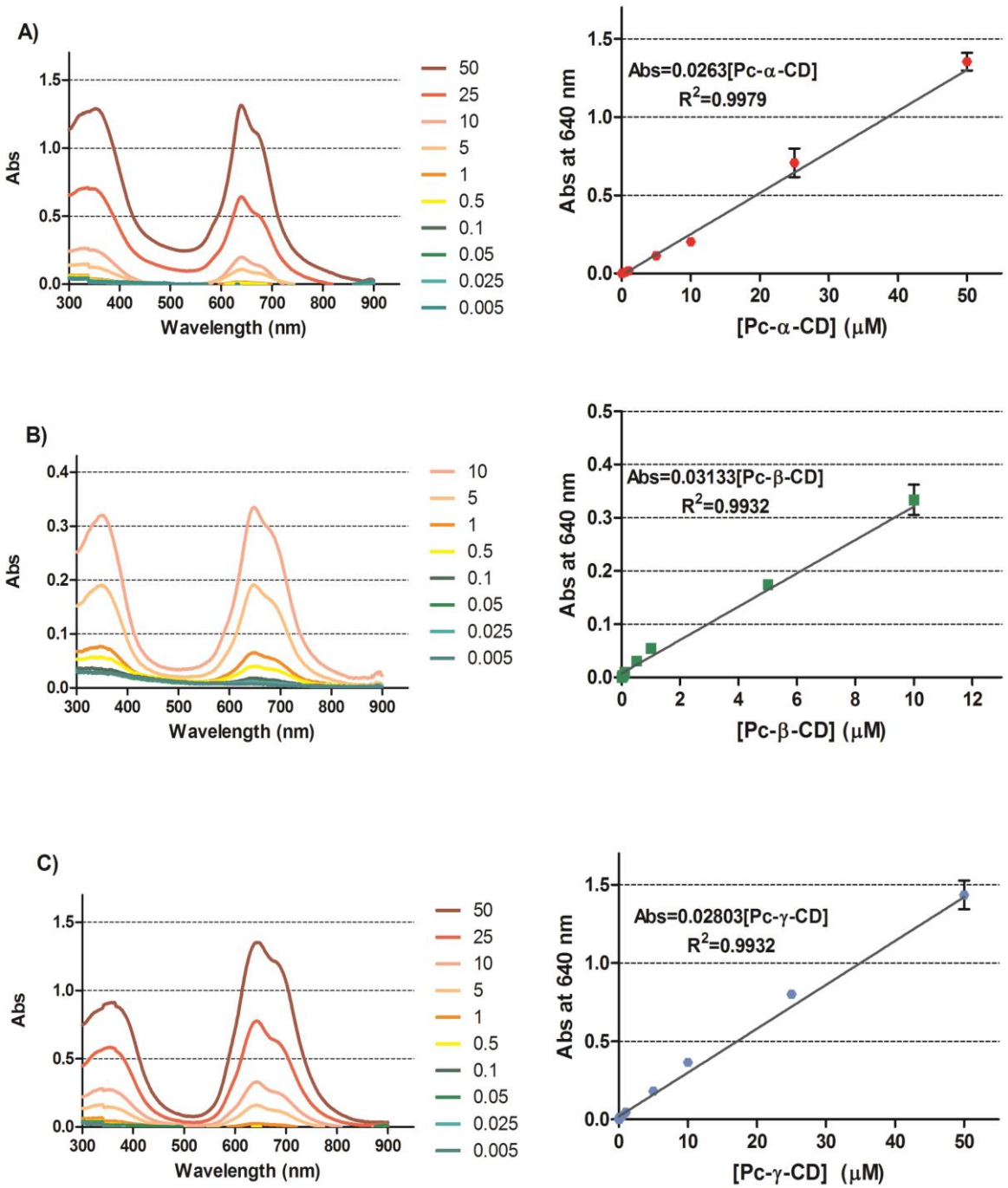

Figure 6.13 UV-Vis spectra of A) **Pc-α-CD 6.1**, B) **Pc-β-CD 6.2** and C) **Pc-γ-CD 6.3** in PBS buffer (<1% v/v DMSO) at concentrations for **Pc-α-CD 6.1** and **Pc-γ-CD 6.3** from 0 to 50 μM, and for **Pc-β-CD 6.2** from 0 to 10 μM. The inset of each spectrum plots the Q-band absorbance *versus* the concentration of the Pc-CD in PBS, and the line represents the best-fitted straight line.

6.3.3 Photostability and ability of the Pc-CD conjugates to generate $^1O_2$

Considering the potential application of Pc-CDs **6.1-6.3** as new PSs, their photostability and ability to generate $^1O_2$ were determined. The photodegradation of PSs impairs their photodynamic effectiveness, as it causes the decrease of PS concentration. For the photostability assays, solutions of Pc-CDs **6.1-6.3** at 1 µM were freshly prepared in PBS buffer (with 0.5% v/v DMSO) and kept in the dark at room temperature. The photostability of Pc-CDs **6.1-6.3** were determined by monitoring the absorption Q-band intensity at different irradiation times. The irradiation experiments were performed in magnetically stirred cuvette solutions (with 2 mL of sample), over a period of 40 min with white (400-800 nm) and red light (620-750 nm) delivered by an illumination system (LC-122 LumaCare, London) equipped with a halogen/quartz 250 W lamp coupled the selected interchangeable optic fibre probe (400-800 nm or 620-750 nm). The lights were delivered at an irradiance rate of 150 mW.cm^{-2}, measured with an energy meter Coherent FieldMaxII-Top combined with a Coherent PowerSens PS19Q energy sensor. The absorbance at 640 nm (maximum absorption band in PBS) was determined at 0, 1, 3, 4, 5, 10, 15, 20, 25, 30 and 40 min periods of time after irradiation. The results were expressed as follows:

$$Photostability\ (\%) = \frac{Abs\ at\ a\ given\ time\ of\ irradiation\ (t = x\ min)}{Abs\ before\ irradiation\ (t = 0\ min)}.$$

The Pc-CD conjugates **6.1-6.3** exhibited similar photostability when compared to **ZnPc** over the investigated irradiation period (40 min; Table 6.3). These results demonstrated that the derivatization of **Pc** with α-, β- and γ-CDs did not compromise their photostability.

It has been demonstrated that the ability of PSs to generate $^1O_2$ is an important feature in the photosensitizing process, since this reactive oxygen specie is important in the induction of cell death pathways which will lead to the destruction of tumours.[8] The ability of Pc-CD conjugates **6.1-6.3** to generate $^1O_2$ was evaluated in DMF/H_2O (9:1 v/v) and in DMSO. On these two solvents the three conjugates strictly followed the Lambert-Beer's law between 0 to 50 µM (Figures 6.12 and 6.14), suggesting that the solubility of Pc-CD conjugates was not compromised during the study.

Table 6.3 Photostability of 1 µM of **ZnPc** and Pc-CDs **6.1-6.3** in PBS, after irradiation with white (400-800 nm) and red light (620-750 nm) at an irradiance rate of 150 mW.cm^{-2} at different periods of time (0-40 min).

Compounds	Light	Irradiation time (min)										
		0	**1**	**3**	**4**	**5**	**10**	**15**	**20**	**25**	**30**	**40**
ZnPc[a]	white	100	99	98	97	97	96	94	93	92	91	90
	red	100	99	98	98	98	97	97	96	96	96	96
Pc-α-CD	white	100	99	98	98	98	97	97	96	95	95	95
	red	100	100	100	100	100	100	100	100	100	99	99
Pc-β-CD	white	100	97	95	95	94	94	94	94	94	94	94
	red	100	99	99	98	97	96	95	95	94	94	93
Pc-γ-CD	white	100	99	99	99	99	99	99	96	96	96	96
	red	100	99	99	99	99	99	99	99	99	98	98

[a]The photostability of **ZnPc** was determined in PBS buffer containing 20% of DMSO due to its low solubility in aqueous solution. The results in percentage are calculated by the ratio of residual absorbance at 640 nm at different periods of time and absorbance before irradiation.

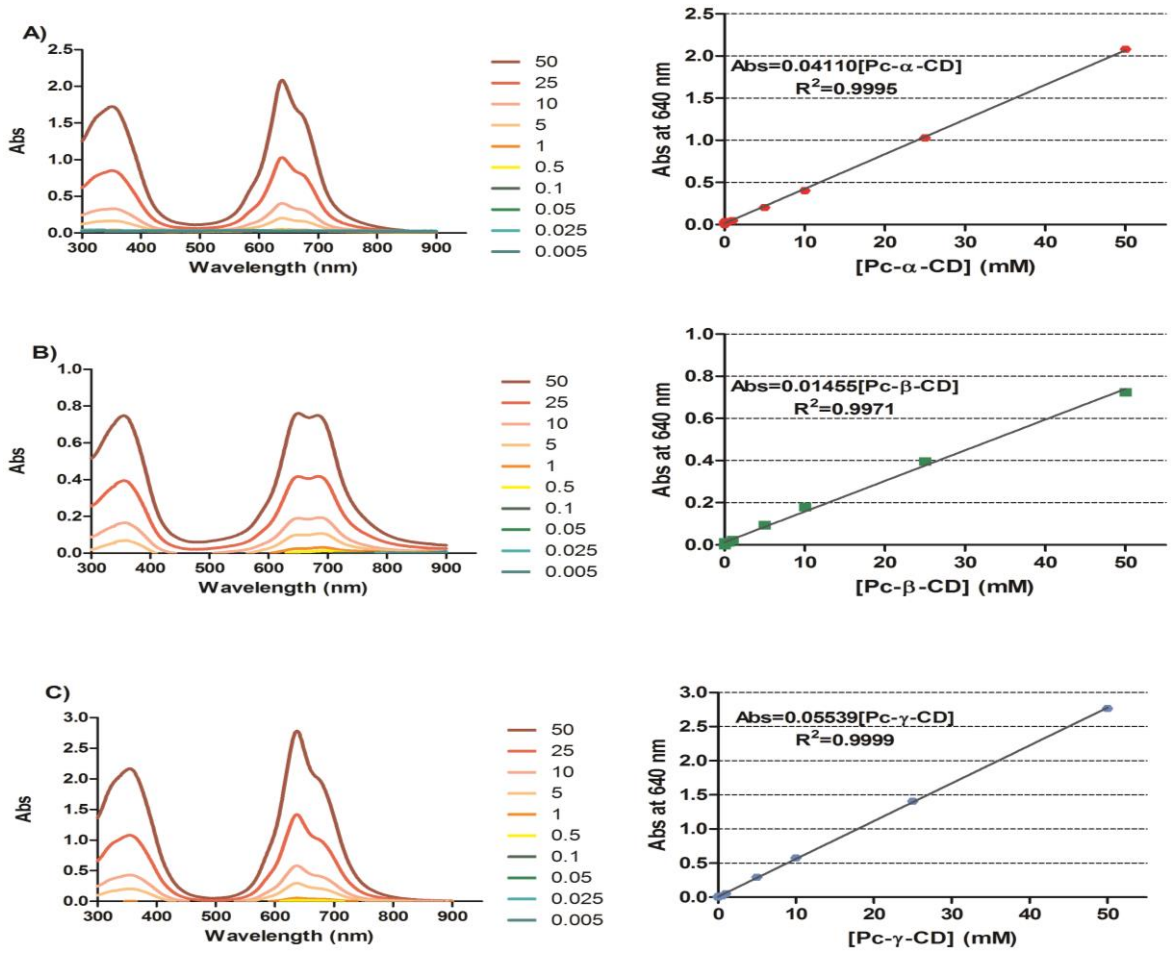

Figure 6.14 UV-Vis spectra of A) **Pc-α-CD 6.1**, B) **Pc-β-CD 6.2** and C) **Pc-γ-CD 6.3** in DMF/H_2O (9:1 v/v) at different concentrations 0 to 50 µM. The inset of each spectrum plots the Q-band absorbance *versus* the concentration of the Pc-CD in DMF/H_2O (9:1 v/v), and the line represents the best-fitted straight line.

The ability of Pc-CDs to generate $^1O_2$, was performed by a steady-state method using 1,3-diphenylisobenzofuran (DPBF) as the $^1O_2$ acceptor; the non-substituted **ZnPc** was used as the $^1O_2$ generator reference.[29,30] The decrease in the absorption of DPBF (monitored at 415 nm) was higher in the presence of all Pc-CDs (Figures 6.15 and 6.16) with the conjugates **6.1** and **6.3** showing similar ability to photooxidize DPBF when compared to **ZnPc**. These results demonstrated that **ZnPc** moiety did not lose its sensitizing properties after binding with α- and γ-CDs. **Pc-β-CD** demonstrated to be a much less efficient $^1O_2$ generator, which could be partially explained by its low solubility in aqueous media like PBS (Figure 6.13).

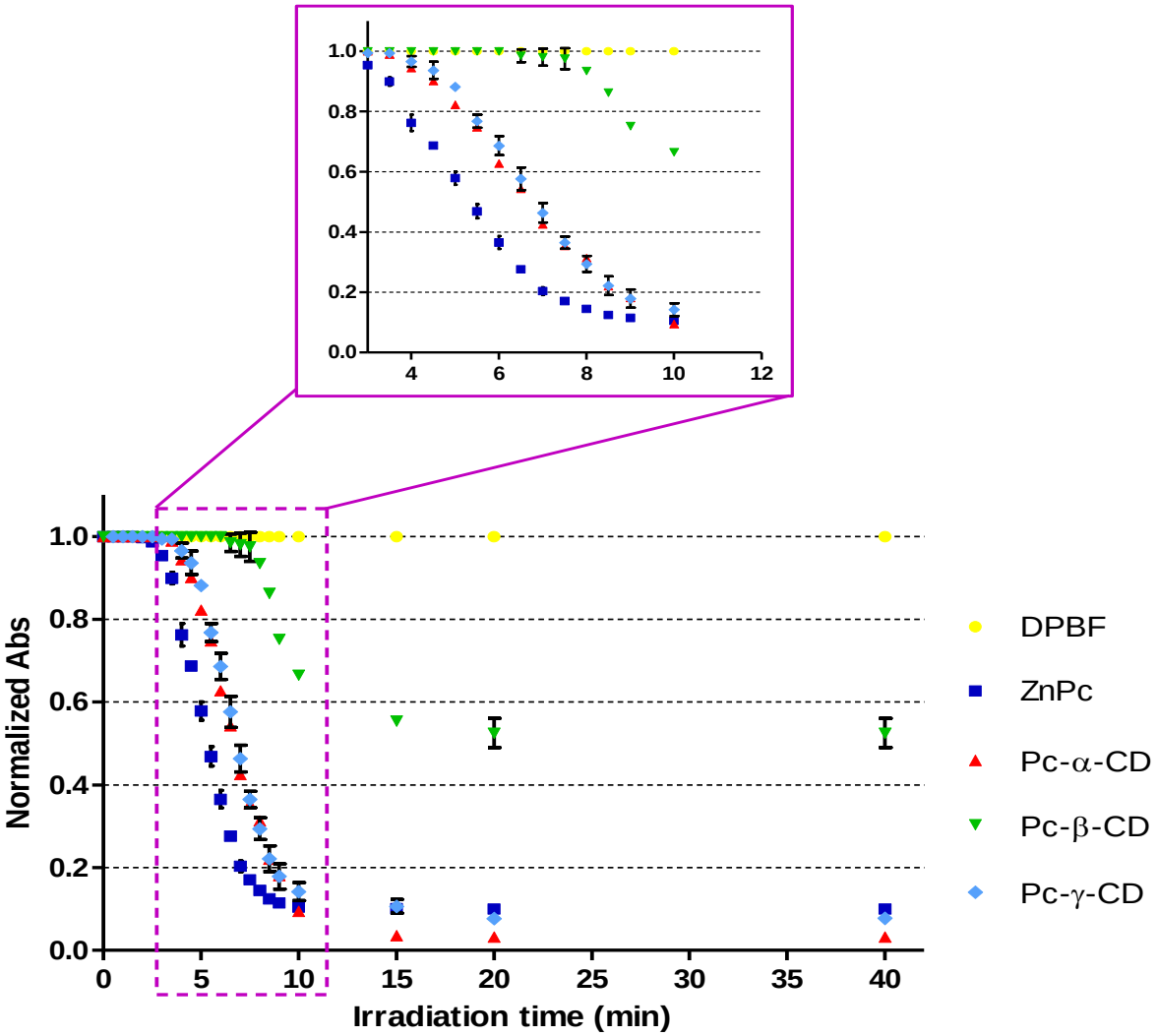

Figure 6.15 Photo-oxidation of DPBF (33 µM) in DMF/H_2O (9:1) with or without **Pc-α-CD 6.1**, **Pc-β-CD 6.2**, **Pc-γ-CD 6.3** or **ZnPc** at 0.33 µM, after irradiation with a LEDs array system emitting red light at a irradiance of 10 mW.cm^{-2}. The DPBF absorbance was recorded at 415 nm.

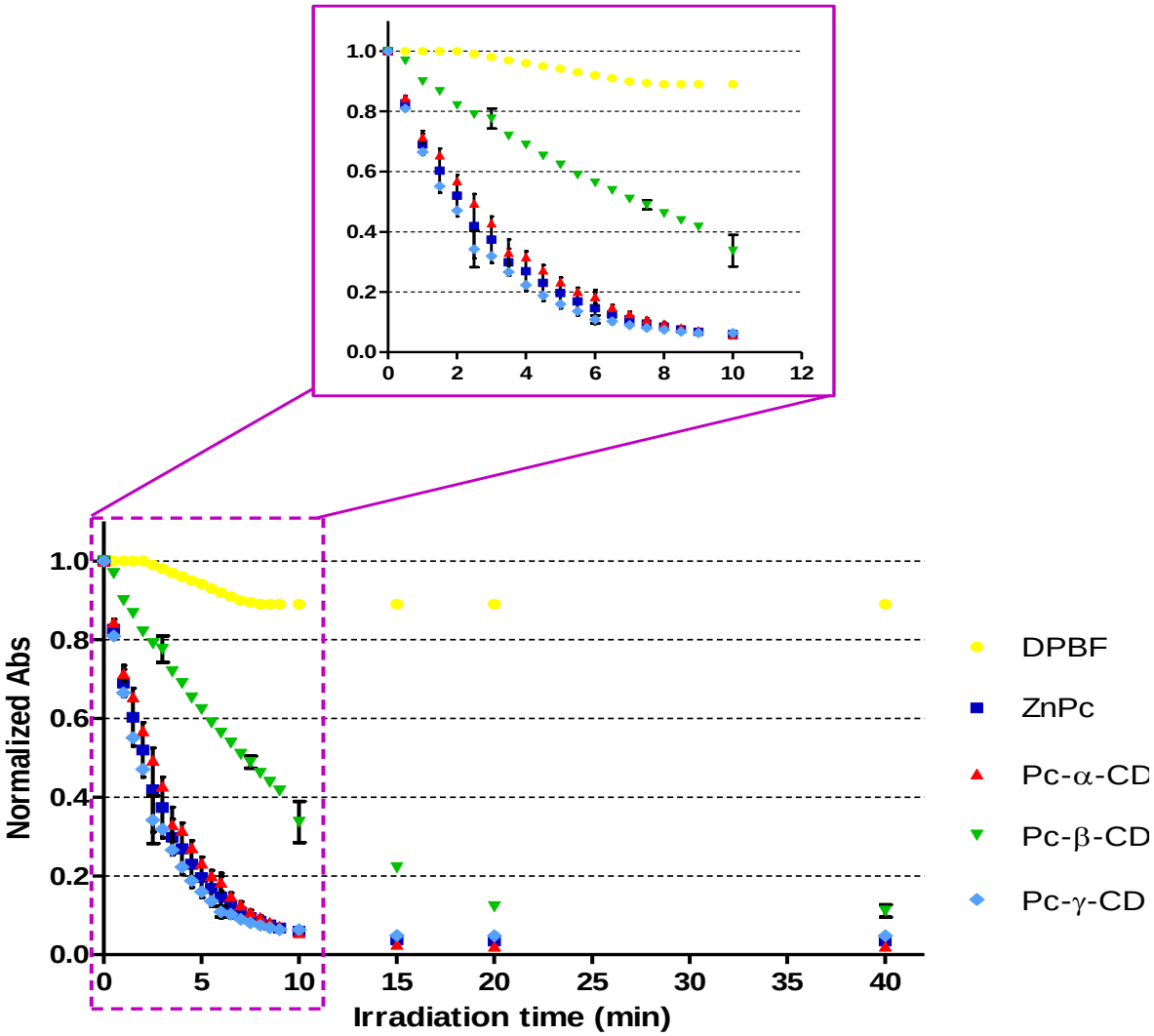

Figure 6.16 Photo-oxidation of DPBF (33 µM) in DMSO with or without **Pc-α-CD 6.1**, **Pc-β-CD 6.2**, **Pc-γ-CD 6.3** or **ZnPc** at 0.33 µM, after irradiation with a LEDs array system emitting red light at a irradiance of 10 mW.cm^{-2}. The DPBF absorbance was recorded at 415 nm.

6.3.4 Human serum albumin interaction assays

Knowing that human serum albumin (HSA) is able to bind anticancer drugs and deliver them to the target organs, the interaction of Pc-CDs **6.1-6.3** with the abundant plasma protein HSA was studied by fluorescence quenching of tryptophan residues in HSA solutions in the presence of increase concentration of Pc-CDs (0-10 µM in PBS <1% v/v DMSO).[29]

For the determination of Pc-CDs interaction with HSA, 2 mL of HSA solution was titrated with increasing additions of Pc-CDs, keeping always the final amount of DMSO

below 1% (v/v). The fluorescence spectrum of the HSA´s tryptophan residues were acquired for the wavelength range between 300-450 nm upon excitation at 280 nm, showing a characteristic emission maximum band at 335 nm (Figure 6.17). The excitation and emission slits width were set at 2.0 nm. The fluorescence quenching curves were obtained by plotting the tryptophan residues quenching (in percentage) against conjugates concentration. The tryptophan residues quenching (in percentage) was calculated, as follows:

$$Trypthophan\ residues\ quenching\ (\%) = \frac{(F_0 - F)}{F_0} \times 100$$

The K_a and *n* values presented in Table 6.4 were determined by plotting the *log((*F_0*-F)/F)* against *log(Pc-CD concentration)*, giving a linear plot, where *log(*K_a*)* and *log(n)* are the ordinate at the origin and slope, respectively.

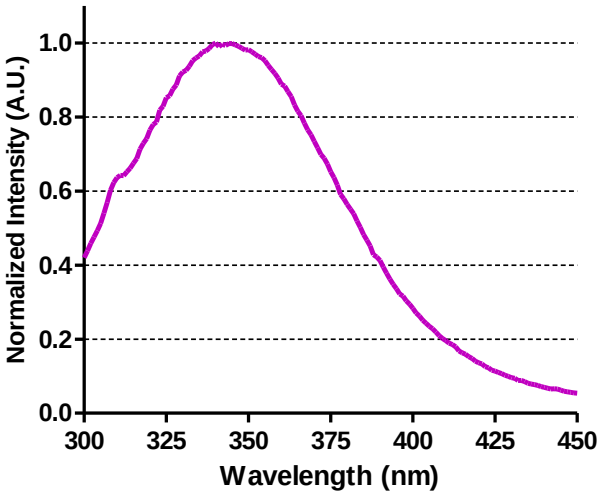

Figure 6.17 Emission spectra of HSA at 2 µM in PBS ($\lambda_{exc.}$ at 280 nm).

The effects of DMSO on HSA emission quenching were tested, since the stock solutions of the Pc-CDs were prepared in this organic solvent. Over a concentration range of 0-1% (v/v), DMSO did not quench HSA emission (data not shown). The addition of Pc-CDs to HSA led to fluorescence quenching of tryptophan residues (Figure 6.18), which was lower for the compound **6.2** when compared with compounds **6.1** and **6.3**.

The binding constant (K_a) and the number of binding sites (n) of compounds **6.1**-**6.3** were determined as described in the literature[29] and compared with the ones obtained

for **ZnPc** (K_a = 7.3×10^3 M^{-1} and n = 0.8). The K_a values of the Pc-CDs decreased in the order **6.3** (**Pc-γ-CD**) > **6.1** (**Pc-α-CD**) > **ZnPc** > **6.2** (**Pc-β-CD**) (Table 6.4).

Table 6.4 Binding constant (K_a) and number of binding sites (n) of compounds **6.1**-**6.3** to HSA.

Compound	HSA interaction	
	K_a (M^{-1})	n
Pc-α-CD (6.1)	3.0 × 10^5	1.2
Pc-β-CD (6.2)	1.1 × 10^2	1.3
Pc-γ-CD (6.3)	7.8 × 10^5	0.9

The number of binding sites indicates that there is only one binding site for the Pc-CDs closes to the tryptophan residues of HSA (Table 6.4). The values of K_a obtained for Pc-CDs **6.1** and **6.3** are in accordance to the ones obtained for Pcs glycodendritic conjugates.[29]

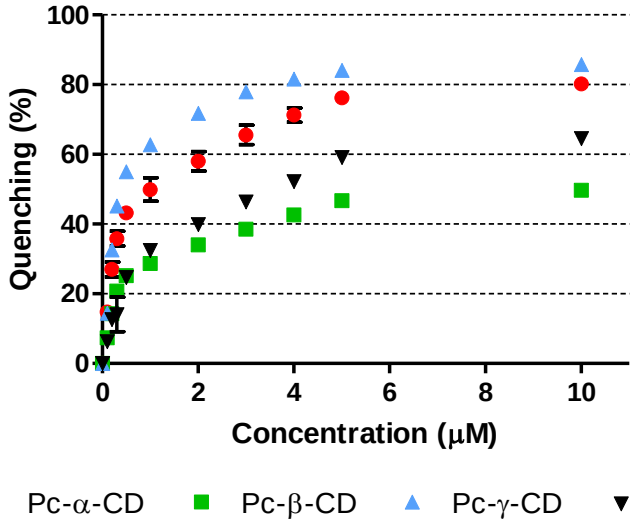

Figure 6.18 Emission quenching curves of 2 μM of HSA after addition of the Pc-CDs **6.1**-**6.3** at concentrations ranging from 0 to 10 μM). Quenching % = (F_0-F)/(F_0)×100, where F_0 and F are the HSA emission intensities in the absence and presence of the Pc-CDs ($\lambda_{exc.}$ = 280 nm and $\lambda_{em.}$ = 335 nm).

Considering that Pc-CDs in PBS have an absorption band (Figure 6.11) in the region of the emission spectra of the HSA protein (Figure 6.17), two additional experiments demonstrates that HSA emission quenching was due to the interaction of HSA with Pc-CDs. On the first experiment, the emission spectra of Pc-CD solutions in the

presence and absence of HSA were recorded after excitation at 610 nm (Figure 6.19). HSA by itself did not produce a signal over the spectral region (data not shown). Note the large increase in emission spectra associated with combining the HSA and the photosensitizer.

The emission and electronic absorption spectra of Pc-CDs were also recorded after addition of HSA at 2 µM, keeping always the final concentration of DMSO below 1% (v/v). The emission spectra of Pc-CDs were acquired for the wavelength range of 650-850 nm. The excitation and emission slits width were set at 2.0 nm.

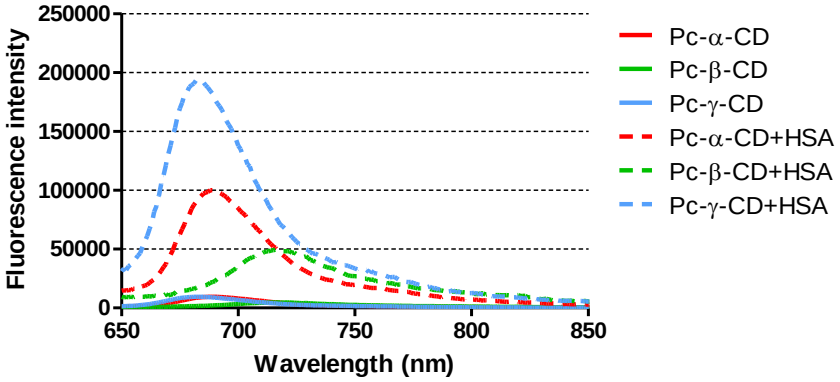

Figure 6.19 Emission spectra of Pc-CDs in PBS before and after addition of HSA ($\lambda_{exc.}$ at 610 nm).

The increase of Pc-CD emission suggests the formation of a complex that substantially enhances the emission characteristics of the photosensitizer. On the second experiment, the absorption spectra of Pc-CDs were recorded upon addition of HSA protein (Figure 6.20). After addition of HAS, it was observed hypochromicity without any Q-band shift, which unequivocally confirms the existence of interaction between HSA and Pc-CDs. The Pc-CD conjugates and their interaction with HAS are not comparing with **ZnPc** reference because this one aggregates in PBS.

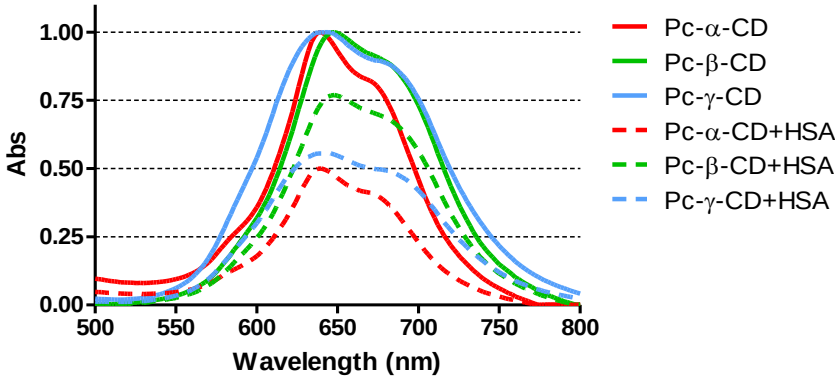

Figure 6.20 Absorption spectra of Pc-CDs in PBS before and after addition of HSA.

6.3.5 *In vitro* photodynamic activities of Pc-CD conjugates

The *in vitro* photosensitizing efficiency of Pc-CDs **6.1-6.3** was performed in the human bladder cancer cell line (UM-UC-3) derived from transitional cell carcinoma, which is the most common malignant tumour arising from the urothelium. The cytotoxicity of Pc-CDs **6.1-6.3** was investigated in the presence and absence of light using 3-(4,5-dimethylthiazol-2-yl)-2,5-diphenyltetrazolium bromide (MTT) colorimetric assay (Figures 6.21 and 6.22).

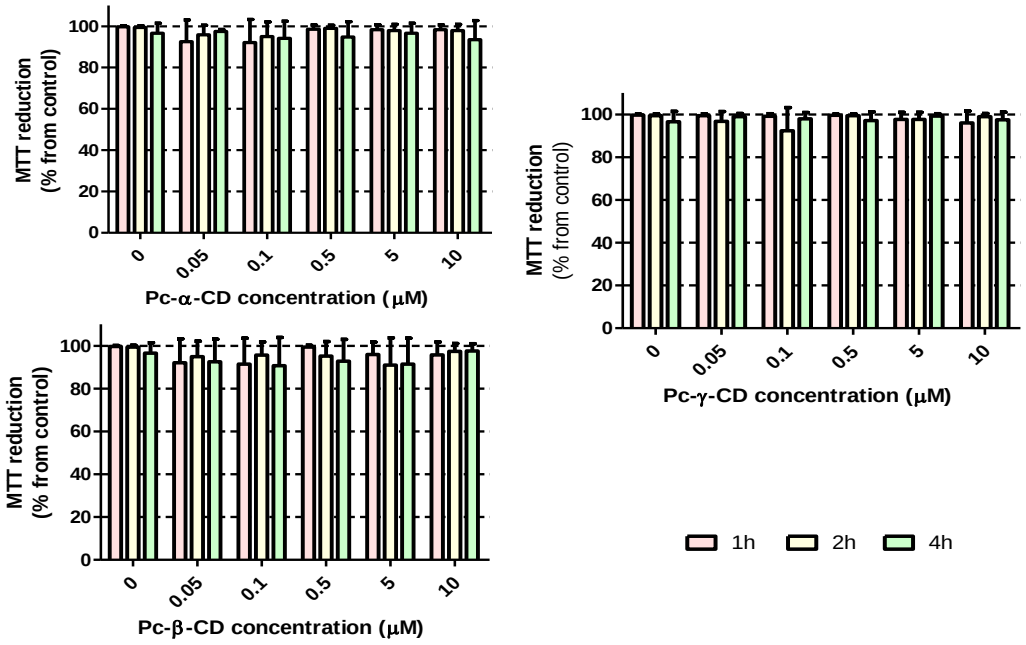

Figure 6.21 Dark toxicity of Pc-CDs **6.1-6.3** in UM-UC-3 bladder cancer cells. Cells were incubated in darkness with Pc-CDs at different concentrations (0, 0.05, 0.1, 0.5, 5 and 10 µM in PBS buffer) for increasing uptake times (1, 2 and 4 h). Cytotoxicity was assessed 24 h after treatment using the MTT colorimetric assay. The percentage of cytotoxicity was calculated relatively to control cells (cells incubated with PBS in darkness) at the respective uptake time. Data are the mean value ± S.D. of at least three independent experiments performed in triplicates.

In this assay, the yellow colored MTT is reduced by mitochondrial dehydrogenases in living cells to a blue-colored formazan precipitate. The absorption of dissolved formazan correlates with the number of living cells. Pc-CDs solutions **6.1-6.3** were non-toxic in the dark up to 10 µM and uptake time up to 4 h. For the PDT assays, the bladder cancer cells were incubated in darkness with Pc-CDs at different concentrations (0-1 µM) during 3 h and irradiated with a white (400–800 nm) or red (620–750 nm) light source, both at an irradiance rate of 50 mW.cm^{-2}. Variable irradiation times of 20 and 40 min were

performed for giving a demonstration of irradiation-time dependence of cell killing. Compounds **6.1** and **6.3** demonstrated a phototoxic effect in a concentration- and irradiation time-dependent manner (Figure 6.22).

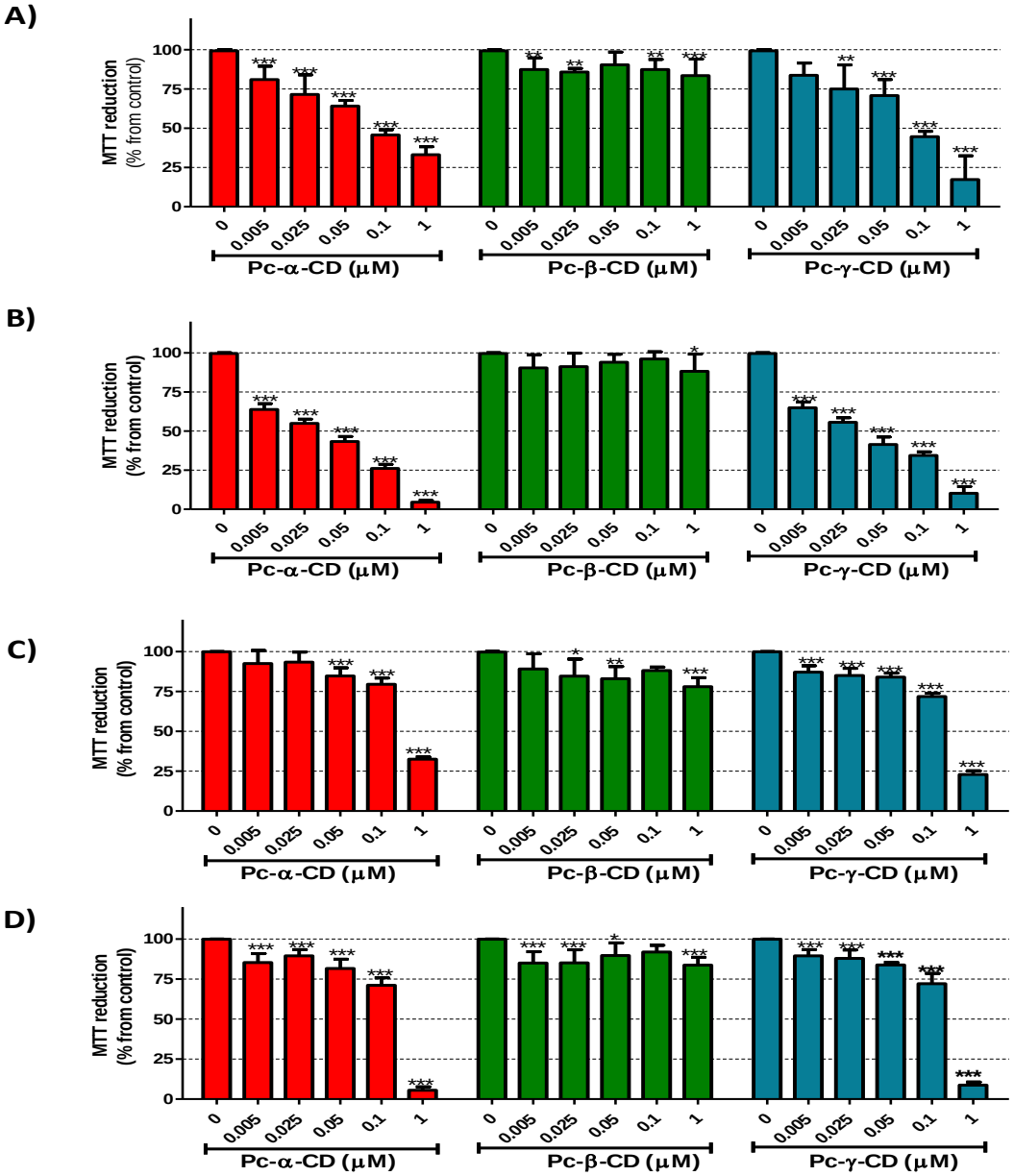

Figure 6.22 Photocytotoxic effects after PDT with Pc-CDs **6.1-6.3** in UM-UC-3 bladder cancer cells. Cells were incubated in darkness with Pc-CDs **6.1-6.3** at different concentrations (0, 0.005, 0.025, 0.1 and 1 μM in PBS) for 3 h and irradiated with red light (620-750 nm) for 20 min (A) and 40 min (B), or with white light (400–800 nm) for 20 min (C) and 40 min (D) at a potency of 50 mW.cm^{-2}. Cytotoxicity was assessed 24 h after PDT using the MTT colorimetric assay. The percentage of phototoxicity was calculated relatively to control cells (cells incubated in darkness with PBS and then irradiated). Data are the mean value ± S.D. of at least three independent experiments performed in triplicates. *($p<0.05$), **($p<0.001$), ***($p<0.0001$) significantly different from control cells.

The incubation concentration (IC_{50}) values are summarized in Table 6.5, being estimated from Figure 6.22, and it is defined as the Pc-CD concentration required to kill 50% of the UM-UC-3 bladder cancer cells. The data show that the cell photokilling is dependent of the Pc-CD, light wavelength range and irradiation time. In case of the white light, only a narrow region of the light was absorbed by the compounds to initiate the photodynamic action. Hence, the IC_{50} values were lower when it was used the red light source. The data showed interesting differences between the photoactivity of Pc-CDs that differ only in the CD nature. Compounds **6.1** and **6.3** are more phototoxic comparatively with compound **6.2**, showing IC_{50} values in the range of 26-87 and 330-460 nM when cells are irradiated for 20 and 40 min with red and white lights, respectively. These IC_{50} values of Pc-CDs **6.1** and **6.3** were similar with the obtained for β-CD-conjugated silicon(IV) Pcs against human colorectal carcinoma and human hepatocarcinoma cells.[3] The lower solubility and $^1O_2$ production of **Pc-β-CD 6.2** could explain the absence of phototoxic effect on UM-UC-3 cells (Figure 6.22). Meanwhile, it is well-known that aggregation can deactivate the excited electronic states of PSs and cause further loss of photoreactivity.[25]

Table 6.5 IC_{50} values of Pc-CDs **6.1** and **6.3** against UM-UC-3 bladder cancer cells.

	Pc-CD	Red light		White light	
		20 min	**40 min**	**20 min**	**40 min**
IC_{50} [$CI_{95\%}$] (nM)	**6.1**	41 [27;64]	33 [23;47]	460 [290;730]	380 [220;660]
	6.2	n/d	n/d	n/d	n/d
	6.3	87 [53;140]	26 [17;38]	430 [300;620]	330 [220;490]

IC_{50}: incubation concentration that inhibits the proliferation of cultures in 50%, after cells incubation with Pc-CD and irradiation for 20 or 40 min with white or red light; [$CI_{95\%}$]: 95% confidence interval; n/d: not determined.

To account for the difference in photocytotoxicity, the intracellular production of ROS of these Pc-CDs was evaluated immediately after PDT using the probe 2´,7´-dichlorodihydrofluorescein diacetate (DCFDA).[29,31] This probe quantitatively reacts with several ROS to yield the fluorescent product 2´,7´-dichlorodihydrofluorescein (DCF). It was found that all the Pc-CDs are able to generate ROS upon irradiation with white or red light and the intracellular ROS production was higher for Pc-CD conjugates **6.1** and **6.3** than for Pc-CD dyad **6.2** (Figure 6.23). This fact is in good agreement with the trend observed for their photocytotoxicity (Table 6.5).

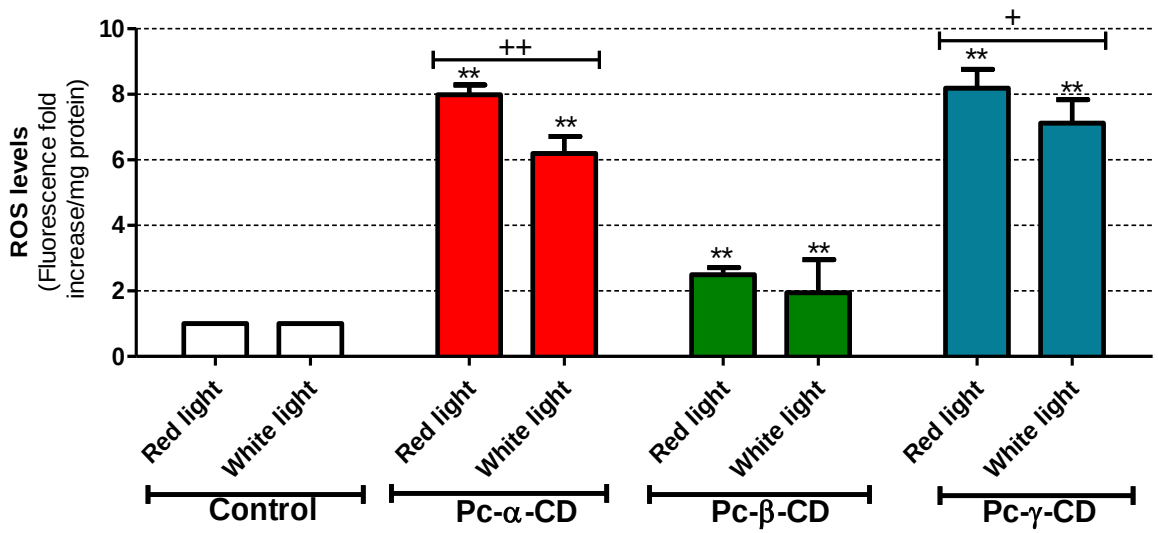

Figure 6.23 Quantification of DCF fluorescence increase (as a measure of ROS production) after PDT. UM-UC-3 bladder cancer cells were incubated with 1 μM of Pc-CD for 3 h in the dark. After PDT with red (620-750 nm) or white light (400-800 nm) during 40 min, it was detected an increase in intracellular oxidative stress observed by oxidation of the fluorescent probe H_2DCFDA (5 μM in PBS). **Significantly different from irradiated-control cells ($p<0.001$), $^{++}$significantly different from cells incubated with **Pc-α-CD** and irradiated with red light ($p<0.001$), $^{+}$significantly different from cells incubated with **Pc-γ-CD** and irradiated with red light ($p<0.05$).

In addition to the cell viability studies, it was also investigated the intracellular uptake of Pc-CDs **6.1-6.3** in bladder cancer cells by fluorescence microscopy (Figure 6.24). It is expected that CDs act as Pc carriers and that the hydrophilic (polar) CD exterior and lipophilic (nonpolar) Pc ring of Pc-CDs **6.1-6.3** resemble the structure of amphiphilic sensitizers. Uptake of these types of PSs by endocytosis has been previously reported.[5,32] On the other hand, it has been reported that CDs can perturb the lipophilic membrane barrier, enhancing the uptake of Pcs in cancer cells.[5]

The results obtained by fluorescence confocal microscopy revealed that incubation of UM-UC-3 cells with the three Pc-CDs at 1 μM for 3 h (in the dark) led to cell incorporation of all compounds resulting in intracellular fluorescence. The fluorescence of all Pc-CDs was observed as bright and granular small spots through the cytoplasm indicating that there was substantial uptake of the dyes. There were marked differences in the cellular uptake of the compound **6.2** when compared with compounds **6.1** and **6.3**, which might be due to its overall solubility and tendency to aggregation. While compound **6.2** is poorly taken up by the cells, compounds **6.1** and **6.3** are accumulated inside the cells to a much higher extent. All these results suggest that the higher phototoxicity of

compounds **6.1** and **6.3** can be attributed to their higher cellular uptake and efficiency in generating intracellular ROS.

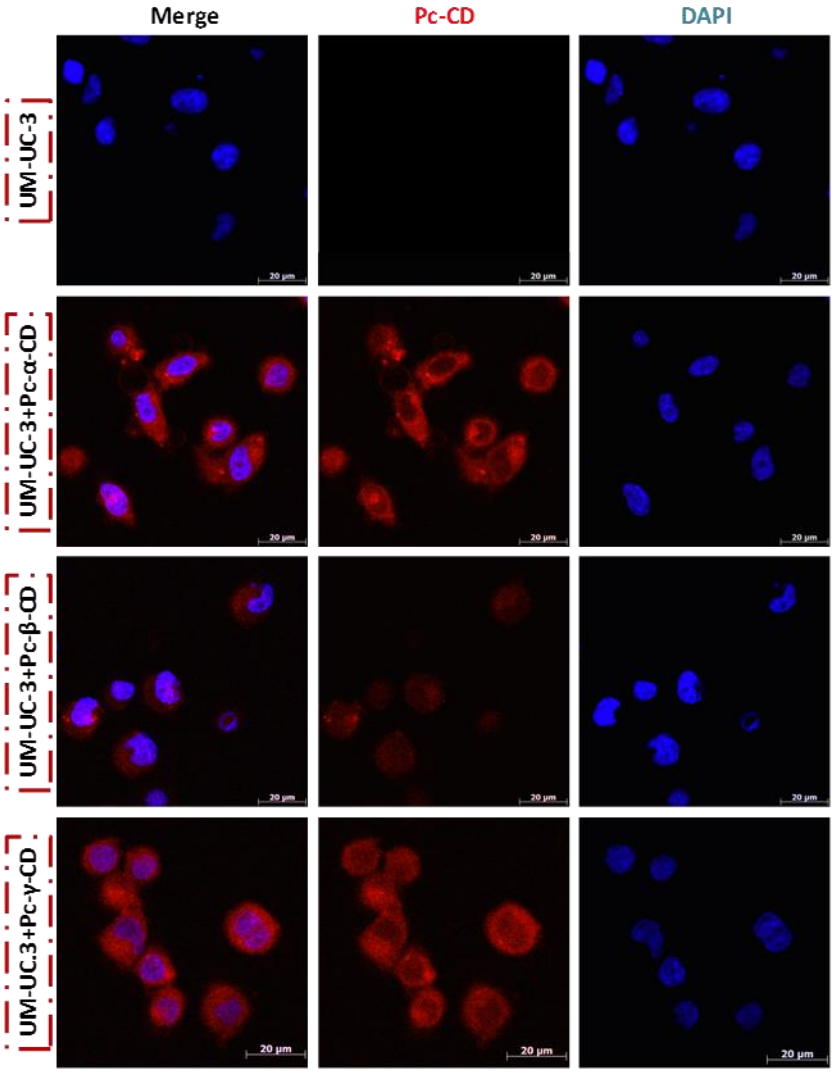

Figure 6.24 Representative fluorescence images of UM-UC-3 bladder cancer cells after incubation with 1 µM of Pc-CDs **6.1**-**6.3** (red) for 3 h in the dark. Nucleus was stained with DAPI (blue). Control fluorescence images were acquired after cells incubation with PBS buffer for 3 h and staining the nucleus with DAPI (blue). Scale bars are indicated on images. Original magnification: 400x.

6.4 Conclusions

In conclusion, we have prepared and characterized three Pc-CD conjugates (**Pc-α-CD**, **Pc-β-CD**, and **Pc-γ-CD**) and investigated their PS capabilities on UM-UC-3 bladder cancer cell line. The structures of the new Pc-CD conjugates were fully characterized by

MALDI-TOF-MS/MS tandem mass spectrometry, in which the observed fragmentation pathways were therefore relevant for the identification of such glycophthalocyanine derivatives. The MS/MS results demonstrated the main fragmentation pathways of $[Pc\text{-}CD+Na]^+$ ions studied that consist of consecutive loss of hexose residues (-162 Da) due to the rupture of $O\text{-}C_{1,4}$ bond in the CD units.

The new **Pc-α-CD** and **Pc-γ-CD** exhibited much higher water-solubility, $^1O_2$ production and intracellular ROS generation than **Pc-β-CD**, with consequently much higher UM-UC-3 bladder cancer cell line phototoxicity by the first two Pc-CDs and almost none phototoxicity by the **Pc-β-CD**. The lower photodynamic activity of the **Pc-β-CD** can be attributed to its lower solubility, lower accumulation in bladder cancer cells and lower intracellular reactive oxygen species generation. The promising photoactivity of **Pc-α-CD** and **Pc-γ-CD** ensure their potential as strong PDT drugs and it opens the possibility to explore these and many other bioconjugates of **PcF_{16}** in different directions.

6.5 Experimental section

6.5.1 General methods

^1H and ^{19}F NMR spectra were recorded on a *Bruker Avance-300* spectrometer at 300.13 and 282.38 MHz, respectively. Tetramethylsilane was used as internal reference. Absorption and fluorescence spectra were recorded using a *Shimadzu UV-2501-PC* and *FluoroMax3 (Horiba JovinYvon)*, respectively. Analytical TLC was carried out on precoated silica gel sheets (Merck, 60, 0.2 mm). Column chromatography was carried out over silica gel (Merck, 63–200 mesh). Reverse phase column chromatography was carried out over Sep-Pak®Vac 35cc (10g) tC18 Cartridges and molecular exclusion column chromatography was carried out over Bio-beads™ S-X1 Beads (200-400 Mesh, 100g), Bio-Rad Laboratories, Inc.

The HPLC chromatograms were recorded on a Merck Hitachi L620A coupled to a detector Merck Hitachi, L4250 UV/Vis detector, set at 690 nm.

MALDI-TOF-MS and MALDI-TOF-MS/MS mass spectra were acquired using a MALDI-TOF/TOF Applied Biosystems 4800 Proteomics Analyzer (Applied Biosystems, Framingham, MA, USA) instrument equipped with a nitrogen laser emitting at 337 nm. Prior to MALDI-TOF-MS analysis, 4 µL of matrix, dithranol (10 mg mL^{-1} in methanol /

0.1% TFA) were mixed with 2 µL of Pc-CD solution in methanol/ (≈10 µg mL^{-1}) and 1 µL of this mixture was deposited on the MALDI plate and let to dry. MALDI-TOF-MS spectra were acquired in the positive ion reflector mode using delayed extraction in the mass range between 600 and 4500 Da with ca. 1500 laser shots. For the following acquisition of tandem mass spectra (MS/MS) a collision energy of 2 keV was used to induce fragmentation and compressed air was used as collision gas.

6.5.2 Synthesis and characterization of Pc-CD dyes 6.1-6.3

*General procedure for the preparation of the Pc-CD derivatives **6.1**-**6.3***:

A mixture of hexadecafluorophthalocyaninatozinc(II) **PcF_{16}** (50 mg) and 1 equivalent of the CD derivative (α-, β- and γ-CD) in dry DMSO (10 mL) was heated in the presence of an excess of K_2CO_3 for 16 h at 50 ºC, until no starting **PcF_{16}** could be detected in the TLC. Then, it was added to the reaction mixture chloroform and the obtained precipitate was filtrated and redissolved in THF/H_2O (6/4). This crude mixture was first purified by silica gel column chromatography using a gradient of THF/H_2O. Further purifications of the main product fractions were performed in a reverse phase column chromatography, using again a gradient of THF/H_2O as eluent, and by molecular exclusion column chromatography using DMF as solvent. The desired products were then directly precipitated from chloroform. Typical yields were over 63%. The structures of **6.1-6.3** were confirmed by NMR spectroscopy, UV–Vis and MALDI-TOF-MS.

*Phthalocyanine-α-cyclodextrin dyad (**Pc-α-CD**, **6.1**)*:

In a 25 mL round-bottom flask, to a mixture of **PcF_{16}** (50.0 mg, 0.058 mmol) and α-CD (57.7 mg, 0.059 mmol, 1.0 equiv.) dissolved in DMSO (10 mL) was added K_2CO_3 (62.5 mg, 0.45 mmol, 7.8 equiv.). The reaction mixture was then stirred for 16 h at 50 ºC. After the workup and the purification described above the product **Pc-α-CD** was crystalized from THF/H_2O and obtained in 73% (76.8 mg) yield. ^{19}F NMR (282 MHz, DMSO-d_6): δ -178.86 to -175.51 (m, 8F, 8-α-F), -166.98 to -164.12 (m, 6F, 6-β-F). UV-Vis (DMSO), $\lambda_{max.}$ (log ε): 694 (3.67). MALDI-TOF-MS: *m/z* 1821 $[M+Na]^+$.

*Phthalocyanine-β-cyclodextrin dyad (**Pc-β-CD**, **6.2**)*:

In a 25 mL round-bottom flask, to a mixture of **PcF_{16}** (52.0 mg, 0.059 mmol) and β-CD (67.0 mg, 0.059 mmol, 1.0 equiv.) dissolved in DMSO (10 mL) was added K_2CO_3 (68.5 mg, 0.50 mmol, 8.4 equiv.). The reaction mixture was then stirred for 16 h at 50 ºC. After the workup and the purification described above the product was crystalized from THF/H_2O and obtained in 66% (77.2 mg) yield. ^{19}F NMR (DMSO-d_6, 282 MHz): δ -178.30 to -175.26 (m, 8F, 8-α-F), -166.78 to -164.15 (m, 6F, 6-β-F). UV-Vis (DMSO), $\lambda_{max.}$ (log ε): 696 (3.03). MALDI-TOF-MS: *m/z* 1981 $[M+Na]^+$.

*Phthalocyanine-γ-cyclodextrin dyad (**Pc-γ-CD**, **6.3**)*:

In a 25 mL round-bottom flask, to a mixture of **PcF_{16}** (50.8 mg, 0.058 mmol) and γ-CD (77.4 mg, 0.060 mmol, 1.0 equiv.) dissolved in DMSO (10 mL) was added K_2CO_3 (66.0 mg, 0.48 mmol, 8.2 equiv). The reaction mixture was stirred for 16 h at 50 ºC. After the workup and the purification described above the product was crystalized from THF/H_2O and obtained in 63% (78.4 mg) yield. ^{19}F NMR (DMSO-d_6, 282 MHz): δ -179.92 to -176.90 (m, 8F, 8-α-F), -167.16 to -165.02 (m, 6F, 6-β-F). UV-Vis (DMSO), $\lambda_{max.}$ (log ε): 699 (3.91). MALDI-TOF-MS: *m/z* 2143 $[M+Na]^+$.

6.5.3 Cell culture

Human bladder transitional cell carcinoma cell line UM-UC-3, established from urinary bladder of a male with a grade 3 bladder carcinoma (World Health Organization grading system classification), was obtained from the American Type Culture Collection (ATCC®, Manassas, VA, USA). UM-UC-3 cells were grown in EMEM medium (ATCC) with Earle's Balanced Salt Solution, nonessential amino acids, sodium pyruvate, 10% (v/v) of heat-inactivated Fetal Bovine Serum (FBS; Life Technologies, Carlsbad, CA, USA) and antibiotic/antimicotic containing 100 units.mL^{-1} penicillin, 100 µg.mL^{-1} streptomycin and 0.25 µg.mL^{-1} amphotericin B (Sigma).

6.5.4 Determination of intracellular Pc-CD fluorescence by fluorescence microscopy

The UM-UC-3 bladder cancer cells were plated in coverslips at a density of 0.9 × 10^5 cells per mL for 24 h before treatment. Cells were incubated with 1 µM Pc-CD in PBS buffer (10 mM NaH_2PO_4, 70 mM Na_2HPO_4 and 145 mM NaCl at pH 7.6) for 3 h in the dark. Immediately after incubation, cells were washed and fixed with 4% paraformaldehyde (PFA) (Merck, Darmstadt, Germany) for 10 min at room temperature. The samples were rinsed in PBS, mounted using VectaSHIELD (Vector Laboratories, CA, Burlingame) mounting medium with DAPI, sealed around the perimeter with nail polish and stored at 4 ºC until visualization under the confocal microscope (LSM 710, Carl Zeiss).

6.5.5 Dark toxicity of Pc-CD dyads

Cells were seeded (9.4 × 10^4 cells.cm^{-2}) in 96-well cell culture plates and maintained in culture medium under an atmosphere of air containing 5% CO_2. After seeding the cells overnight, they were washed twice with PBS and incubated in darkness (at 37 ºC under an atmosphere of air containing 5% CO_2) with solutions of Pc-CDs in PBS. The cells were then washed twice with PBS and covered with 100 µL of fresh medium. After uptake, cells were incubated in a humidified incubator in an atmosphere containing 5% CO_2 and 95% air. After 24 h, cell toxicity was determined by the MTT colorimetric assay, using 3-[4,5-dimethylthiazol-2-yl]-2,5-diphenyl-tetrazolium bromide (MTT, yellow, Sigma). In this assay, the yellow colored MTT is reduced by mitochondrial dehydrogenases in living cells to a blue-colored formazan precipitate. The absorption of dissolved formazan correlates with the number of living cells.

6.5.6 Phototoxicity of Pc-CD dyads

Cells were seeded (9.4 × 10^4 cells.cm^{-2}) in 96-well cell culture plates and maintained in culture medium under an atmosphere of air containing 5% of CO_2. After seeding the cells overnight, these were washed twice with PBS and incubated in darkness

(at 37 ºC under an atmosphere of air containing 5% of CO_2) with solutions of Pc-CDs in PBS. The cells were then washed twice with PBS and covered with 100 µL of fresh medium. Cells were irradiated (using the illumination system referred above for the photostability assays) for 20 or 40 min with white (400-800 nm) and red light (620-750 nm) at an irradiance rate of 50 $mW.cm^{-2}$. After irradiation, cells were incubated in a humidified incubator in an atmosphere containing 5% of CO_2 and 95% of air. After 24h of PDT, cell phototoxicity was determined by the MTT colorimetric assay using 3-[4,5-dimethylthiazol-2-yl]-2,5-diphenyl-tetrazolium bromide (MTT, yellow, Sigma).

The IC_{50} values (i.e. concentration of PS required to reduce cell viability by 50% as compared to the control cells) were calculated using non-linear regression analysis the sigmoidal dose-response curves (using GraphPad Prism).

6.5.7 Determination of Reactive Oxygen Species (ROS) after PDT

Immediately after photodynamic treatment, cells were washed and incubated with 5 µM of 6-carboxy-2',7'-dichlorodihydrofluorescein diacetate (H_2DCFDA) from Invitrogen (Carlsbad, CA, USA) in PBS, for 1 h at 37 °C and protected from light. This probe quantitatively reacts with several ROS to yield the fluorescent product DCF. The cells were mechanically scrapped in 130 µL of 1% (m/v) sodium dodecyl sulphate (SDS from Sigma) solution in PBS (pH 7.0) and the plate was stirred on an automatic plate shaker in the dark at room temperature. Cell suspension (100 µL) was transferred into a 96-well black plate (Greiner Bio-One) and used for fluorescence measurements of DCF. The measurements were performed using a microtiter plate reader (Synergy HT, Biotek Instruments) with the excitation and emission filters set at 485/20 and 528/20 nm, respectively. It was used 25 µL of the cell suspension to determine the protein concentration using the Pierce® BCA Protein Assay Kit (Pierce, Rockford, IL, USA).

6.5.8 Statistical analysis

GraphPad Prism (v.5.00, GraphPad Software) was used to perform the statistical analysis. The Mann-Whitney non-parametric test was applied to determine the differences between the selected two groups. Level of significance was set at $p < 0.05$.

6.6 References

1. Sallas, F., Darcy, R., *Eur. J. Org. Chem.*, **2008**, 6, 957–969.
2. Ribeiro, A. O., Tomé, J. P. C., Neves, M. G. P. M. S., Tomé, A. C., Cavaleiro, J. A. S., Serra, O. A., Torres, T., *Tetrahedron Lett.*, **2006**, 47, 6129–6132.
3. Lau, J. T. F., Lo, P. C., Tsang, Y. M., Fong, W. P., Ng, D. K. P., *Chem. Commun.*, **2011**, 47, 9657–9659.
4. Lau, J. T. F., Lo, P. C., Fong, W. P., Ng, D. K. P., *Chem.-Eur.*, **2011**, 17, 7569–7577.
5. Del Valle, E. M. M., *Process Biochem.*, **2004**, 39, 1033–1046.
6. Mitsunaga, M., Ogawa, M., Kosaka, N., Rosenblum, L. T., Choyke, P. L., Kobayashi, H., *Nat. Med.*, **2011**, 17, 1685–1691.
7. Garland, M. J., Cassidy, C. M., Woolfson, D., Donnelly, R. F., *Future Med. Chem.*, **2009**, 1, 667–691.
8. Agostinis, P., Berg, K., Cengel, K. A., Foster, T. H., Girotti, A. W., Gollnick, S. O., Hahn, S. M., Hamblin, M. R., Juzeniene, A., Kessel, D., Korbelik, M., Moan, J., Mroz, P., Nowis, D., Piette, J., Wilson, B. C., Golab, *CA Cancer J. Clin.*, **2011**, 61, 250–281.
9. Sortino, S., Mazzaglia, A., Scolaro, L. M., Merlo, F. M., Valveri, V., Sciortino, M. T., *Biomaterials*, **2006**, 27, 4256–4265.
10. Mazzaglia, A., Angelini, N., Darcy, R., Donohue, R., Lombardo, D., Micali, N., Sciortino, M. T., Villari, V., Scolaro, L. M., *Chem.-Eur*, **2003**, 9, 5762–5769.
11. Kralova, J., Synytsya, A., Pouckova, P., Koc, M., Dvorak, M., Kral, V., *Photochem. Photobiol.*, **2006**, 82, 432–438.
12. Silva, J. N., Silva, A. M. G., Tomé, J. P. C., Ribeiro, A. O., Domingues, M. R. M., Cavaleiro, J. A. S., Silva, A. M. S., Neves, M. G. P. M. S., Tomé, A. C., Serra, O. A., Bosca, F., Filipe, P., Santuse, R., Morliere, P., *Photochem. Photobiol. Sci.*, **2008**, 7, 834–843.
13. Kralova, J., Kejik, Z., Briza, T., Pouckova, P., Kral, A., Martasek, P., Kral, V., *J. Med. Chem.*, **2010**, 53, 128–138.
14. Chen, G., Jiang, M., *Chem. Soc. Rev.*, **2011**, 40, 2254–2266.
15. Naidoo, K. J., Gamieldien, M. R., Chen, J. Y. J., Widmalm, G., Maliniak, A., *J. Phys. Chem. B.*, **2008**, 112, 15151–15157.

16. Simões, J., Domingues, P., Reis, A., Nunes, F. M., Coimbra, M. A., Domingues, M. R. M., *Anal. Chem.*, **2007**, 79, 5896–5905.
17. Silva, E. M. P., Serra, V. V., Ribeiro, A. O., Tomé, J. P. C., Domingues, P., Faustino, M. A. F., Neves, M. G. P. M. S., Tomé, A. C., Cavaleiro, J. A. S., Ferrer-Correia, A. J., Iamamoto, Y., Domingues, M. R. M., *Rapid Commun. Mass Spectrom.*, **2006**, 20, 3605–3611.
18. Lourenco, L. M. O., Tomé, J. P. C., Domingues, M. R. M., Domingues, P., Costa, P. J., Felix, V., Neves, M. G. P. M. S., Cavaleiro, J. A. S., *Rapid Commun. Mass Spectrom.*, **2009**, 23, 3478–3483.
19. Soares, A. R. M., Neves, M. G. P. M. S., Santos, S. M., Tomé, J. P. C., Tomé, A. C., Cavaleiro, J. A. S., Torres, T., Domingues, M. R. M., *Rapid Commun. Mass Spectrom.*, **2013**, 27, 1019–1026.
20. Cinar, H., Kretschmann, O., Ritter, H., *Macromolecules*, **2005**, 38, 5078–5082.
21. Zaia, J., *Mass Spectrom. Rev.*, **2004**, 23, 161–227.
22. Harvey, D. J., *Mass Spectrom. Rev.*, **2012**, 31, 183–311.
23. Sforza, S., Galaverna, G., Corradini, R., Dossena, A., Marchelli, R., *J. Am. Soc. Mass Spectrom.*, **2003**, 14, 124–135.
24. Ogunsipe, A., Chen, J. Y., Nyokong, T., *New J. Chem.*, **2004**, 28, 822–827.
25. Messner, M.; Kurkov, S. V., Jansook, P., Loftsson, T., *Int. J. Pharm.*, **2010**, 387, 199–208.
26. Soares, A. R. M., Neves, M. G. P. M. S., Tomé, A. C., Iglesias-de la Cruz, M. C., Zamarron, A., Carrasco, E., Gonzalez, S., Cavaleiro, J. A. S., Torres, T., Guldi, D. M., Juarranz, A., *Chem. Res. Toxicol.*, **2012**, 25, 940–951.
27. Coleman, A. W., Nicolis, I., Keller, N., Dalbiez, J. P., *J. Inclus. Phenom. Mol.*, **1992**, 13, 139–143.
28. Silva, S., Pereira, P. M. R., Silva, P., Paz, F. A. A., Faustino, M. A. F., Cavaleiro, J. A. S., Tomé, J. P. C., *Chem. Commun.*, **2012**, 48, 3608–3610.
29. Zhang, Y. Z., Zhou, B., Zhang, X. P., Huang, P., Li, C. H., Liu, Y., *J. Hazard Mater.*, **2009**, 163, 1345–1352.
30. Pereira, P. M. R., Carvalho, J. J., Silva, S., Cavaleiro, J. A. S., Schneider, R. J., Fernandes, R., Tomé, J. P. C., *Org. Biomol. Chem.*, **2014**, 12, 1804–1811.

31. Shen, H. M., Shi, C. Y., Shen, Y., Ong, C. N., *Free Radic. Biol. Med.*, **1996**, 21, 139–146.
32. Kelbauskas, L., Dietel, W., *Photochem. Photobiol.*, **2002**, 76, 686–694.

Chapter 7

General conclusions

7.1 Conclusions

In summary, the global goal of this multidisciplinary project allowed the synthesis and characterization of remarkable compounds/materials based on neutral and cationic Pcs and to study their potential in electron donor-acceptor and biomedical areas. To this purpose, original Pc derivatives were prepared with appropriate groups on their periphery to investigate their supramolecular interactions with carbon nanostructures, and their use as PDT drugs against human bladder cancer cells and PDI agents against Gram-negative bacteria *E. coli*.

Newly synthesized thiopyridylphthalocyanines **2.6**-**2.8,** as novel electron accepting building blocks of variable strengths, showed great promise for the exfoliation of graphite *via* their immobilization onto the basal plane of graphene in DMF to afford single layer and turbostratic graphene based **G2.6**-**G2.8**. **G2.6**-**G2.8** were fully characterized (AFM, TEM, Raman, pump probe transient absorption spectroscopy, etc.) and were studied in terms of electron donor-acceptor interactions in the ground and excited state. In the context, it was noted a photoinduced electron transfer from graphene to the electron accepting Pcs that was confirmed in a series of steady-state and time-resolved spectroscopy experiments.

Following the use of thiopyridylphthalocyanines **2.6**-**2.8** and the corresponding thiopyridiniumphthalocyanines **3.1**-**3.3**, it was evidenced the syntheses and full characterization of these Pc derivatives. The preliminary photophysical studies of Pcs **2.6**-**2.8** evidence π-π interactions with SWNTs ($\Delta\lambda$ = 17–24 nm) in DMF, were the SPy groups have ability to coordinate the metal of the macrocycle core of the neighbouring Pcs, approaching these molecules around the SWNTs surface. Cationic Pcs **3.1** and **3.2** presents also noncovalent interactions but with smaller intensity comparatively with the corresponding neutral Pcs **2.6** and **2.8**. With regards to the electron donor/acceptor character of these assemblies more studies will be necessary, in order to take final conclusions.

Thiopyridylporphyrins and **RuPcs** proved to be versatile building blocks of novel supramolecular arrays **4.10**-**4.12** by axial ruthenium coordination. The thiopyridyl groups placed at the bay region of the porphyrins coordinate the RuPc dye, showing notable heterochromophore structures that evidenced electron-donating/-accepting communication between both dyes in the supramolecular hybrids. Photophysical investigation by time-

resolved transient absorption, mainly fluorescence and femtosecond spectroscopy, demonstrated efficient intermolecular energy transfer from the photoexcited central porphyrin to the peripheral **RuPcs** in the supramolecular multichromophore ensembles **4.11** and **4.12**. However, in case of the hybrid **4.10** occurs an unidirectional energy transfer from the Por to **RuPc**. The outcome forms the source to architect interesting materials in solar light converting systems.

The new inverted pyridinone and pyridinium Pc derivatives **5.6**-**5.9** were structurally characterized by NMR spectroscopy and mass spectrometry, in which the observed data were therefore relevant for the identification of such pyridinone and/or pyridinium Pc derivatives. Moreover, derivative **5.9** proved to be an efficient PS against bioluminescent *E. coli*. Interestingly, PSs **3.1** and **3.2** have higher absorbance in the wavelengths where white light system emits compared with Pc **5.9**; and the better performance of **5.9** under red light system can be due to its higher production of $^1O_2$ and/or higher overlap with the absorbance spectrum of the red light, comparing to thiopyridiniumphthalocyanines **3.1** and **3.2**.

Three Pcs conjugated with α-, β- and γ-CDs were prepared and their application as PS agents assessed by photophysical, photochemical and *in vitro* photobiological studies. The photoactivity of **Pc-α-CD** and **Pc-γ-CD** ensure their potential as PDT drugs against UM-UC-3 human bladder cancer cells due to the higher water-solubility, $^1O_2$ production and intracellular ROS generation than **Pc-β-CD**, with consequently much higher UM-UC-3 bladder cancer cell line phototoxicity by the first two Pc-CDs and almost none toxicity by the **Pc-β-CD**. The promising photoactivity of **Pc-α-CD** and **Pc-γ-CD** ensure their potential as strong PDT drugs.